NOTICE: When government or other drawings, specifications or other data are used for any purpose other than in connection with a definitely related government procurement operation, the U. S. Government thereby incurs no responsibility, nor any obligation whatsoever; and the fact that the Government may have formulated, furnished, or in any way supplied the said drawings, specifications, or other data is not to be regarded by implication or otherwise as in any manner licensing the holder or any other person or corporation, or conveying any rights or permission to manufacture, use or sell any patented invention that may in any way be related thereto.

DISCLAIMER NOTICE

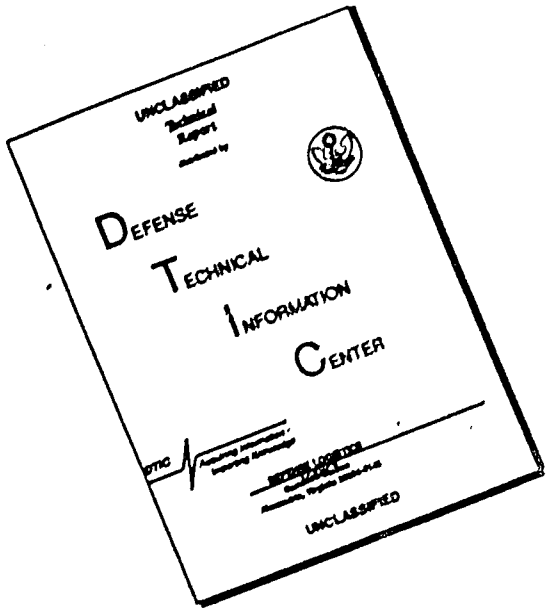

THIS DOCUMENT IS BEST QUALITY AVAILABLE. THE COPY FURNISHED TO DTIC CONTAINED A SIGNIFICANT NUMBER OF PAGES WHICH DO NOT REPRODUCE LEGIBLY.

TRANSLATION

COSMIC RESEARCH

Volume Nr. 1 - Issue Nr. 3 - 1963

FOREIGN TECHNOLOGY DIVISION

AIR FORCE SYSTEMS COMMAND

WRIGHT-PATTERSON AIR FORCE BASE

OHIO

432005

UNEDITED ROUGH DRAFT TRANSLATION

COSMIC RESEARCH

English Pages: 217

PREPARED BY:

TRANSLATION DIVISION
FOREIGN TECHNOLOGY DIVISION
WP-AFB, OHIO.

Akademiya Nauk SSSR

KOSMICHESKIYE ISSLEDOVANIYA

Tom I -Vypusk 3

Noyabr' - Dekabr'

Izdatel'stvo Akademii Nauk SSSR

Moskva 1963

pages 339—430

TABLE OF CONTENTS

THE EVOLUTION OF THE ROTATION OF A DYNAMICALLY SYMMETRICAL SATELLITE

V. V. Beletskiy

A complete system of equations in osculating elements for describing the rotational motion of a dynamically symmetrical satellite is proposed. The use of averaging with respect to one or two fast variables reduces the complete system of equations to simpler equations; in a number of important cases the averaged system can be integrated to completion in closed form. The theory thus formulated is used to investigate motion under the action of various perturbing factors (moments of gravitational, aerodynamic, and magnetic forces and of the forces of light pressure, aerodynamic dissipation, and Foucault currents). This article is a development and continuation of previous articles by the author [8, 9].

Many authors have investigated perturbed motion of artificial satellites around a center of mass. The interesting articles by Naumann [1] and Colombo [2] on the effect of magnetization of the shell of a satellite (and also gravitational moments) should be noted. Their investigation [1, 2] was limited by its framework of application to the specific satellite Explorer XI. Hagihara [3] considered a large number of perturbing factors and their effect

on the rotation of a satellite. However, some of his hypotheses and results [3] seem questionable. For example, his dependence of the moment of the aerodynamic forces on the angle of attack is questionable. His investigation [3] sometimes leads to results contradicting well-known gyroscopic effects: instead of a precession of the axis of a rapidly swirling body under the action of a restoring moment, Hagihara obtained [3] an asymptotic tending of this axis to a certain position. The formulation of the problem by Naumann, Colombo, and Hagihara [1-3] is somewhat restricted by the assumption that unperturbed motion of a satellite is pure rotation around one axis (longitudinal or transverse). This same assumption was also used by other authors: Notni and Oleak [4], Warwick [5] — in investigating the effect of the atmosphere; Zonov [6], Rosenstock [7] — in investigating the effect of eddy currents. Often, as a result, the change in only one characteristic of motion is considered (for example, Warwick, Zonov, and Rosenstock [5-7] considered only the angular velocity), and the evolution of the motion as a whole is not considered.

In the author's previous articles [8, 9] he considered the evolution of the parameters of rotation and orientation of a satellite under the action of gravitational moments and moments of the forces of aerodynamic pressure (allowing for the effect of regression of the orbit).

These articles dealt only with secular perturbations which describe the motion in the first approximation, but did not consider higher approximations and did not present a closed system of equations enabling us to obtain such approximations. On the other hand, the author [8, 9] did not consider the effect of a number of

external factors on the motion.

Therefore it seems necessary to carry out a more detailed investigation, firstly, in the direction of refining the analysis of the motion, and secondly, in the direction of allowing for the effect exerted on the motion by a large number of external factors, such as electromagnetic effects, the effect of light pressure, and the effect of moments of dissipative forces.

The main results of this investigation are set forth in the present article.

The initial basis for a description of the evolution of the rotational motion of a satellite is a system of equations in osculating elements. In the author's previous articles [8, 9] such a system of equations was not presented completely. A complete system of equations in osculating elements (for the case of a dynamically symmetrical satellite) is proposed and investigated in Section 1 of the present article. These equations allow us to ascertain not only the secular perturbations, but to obtain higher approximations to the solution, in some cases in a fairly simple closed form. The secular perturbations are ascertained by averaging the equations in osculating elements over the precession and orbital periods. The solution of the equations in osculating elements averaged only over the precession period may be called a "second approximation". In Section 1, in particular, it is shown that in the important case where the moments of the external forces have a force function, motion even in the "second approximation" is divided into a regular precession (with constant and quasi-constant parameters) around a kinetic-momentum vector of constant magnitude and the precessional-nutational motion of the

kinetic-momentum vector itself. As a result, the equations of motion of the kinetic-momentum vector in certain cases can be integrated in closed form. The problem is even further simplified, if we limit ourselves to just secular motion. It is shown that the equation of the secular-motion trajectory of the kinetic-momentum vector is obtained by equating the twice-averaged force function to an arbitrary constant.

The theory developed in Section 1 is used in the following sections to analyze the effect of specific perturbing factors on the motion.

In Section 2 gravitational perturbations are considered. In particular, it is shown that in a circular orbit the motion of the "second approximation" is described in Jacobian elliptical functions. Motion in an elliptical orbit is also considered, and a comparison of the approximate solutions and solutions obtained by numerical integration of the exact equations is made. This comparison shows that the "second approximation" describes the motion with a very high accuracy (to hundredths of a degree in actual cases).

In Section 3 moments of the forces of aerodynamic pressure and friction are derived, analyzed, and approximated.

The effect of a moment of the forces of aerodynamic pressure is investigated in detail in Section 4. In particular, the effect of the rotation of the earth's atmosphere is considered. The ascertained effect of the "tracking" of the instantaneous velocity vector of the center of mass of the satellite by the kinetic-momentum vector should be noted. This "tracking" occurs in such a way that, for example, in a circular orbit the kinetic-momentum vector precesses around a certain axis stationarily positioned in the plane contain-

ing the instantaneous velocity vector and the normal to the orbital plane.

Section 5 deals with the effect of a moment of the forces of aerodynamic friction, under the action of which, as is shown, the satellite asymptotically tends to establish itself in a regime of maximum aerodynamic resistance.

An analysis of motion under the action of electromagnetic factors is made in Sections 6-7. The effect of the intrinsic magnetic field of the satellite and of the magnetization of the shell of the satellite in the earth's magnetic field is considered in Section 6; the possible sets of motions of the kinetic-momentum vector are analyzed. The asymptotic effects of the motion, caused by eddy currents in the shell of the satellite, are considered in Section 7. It is shown that the satellite tips over or else is stabilized relative to the kinetic-momentumvector, while this vector itself seeks to coincide with a certain intermediate direction of the earth's magnetic field. The effect of moments of the forces of light pressure on a space vechicle moving in an orbit around the sun is considered in Section 8. It is shown that the kinetic-momentum vector describes a closed trajectory around an axis stationarily positioned in the plane containing the direction toward the sun and the normal to the orbital plane.

The main qualitative effects of the motion are systematized in the concluding table.

The formulas obtained in the present article enable us to calculate the evolution of the parameters of rotation and orientation of a satellite sufficiently simply and efficiently in a number of cases. The main purpose of the present article is to describe

the method of investigating the evolution of the motion and to ascertain the qualitative effects, and not to calculate specific problems; therefore the few numerical calculations described in the article are mainly of methodical nature.

The author thanks D. Ye. Okhotsimskiy for his discussion of the article.

1. Equations in Osculating Elements for a Dynamically Symmetrical Satellite and a Method of Investigating Them

We take as the unperturbed motion a regular precession described by the following constant parameters (Fig. 1): L is the modulus of the kinetic-momentum vector, σ and ρ are spherical coordinates of the latter in a coordinate system with its origin at the center of mass of the satellite and with invariable directions of the axes, ϑ is the angle of nutation, $\dot{\varphi}$ and $\dot{\psi}$ are the angular velocities of the proper rotation and the precession.

In the general case it is convenient to take as the osculating elements the quantities L, ρ, σ, and ϑ, which are constant in unperturbed motion, and the quantities $\dot{\psi}$ and $\dot{\varphi}$, which are linear with respect to time. Since the component of the angular velocity along the axis of symmetry $n = \dot{\varphi} + \cos\vartheta \cdot \dot{\psi}$ is constant in unperturbed motion, it is convenient to also consider the quantity n as an osculating element.

If the moments of the perturbing forces do not depend on φ, we shall use as the osculating elements the system of elements

$$L,\ \sigma,\ \rho,\ \vartheta,\ n,\ \psi. \qquad (1.1)$$

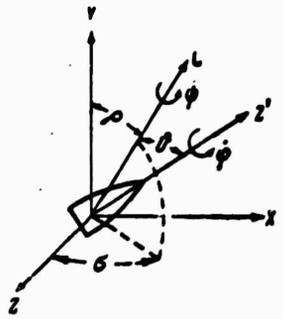

Fig. 1.

If the moments of the perturbing forces depend on φ, we shall use as the osculating elements the system

$$L,\ \sigma,\ \rho,\ \delta,\ \varphi,\ \psi. \tag{1.2}$$

If the differential equations for System (1.1) are unknown, it is, in principle, a simple matter to set up still another differential equation for φ. Therefore (1.1) is the main system for which we shall derive the differential equations of perturbed motion.

Let $\mathbf{L}$ (L_x, L_y, L_z) be the kinetic-momentum vector and $\mathbf{M}$ (M_x, M_y, M_z) be the moment of the external forces,

Then

$$\dot{L}_x = M_x;\ \dot{L}_y = M_y;\ \dot{L}_z = M_z. \tag{1.3}$$

Henceforth we shall always assume that the axis X is directed parallel to the tangent to a Keplerian orbit at its pericenter; the axis Y is directed along the normal to the orbital plane; Z is directed along the radius vector of the pericenter of the orbit. The origin coincides with the center of mass of the satellite. Then ρ is the angular distance between the vector $\mathbf{L}$ and the normal to the orbital plane, σ is the angular distance between the radius vector of the orbit at the pericenter and the projection l of the vector $\mathbf{L}$ on the plane XZ.

We shall determine the location of the axis of symmetry z' of the satellite in the coordinate system XYZ by the direction cosines α'', β'', γ''.

For a dynamically symmetrical body we can obtain

$$\frac{d\alpha''}{dt} = \frac{1}{A}[L_y\gamma'' - L_z\beta''],\quad \frac{d\beta''}{dt} = \frac{1}{A}[L_z\alpha'' - L_x\gamma''],\quad \frac{d\gamma''}{dt} = \frac{1}{A}[L_x\beta'' - L_y\alpha'']. \tag{1.4}$$

Here A is the transverse moment of inertia. Taking into account the notation introduced

$$\alpha'' = \sin\psi \sin\vartheta \cos\rho \sin\sigma - \cos\psi \sin\vartheta \cos\sigma + \cos\vartheta \sin\rho \sin\sigma,$$
$$\beta'' = -\sin\psi \sin\vartheta \sin\rho + \cos\vartheta \cos\rho, \tag{1.5}$$
$$\gamma'' = \sin\psi \sin\vartheta \cos\rho \cos\sigma + \cos\psi \sin\vartheta \sin\sigma + \cos\vartheta \sin\rho \cos\sigma,$$

$$L_x = L \sin\rho \sin\sigma, \quad L_y = L\cos\rho, \quad L_z = L \sin\rho \cos\sigma. \tag{1.6}$$

Let us now require that in perturbed motion the direction cosines and their derivatives, which completely characterize the motion of the body, have the same form as in unperturbed motion, i.e., the form of (1.4) and (1.5). This requirement uniquely determines the differential equations of perturbed motion, which, as it turned out, have the form:

$$\dot{L} = (M_x \sin\sigma + M_z \cos\sigma)\sin\rho + M_y \cos\rho,$$
$$\dot{\rho} = \frac{1}{L}[(M_x \sin\sigma + M_z \cos\sigma)\cos\rho - M_y \sin\rho],$$
$$\dot{\sigma} = \frac{1}{L\sin\rho}(M_x \cos\sigma - M_z \sin\sigma),$$
$$\dot{n} = \frac{1}{C}[M_x\alpha'' + M_y\beta'' + M_z\gamma''], \tag{1.7}$$
$$\dot{\psi} = \frac{L}{A} + \frac{1}{L}\{-M_x[\operatorname{cot}\vartheta(\cos\sigma\sin\psi + \sin\sigma\cos\rho\cos\psi) +$$
$$+ \operatorname{cot}\rho\cos\sigma] + M_y \sin\rho \operatorname{cot}\vartheta \cos\psi + M_z[\operatorname{cot}\vartheta(\sin\sigma\sin\psi -$$
$$- \cos\sigma\cos\rho\cos\psi) + \operatorname{cot}\rho\sin\sigma]\},$$
$$\cos\vartheta = \frac{Cn}{L}.$$

Here C is the longitudinal moment of inertia.

Notes. 1) If M_x, M_y, M_z do not contain $\dot{\varphi}$, System (1.7) is closed. Otherwise it must be supplemented with the kinetic relationship

$$n = \dot{\varphi} + \dot{\psi}\cos\vartheta + \dot{\sigma}(-\sin\psi\sin\vartheta\sin\rho + \cos\vartheta\cos\rho) +$$
$$+ \dot{\rho}(-\cos\psi\sin\vartheta), \tag{1.8}$$

which determines the projection of the total angular velocity on the axis of symmetry of the satellite in perturbed motion.

2) As can be seen, System (1.7) consists of five differential equations and one finite relationship for determining Φ. This kinematic relationship occurs in unperturbed and perturbed motion. Thus System (1.7) is of the fifth order, since $\mathbf{M}$ does not depend on φ. System (1.7)-(1.8) is of the sixth order.

3) Instead of the first three equations in (1.7), it is sometimes more convenient to use Eqs. (1.3) directly.

The moments of the forces in the specific problems considered below in the present article do not depend on φ. Let us analyze an important particular case. Let the moments of the forces have the force function

$$U = U(t, \alpha'', \beta'', \gamma'') \tag{1.9}$$

i.e., they depend only on the location of the axis of symmetry of the satellite in space. In the cases being considered by us U depends on time only through the true anomaly of the satellite $\nu(t)$, i.e.,

$$U = U(\nu\ (t), \alpha'', \beta'', \gamma'').$$

Then

$$M_x = \frac{\partial U}{\partial \gamma''}\beta'' - \frac{\partial U}{\partial \beta''}\gamma''; \quad M_y = \frac{\partial U}{\partial \alpha''}\gamma'' - \frac{\partial U}{\partial \gamma''}\alpha''; \quad M_z = \frac{\partial U}{\partial \beta''}\alpha'' - \frac{\partial U}{\partial \alpha''}\beta'', \tag{1.10}$$

and the system of equations (1.7) assumes the form

$$\begin{aligned} \dot{L} &= \frac{\partial U}{\partial \psi}, \\ \dot{\rho} &= \frac{1}{L \sin \rho}\left\{\frac{\partial U}{\partial \psi}\cos \rho - \frac{\partial U}{\partial \sigma}\right\}, \\ \dot{\sigma} &= \frac{1}{L \sin \rho}\frac{\partial U}{\partial \rho}, \\ \dot{n} &= 0, \\ \dot{\psi} &= \frac{L}{A} - \frac{1}{L}\left\{\frac{\partial U}{\partial \rho}\cot \rho + \frac{\partial U}{\partial \delta}\cot \theta\right\}, \\ \cos \theta &= \frac{C_R}{L}. \end{aligned} \tag{1.11}$$

System (1.11) admits the first integral

$$n = n_0. \tag{1.12}$$

From (1.11) we can obtain the relationship

$$\frac{d}{dt}(L^2 - 2AU) = -\frac{\partial}{\partial t}(2AU).$$

If U does not depend explicitly on time, the following energy integral occurs

$$L^2 - 2AU = \text{const} \tag{1.12a}$$

From the first two equations in (1.11) we find

$$\frac{d}{dt}(L\cos\rho) = \frac{\partial U}{\partial \sigma}.$$

Let U depend on the time t and the coordinate σ only through the parameter

$$\varphi = \sigma - \omega_0 t.$$

This case occurs when the center of mass of the satellite moves in a circular orbit with an angular velocity ω_0. Then

$$\frac{\partial U}{\partial t} = -\omega_0 \frac{\partial U}{\partial \sigma},$$

and, comparing the relationship for d/dt (L^2 - 2AU) and d/dt (L cos ρ), we obtain an energy integral of Jacobian type

$$L^2 - 2AU - 2A\omega_0 L\cos\rho = \text{const} \tag{1.12b}$$

Equations (1.7) or (1.11) enable us to investigate any motion: fast rotations and oscillations. For example, in (1.11) let $n_0 = 0$. Then cos $ = 0 and U does not depend on $. We can seek a solution such that $\rho = 0$, $\sigma = \sigma_0 = \text{const}$, which is possible, if the following condition is fulfilled

$$\left.\frac{1}{\sin\rho}\frac{\partial U}{\partial \rho}\right|_{\substack{\rho=0 \\ \theta=\frac{\pi}{3}}} = 0.$$

Then only the following equations remain

$$\dot{\psi} = \frac{L}{A}; \quad L = \frac{\partial H'}{\partial \psi}.$$

from which it is easy to obtain

$$\ddot{\psi} - \frac{1}{A}\frac{\partial U}{\partial \psi} = 0.$$

This is an equation for the oscillations in the orbital plane. However, by the very choice of variables, Eqs. (1.7) or (1.11) are most suitable for investigating fast perturbed motion. To these equations it is convenient to apply various approximate methods, for example, the Bogolyubov-Krylov asymptotic method [10].

Note that, as can be seen from (1.7) and (1.11), the angular velocity of precession $\dot{\psi}$ may be expressed approximately as:

$$\dot{\psi} \approx \frac{L}{A}, \qquad (1.13)$$

since the remaining terms in the case of fast rotations, i.e., in the case of large L, are fairly small. These terms introduce a small quantitative correction into the precession velocity, but the qualitative picture of the motion does not change as long as the precession velocity is fairly great. Therefore, instead of the equations for $\dot{\psi}$ written in (1.7) and (1.11), we can limit ourselves to Eq. (1.13).

Since, according to (1.13), ψ increases almost linearly and fairly fast (in comparison not only with the rate of change in the osculating elements, but even with the angular velocity $\dot{\nu}$ of the motion of the center of mass of the satellite in orbit), for ascertaining the main effects of the motion it is convenient to average the right-hand sides of the equation of motion with respect to the variable ψ. Carrying out such an averaging, for example,

in (1.11) and taking into account that U, according to (1.9) and (1.5), depends on ψ periodically with a period of 2π, we obtain for the averaged motion

$$\dot{L} = 0, \text{ i.e., } L = L_0, \tag{1.14}$$

and, consequently,

$$\cos i = \cos i_0; \ \dot{\psi} \approx \dot{\psi}_0 \tag{1.15}$$

Moreover,

$$\dot{\rho} = -\frac{1}{L_0 \sin i} \frac{\partial \overline{U}}{\partial \sigma}, \qquad \dot{\sigma} = \frac{1}{L_0 \sin i} \frac{\partial \overline{U}}{\partial \rho}, \tag{1.16}$$

where

$$\overline{U} = \frac{1}{2\pi} \int_0^{2\pi} U \, d\psi. \tag{1.17}$$

In other words, the satellite precesses regularly around a kinetic-momentum vector of constant magnitude, the direction of which varies in space, according to Eqs. (1.16) and (1.17).

We thus see that the problem of the evolution of motion in this case reduced to an investigation of System (1.16), which is easily converted to canonical form. Assumption (1.13) is not fundamental, since an averaging of the exact system (1.11) leads to its division into System (1.16), which does not depend on ψ, and an equation for ψ:

$$\dot{\psi} = \frac{L}{A} - \frac{1}{L}\left\{\frac{\partial \overline{U}}{\partial \rho} \cot i + \frac{\partial \overline{U}}{\partial \theta} \cot \theta\right\}. \tag{1.18}$$

Note that averaging the right-hand sides of the equations of motion (1.11) was equivalent to averaging the force function.

Equations (1.16) in the general case are not integrated to completion, since U depends on time (through the true anomaly ν).

However, for ascertaining the secular variations in ρ and σ it is permissible to average Eqs. (1.16) again with respect to the true anomaly, since the variation in ρ and σ occurs fairly slowly in comparison with the variation in ν. Since in an elliptical orbit ν varies nonuniformly in time, while the averaging must be carried out with respect to uniformly varying variables, in Eqs. (1.16) let us pass from the independent variable $\underline{t}$ to the new independent variable ν. We shall assume that the orbit of the satellite is an unperturbed elliptical orbit. Then

$$\frac{d\nu}{dt} = \frac{\sqrt{\mu P}}{P^2}(1 + e\cos\nu)^2, \qquad (1.19)$$

where P is a focal parameter, $\underline{e}$ is the eccentricity, and μ is the product of the gravitational constant times the mass of the central body. Let us introduce the function

$$U_\nu = \frac{P^2}{\sqrt{\mu P}\,(1 + e\cos\nu)^2} U \cdot \qquad (1.20)$$

and its average value with respect to ψ

$$\overline{U}_\nu = \frac{1}{2\pi}\int_0^{2\pi} U_\nu d\psi. \qquad (1.21)$$

Then Eqs. (1.16) can be written in the form

$$\frac{d\rho}{d\nu} = -\frac{1}{L_0 \sin\rho}\frac{\partial \overline{U}_\nu}{\partial\sigma}, \quad \frac{d\sigma}{d\nu} = \frac{1}{L_0\sin\rho}\frac{\partial\overline{U}_\nu}{\partial\rho}. \qquad (1.22)$$

Note that Eqs. (1.22) are invariant with respect to the transformation ρ, $\sigma \to \theta$, λ, where θ, λ are the coordinates of the kinetic-momentum vector read off analogously to ρ, σ, but relative to other axes (for example, θ is the angle between **L** and the axis X, while λ is read off in the plane ZY from the axis Z).

From the point of view of mechanics, averaging with respect to ψ is equivalent to neglecting in the solution high-frequency

oscillations of very small amplitude, which are superimposed on the slower oscillations described by Eqs. (1.22). We shall call the high-frequency oscillations caused by the effect of ψ vibration oscillations.

Equations (1.22) give the very slow secular and long-period terms of the solution, and also the periodic terms resulting from the effect of ν. The period of these periodic oscillations is commensurate with the orbital period of the satellite. The secular and long-period terms vary very slowly in comparison with the velocity of motion of the center of mass of the satellite in orbit. In order to ascertain them, it is necessary to average the equations of motion not only with respect to ψ, but also with respect to ν. An independent averaging with respect to each variable ψ, ν is permissible, if the frequencies of these variables are incommensurable, which is what we shall always assume. Such a twofold averaging, for example, of Eqs. (1.11) reduces, obviously, to averaging Eqs. (1.22) with respect to ν. We obtain

$$\frac{d\rho}{d\nu} = -\frac{1}{L_0 \sin\rho}\frac{\partial \overline{\overline{U}}_\nu}{\partial \sigma}, \qquad \frac{d\sigma}{d\nu} = +\frac{1}{L_0 \sin\rho}\frac{\partial \overline{\overline{U}}_\nu}{\partial \rho}, \tag{1.23}$$

where

$$\overline{U}_\nu = \frac{1}{(4\pi)^2}\int_0^{2\pi}\int_0^{2\pi} \frac{p^2}{\sqrt{\mu p}\,(1+e\cos\nu)^2} U\, d\psi\, d\nu. \tag{1.24}$$

In (1.23) $\overline{\overline{U}}_\nu$ no longer depends on ν; therefore there exists a first integral of Eqs. (1.23)

$$\overline{\overline{U}}_\nu(\rho, \sigma) = \text{const} \tag{1.25}$$

which determines the trajectory of the terminus of the kinetic-momentum vector (in its secular and long-period motion). Using (1.25), it is not difficult to integrate Eqs. (1.23) to completion,

thus, also ascertaining the law of change in the kinetic-momentum vector.

Returning to Eqs. (1.22), let us note that their solution gives a picture of motion substantially more accurate than the solution of Eqs. (1.23). Although in the general case Eqs. (1.22) are not integrated, their solution is, in principle, not difficult to obtain to any desired degree of accuracy, for example, by the method of successive approximations, the Bogolyubov-Krylov asymptotic method, and finally by numerical integration. Moreover, let us mention the interesting particular case, encountered in practice, where even Eqs. (1.22) are integrated in closed form. Let $\overline{U}_\nu$ depend on σ and ν only through their difference $\varphi = \sigma - \nu$:

$$\overline{U}_\nu = \overline{U}_\nu(\rho, \overline{\varphi}). \qquad (1.25a)$$

The coordinate $\overline{\varphi}$ is the angle between the instantaneous radius vector of the orbit **R** and the projection of the vector **L** on the orbital plane. Thus the angles ρ, $\overline{\varphi}$ give the position of the vector **L** in a rotating coordinate system **n**, τ, **R**, where **n** is directed along the normal to the orbital plane and τ is directed along the transversal to the orbit. Equations (1.22) assume the form

$$\frac{d\rho}{d\nu} = -\frac{1}{L_0 \sin\rho}\frac{\partial\Phi}{\partial\overline{\varphi}}, \qquad \frac{d\overline{\varphi}}{d\nu} = \frac{1}{L_0 \sin\rho}\frac{\partial\Phi}{\partial\rho}, \qquad (1.26)$$

where

$$\Phi = L_0 \cos\rho + \overline{U}_\nu. \qquad (1.27)$$

Here $\overline{U}_\nu$, as before, is determined by Formulas (1.21) and (1.20). Since U_ν contains only ρ and $\overline{\varphi}$ and does not depend on ν explicitly, Eqs. (1.26) have a first integral which gives the trajectory of the terminus of the vector **L** in a rotating coordinate system

$$\Phi = \text{const} \tag{1.28}$$

This integral enables us to integrate Eq. (1.26) to completion. It can be considered as a corollary of (1.12b) and (1.14). As will be shown below, we can reduce to form (1.26) equations of rotational motion under the action of such important perturbations as gravitational and aerodynamic perturbations in the case of a circular orbit of the center of mass of a satellite and perturbations due to light pressure in the case of an arbitrary elliptical orbit of a solar satellite.

In the general case of Eqs. (1.7) (in the presence of arbitrary force moments which do not have a force function) it is also expedient to use the method of averaging to ascertain the principal effects of the motion. This method will be used below, for example, to investigate secular perturbations under the action of dissipative-force moments caused by aerodynamic friction and eddy currents.

2. Gravitational Perturbations

Gravitational-force moments acting on a dynamically symmetrical satellite in a central Newtonian field have, as follows from a previous article by the author [11], a force function, which may be expressed approximately as:

$$U = \frac{3}{2}\frac{\mu}{p^3}(1 + e\cos\nu)^3 (A - C)(\gamma'' \cos\nu + \alpha'' \sin\nu)^2. \tag{2.1}$$

Then, using the formulas of the preceding section, we obtain:

$$U_\nu = \frac{3}{2}\frac{\sqrt{\mu}}{p^{3/2}}(1 + e\cos\nu)(A - C)(\gamma'' \cos\nu + \alpha'' \sin\nu)^2, \tag{2.2}$$

$$\overline{U}_\nu = \frac{3}{2}\frac{\sqrt{\mu}}{p^{3/2}}(A - C)(1 + e\cos\nu)\left[1 - \frac{3}{2}\sin^2\vartheta\right]\sin^2\rho\cos^2(\sigma - \nu), \tag{2.3}$$

$$\overline{U}_\nu = \frac{3}{4}\frac{\sqrt{\mu}}{p^{3/2}}(A - C)\left[1 - \frac{3}{2}\sin^2\vartheta\right]\sin^2\rho. \tag{2.4}$$

In Formulas (2.1)-(2.4) the terms not affecting the motion relative to the center of mass are omitted.

According to (1.25) and (2.4), we see that for the trajectory of the terminus of the kinetic-momentum vector

$$\rho = \rho_0. \tag{2.5}$$

Substituting (2.4) in (1.23), we obtain the velocity of the secular motion of the terminus of the kinetic-momentum vector

$$\frac{d\sigma}{d\nu} = \frac{3}{2}\frac{\sqrt{\mu}}{p^{3/2}}\frac{(A-C)}{L_0}\left[1-\frac{3}{2}\sin^2\vartheta_0\right]\cos\rho_0. \tag{2.6}$$

Thus, in secular motion the kinetic-momentum vector precesses around the normal to the orbital plane at a constant angular distance (2.5) with an angular velocity proportional (with the proportionality coefficient in (2.6)) to the angular velocity of motion of the center of mass in an elliptical orbit. In a particular case we obtain for a circular orbit a well-known result [8]. In this case $\nu = \omega_0 t$, $\sqrt{\mu/p}^{3/2} = \omega_0$, where ω_0 is a constant angular velocity of motion of the center of mass.

From (1.22) and (2.3) we obtain more accurate equations, when averaging only with respect to ψ

$$\begin{aligned}\frac{d\rho}{d\nu} &= N_0(1+e\cos\nu)\cos(\sigma-\nu)\sin(\sigma-\nu)\sin\rho,\\ \frac{d\sigma}{d\nu} &= N_0(1+e\cos\nu)\cos^2(\sigma-\nu)\cos\rho,\end{aligned} \tag{2.7}$$

where

$$N_0 = 3\frac{\sqrt{\mu}}{p^{3/2}}\frac{(A-C)}{L_0}\left(1-\frac{3}{2}\sin^2\vartheta_0\right). \tag{2.8}$$

In solving these equations, periodic oscillations of σ and ρ with a small (for small values of N_0) amplitude and a period comparable to 2π are also superimposed on the secular motion (2.6). Since ν varies comparatively rapidly, while σ varies slowly, $\sigma - \nu$ varies

rapidly and therefore repeatedly passes through the extremal values, which are multiples of $\pi/2$.

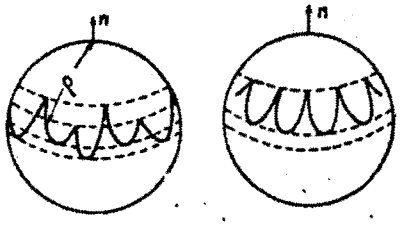

Fig. 2.

In this case on the trajectory $\rho(\sigma)$, which is the trace of the kinetic-momentum vector on a unit sphere, points of tangency to the parallels of the unit sphere alternate with points of return (Fig. 2). Indeed, the angle V between the tangent to the trajectory and the meridian on the unit sphere is given by the formula

$$\tan V = \sin\rho \frac{d\sigma}{d\rho} = \operatorname{cot}(\sigma - \nu)\cos\rho. \qquad (2.9)$$

When $\sigma - \nu = 0$ and $\sigma - \nu = \pm\pi$, we obtain $\tan V = \infty$, and consequently the trajectory is tangent to the parallel, having an extremum at the point of tangency. When $\sigma - \nu = \pm\pi/2$ and $\sigma - \nu = \pm 3/2\pi$, we obtain $\tan V = 0$, i.e., the trajectory has a point of return. From (2.9) it also follows that the trajectory can pass through $\rho = 90^\circ$ only at a right angle to the equator of the unit sphere. From (2.9) it follows further that when $\rho < 90^\circ$ the points of return are always minimum points of ρ, while the points of tangency are maximum points of ρ (Fig. 2). When $\rho > 0$, the picture is reversed. When $\rho < 90^\circ$, the trajectory passes in one direction, but when $\rho > 90^\circ$, it passes in the opposite direction. It should also be noted that the oscillation amplitude of ρ is all the smaller and the rate of change in σ all the greater, the closer the value of ρ is to 0 or π. Since the direction of motion of a trajectory changes when it passes through $\rho = \pi/2$, in the neighborhood of $\rho = \pi/2$ the trajectories have a specific character: they have loops.

These trajectories are shown in Fig. 3. In the neighborhood of $\rho = \pi/2$ the rate of change in σ, as can be seen from the second equation in (2.7), is very low; therefore the trajectory loops have a small width and move very slowly. In particular, there exist periodic trajectories (with a stationary loop). Let us recall that in the first approximation, when $\rho = 90^\circ$, there is no secular motion, as follows from (2.6). Such are the basic features of the motion. Let us pass now to an analytical description of it.

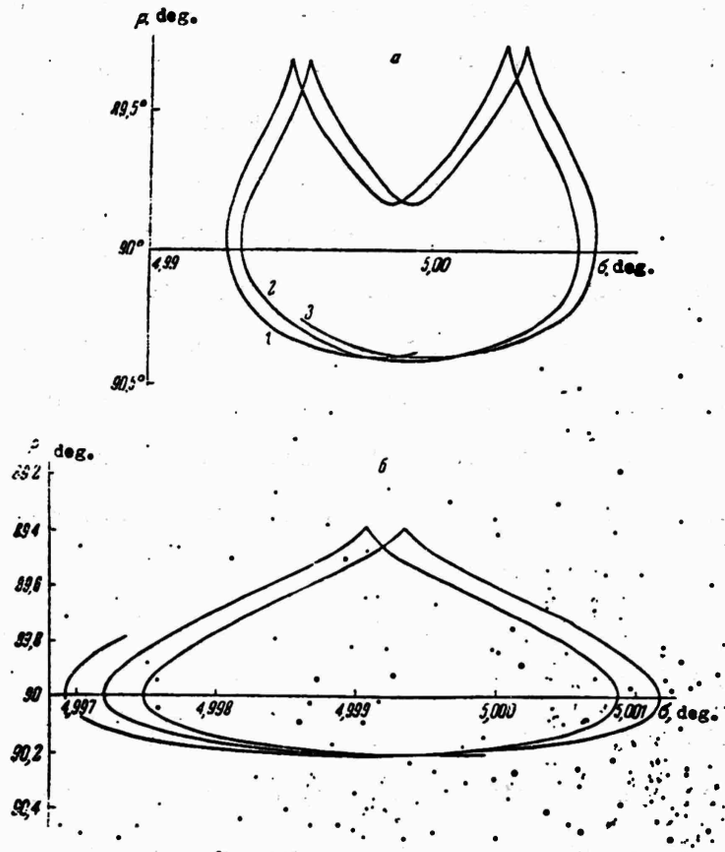

Fig. 3.

Let us consider the case of a circular orbit ($e = 0$). Then Eqs. (2.7) can be reduced to the form (1.26) by the substitution $\bar{\varphi} = \sigma - \nu$ and, according to (1.28), have the first integral

$$L_0 \cos\rho + L_0 \frac{N_0}{2} \sin^2\rho \cos^2\bar{\varphi} = \text{const.} \qquad (2.10)$$

Note that

$$\sin\rho\cos\bar{\varphi} = \cos\Psi, \qquad (2.11)$$

where Ψ is the angle between the kinetic-momentum vector and the instantaneous radius vector of the orbit. From (2.10) and (2.11) it follows that the trajectory of the terminus of the kinetic-momentum vector is closed in a coordinate system rigidly connected to the radius vector of the orbit. An analysis of the trajectory is not difficult to carry out by the method given by the author [8, 9]. By the nature of the problem, an approximate solution will differ fairly little from the exact solution over an interval of change in ν that is all the greater, the lower the value of N_0. When $|N_0| < 1$, the trajectories have the character shown in Fig. 4: elongated along the meridian **n**, **R** at one pole and along the meridian **n**, τ at the other pole (**-n**). The trajectory depicted in Fig. 4 is shown in absolute motion in Fig. 2b. Over a small interval of values of ν (of the order of one orbital pass, which is of interest, for example, in studying the motion of a solar satellite) a consideration of the case $N_0 > 1$ is permissible. Then the family of trajectories has the form shown in Fig. 5. The appearance of new slanting poles of motion gravitating toward **R** reflects the fact that in the case of a low kinetic energy of rotation the direction of the instantaneous radius vector is the direction of stable equilibrium of the body. This effect makes itself felt even in our analysis, although in the case of low kinetic energies the method used gives a cruder result than in the case of high kinetic energies. Examples of the comparison of the theory and the exact solution

will be given below. The location ρ^*, $\bar{\varphi}^*$ of the slanting poles is determined by the formula

$$\cos\rho^* = \frac{1}{N_0}, \quad \bar{\varphi}^* = 0, \ |N_0| > 1.$$

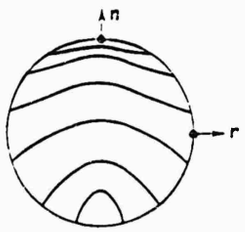

Fig. 4.

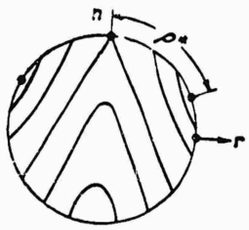

Fig. 5.

Let us return to the basic case $|N_0| < 1$. Using Integral (2.10), we can integrate Eqs. (2.7) to completion in Jacobian elliptic functions. For $N_0 > 0$ the solution has the form

$$\cos\rho = \cos\rho_0 + \frac{N_0}{2}\sin^2\rho_0\,\mathrm{sn}^2(u, k), \tag{2.12}$$

$$\cos\bar{\varphi} = \frac{\mathrm{cn}(u, k)}{\sqrt{1 - N_0\cos\rho_0\,\mathrm{sn}^2(u, k) - \frac{N_0^2}{4}\sin^2\rho_0\,\mathrm{sn}^4(u, k)}}, \tag{2.13}$$

$$u = \sqrt{1 - N_0\cos\rho_0}\,\nu, \tag{2.14}$$

$$k = \frac{N_0\sin\rho_0}{2\sqrt{1 - N_0\cos\rho_0}}. \tag{2.15}$$

Moreover,

$$\cos\Psi = \cos\Psi_0\,\mathrm{cn}(u, k), \ (\cos\Psi_0 = \sin\rho_0). \tag{2.15a}$$

Here it is assumed that the coordinate system is chosen in such a way that when $\nu = 0$, $\sigma = 0$ and, consequently, $\bar{\varphi} = 0$ (on a circular orbit such a coordinate system can always be chosen). The modulus of the elliptic functions $k < 1$, when $N_0 < 1$, as follows from (2.15). If, instead of ρ, we put in these formulas $\bar{\rho} = \pi - \rho$ and replace N_0 by $|N_0|$, we obtain the formulas for the case $N_0 < 0$.

Let us analyze (2.12)-(2.15). The oscillation amplitude is equal to $(N_0/2)\sin^2\rho_0$ and tends to 0, when $\rho_0 \to 0, \pi$; $\cos\rho$ varies from $\cos\rho_0$ to $\cos\rho_0 + (N_0/2)\sin^2\rho_0$; the period T_ρ of the

oscillations of the angle ρ:

$$T_\rho = \frac{2K(k)}{\sqrt{1 - N_0 \cos \rho_0}}, \tag{2.16}$$

where

$$K(k) = \int_0^{\frac{\pi}{2}} \frac{d\alpha}{\sqrt{1 - k^2 \sin^2 \alpha}}$$

is a complete elliptic integral of the first kind.

Using the smallness of N_0, we have approximately

$$T_\rho \approx \pi \left[1 + \frac{N_0}{2} \cos \rho_0 + \frac{N_0^2}{8}\left(3 \cos^2 \rho_0 + \frac{1}{2} \sin^2 \rho_0\right) + \ldots\right]. \tag{2.17}$$

The oscillation period of $\cos \overline{\varphi}$ is twice as great as T_ρ:

$$T_\varphi = 2T_\rho, \tag{2.18}$$

i.e., when the true anomaly ν varies by $2T_\rho$, the angle $\overline{\varphi}$ decreases by 2π. During this same time σ varies by $\Delta\sigma$.

$$\Delta\sigma = 2(T_\rho - \pi). \tag{2.19}$$

Approximately, according to (2.17):

$$\Delta\sigma \approx 2\pi \left[\frac{N_0}{2} \cos \rho_0 + \frac{N_0^2}{8}\left(3\cos^2 \rho_0 + \frac{1}{2} \sin^2 \rho_0\right) + \ldots\right]. \tag{2.20}$$

The first term in (2.20) corresponds to the secular variation determined by Formula (2.6). The more accurate formula (2.20) shows that a secular variation will occur at $\rho_0 = \pi/2$ (in constrast to Formula (2.6)). However, from (2.20) we can determine a $\rho_0 = \rho_0^*$ such that $\Delta\sigma = 0$, i.e., there will be no secular variation. It turns out that

$$\cos \rho_0^* \approx -\frac{4}{5N_0}\left[1 - \sqrt{1 - \frac{5}{16} N_0^2}\right] \approx -\frac{N_0}{8}. \tag{2.21}$$

At the value $\rho_0 = \rho_0^*$ the trajectory $\rho(\sigma)$ is obtained closed (periodic). In this case ρ_0^* corresponds exactly to the solution

of the transcendental equation $T_\rho = \pi$.

Let us consider the case of an elliptical orbit. Then Eqs. (2.7) are not integrated exactly. We obtain their solution by the method of successive approximations. We take as the zero approximation an unperturbed motion, i.e.,

$$\rho = \rho_0, \quad \sigma = \sigma_0.$$

Then in the first approximation

$$\rho = \rho_0 + \frac{N_0}{4}\sin\rho_0\left\{[\cos 2(\sigma_0 - \nu) - \cos 2\sigma_0] + \right.$$
$$\left. + e\,[\cos(2\sigma_0 - \nu) - \cos 2\sigma_0] + \frac{e}{3}[\cos(2\sigma_0 - 3\nu) - \cos 2\sigma_0]\right\}, \tag{2.22}$$

$$\sigma = \sigma_0 + \frac{N_0}{2}\cos\rho_0\left\{\nu - e\sin\nu + \frac{1}{2}[\sin 2\sigma_0 - \sin 2(\sigma_0 - \nu)] + \right.$$
$$\left. + \frac{e}{2}[\sin 2\sigma_0 - \sin(2\sigma_0 - \nu)] + \frac{e}{6}[\sin 2\sigma_0 - \sin(2\sigma_0 - 3\nu)]\right\}. \tag{2.23}$$

The structure of Formulas (2.22)-(2.23) shows that the rotation is by nature close to rotation in a circular satellite orbit: the oscillations in ρ and σ are superimposed on the secular variation of σ; the main difference is that the alternating maximum and minimum values of ρ are not equal to each other in the case of an elliptical orbit (from (2.7)) it can be seen that ρ will have extrema when $\sin 2(\sigma - \nu) = 0$:

$$\begin{aligned}
\rho_1 &= \rho_0 + N_0 \sin\rho_0\left\{\frac{1}{2}\sin^2\sigma_0 + \frac{e}{3}(\cos\sigma_0 - \cos 2\sigma_0)\right\}, \\
\rho_2 &= \rho_0 - N_0 \sin\rho_0\left\{\frac{1}{2}\cos^2\sigma_0 - \frac{e}{3}(\sin\sigma_0 - \cos 2\sigma_0)\right\}, \\
\rho_3 &= \rho_0 + N_0 \sin\rho_0\left\{\frac{1}{2}\sin^2\sigma_0 - \frac{e}{3}(\cos\sigma_0 + \cos 2\sigma_0)\right\}, \\
\rho_4 &= \rho_0 - N_0 \sin\rho_0\left\{\frac{1}{2}\cos^2\sigma_0 + \frac{e}{3}(\sin\sigma_0 + \cos 2\sigma_0)\right\},
\end{aligned} \tag{2.24}$$

when $0 < \sigma_0 < 90^\circ$ and $N_0 > 0$, we obtain

$$\rho_1 > \rho_2, \quad \rho_2 < \rho_3, \quad \rho_2 > \rho_4, \quad \rho_1 < \rho_3$$

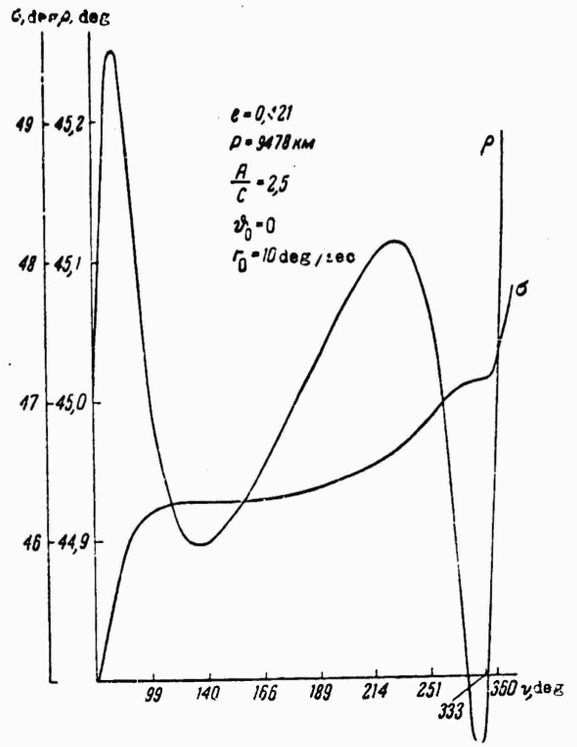

Fig. 6.

The nature of the dependence $\rho(\nu)$ is shown in Fig. 6. The trajectory-trace of the kinetic-momentum vector on a unit sphere will have the character shown in Fig. 2a.

In conclusion, let us cite an example which illustrates the accuracy of the approximate method of investigation that we used. Figure 7 gives the characteristics of the motion, calculated, on the one hand, according to the formulas of this section (broken line), and on the other hand, according to the exact equations in osculating elements without averaging. We see that the vibration terms thus added are actually negligibly small. The following values of the parameters and initial data were taken in the example: $A = 50$ kg-m sec^2, $C = 20$ kg-m sec^2, $L_0 = 3.49$ kg-m sec, $\vartheta_0 = 70^\circ$,

which corresponds to an initial precession velocity $\dot{\psi}$ = 4 deg/sec and to a projection of the angular velocity on the axis of symmetry of the satellite r = 3.4 deg/sec, e = 0.421, P = 9478 km, i.e., for an orbit with a perigee h_{π} = 300 km and an apogee h_{α} = 10,000 km.

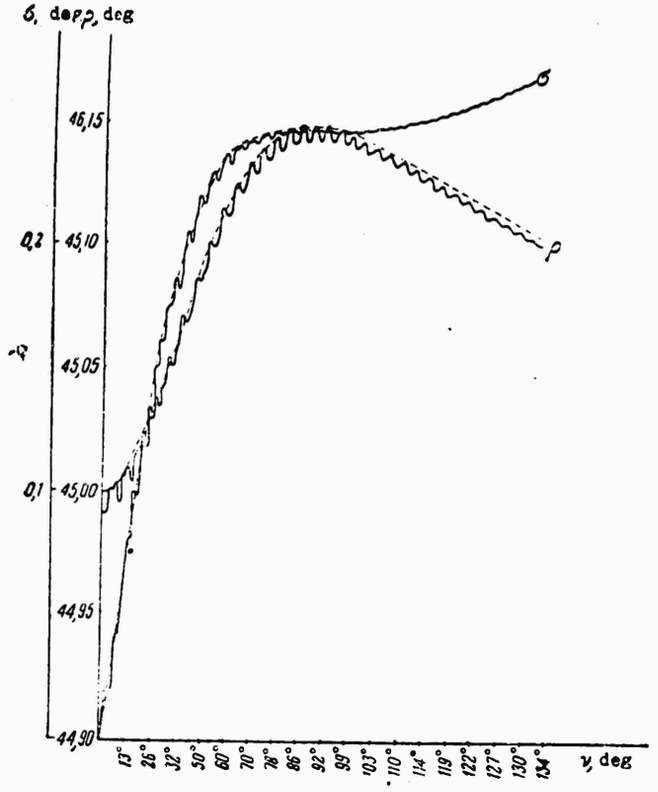

Fig. 7.

3. Moments of Aerodynamic Forces and Their Approximation

When a satellite moves in the rarefied layers of the atmosphere, owing to the interaction between the molecular flux and the shell of the satellite, a number of effects arise in the rotational motion of the satellite. Let us note some of the possible effects.

1. The center of pressure does not coincide with the center of mass. A torque arises. As a result of the rotation of the earth's atmosphere, the velocity vector of the incident flux does not lie in the orbital plane.

2. The rotation of the satellite gives rise to dissipative moments, which cause, in particular, a slowing down of the rotation of the satellite.

3. The density of the atmosphere varies at different points of the satellite shell (closer to the earth it is denser), thus creating an additional small moment [4] (the gradient effect).

4. A small effect related to the presence of the proper thermal velocities of the molecules.

Only the effects mentioned in items 1 and 2 are considered below.

The components of an aerodynamic-force moment along axes rigidly connected to a satellite in the general case depend on the orientation of these axes relative to the incident flux and on the components p, q, r of the angular velocity of rotation of the satellite relative to the flux. In view of the smallness of the linear velocity of rotation of the satellite shell in comparison with the velocity of motion of the center of mass of the satellite, the dependence of the force moment on p, q, r may be regarded as linear. Let $\mathbf{i}'$, $\mathbf{j}'$, $\mathbf{k}'$ be unit vectors of the principal central axes of inertia of the satellite. Then the aerodynamic-force moment can be written in the form

$$\mathbf{M} = \tfrac{1}{2}\rho_a V_0^2 \mathbf{e}_v \times \mathbf{c}^m + \tfrac{1}{2}\rho_a V_0 \mathbf{P},$$

$$\mathbf{c}^m = c_1^m \mathbf{i}' + c_2^m \mathbf{j}' + c_3^m \mathbf{k}', \quad \mathbf{P} = P_1 \mathbf{i}' + P_2 \mathbf{j}' + P_3 \mathbf{k}',$$

(continued)

(formula continued)

$$\begin{pmatrix} P_1 \\ P_2 \\ P_3 \end{pmatrix} = \begin{pmatrix} I_{11} I_{12} I_{13} \\ I_{21} I_{22} I_{23} \\ I_{31} I_{32} I_{33} \end{pmatrix} \begin{pmatrix} p \\ q \\ r \end{pmatrix}.$$

Here V_0 is the velocity of the center of mass of the satellite relative to the flux, $\mathbf{e}_v$ is a unit vector in the direction of this velocity, ρ_a is the density of the flux. The coefficients c_1^m and I_{jk} depend on the location of the satellite relative to the flux.

In the particular case for a symmetrical configuration of the satellite (the axis of symmetry coincides with $\mathbf{k}'$) we have $c_1^m = c_2^m = 0$. The coefficient c_3^m and the coefficients I_{jk} (some of them may be equal to zero) depend only on the angle of attack δ, the angle between $\mathbf{e}_v$ and $\mathbf{k}'$. The explicit dependence of the coefficients on the angles is determined by the nature of the collision between the molecules of the incident flux and the surface of the satellite.

According to prevailing notions, the following mechanism of interaction between the molecules of the incident flux and the surface of the satellite is most probable. During a collision the particle gives up practically all of its energy and comes into a temperature equilibrium with the site of impact (somewhat heated now). When this heating passes through, the particle moves out into space with a thermal velocity equal to the thermal velocity of the molecules of the satellite shell. Since this thermal velocity is substantially less than the thermal velocity of the external particles, we can idealize this picture by hypothesizing an absolutely inelastic impact, where the particles completely lose their energy during a collision with the satellite. Let us analyze this case in

detail, assuming that the satellite is axisymmetrical.

The elementary force $d\mathbf{F}$ acting on a surface dS will be:

$$d\mathbf{F} = -I\frac{\mathbf{V}}{V}, \quad I = \frac{1}{2}c\rho_a V^2 \cos\gamma dS. \tag{3.1}$$

Here $\mathbf{V}$ is the velocity of the surface relative to the incident flux, ρ_a is the density of the flux, $\underline{c}$ is a constant coefficient, γ is the local angle of attack: the angle between the external normal $\mathbf{n}$ to the surface and the vector $\mathbf{V}$. The elementary moment

$$d\mathbf{M} = \mathbf{r}_s \times d\mathbf{F}, \tag{3.2}$$

where $\mathbf{r}_s$ is the radius vector of the surface dS, drawn from the center of mass of the satellite. Substituting (3.1) in (3.2) and taking into account that

$$\cos\gamma = \frac{(n\mathbf{V})}{|n||\mathbf{V}|} = \frac{(n\mathbf{V})}{V}, \tag{3.3}$$

we obtain

$$d\mathbf{M} = \frac{1}{2}c\rho_a (n\mathbf{V})\,\mathbf{V}\times\mathbf{r}_s dS, \tag{3.4}$$

in which

$$\mathbf{V} = \mathbf{V}_0 + \Omega \times \mathbf{r}_s, \tag{3.5}$$

where $\mathbf{V}_0$ is the velocity of the center of mass of the satellite relative to the incident flux, Ω is the vector of the angular velocity of rotation of the satellite. (Strictly speaking, Ω is the vector of the angular velocity of rotation of the satellite relative to the flux, but for the case being considered here, where the rotations are fairly fast, we can assume that Ω is the vector of the absolute angular velocity, since the translational angular velocity is small in comparison with $|\Omega|$).

The quantity $|\Omega \times \mathbf{r}_s|$ is very small in comparison with V_0. Therefore, substituting (3.5) in (3.4), let us neglect terms of the

order of Ω^2. Integrating over the part S* of the surface of the satellite around which the flux is flowing, we obtain an expression for the total moment of the aerodynamic forces in the form

$$\mathbf{M} = \tfrac{1}{2} c\rho_a V_0^2 \int_{S^*} (\mathbf{ne}_v)\, \mathbf{e}_v \times \mathbf{r}_s\, dS + \\ + \tfrac{1}{2} c\rho_a V_0 \int_{S^*} \{(\mathbf{n}\,[\Omega \times \mathbf{r}_s])\,[\mathbf{e}_v \times \mathbf{r}_s] + (\mathbf{ne}_v)\,[\Omega \times \mathbf{r}_s] \times \mathbf{r}_s\}\, dS, \tag{3.6}$$

where

$$\mathbf{e}_V = \frac{\mathbf{V}_0}{V_0} \tag{3.7}$$

is the unit vector of the direction of the velocity of the center of mass of the satellite relative to the incident flux. The region S* of integration is determined by the inequality

$$(\mathbf{Vn}) > 0, \tag{3.8}$$

However, neglecting the small second term in (3.5), we find that the region of integration is approximately determined by the inequality

$$(\mathbf{V}_0\mathbf{n}) > 0. \tag{3.9}$$

Then for an axisymmetrical satellite

$$S^* = S^*(\delta). \tag{3.9a}$$

Let

$$\Phi(z^*, \rho^{*2}) = 0, \quad \rho^{*2} = x^{*2} + y^{*2} \tag{3.10}$$

be the equation of the surface of a satellite symmetrical with respect to the axis z*. Then the components of the unit vector $\mathbf{n}$ will be:

$$n_{z^*} = \frac{\Phi_{z^*}}{\sqrt{\Phi_{z^*}^2 + 4\rho^{*2}\Phi_{\rho^{*2}}^2}}, \quad n_{x^*} = \sigma^* x^*, \quad n_{y^*} = \sigma^* y^*, \\ \sigma^* = \frac{2\Phi_{\rho^{*2}}}{\sqrt{\Phi_{z^*}^2 + 4\rho^{*2}\Phi_{\rho^{*2}}^2}}, \quad \Phi_{z^*} = \frac{\partial \Phi}{\partial z^*}, \quad \Phi_{\rho^{*2}} = \frac{\partial \Phi}{\partial \rho^{*2}}. \tag{3.11}$$

This coordinate system x*y*z* is chosen in such a way that the x-axis always lies in the plane passing through the axis z* and the vector $\mathbf{V}_0$ (Fig. 8). The angle of attack (the angle between $\mathbf{V}_0$ and z*) will be denoted by δ. Moreover, the location of the point of the surface of the satellite in the coordinate system x*y*z* will be determined by the cylindrical coordinates z*, ρ*, φ*, where φ* is read off in the plane normal to z* from the axis x* in such a way that

$$x^* = \rho^* \cos\varphi^*, \quad y^* = \rho^* \sin\varphi^*. \tag{3.12}$$

Then Φ, n_z*, and σ* from (3.11) do not depend on φ*. The region of integration S* depends only on the angle of attack δ, the integration with respect to φ* going from a certain $\varphi^*_0(\delta)$ to $-\varphi^*_0(\delta)$. Let us relate the unit reference point **i**, **j**, **k** to x*y*z*.

Then

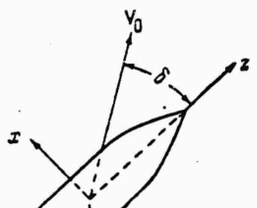

Fig. 8.

$$\begin{gathered} \mathbf{r} = x^*\mathbf{i} + y^*\mathbf{j} + z^*\mathbf{k}, \\ \mathbf{e}_v \times \mathbf{k} = -\sin\delta\mathbf{j}, \quad \mathbf{e}_v \times \mathbf{i} = \cos\delta\cdot\mathbf{j}, \\ \mathbf{e}_v \times \mathbf{j} = \sin\delta\mathbf{k} - \cos\delta\mathbf{i}, \\ \mathbf{e}_v \times \mathbf{k} = -\cot\delta\,(\mathbf{e}_v \times \mathbf{i}). \end{gathered} \tag{3.13}$$

According to the formulas of vector algebra, we have, in addition,

$$\mathbf{n}\,[\Omega \times \mathbf{r}_s] = \begin{vmatrix} \bar{p} & \bar{q} & \bar{r} \\ x^* & y^* & z^* \\ n_{x^*} & n_{y^*} & n_{z^*} \end{vmatrix}, \tag{3.14}$$

$$[\Omega \times \mathbf{r}_s] \times \mathbf{r}_s = -r_s^2(\mathbf{i}\bar{p} + \mathbf{j}\bar{q} + \mathbf{k}\bar{r}) + (x\bar{p} + y\bar{q} + z\bar{r})\,(\mathbf{i}x^* + \mathbf{j}y^* + \mathbf{k}z^*), \tag{3.15}$$

where $\bar{p}$, $\bar{q}$, $\bar{r}$ are the components of Ω along **i**, **j**, **k**. Performing the integration in (3.6), using Relationships (3.11)-(3.15), and discarding terms proportional to sin φ, which give zero during integration, we obtain

$$\mathbf{M}=\frac{1}{2}\rho_a V_0^2\ \bar{c}(\delta)\,\mathbf{e}_v\times\mathbf{k}+\frac{1}{2}c\rho_a V_0\{\mathbf{i}[-\bar{p}\tilde{I}_3+\bar{r}\tilde{I}_4]+$$
$$+\mathbf{j}[-\tilde{I}_5\bar{q}]+\mathbf{k}[-\tilde{I}_1\bar{r}+\tilde{I}_2\bar{p}]\},$$
$$\bar{c}(\delta)=c\{W_1\cos\delta+W_2\sin\delta-W_3\cos\delta\operatorname{sgn}t\ \delta\}. \tag{3.16}$$

The first term in this formula gives the torsional (restoring) moment of the aerodynamic forces, while the remaining terms give the moment of the forces of aerodynamic dissipation.

In (3.16) W_i ($i = 1, 2, 3$) and $\tilde{I}_j$ ($j = 1, 2, 3, 4, 5$) depend only on δ and are given by the following integrals over the region $S^*(\delta)$ of the surface of the body:

$$W_1=\int\{z^*n_{z^*}-\sigma^*\rho^{*2}\cos^2\varphi^*\}\,dS,$$
$$W_2=\int z^*\sigma^*\rho^*\cos\varphi^*\,dS, \tag{3.17}$$
$$W_3=\int n_{z^*}\rho^*\cos\varphi^*\,dS,$$

$$\tilde{I}_1=\cos\delta\int n_{z^*}\rho^{*2}\,dS+\sin\delta\int\sigma^*\rho^{*3}\cos\varphi^*\,dS,$$
$$\tilde{I}_2=\cos\delta\int z^*n_{z^*}\rho^*\cos\varphi^*dS+\sin\delta\int[\sigma^*z^*\rho^{*2}\cos^2\varphi^*+\rho^{*2}\sin^2\varphi^*(n_{z^*}-\sigma^*z^*)]dS,$$
$$\tilde{I}_3=\cos\delta\int[(n_{z^*}-\sigma^*z^*)\rho^{*2}\sin^2\varphi^*+n_{z^*}(z^{*2}+\rho^{*2}\sin^2\varphi^*)]\,dS+$$
$$+\sin\delta\int(z^{*2}+\rho^{*2}\sin^2\varphi^*)\,\sigma^*\rho^*\cos\varphi^*dS,$$
$$\tilde{I}_4=\sin\delta\int z^*\sigma^*\rho^{*2}\cos^2\varphi^*\,dS+\cos\delta\int n_{z^*}z^*\rho^*\cos\varphi^*\,dS, \tag{3.18}$$
$$\tilde{I}_5=\cos\delta\int[(z^{*2}+\rho^{*2}\cos^2\varphi^*)\,n_{z^*}+(n_{z^*}-\sigma^*z^*)\rho^{*2}\cos^2\varphi^*]\,dS+$$
$$+\sin\delta\int[(z^{*2}+\rho^{*2}\cos^2\varphi^*)\,\sigma^*\rho^*\cos\varphi^*-z^*(n_{z^*}-\sigma^*z^*)\,\rho^*\cos\varphi^*]\,dS.$$

In order to ascertain the principal qualitative and quantitative effects common to bodies of different shapes, it is convenient to take, instead of the exact values of W_i and $\tilde{I}_j$, certain approximate expressions, which reflect the structure of these integrals.

Let us deal first with the restoring moment, i.e., with the approximation of the coefficient $\bar{c}(\delta)$. Transforming the first

integral from (3.6) with the aid of Ostrogradskiy's formula [12], we find that the coefficient $\bar{c}(\delta)$ is determined by the relationship

$$\bar{c}(\delta) = cS(\delta) z_0(\delta), \tag{3.19}$$

where $S(\delta)$ is the area of the cross section of the satellite cut by the flow and $z_0(\delta)$ is the distance from the center of gravity of the cross section S to the center of mass. Obviously,

$$\bar{c}(\pi - \delta) = \bar{c}(\delta). \tag{3.20}$$

This reflects the properties of an absolutely inelastic collision: the force moment depends only on the magnitude and location of the cross section $S(\delta)$ relative to the satellite; therefore $\bar{c}(\delta)$ does not change during this turn.

From the appearance of W_2 and W_3 (3.17) it follows that $W_3(0) = W_2(0) = 0$, since the integration then passes over the entire lateral surface of the body from $\varphi^* = 0$ to $\varphi^* = 2\pi$. Therefore it may be assumed that

$$\begin{aligned} W_2 &= \sin\delta f_2(\delta), \\ W_3 &= \sin\delta f_3(\delta), \end{aligned} \tag{3.21}$$

and then $\bar{c}(\delta)$ from (3.16) will be represented in the form:

$$\bar{c}(\delta) = c\{W_1(\delta)\cos\delta + f_2(\delta) - [f_2(\delta) + f_3(\delta)]\cos^2\delta\}. \tag{3.21a}$$

We shall seek $\bar{c}(\delta)$ in the form of a power series in powers of $\cos\delta$. From (3.20) it follows that (3.21) can be approximated most simply as:

$$cW_1(\delta)\cos\delta + f_2(\delta) = a_0, \quad -c[f_2(\delta) + f_3(\delta)] = a_2,$$

where a_0 and a_2 are constants. Then

$$\bar{c}(\delta) = a_0 + a_2\cos^2\delta. \tag{3.22}$$

In this case, according to (3.19), it is easy to calculate the coefficients a_0 and a_2 in terms of the constants $S(0)z_0(0)$ and $S(\pi/2)z_0(\pi/2)$. In the case of an elongated body, for example, we can have $a_0 > 0$, $a_2 < 0$. In the simplest case we can put

$$a_2 = 0, \ \bar{c}(\delta) = a_0. \tag{3.23}$$

From (3.19) it can be seen that when $a_0 > 0$ the center of pressure lies "in front of" the center of mass ($z_0 > 0$), but when $a_0 < 0$ it lies "in back of" the center of mass ($z_0 < 0$), when $\delta < \pi/2$. If a portion of the molecules is not reflected absolutely inelastically, Condition (3.20) may be unfulfilled, since it is then not a matter of indifference whether the satellite is flying "nose forward" or "bottom forward". In this case we can use an approximate formula of the type

$$\bar{c}(\delta) = a_0 + a_1 \cos\delta + a_2 \cos^2\delta, \tag{3.24}$$

which corresponds to the condition

$$\bar{c}(\pi - \delta) \neq \bar{c}(\delta). \tag{3.25}$$

From this point on, as in [8-9], we shall operate mainly with approximate formula (3.22). But, in addition, let us consider the effects related to Condition (3.25). In this case we shall use approximate formula (3.24), which, when $a_1 = 0$, coincides with (3.22).

Let us now deal with the approximation of $\tilde{I}_j$. Let us limit ourselves in the approximate formulas to the principal terms of the quantities $\tilde{I}_j$. The integrals containing the factor cos φ^* in the integrand, as was noted above, can be represented in the form $\sin\delta f(\delta)$. Taking this into account, we see that $\tilde{I}_1$, $\tilde{I}_3$, and $\tilde{I}_5$ are positive for any value of δ; therefore the principal terms of

the functions will be positive constants. With reference to $\tilde{I}_3$ and $\tilde{I}_5$ it should also be noted that the difference $I_3 - I_5$ vanishes during integration over the entire lateral surface (i.e., when $\delta = 0, \pi$). Therefore the principal terms in $\tilde{I}_3$ and $\tilde{I}_5$, approximated by the constants, are equal to each other. The quantities $\tilde{I}_2$ and $\tilde{I}_4$ cannot be approximated by constants, since they always depend on the angle of attack approximately according to a sine law. We shall therefore assume that

$$\tilde{I}_1 \approx I_1,\ \tilde{I}_3 \approx I_3,\ \tilde{I}_5 \approx I_3,\ \tilde{I}_2 \approx I_2 \sin\delta,\ \tilde{I}_4 = I_4 \sin\delta, \tag{3.26}$$

where $I_k = \text{const}$ $(k = 1, 2, 3, 4)$.

From (3.18) it follows that in the general case $I_2 \neq I_4$, but this is not essential for an investigation of the motion.

The actual calculation of the quantities in (3.26) can be made according to the same formulas (3.18), setting $\delta = 0$ and $\delta = \pi/2$ and taking the arithmetic mean of the values of I obtained. We may also seek other approximate evaluations for I. Their calculation is simplified substantially for specific bodies (e.g., a cylinder, a cone, a sphere, etc.).

4. The Effect of a Restoring Aerodynamic Moment

Let us consider the effect exerted on the evolution of the rotation of a satellite by a restoring aerodynamic moment

$$\begin{gathered}\mathbf{M} = \tfrac{1}{2}\rho_a V_0^2\, \bar{c}\,(\delta)\, \mathbf{e}_v \times \mathbf{k}, \\ \bar{c}\,(\delta) = a_0 + a_1 \cos\delta + a_2 \cos^2\delta.\end{gathered} \tag{4.1}$$

We have

$$\cos\delta = \tfrac{1}{V_0}\{V_x^0\alpha^* + V_y^0\beta^* + V_z^0\gamma^*\}, \tag{4.2}$$

where V_x^0, V_y^0, V_z^0 are the components of V_0 along the axes of a coordinate system XYZ:

$$\begin{gathered} V_x^0 = \sqrt{\frac{\mu}{P}}(e + \cos\nu) - W_0 \frac{P}{1+e\cos\nu}\cos i\cos\nu, \\ V_y^0 = W_0 \frac{P}{1+e\cos\nu}\sin i\cos(\omega+\nu), \\ V_z^0 = -\sqrt{\frac{\mu}{P}}\sin\nu + W_0 \frac{P}{1+e\cos\nu}\cos i\sin\nu, \\ V_0 = \sqrt{(V_x^0)^2 + (V_y^0)^2 + (V_z^0)^2}. \end{gathered} \tag{4.3}$$

where W_0 is the angular velocity of rotation of the earth, $\underline{i}$ is the inclination of the orbit toward the equator, ω is the longitude of the perigee. Since the terms which are proportional to W_0 comprise 1-5% of the total velocity V_0, we can neglect them when analyzing the principal effects. Let us assume first that $W_0 = 0$.

From (4.1) we can find the components M_x, M_y, M_z in the form (1.10), where

$$U = -\frac{1}{2}\rho_a V_0^2 \int \bar{c}\,(\cos\delta)\,d\cos\delta, \tag{4.4}$$

which, with the aid of Approximation (3.24), is converted to the form

$$U = -\frac{1}{2}\rho_a V_0^2 \left\{a_0\cos\delta + \frac{a_1}{2}\cos^2\delta + \frac{a_2}{3}\cos^3\delta\right\}. \tag{4.5}$$

When $W_0 = 0$, we have

$$V_0 = \sqrt{\frac{\mu}{P}}\sqrt{1 + e^2 + 2e\cos\nu}, \tag{4.6}$$

$$\cos\delta = \frac{(e+\cos\nu)\alpha'' - \sin\nu\gamma''}{\sqrt{1+e^2+2e\cos\nu}}. \tag{4.7}$$

Let us find, in addition, U_ν from Relationships (1.20) and (4.5):

$$U_\nu = -\frac{1}{2}\rho_\pi\sqrt{\mu P}\,\bar{\rho}\,\frac{1+e^2+2e\cos\nu}{(1+e\cos\nu)^2}\left(a_0\cos\delta + \frac{a_1}{2}\cos^2\delta + \frac{a_2}{3}\cos^3\delta\right). \tag{4.8}$$

Here ρ_π is the density of the atmosphere at the perigee of the orbit, while $\bar{\rho}$ is a dimensionless function determined by the

relationship:

$$\bar{\rho} = \frac{\rho_a(h)}{\rho_\pi}, \quad \bar{\rho}(0) = 1, \tag{4.9}$$

where

$$h = r - r_\pi = \frac{P}{1 + e\cos\nu} - \frac{P}{1 + e}. \tag{4.10}$$

Let us take, for example,

$$\bar{\rho} = \exp\left(-\frac{h}{H}\right), \tag{4.11}$$

where H is the so-called altitude of the homogeneous atmosphere.

Secular Perturbations

In order to investigate the secular perturbations, let us average U_ν, as determined by Formula (4.8), with respect to ψ and ν. Let

$$\begin{aligned}
J_1 &= \frac{1}{2\pi}\int_0^{2\pi} \bar{\rho}\,\frac{\sqrt{1 + e^2 + 2e\cos\nu}}{(1 + e\cos\nu)^2}(e + \cos\nu)\,d\nu,\\
J_2 &= \frac{1}{2\pi}\int_0^{2\pi} \bar{\rho}\,\frac{(e + \cos\nu)^2}{(1 + e\cos\nu)^2}d\nu,\\
J_3 &= \frac{1}{2\pi}\int_0^{2\pi} \bar{\rho}\,\frac{\sin^2\nu}{(1 + e\cos\nu)^2}d\nu,\\
J_4 &= \frac{1}{2\pi}\int_0^{2\pi} \bar{\rho}\,\frac{(e + \cos\nu)^3\,d\nu}{(1 + e\cos\nu)^2\sqrt{1 + e^2 + 2e\cos\nu}},\\
J_5 &= \frac{1}{2\pi}\int_0^{2\pi} \bar{\rho}\,\frac{(e + \cos\nu)\sin^2\nu\,d\nu}{(1 + e\cos\nu)^2\sqrt{1 + e^2 + 2e\cos\nu}}.
\end{aligned} \tag{4.12}$$

The quantities J for certain values of h and H are given in Fig. 9.

The twice-averaged value of the function U_ν will be:

$$\overline{\overline{U}}_\nu = \overline{\overline{U}}_{\nu_1} + \overline{\overline{U}}_{\nu_2}, \tag{4.13}$$

where

$$\begin{aligned}
\overline{\overline{U}}_{\nu_1} = -\frac{\sqrt{\mu P}}{2}\rho_\pi\Big\{&\cos\theta\cos\vartheta\Big[a_0 J_1 + \frac{a_2}{2}J_4\sin^2\vartheta + \\
&+ a_2 J_5\Big(\frac{\sin^2\vartheta}{2} + \Big(1 - \frac{5}{2}\sin^2\vartheta\Big)\cos^2\lambda\Big)\Big] + \\
&+ \frac{a_1}{2}(J_2 - J_3)\Big(1 - \frac{3}{2}\sin^2\vartheta\Big)\cos^2\theta + \qquad \text{(cont.)}
\end{aligned} \tag{4.14}$$

(Eq. 14 cont.) $$+\left(1-\frac{5}{2}\sin^2\theta\right)\left[\frac{a_2}{3}J_4-a_2J_6\cos^2\lambda\right]\cos^2\theta\cos\theta\Big\},$$

$$\overline{U}_{\nu_1}=-\frac{1}{4}\rho_\pi\sqrt{\mu P}\,a_1J_3\left(1-\frac{3}{2}\sin^2\theta\right)\sin^2\rho, \qquad (4.15)$$

where we have used the variables ρ, θ, λ which are related by the relationships:

$$\cos\rho=-\sin\theta\sin\lambda,\quad \cos\theta=\sin\rho\sin\sigma,\quad \sin\rho\cos\sigma=\sin\theta\cos\lambda.$$

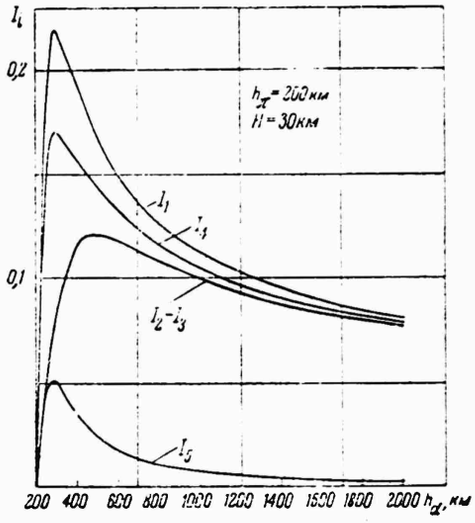

Fig. 9.

The trajectory $\theta(\lambda)$ of the terminus of the vector **L** in secular motion, according to (1.25) will be

$$\overline{\overline{U}}_\nu=\overline{\overline{U}}_{\nu_0}. \qquad (4.16)$$

The portion $\overline{\overline{U}}_{\nu_2}$ has the same structure as the secular portion of the force function of the gravitational moments (2.4). They give a total

$$\overline{\overline{U}}_\pi=\frac{1}{4}\left(1-\frac{3}{2}\sin^2\theta\right)\left[3\frac{\sqrt{\mu}}{P^{3/2}}(A-C)-\rho_\pi\sqrt{\mu P}\,a_1J_3\right]\sin^2\rho\equiv\tilde{k}\sin^2\rho. \qquad (4.17)$$

From (1.23) and (4.17) we obtain an equation determining the precession of the kinetic-momentum vector around the normal to the orbital plane

$$\frac{d\sigma}{dv}=\frac{2\tilde{k}}{L_0}\cos\rho_0. \qquad (4.18)$$

Thus the term $\overline{\overline{U}}_{\nu_2}$ introduces only a certain correction to the gravitational effect already considered; in an analysis of the combined effect of aerodynamic and gravitational perturbations the term $\overline{\overline{U}}_{\nu_2}$ has no effect on the qualitative picture; therefore the principal term is (4.14).

For the case $a_1 = 0$ a combined analysis of gravitational and aerodynamic secular perturbations is given in another article by the author [9]. The equations of perturbed motion, in accordance with the results of Section 1, will have the form:

$$\begin{aligned}
\frac{d\lambda}{d\nu} &= \frac{\rho_\pi}{2}\frac{\sqrt{\mu P}}{L_0}\left\{\cos\vartheta\left[a_0 J_1 + \frac{a_2}{2}J_3\sin^2\vartheta - a_2 J_5\left(\frac{1}{2}\sin^2\vartheta + \right.\right.\right. \\
&+ \left.\left.\left.\left(1 - \frac{5}{2}\sin^2\vartheta\right)\cos^2\lambda\right)\right] + a_1(J_2 - J_4)\left(1 - \frac{3}{2}\sin^2\vartheta\right)\cos\theta - \right. \\
&\left. + 3\cos\vartheta\left(1 - \frac{5}{2}\sin^2\vartheta\right)\left[\frac{a_2}{3}J_4 - a_2 J_5\cos^2\lambda\right]\cos^2\theta\right\}, \qquad (4.19) \\
\frac{d}{d\nu}\cos\theta &= \frac{\rho_\pi\sqrt{\mu P}}{L_0}a_2 J_5\cos\vartheta\left(1 - \frac{5}{2}\sin^2\vartheta\right)\cos\theta\sin^2\theta\cos\lambda\sin\lambda.
\end{aligned}$$

Let us indicate the basic properties of the perturbations, caused by $\bar{\bar{U}}_{\nu_1}$, making simplifications in passing.

1. Since, when $e = 0$, $J_1 = J_2 - J_3 = J_4 = J_5 = 0$, in a circular orbit of a satellite there are no secular perturbations in its rotational motion.

2. From Fig. 9 and Relationships (4.12) it is obvious that the quantity J_5 is an order lower than the other coefficients J_j. Therefore the term proportional to J_5 can be neglected. Then from (4.19) we obtain $\theta \approx \theta_0$, i.e., the vector **L** precesses around the direction of the perigean tangent with a velocity $d\lambda/d\nu$ determined by Eq. (4.19), in which we have to set $\theta \approx \theta_0$, $J_5 = 0$. Investigations show [8, 9] that the effect of the term proportional to J_5 causes small oscillations in the angle θ.

3. The quantity $a_1 \neq 0$, if the following two conditions are fulfilled simultaneously: a) the number of molecules reflected from the satellite according to laws different from absolute inelastic collision is fairly large, b) the shape of the satellite differs from bisymmetrical (i.e., the satellite does not possess a plane of symmetry perpendicular to its axis of symmetry). Since

Condition "a" is most often poorly fulfilled, we can assume that $a_1 \ll a_0$, a_2 and set $a_1 \approx 0$. In the case of bisymmetrical satellites the equality $a_1 = 0$ is fulfilled regardless of whether Condition "a" is fulfilled. Taking items 2 and 3 into account, we can assert in this approximation that the entire secular effect of the restoring moment of the aerodynamic forces is manifested in the precession of the kinetic-momentum vector around the direction of the perigean tangent at a constant value of θ_0 and with an angular velocity

$$\frac{d\lambda}{dv} = \frac{p\pi\sqrt{\mu P}}{2L_0}\cos\vartheta\,[k_0 - k_1\cos^2\theta_0], \tag{4.20}$$

where

$$k_0 = a_0 J_1 + \frac{a_2}{2} J_4 \sin^2\vartheta, \quad k_1 = \left(1 - \frac{5}{2}\sin^2\vartheta\right) a_2 J_4.$$

In the simplest case (3.23) we obtain

$$\frac{d\lambda}{dv} = \frac{p\pi\sqrt{\mu P}}{2L_0}\cos\vartheta a_0 J_1. \tag{4.20a}$$

These results are equivalent to previous results obtained by the author [8, 9]. However, in these articles in the formulas for J_1, J_4, J_5 errors were made, which insignificantly change the quantitative results, while the qualitative picture remains unchanged.

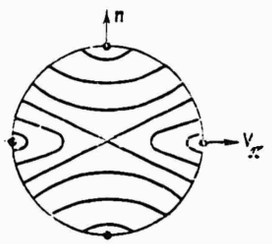

Fig. 10.

Note that, as follows from (4.20) and (4.20a) in the case of a satellite rotating in a somersault regime ($\$ = 90^\circ$) the aerodynamic restoring moment does not create a secular effect. As is obvious from (4.19), this assertion is incorrect, if $a_1 \neq 0$.

For an estimate of the effect of a_1 let us consider the limiting case $a_1 \neq 0$, $a_0 = a_2 = 0$, which corresponds to the hypothesis used by Hagihara [3]. Then the trajectory of the terminus of the

vector **L**

$$\bar{U}_{\nu_1} + \bar{U}_{\nu_2} = \text{const}$$

assumes the form

$$(J_2 - J_3)\cos^2\theta + J_3 \sin^2\rho = \text{const}.$$

A family of these trajectories for an elliptical satellite orbit ($e \neq 0$, $J_2 \neq J_3$) is shown in Fig. 10. The kinetic-momentum vector will precess around the normal $\underline{n}$ to the orbital plane or around the perigean tangent $\mathbf{V}_\pi$, if correspondingly

$$|\cos\rho_0| \gtrless \sqrt{\frac{J_2 - J_3}{J_3}}\cos\theta_0,$$

where ρ_0, θ_0 are the initial coordinates of the kinetic-momentum vector. Let us note again that the case $|a_1| \ll |a_0|$ is much more likely.

The Effect of the Rotation of the Atmosphere on Secular Perturbations

In the case $W_0 \neq 0$ the expression for cos δ is determined by the complete formulas (4.2)-(4.3).

In order to understand the principal effects caused by the rotation of the atmosphere, let us use for $c(\delta)$ the simplest approximate formula (3.23). Then, retaining only terms of the first order of smallness relative to W_0, we obtain

$$\begin{aligned} U_\nu = &-\frac{1}{2}\rho_\pi\sqrt{\mu p}\,\frac{\bar{\rho}a_0}{(1+e\cos\nu)^2}\left\{\left[(e+\cos\nu)\sqrt{1+2e\cos\nu+e^2}-\right.\right. \\ &-\left.\frac{p^{3/2}W_0}{\sqrt{\mu}}\cos i\,\frac{e+\cos\nu}{\sqrt{1+e^2+2e\cos\nu}}\right]\alpha'' - \left[\sin\nu\sqrt{1+e^2+2e\cos\nu}-\right. \\ &\left.\left.-\frac{p^{3/2}W_0\cos i}{\sqrt{\mu}}\,\frac{\sin\nu}{\sqrt{1+e^2+2e\cos\nu}}\right]\gamma''\right\} - \frac{1}{2}\rho_\pi p^2 W_0\bar{\rho}\,\frac{a_0}{1+e\cos\nu}\times \\ &\times\{-\cos i\cos\nu\,\alpha'' + \sin i\cos(\omega+\nu)\,\beta'' + \cos i\sin\nu\,\gamma''\}. \end{aligned} \tag{4.21}$$

Let

$$F_0 = J_1 - \frac{P^{3/2}W_0}{\sqrt{\mu}} \cos i \frac{1}{2\pi} \int_0^{2\pi} \frac{\bar{\rho}(e + \cos\nu)\,d\nu}{(1 + e\cos\nu)^2 \sqrt{1 + e^2 + 2e\cos\nu}}, \tag{4.22}$$

where J_1 is determined by Formula (4.12), and

$$S_0 = \frac{1}{2\pi} \int_0^{2\pi} \bar{\rho} \frac{\sqrt{1 + 2e\cos\nu + e^2}}{(1 + e\cos\nu)^2} d\nu. \tag{4.23}$$

Averaging the function U_ν with respect to ψ and ν, we obtain

$$\overline{U}_\nu = -\frac{1}{2}\rho_\pi \sqrt{\mu P} a_0 F_0 \cos\vartheta \cos\theta + \tag{4.24}$$
$$+ \frac{1}{2}\rho_\pi W_0 P^2 a_0 S_0 \cos\vartheta (\cos i \cos\theta + \sin i \sin\omega \sin\theta \sin\lambda).$$

Also let

$$\sin\theta^* = \frac{\sin i \sin\omega}{\sqrt{\cos^2 i + \sin^2 i \cos^2\omega}}, \tag{4.25}$$
$$\cos\theta^* = \frac{\cos i}{\sqrt{\cos^2 i + \sin^2 i \cos^2\omega}},$$
$$k^\circ = \frac{1}{2}\rho_\pi W_0 P^2 a_0 S_1 \cos\vartheta \sqrt{\cos^2 i + \sin^2 i \cos^2\omega},$$

$$k' = \frac{1}{2}\rho_\pi \sqrt{\mu P}\, a_0 F_0 \cos\vartheta, \tag{4.26}$$
$$\cos\varkappa = \cos\theta^* \cos\theta + \sin\theta^* \sin\theta \sin\lambda. \tag{4.27}$$

Then

$$\overline{U}_\nu = -k' \cos\theta + k^\circ \cos\varkappa = \overline{U}_\nu^* \tag{4.28}$$

is the equation of the trajectory, which can also be written as:

$$\cos\theta = c_0 - \alpha\cos\varkappa \tag{4.29}$$

Since

$$\alpha = \frac{PW_0\sqrt{\cos^2 i - \sin^2 i\cos^2\omega}}{\sqrt{\frac{\mu}{P}}} \frac{S_0}{F_0} \approx \frac{PW_0}{\sqrt{\frac{\mu}{P}}}. \tag{4.30}$$

is a small quantity, the trajectory differs very little from

$$\cos\theta = \cos\theta_0,$$

i.e., as was to be expected, the effect of the rotation of the atmosphere is slight in comparison with the principal atmospheric effect.

Let us determine the poles of the trajectory.

The equations of motion will be:

$$\begin{aligned} \frac{d\lambda}{dv} &= \frac{1}{L_0 \sin\theta}\frac{\partial U}{\partial\theta} = \frac{k'}{L_0} - \frac{k^\circ}{L_0}\cos\theta^\circ + \frac{k^\circ}{L_0}\sin\theta^\circ \operatorname{ctg}\theta \sin\lambda, \\ \frac{d\theta}{dv} &= -\frac{1}{L_0 \sin\theta}\frac{\partial U}{d\lambda} = -\frac{k^\circ}{L_0}\sin\theta^\circ \sin\theta\cos\lambda. \end{aligned} \tag{4.31}$$

From the second equation it is obvious that the pole lies on the meridian $\lambda_\pi = 90^\circ$ (270°). Then from the first equation we obtain the coordinate θ_π of the pole

$$\pm\tan\theta_\pi = \frac{k^\circ \sin\theta^\circ}{k' - k^\circ\cos\theta^\circ}. \tag{4.32}$$

Since $k^\circ \ll k'$, the pole is close to $\theta_\pi^\circ = 0, \pi$. The equation of the trajectory (4.28) can be represented in the form

$$\sqrt{k'^2 + k'^2 - 2k'k^\circ\cos\theta^\circ}\cos\varkappa_1 = \text{const}, \tag{4.33}$$

where $\varkappa_1$ is the angular distance of the kinetic-momentum vector from the precession pole λ_π, θ_π. Hence it follows that the kinetic-momentum vector precesses around Pole (4.32) (and $\lambda_\pi = 90^\circ$ or 270°) at a constant angular distance $\varkappa_1$ with a velocity

$$\frac{d\alpha}{dv} = -\frac{1}{L_0}\sqrt{k'^2 + k^{\circ 2} - 2k'k^\circ\cos\theta^\circ}. \tag{4.34}$$

The Case of a Circular Orbit. Effects of the Second Order.

In the case of a circular orbit, as has been shown, aerodynamic forces do not cause perturbations (if we make the highly justified assumption that $a_1 \approx 0$). Let us see, nevertheless, what kind of motion is described by the vector **L** in this case, for which purpose we must turn to more accurate equations, averaged only with respect to ψ. For simplicity of analysis let us again turn to Approximation (3.23) and neglect the rotation of the atmosphere. Then the force

function averaged with respect to ψ has the form

$$\overline{U}_v = -\frac{1}{2}\rho_* \sqrt{\mu P}\, a_0 \cos\theta \sin\rho \sin(\varsigma - \nu), \tag{4.35}$$

i.e., is related to Type (1.25a). Therefore, according to (1.27)-(1.28), the trajectory of the trace of the kinetic-momentum vector in a rotating coordinate system has the form

$$\cos\rho - n\cos\Lambda = \text{const}, \tag{4.36}$$

$$n = \frac{\frac{1}{2}\rho_* \sqrt{\mu P}\, a_0 \cos\theta}{L_0}. \tag{4.37}$$

Where Λ is the angle between **L** and the velocity vector of the center of mass of the satellite

$$\cos\Lambda = \sin\rho \sin\overline{\varphi}. \tag{4.38}$$

Using (4.36) and the results of Section 1, it is not difficult to verify that the trajectory of the trace of the vector **L** on a unit sphere in a rotating coordinate system is a circle, the center of which lies in the meridian passing through the trace of the normal to the orbital plane and the trace of the velocity vector of the center of mass (the instantaneous tangent to the orbit); the center of the circle lies at the angular distance ρ^* from the normal to the orbital plane and consequently

$$\tan\rho^* = -n. \tag{4.39}$$

It also happens that the velocity of rotation of the kinetic-momentum vector **L** around this circle is constant and may be written as

$$\frac{d\lambda_\Lambda}{d\nu} = -\sqrt{1-n^2}. \tag{4.40}$$

We see that if n is very small (i.e., the effect of perturbations is very small), $\rho^* \approx 0$, and the kinetic-momentum vector in the rotating coordinate system under consideration rotates around

the normal to the orbital plane with an angular velocity $\lambda'_\Lambda \approx -1$, i.e., it remains stationary in absolute space. If, on the other hand, $\underline{n}$ is large, p^* is close to $\pi/2$, and the kinetic-momentum vector precesses around the direction of the incident flux. Note that the criterion of applicability of the theory is, roughly speaking, the following: the motion obtained by averaging should occur considerably more slowly than the motion according to which the averaging was done. In the given case it is required that $|d\lambda_\Lambda/d\nu| \ll |d\Psi/d\nu|$. For example, let $\Psi = 14$ deg/sec, while the angular velocity of motion in orbit $d\nu/dt = 0.07$ deg/sec. Then the theory will be fairly accurate when $|d\lambda_\Lambda/d\nu| \ll 200$, i.e., when $n \approx 10\text{-}20$. Twofold averaging occurs here only when $n \ll 1$.

5. The Effect of a Moment of the Forces of Aerodynamic Dissipation

The moment of the forces of aerodymamic dissipation is determined by the second term in Formula (3.16). For the dissipation coefficients let us take approximate formulas (3.26).

Let us introduce, instead of a semiconnected coordinate system, a system rigidly connected to the satellite. Let the reference point of this system be $\mathbf{i}'$, $\mathbf{j}'$, $\mathbf{k}'$, the axis of symmetry of the satellite being directed along $\mathbf{k}'$. Then

$$\begin{aligned} \mathbf{k} &= \mathbf{k}', \\ \mathbf{j} &= \mathbf{j}' \cos\varphi_0 - \mathbf{i}' \sin\varphi_0, \\ \mathbf{i} &= -\mathbf{j}' \sin\varphi_0 + \mathbf{i}' \cos\varphi_0, \end{aligned} \tag{5.1}$$

where $\mathbf{i}$, $\mathbf{j}$, $\mathbf{k}$ is the reference point of the semiconnected system, while φ_0 is the angle of rotation of the connected system relative to the semiconnected system. It can be shown that

$$\cos\varphi_0 = \frac{\cos(e_v, i')}{\sin\delta}, \quad \sin\varphi_0 = -\frac{\cos(e_v, j')}{\sin\delta} \tag{5.2}$$

Next let p, q, r be the angular-velocity components along the connected axes. Then

$$\begin{aligned} \bar{r} &= r, \\ \bar{p} &= -q\sin\varphi_0 + p\cos\varphi_0, \\ \bar{q} &= q\cos\varphi_0 + p\sin\varphi_0. \end{aligned} \tag{5.3}$$

Let us now substitute in (3.16) (in the dissipative portion) Expressions (5.1) and (5.3), taking (5.2) into account, and let us introduce the approximate values (3.26) of Functions (3.18). Then the moment of the dissipative forces will be written in the form

$$\begin{aligned} \mathbf{M}_д = \tfrac{1}{2}c\rho_n V_0 \{ & i'[-pI_3 + r\cos(e_v, i')I_4] + \\ & + j'[-qI_3 + r\cos(e_v, j')I_4] + \\ & + k'[-rI_1 + (p\cos(e_v, i') - q\cos(e_v, j')I_2]\}. \end{aligned} \tag{5.4}$$

Hence it is obvious what the meaning of the quantities I_1 is: I_1 is the coefficient of dissipation along the axis of symmetry, I_3 is the coefficient of dissipation along the transverse axis. These terms lead to the attenuation of the velocities of rotation of the satellite. The terms containing I_2 and I_4 will cause a change in the orientation of the satellite. Let the position of the reference point **i'**, **j'**, **k'** relative to the coordinate system XYZ be given by the table of direction cosines

	i'	j'	k'
X	α	α'	α''
Y	β	β'	β''
Z	γ	γ'	γ''

(5.5)

Then, without taking the rotation of the atmosphere into account, we obtain:

$$\cos(e_v, i') = \frac{1}{V_0}[V_x\alpha + V_z\gamma], \quad \cos(e_v, j') = \frac{1}{V_0}[V_x\alpha' + V_z\gamma']. \tag{5.6}$$

$$V_0 = \sqrt{\frac{\mu}{p}}\sqrt{1 + e^2 + 2e\cos\nu},$$
$$V_x = \sqrt{\frac{\mu}{p}}(e + \cos\nu), \quad V_z = -\sqrt{\frac{\mu}{p}}\sin\nu, \tag{5.7}$$

$$p\cos(e_v, i') + q\cos(e_v, j') = \frac{1}{V_0}\{V_x(p\alpha + q\alpha') + V_z(p\gamma + q\gamma')\}. \tag{5.8}$$

Since

$$q\alpha' + p\alpha = \frac{L_x - Cr\alpha''}{A}, \quad q\gamma' + p\gamma = \frac{L_z - Cr\gamma''}{A}, \tag{5.9}$$

as can be seen from the last component in (5.4), the equation for the angular-velocity component along the axis of symmetry k' can be written in the form

$$C\frac{dr}{dt} = -\frac{1}{2}c\rho_a V_0 I_1 r + \frac{1}{2}c\rho_0\frac{I_2}{A}\{V_x(L_x - Cr\alpha'') + V_z(L_z - Cr\gamma'')\}. \tag{5.10}$$

Now taking (5.4)-(5.9) into account, we can write the components of the moment of the forces along the axes of the coordinates XYZ:

$$\begin{aligned}
M_x &= \frac{1}{2}c\rho_a V_0\left\{-\frac{I_3}{A}(L_x - Cr\alpha'') - I_1 r\alpha'' + I_4 r\frac{1}{V_0}[V_x(1-\alpha''^2) + V_z(-\alpha''\gamma'')] + \right.\\
&\left. + \frac{I_2}{V_0 A}\alpha''[V_x(L_x - Cr\alpha'') + V_z(L_z - Cr\gamma'')],\right.\\
M_y &= \frac{1}{2}c\rho_a V_0\left\{-\frac{I_3}{A}(L_y - Cr\beta'') - I_1 r\beta'' + I_4\frac{r}{V_0}[V_x(-\alpha''\beta'') + V_z(-\beta''\gamma'')] + \right.\\
&\left. + \frac{I_2}{V_0 A}\beta''[V_x(L_x - Cr\alpha'') + V_z(L_z - Cr\gamma'')]\right\},\\
M_z &= \frac{1}{2}c\rho V_0\left\{-\frac{I_3}{A}(L_z - Cr\gamma'') - I_1 r\gamma'' + I_4\frac{r}{V_0}[V_x(-\alpha''\gamma'') + V_z(1-\gamma''^2)] + \right.\\
&\left. + \frac{I_2}{V_0 A}\gamma''[V_x(L_x - Cr\alpha'') + V_z(L_z - Cr\gamma'')]\right\}.
\end{aligned} \tag{5.11}$$

The equations of motion of the vector **L** will be written in the form

$$\dot{L}_x = M_x, \quad \dot{L}_y = M_y, \quad L_z = M_z. \tag{5.12}$$

We are interested in the evolution of the motion. In perturbed motion, as was shown earlier, we can take approximately

$$\psi \approx \frac{L}{A}. \tag{5.13}$$

Moreover, the following kinematic relationship remains valid:

$$\cos \vartheta = \frac{Cr}{L} \tag{5.14}$$

Therefore Eqs. (5.10)-(5.12), together with Relationships (5.13)-(5.14), enable us to follow the evolution of the motion. We shall seek only the secular perturbations of the motion, which are obtained as a result of averaging the equations of motion with respect to ψ and ν. Before averaging with respect to ν, let us pass from the independent variable t to the variable ν.

Let us introduce

$$N_0 = \frac{1}{2} c\rho_\pi P \frac{1}{2\pi} \int_0^{2\pi} \overline{\rho} \frac{\sqrt{1-e^2-2e\cos\nu}}{(1+e\cos\nu)^2}\, d\nu,$$
$$N_1 = \frac{1}{2} c\rho_\pi P \frac{1}{2\pi} \int_0^{2\pi} \overline{\rho} \frac{e+\cos\nu}{(2+e\cos\nu)^2}\, d\nu, \tag{5.15}$$

where $\overline{\rho} = \rho_a/\rho_\pi$, ρ_π is the density of the atmosphere at the perigee of the orbit.

The combinations of direction cosines averaged with respect to the precession can be written in the form

$$\overline{\alpha''} = \cos\vartheta \frac{L_x}{L}, \overline{\beta''} = \cos\vartheta \frac{L_y}{L}, \overline{\gamma''} = \cos\vartheta \frac{L_z}{L},$$
$$\overline{\alpha''^2} = \frac{1}{2}\sin^2\vartheta + \left(1 - \frac{3}{2}\sin^2\vartheta\right)\frac{L_x^2}{L^2}, \tag{5.16}$$
$$\overline{\alpha''\beta''} = \left(1 - \frac{3}{2}\sin^2\vartheta\right)\frac{L_x L_y}{L^2}, \overline{\alpha''\gamma''} = \left(1 - \frac{3}{2}\sin^2\vartheta\right)\frac{L_x L_z}{L^2}.$$

The bar indicates averaging with respect to ψ. Now averaging (5.10)-(5.12) and taking (5.15)-(5.16) into account, we obtain the following equations of secular motion:

$$L_x' = -k_0' L_x + k_1' \cos\vartheta \frac{L_x^2}{L} - k_2' \cos\vartheta L,$$
$$L_y' = -k_0' L_y + k_1' \cos\vartheta \frac{L_x L_y}{L}, \quad L_z' = -k_0' L_z + k_1' \cos\vartheta \frac{L_x L_z}{L}, \tag{5.17}$$
$$Cr' = -N_0 I_1 r + \frac{I_2 N_1}{L} \sin^2\vartheta L_x.$$

To these equations we must add (5.14). The prime indicates the derivative with respect to ν, while k_0', k_1', k_2' have the values:

$$k_0'(\vartheta) = N_0\left(\frac{I_3}{A}\sin^2\vartheta + \frac{I_1}{C}\cos^2\vartheta\right),$$
$$k_1'(\vartheta) = \left\{-\frac{I_4N_1}{C}\left(1 - \frac{3}{2}\sin^2\vartheta\right) + \frac{I_3N_1}{A}\cdot\frac{3}{2}\sin^2\vartheta\right\},$$
$$k_2'(\vartheta) = \left\{\frac{I_4N_1}{C}\left(1 - \frac{1}{2}\sin^2\vartheta\right) - \frac{I_3N_1}{A}\cdot\frac{1}{2}\sin^2\vartheta\right\}. \qquad (5.18)$$

Note that for a circular orbit $N_1 = 0$, $k_1' = k_2' = 0$, and the motion will be of very simple nature. Let us discuss this case in passing. In the general case of an elliptical orbit $N_1 \neq 0$. Let us turn now to a study of Eqs. (5.17). From the equation for L_y' and L_z' it follows that

$$L_zL_y' - L_yL_z' = 0$$

i.e.,

$$\frac{L_z}{L_y} = \text{const} \qquad (5.19)$$

This means that the plane passing through the vector **L** and the axis X maintains its position in space, and the vector **L** can move only in this plane. Then, from the first three equations in (5.17) we have

$$L' = -k_0'L_x + \cos\vartheta L_x(k_1' + k_2'). \qquad (5.20)$$

Let θ be the angle between L and the axis X; then

$$L_x = L\cos\theta, \qquad -L\sin\theta\theta' = L_x' - L'\cos\theta. \qquad (5.21)$$

Substituting L' from (5.20) and L_x' from (5.17) into the right-hand side of (5.21), we obtain

$$\theta' = -k_2'\cos\vartheta\sin\theta,$$

whence

$$\tan\frac{\theta}{2} = \tan\frac{\theta_0}{2}\exp\left[-\int_{\nu_0}^{\nu} k_2'\cos\vartheta\,d\nu\right], \qquad (5.22)$$

$k_2'(\$)$ and cos \$, generally speaking, vary slowly, by virtue of the equations of motion (5.17). In the first approximation we can take

$k_2'(\vartheta)\cos\vartheta \approx k_2'(\nu_0)\cos\nu_0$. However, even when the slow variation in $k_2'(\vartheta)\cos\vartheta$ is taken into account, the same asymptotic picture is maintained as in the case of a constant $k_2'\cos\vartheta$, since for all fairly large values of ν $k_2'\cos\vartheta$ has a completely determined sign. We see from (5.22) that when $k_2'\cos\vartheta > 0$ $\theta \to 0$, but when $k_2'\cos\vartheta < 0$ $\theta \to \pi$, as $\nu \to \infty$. Both cases indicate that the kinetic-momentum vector seeks to coincide with the direction of the tangent to the orbit at its perigee. We can assume approximately that

$$\tan\frac{\theta}{2} = \tan\frac{\theta_0}{2}\exp\{-k_2'(\vartheta_0)\cos\vartheta_0\}(\nu-\nu_0). \tag{5.23}$$

For a circular orbit $k_2' = 0$, and the direction of the vector **L** remains invariable. Returning to (5.20), we have

$$L' = L\left\{-k_0' + \cos\vartheta\sin^2\vartheta\cos\vartheta N_1\left(\frac{I_3}{A}+\frac{I_3}{C}\right)\right\},$$

whence

$$L = L_0\exp\int\left\{-k_0' + \cos\vartheta\sin^2\vartheta\cos\vartheta N_1\left(\frac{I_3}{A}+\frac{I_3}{C}\right)\right\}d\nu, \tag{5.24}$$

since k_0' is an essentially positive quantity and does not vanish on a circular orbit, while $N_1 = 0$ when $e = 0$, we must assume that N_1 is small in comparison with k_0'; moreover, it will be shown below that $\vartheta \to 0$ or $\nu \to \pi/2$; therefore at fairly large values of ν the quantity in the braces is essentially negative, and $L \to 0$ as $\nu \to \infty$; in addition, the angular velocity of the precession $\dot{\psi} = L/A$ decreases.

We can take approximately $k_0' = \text{const}$ and neglect N_1 in (5.24). Then

$$L = L_0\exp\{-k_0'(\nu-\nu_0)\}. \tag{5.25}$$

With the same degree of accuracy we can obtain from the last equation in (5.17) the projection of the angular velocity on the axis of symmetry of the satellite

$$r = r_0 \exp\left\{-\frac{N_0 I_1}{C}(\nu - \nu_0)\right\}. \qquad (5.26)$$

Let us consider the behavior of the angle ϑ. We have

$$\cos\vartheta = Cr/L, \text{ whence } \frac{d\cos\vartheta}{d\nu} = -\frac{Cr}{L^2}\dot{L} + \frac{C}{L}\dot{r}.$$

Substituting the values of $\dot{L}$ and $\dot{r}$, we obtain

$$\frac{d\cos\vartheta}{d\nu} = -\frac{Cr}{L^2}\left\{-k_0 L + \cos\vartheta\,(k_1 + k_2)\,L\cos\theta\right\} +$$
$$+\frac{C}{L}\left\{-\frac{N_0 I_1}{C}r + \frac{I_2 N_1}{AC}\sin^2\vartheta\, L\cos\theta\right\} = \cos\vartheta\left\{k_0 - \frac{N_0 I_1}{C}\right\} +$$
$$+ N_1\cos\theta\sin^2\vartheta\left\{\frac{I_2}{A}\sin^2\vartheta - \frac{I_1}{C}\cos^2\vartheta\right\}.$$

By virtue of (5.18), we have

$$k_0 - \frac{N_0 I_1}{C} = \sin^2\vartheta\left(\frac{I_2}{A} - \frac{I_1}{C}\right)N_0.$$

Again neglecting N_1 (on a circular orbit $N_1 = 0$, while $N_0 \neq 0$), we obtain the equation

$$\frac{d\cos\vartheta}{d\nu} = \cos\vartheta\sin^2\vartheta\left(\frac{I_2}{A} - \frac{I_1}{C}\right)N_0,$$

the integration of which gives

$$\tan\vartheta = \tan\vartheta_0 \exp\left\{\frac{I_1}{C} - \frac{I_2}{A}\right\}N_0(\nu - \nu_0). \qquad (5.27)$$

Hence $\vartheta \to 0$ when $I_1/C - I_3/A < 0$ and $\vartheta \to \pi/2$ when $I_1/C - I_3/A > 0$. If we assume that the dissipation coefficients are approximately the same $I_1 \approx I_3$, then $\vartheta \to 0$ when $A < C$ and $\vartheta \to \pi/2$ when $A > C$. In other words, a dynamically compressed satellite is stabilized around the axis of symmetry ($\vartheta \to 0$), while a dynamically elongated satellite tips over ($\vartheta \to \pi/2$). Taking into account the asymptotic behavior of the kinetic-momentum vector (see (5.22)-(5.23)), we can formulate the following general law: under the action of the forces of aerodynamic dissipation the satellite seeks to establish itself in a regime of maximum aerodynamic resistance. Actually, the vector

L seeks to establish itself along the line of maximum aerodynamic pressure (the tangent to the perigee of the orbit), while the angle $ varies in such a way that the maximum surface area of the satellite is facing the incident flux at the perigee of the orbit.

Note 1. At low angular velocities the above consideration is incorrect, since the method of averaging is correct only for fairly large angular velocities of rotation. Therefore we cannot consider the asymptotics all the way to the end. However, the asymptotics correctly describe the tendencies of the motion.

Note 2. Attenuation of the rotation will occur more rapidly than the motion of the vector **L** toward the tangent of the orbit, since the first velocities are determined by the parameter N_0, while the second velocity is determined by the parameter N_1, the order of which is $\sim eN_0$.

6. The Effect of the Interaction Between the Magnetic Field of the Satellite and the Earth's Magnetic Field

As is known [13], the moment **M** of the forces arising as a result of the interaction between an external magnetic field with a strength **H** and the intrinsic magnetic field of a body possessing a magnetic moment **I** is given by the vector product

$$\mathbf{M} = \mathbf{H} \times \mathbf{I} \tag{6.1}$$

Of the factors causing the appearance of the magnetic moment **I** let us note the following:

a) The presence of current systems on the satellite and permanent magnets in the instruments. For simplicity, we shall assume that these factors cause a constant magnetic moment I_0 directed along the

axis of symmetry of the satellite:

$$\mathbf{I}_0 = \mathbf{k}' I_0 \tag{6.2}$$

Here $\mathbf{k}'$ is a unit vector of the axis of symmetry.

b) The magnetization of the satellite shell in the earth's magnetic field. In the case of fairly elongated bodies the magnetic moment $\mathbf{I}_1$ thus arising may be assumed to be directed along the axis of symmetry of the body, while its magnitude may be regarded as being proportional to the component of the external field along this axis:

$$\mathbf{I}_1 = \frac{\mu_0 - 1}{4\pi} v(\mathbf{H}\mathbf{k}')\,\mathbf{k}'. \tag{6.3}$$

Here μ_0 is the permeability, $\underline{v}$ is the volume of the satellite shell. Thus the total magnetic moment will be written in the form

$$\mathbf{I} = \left\{ I_0 + \frac{\mu_0 - 1}{4\pi} v(\mathbf{H}\mathbf{k}') \right\} \mathbf{k}'. \tag{6.4}$$

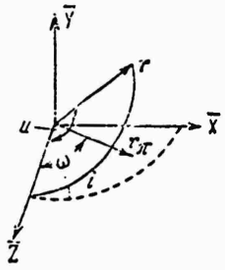

Fig. 11.

According to (6.4), the magnetic-moment is directed along the longitudinal axis of the satellite. Consequently, in this case we can neglect the transverse component $\mathbf{I}_\pi$ of the vector $\mathbf{I}$. Naumann and Colombo [1, 2] considered secular effects in the presence of a moment of type (6.4) as applied to the satellite Explorer XI in the assumption that the satellite is moving in a somersault regime ($\$ = 90^\circ$). In this section we are considering the main properties of motion under the action of a moment determined by Formulas (6.1) and (6.4) in the general case. We shall take the vector $\mathbf{H}$ of the earth's magnetic strength in the form

$$\mathbf{H} = \frac{\mu_E}{R^3} \{ \mathbf{k}_0 - 3(\mathbf{k}_0 \mathbf{e}_R)\,\mathbf{e}_R \}, \tag{6.5}$$

where $\mathbf{k}_0$ is the direction of the axis of the earth's magnetic dipole, $\mathbf{e}_R$ is a unit vector of the direction of the radius vector **R** of an orbital satellite, μ_E is the magnitude of the magnetic moment of the earth's dipole. For simplicity, let us assume that $\mathbf{k}_0$ coincides with the earth's axis. Let us introduce a stationary coordinate system $\overline{XYZ}$ (Fig. 11), the axis $\overline{Y}$ of which coincides with the earth's axis, the axis $\overline{Z}$ is directed into the node of the orbit. Let $\underline{i}$ be the inclination of the orbit toward the equator, $u = \omega + \nu$ is the argument of the latitude, ω is the longitude of the perigee. Then the components of **H** will be:

$$\begin{aligned} H_{\bar{z}} &= -\frac{\mu_E}{R^3} \cdot 3 \sin i \sin u \cos u, \\ H_{\bar{x}} &= -\frac{\mu_E}{R^3} 3 \sin i \cos i \sin^2 u, \\ H_{\bar{y}} &= \frac{\mu_E}{R^3} [1 - 3 \sin^2 u \sin^2 i]. \end{aligned} \tag{6.6}$$

We can write the force function U characterizing the action of the magnetic moment under consideration. It turns out that

$$U = -I_0 \left\{ H_{\bar{x}} \alpha_1 + H_{\bar{y}} \beta_1 + H_{\bar{z}} \gamma_1 + \frac{1}{2} \bar{k}_0 (H_{\bar{x}} \alpha_1 + H_{\bar{y}} \beta_1 + H_{\bar{z}} \gamma_1)^2 \right\}, \tag{6.7}$$

where α_1, β_1, γ_1 are the direction cosines of the axis of symmetry of a satellite with the axes XYZ;

$$\bar{k}_0 = \frac{\mu_0 - 1}{4\pi} \frac{v}{I_0}. \tag{6.8}$$

From there on the theory set forth in Section 1 is again completely applicable for studying the motion. Let us introduce the function U_ν (1.20) and average it twice, as in (1.24); then we can easily write the secular-motion equations (1.23) of the kinetic-momentum vector and the trajectory of its terminus (1.25). We have

$$\begin{aligned} U_\nu = -\frac{I_0 P^2}{\sqrt{\mu P}} \frac{1}{(1 + e \cos \nu)^2} \Big\{ & H_{\bar{x}} \alpha_1 + H_{\bar{y}} \beta_1 + H_{\bar{z}} \gamma_1 + \\ & + \frac{1}{2} \bar{k}_0 (H_{\bar{x}} \alpha_1 + H_{\bar{y}} \beta_1 + H_{\bar{z}} \gamma_1)^2 \Big\}. \end{aligned} \tag{6.9}$$

Let us introduce the angular coordinates ρ_1, σ_1, which are similar to the coordinates ρ, σ (the angle ρ_1 is the angle between **L** and the axis Y). The direction cosines α_1, β_1, γ_1 will have the same form as α'', β'', γ'' in (1.5), except that in the right-hand sides of the equations, instead of ρ and σ, we must write ρ_1, σ_1. Averaging (6.9) with respect to ψ and discarding in the average values $\overline{\alpha}_1^2$, $\overline{\beta}_1^2$, $\overline{\gamma}_1^2$ the term $1/2 \sin^2 \$$ (which has no effect on the motion of the kinetic-momentum vector), we obtain the averaged value $\overline{U}_\nu$ in the form

$$\overline{U}_\nu = -\frac{I_0 p^2}{\sqrt{\mu p}} \frac{1}{(1+e\cos\nu)^2} \left\{ \cos\vartheta \left(H_{\bar{x}} \alpha_1^0 + H_{\bar{y}} \beta_1^0 + H_{\bar{z}} \gamma_1^0\right) + \right.$$
$$\left. + \frac{1}{2} \overline{k}_0 \left(1 - \frac{3}{2} \sin^2 \vartheta\right) \left(H_{\bar{x}} \alpha_1^0 + H_{\bar{y}} \beta_1^0 + H_{\bar{z}} \gamma_1^0\right)^2 \right\}. \tag{6.10}$$

Here α_1^0, β_1^0, γ_1^0 are the direction cosines of a kinetic-momentum vector with the axes XYZ, i.e.,

$$\alpha_1^0 = \sin\rho_1 \sin\sigma_1, \; \beta_1^0 = \cos\rho_1, \; \gamma_1^0 = \sin\rho_1 \cos\sigma_1. \tag{6.11}$$

The equations of rotational motion will now have the form (1.22) with ρ replaced by ρ_1 and σ by σ_1), where $\overline{U}_\nu$ is determined by Formulas (6.10), (6.11), and (6.6). From (6.10), in particular, it follows that if the satellite shell is not magnetized ($\overline{k}_0 = 0$), there will nevertheless occur a perturbed motion of the vector **L** caused by the intrinsic magnetic field of a satellite with a moment I_0. Only in the particular case $\$ = \pi/2$, i.e., when the satellite rotates around the transverse axis, does I_0 not cause perturbations in the motion. However, when $\$ = \pi/2$, there remain perturbations as a result of magnetization of the satellite shell $\overline{k}_0 \neq 0$.

Let us consider the secular perturbations in ρ_1, σ_1. For this purpose, let us average (6.10) with respect to the true anomaly ν.

Let

$$I_s = \frac{1}{2\pi}\int_0^{2\pi} \frac{H_s\,d\nu}{\frac{\mu_E}{p^3}(1+e\cos\nu)^3} \quad (s = \bar{x}, \bar{y}, \bar{z}),$$
$$I_{sk} = \frac{1}{2\pi}\int_0^{2\pi} \frac{H_s H_k\,d\nu}{\frac{\mu_E^2}{p^6}(1+e\cos\nu)^3} \quad (s = \bar{x}, \bar{y}, z, k = \bar{x}, \bar{y}, \bar{z}). \tag{6.12}$$

Then

$$I_{\bar{x}} = -\frac{3}{2}\sin i\cos i,\ I_{\bar{y}} = \left(1 - \frac{3}{2}\sin^2 i\right),\ I_{\bar{z}} = 0,$$
$$I_{\bar{x}\bar{x}} = 9\sin^2 i\cos^2 i\, f_1(e,\omega),\ I_{\bar{y}\bar{y}} = \left(1 + 3e^2 + \frac{3}{8}e^4\right) -$$
$$- 6\sin^2 i f_2(e,\omega) + 9\sin^4 i\, f_1(e,\omega),$$
$$I_{\bar{z}\bar{z}} = 9\sin^2 i\,[f_2 - f_1],$$
$$I_{\bar{x}\bar{y}} = -3\sin i\cos i\,[f_2 - 3\sin^2 i f_1],\ I_{\bar{z}\bar{x}} = 0,\ I_{\bar{z}\bar{y}} = 0, \tag{6.13}$$
$$f_1(e,\omega) = \frac{3}{8} + 6e^2\left[\frac{3}{16}\cos^4\omega + \frac{18}{16}\cos^2\omega\sin^2\omega + \frac{5}{16}\sin^4\omega\right] +$$
$$+ e^4\left[\frac{9}{128}\cos^4\omega + \frac{90}{128}\cos^2\omega\sin^2\omega + \frac{35}{128}\sin^4\omega\right],$$
$$f_2(e,\omega) = \frac{1}{2} + \frac{3}{4}e^2[\cos^2\omega + 3\sin^2\omega] + \frac{e^4}{16}[3\cos^2\omega + 5\sin^2\omega].$$

Since the eccentricity figures in these expressions in a power higher than the first, for orbits with a small eccentricity the motion is practically independent of e and, consequently, of ω. In this case, neglecting terms containing e^2 and e^4, we obtain

$$I_{\bar{x}\bar{x}} = \frac{27}{8}\sin^2 i\cos^2 i,\ I_{\bar{y}\bar{y}} = 1 - 3\sin^2 i + \frac{27}{8}\sin^4 i,$$
$$I_{\bar{z}\bar{z}} = \frac{9}{8}\sin^2 i,\ I_{\bar{x}\bar{y}} = -3\sin i\cos i\left[\frac{1}{2} - \frac{9}{8}\sin^2 i\right]. \tag{6.14}$$

The twice-averaged value of U_ν can now be written in the form:

$$\overline{U}_\nu = -\frac{I_0\mu_E}{p^{3/2}\sqrt{\mu}}\left\{\cos\vartheta\,(I_{\bar{x}}\alpha_1^0 + I_{\bar{y}}\beta_1^0) + \frac{1}{2}k_0\left(1 - \frac{3}{2}\sin^2\vartheta\right)\times\right.$$
$$\left.\times\frac{\mu_E}{p^3}(I_{\bar{x}\bar{x}}(\alpha_1^0)^2 + I_{\bar{y}\bar{y}}(\beta_1^0)^2 + I_{\bar{z}\bar{z}}(\gamma_1^0)^2 + 2I_{\bar{x}\bar{y}}\alpha_1^0\beta_1^0)\right\}. \tag{6.15}$$

According to the general theory of Section 1, the equation

$$\overline{\overline{U}}_\nu = \text{const} \tag{6.16}$$

gives the trajectory of the trace of the kinetic-momentum vector, while Eqs. (1.23) give the law of motion.

Taking into account that $(\gamma_1^0)^2 = 1 - (\alpha_1^0)^2 - (\beta_1^0)^2$, we can write

$$\overline{U}_* = -\frac{I_0\mu_E}{P^{3/2}\sqrt{\overline{\mu}}}\left\{\cos\vartheta\,(I_{\bar{x}}\,\alpha_1^0 + I_{\bar{y}}\beta_1^0) + \frac{1}{2}\bar{k}_0\left(1-\frac{3}{2}\sin^2\vartheta\right)\times\right.$$
$$\left.\times\frac{\mu_E}{P^3}\left[(I_{\bar{x}\bar{x}} - I_{\bar{z}\bar{z}})(\alpha_1^0)^2 + (I_{\bar{y}\bar{y}} - I_{\bar{z}\bar{z}})(\beta_1^0)^2 + 2I_{\bar{x}\bar{y}}\alpha_1^0\beta_1^0\right]\right\} = \text{const.} \tag{6.17}$$

Then Eqs. (1.23), with (6.11) taken into account, give

$$\frac{d\sigma_1}{dv} = -\frac{I_0\mu_E}{P^{3/2}\sqrt{\overline{\mu}}L_0}\left\{\cos\vartheta\,(I_{\bar{x}}\cos t\;\rho_1\sin\sigma_1 - I_{\bar{y}}) + \bar{k}_0\left(1-\frac{3}{2}\sin^2\vartheta\right)\times\right.$$
$$\times\frac{\mu_E}{P^3}\left[(I_{\bar{x}\bar{x}} - I_{\bar{z}\bar{z}})\cdot\cos\rho_1\sin^2\sigma_1 - (I_{\bar{y}\bar{y}} - I_{\bar{z}\bar{z}})\cos\rho_1 + I_{\bar{x}\bar{y}}\sin\sigma_1\times\right.$$
$$\left.\left.\times\frac{\cos 2\rho_1}{\sin\rho_1}\right]\right\}, \tag{6.18}$$
$$\frac{d\rho_1}{dv} = \frac{I_0\mu_E}{P^{3/2}\sqrt{\overline{\mu}}L_0}\left\{\cos\vartheta I_{\bar{x}}\cos\sigma_1 + \bar{k}_0\left(1-\frac{3}{2}\sin^2\vartheta\right)\times\right.$$
$$\left.\times\frac{\mu_E}{P^3}\left[(I_{\bar{x}\bar{x}} - I_{\bar{z}\bar{z}})\sin\rho_1\sin\sigma_1\cos\sigma_1 + I_{\bar{x}\bar{y}}\cos\rho_1\cos\sigma_1\right]\right\}.$$

Particular Cases

1. $i = 0$ (equatorial orbit). The vector **L** precesses around the normal to the orbital plane at a constant angular distance

$$\rho_1 = \rho_1^0 \tag{6.19}$$

with a constant angular velocity

$$\frac{d\sigma_1}{dv} = \frac{I_0\mu_E}{P^{3/2}\sqrt{\overline{\mu}}L_0}\left\{\cos\vartheta + \bar{k}_0\left(1-\frac{3}{2}\sin^2\vartheta\right)\frac{\mu_E}{P^3}\cos\rho_1^0\right\}. \tag{6.20}$$

2. The shell is not magnetized ($\bar{k}_0 = 0$). The motion occurs only as a result of the constant magnetic moment I_0 of the satellite. Then the kinetic-momentum vector **L** precesses at a constant angular distance

$$\varkappa = \varkappa_0 \tag{6.21}$$

from the pole, the coordinates of which σ_1^*, ρ_1^* are determined by the formulas

$$\text{cot}\quad \rho_1^{\cdot} = \frac{I_{\bar{y}}}{I_{\bar{x}}} = -\frac{1-\frac{3}{2}\sin^2 i}{\frac{3}{2}\sin i\cos i},\quad \sigma_1^{\cdot} = \pm\frac{\pi}{2} \tag{6.22}$$

(i.e., the pole lies in the plane $\bar{X}\bar{Y}$, which is normal to the nodal line $\bar{Z}$ and passes through the earth's axis $\bar{Y}$). The rate of precession of the vector **L** is constant and is given by the expression

$$\frac{d\lambda_{\varkappa}}{dv} = \frac{I_0\mu_{\bar{z}}}{2P^{3/2}\sqrt{\mu L_0}}\cos\vartheta\sqrt{1+3\cos^2 i}. \tag{6.23}$$

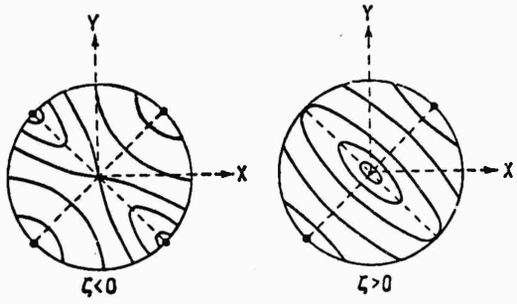

Fig. 12.

3. $I_0 = 0$, i.e., the original magnetic field of the satellite can be neglected; we take into account only the magnetization of the shell ($\bar{k}_0 I_0 \neq 0$). Let $\alpha_1^0 = \cos\Phi$, $\beta_1^0 = \cos\rho_1$; thus Φ is the angle between the vector **L** and the axis X; from (6.17) it follows that the trajectories are symmetrical relative to the plane $\bar{Y}\bar{X}$, i.e., to the plane which is normal to the nodal line of the orbit. Solving Eq. (6.17) for cos Φ, we obtain:

$$\cos\Phi = -\lambda\cos\rho \pm \sqrt{C_0 + \zeta\cos^2\rho}. \tag{6.24}$$

Here C_0 is a constant of integration, while

$$\lambda = \frac{I_{\bar{x}\bar{y}}}{I_{\bar{x}\bar{x}} - I_{\bar{z}\bar{z}}},\quad \zeta = \frac{I_{\bar{x}\bar{y}}^2}{(I_{\bar{x}\bar{x}} - I_{\bar{z}\bar{z}})} - \frac{I_{\bar{y}\bar{y}} - I_{\bar{z}\bar{z}}}{I_{\bar{x}\bar{x}} - I_{\bar{z}\bar{z}}}. \tag{6.25}$$

Depending on the values ofthe orbital parameters (the angle i), we can have $\lambda \gtrless 0$ and $\zeta \gtrless 0$. Taking into account that

$$\cos\Phi = \sin\rho_1\sin\sigma_1,\ \text{i.e.,}\ -\sin\rho_1 < \cos\Phi < \sin\rho_1,$$

with the aid of (6.24) we can plot in the usual manner [9] the

trajectories of the trace of the vector **L** on a unit sphere. These trajectories are shown in Fig. 12 for the case $\lambda < 0$; for the case $\lambda > 0$ the picture will be symmetrically reversed with respect to the axis $\overline{Y}$. The family of trajectories contains two pairs of poles on the meridian of symmetry (i.e., on the meridian $\overline{YX}$) and one more pair of poles, which constitute the trace of the axis $\overline{Z}$ ($+\overline{Z}$ and $-\overline{Z}$); one of these pairs represents the unstable poles. When $\zeta < 0$, the unstable poles are the poles which are traces of the axis $\overline{Z}$ (i.e., $\sigma_1 = 0, \pi$; $\rho_1 = \pi/2$); when $\zeta > 0$, the unstable poles are one of the pairs on the meridian of symmetry. The location of the poles σ_1 on the meridian of symmetry can be determined most easily from the equations of motion (6.18) by equating the right-hand sides to zero. We obtain

$$\sigma_1^* = \pm\frac{\pi}{2}, \quad \tan 2\rho_1^* = \pm\frac{2I_{\overline{xy}}}{I_{\overline{xx}} - I_{\overline{yy}}}. \tag{6.26}$$

Hence, in particular, it follows that for a polar orbit ($i = 90^\circ$) $\rho_1^* = 0, \pi/2, \pi$; but since for $i = 90^\circ$ $\zeta > 0$, depending on the initial data, the precession will occur either around the line $\overline{X}$ or around the axis $\overline{Y}$. Naturally, the precession occurs nonuniformly: a precessional-nutational motion with variable velocities occurs, according to (6.18). Using (6.17), we can reduce the problem to quadratures.

4. When $I_0 \neq 0$, the qualitative picture shown in Fig. 12 is distorted: the poles shift (although the plane $\overline{YX}$ remains the plane of symmetry), the regions of motion around each pole of one pair are not equal to each other (one region expands, the other contracts); the location of the poles will depend not only on the parameters of the orbit, but also on the parameters of the satellite.

Notes. 1) In this case we did not take into account that the axis of the earth's magnetic dipole does not coincide with the axis of rotation. This fact was taken into account by Colombo [2], who introduced one more averaging, an averaging with respect to the earth's period of rotation.

2) A study of the effect of the transverse component $\mathbf{I}_\pi$ of the magnetic moment **I** of the satellite shows [15] that under certain conditions a qualitative change in the motion relative to the vector **L** is possible: instead of a continuous rotation around the axis of symmetry of the satellite, oscillations relative to this axis may appear.

7. The Effect of Eddy Currents

When a satellite rotates around a center of mass in the earth's magnetic field, eddy currents (Foucault currents) will arise in the metal shell of the satellite; the interaction between these currents and the earth's magnetic field creates a force moment applied to the satellite. This moment will slow down the rotation of the satellite, as a result of the dissipation of energy.

Concerning the moment of these forces, we can make the following assumptions from obvious physical premises.

a) When a body rotates around a line of force of an external magnetic field, eddy currents do not arise in the shell of the body; they arise only during rotation across the lines of force. Let ω be a certain component of the angular velocity of rotation of the body, while **H** is the external magnetic field strength vector; then eddy currents arise as a result of $\omega_\perp$ (that component of ω which is normal to **H** and lies in the plane of the vectors ω and **H**.

b) Eddy currents lead to dissipation of energy, and, consequently to a decrease in the angular velocity ω, namely, to a decrease in its component $\omega_\perp$. This means that there appears a force moment **M** directed contrariwise to the vector $\omega_\perp$ and, as may be assumed, proportional to $\omega_\perp$, $|\omega_\perp| = |\omega \sin \delta|$ (Fig. 13).

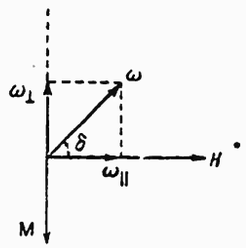

Fig. 13

c) Since the force moment should have the form (6.1), while the magnitude of the moment I resulting from eddy currents is governed by the magnitude of the external magnetic field strength H, assuming I proportional to H, we find, according to (6.1), that **M** is proportional to H^2. By virtue of the above-said, the moment resulting from eddy currents has the form

$$\mathbf{M} = -k''H^2\omega \sin\delta\, \mathbf{e}_{\perp H}, \tag{7.1}$$

where δ is the angle between $\bar{\boldsymbol{\omega}}$ and **H**, $\mathbf{e}_{\perp H}$ is a unit vector of the direction $\boldsymbol{\omega}_\perp$, k" is a dissipation coefficient depending on the parameters of the shell of the body, and also on the orientation of the body. For the sake of generality, let us assume that the dissipation coefficients are different along the longitudinal and transverse axes of the satellite. Let x', y', z' be a coordinate system rigidly connected to a satellite which has a symmetrical shell and possesses dynamic symmetry with respect to the axis z'. Then the components of the moment of the forces under consideration along axes which are normal to x', y', z' and lie, respectively, in the planes x'H, y'H, z'H will be written in the form:

$$\begin{aligned} \mathbf{M}_{Hx'} &= -k_0'' H^2 r \sin(\widehat{z'H})\, \mathbf{e}_{Hx'}, \\ \mathbf{M}_{Hx'} &= -k_1'' H^2 p \sin(\widehat{x'H})\, \mathbf{e}_{Hx'}, \\ \mathbf{M}_{Hy'} &= -k_1'' H^2 q \sin(\widehat{y'H})\, \mathbf{e}_{Hy'}. \end{aligned} \tag{7.2}$$

Here p, q, r are the components of the angular velocity of the body along the axes x', y', z'; $\mathbf{e}_{Hz'}$, $\mathbf{e}_{Hx'}$, $\mathbf{e}_{Hy'}$ are unit vectors of the directions $\mathbf{r}_\perp$, $\mathbf{q}_\perp$, $\mathbf{p}_\perp$, which are determined analogously to the direction $\bar{\boldsymbol{\omega}}_\perp$ in Fig. 13. Let $\delta = \hat{z'H}$; correspondingly, $\delta_1 = \hat{x'H}$, $\delta_2 = \hat{y'H}$. Then the table of direction cosines of the axes x'y'z' and $\mathbf{e}_{Hx'}$, $\mathbf{e}_{Hy'}$, $\mathbf{e}_{Hz'}$ has the form

	$e_{Hx'}$	$e_{Hy'}$	$e_{Hz'}$
x'	$\sin\delta_1$	$-\cos\delta_1\cot\delta_2$	$-\cos\delta_1\cot\delta$
y'	$-\cos\delta_2\cot\delta_1$	$\sin\delta_2$	$-\cos\delta_2\cot\delta$
z'	$-\cos\delta\cot\delta_1$	$-\cos\delta\cot\delta_2$	$\sin\delta$

(7.3)

Let us introduce another right-handed coordinate system XYZ, the axis Y being directed along **H**, while X and Z are, for the time being, arbitrary. Let the position of x'y'z' relative to XYZ be given by the table of direction cosines:

	x'	y'	z'
X	α	α'	α''
Y	β	β'	β''
Z	γ	γ'	γ''

(7.4)

The total moment

$$\mathbf{M} = \mathbf{M}_{Hz'} + \mathbf{M}_{Hx'} + \mathbf{M}_{Hy'}, \tag{7.5}$$

made up of the components of (7.2), can now be broken down along the axes x'y'z' by using Tables (7.3) and (7.4) and taking into account that $\sin^2\delta = 1 - \beta^2$, etc. We then obtain the components of **M** along the axes x'y'z':

$$\begin{aligned} M_{x'} &= -H^2\{k_1''p - k_1''\beta(\beta p + \beta' q) - k_0''\beta\beta'' r\},\\ M_{y'} &= -H^2\{k_1''q - k_1''\beta'(\beta p + \beta' q) - k_0''\beta'\beta'' r\},\\ M_{z'} &= -H^2\{k_0''r - k_1''\beta''(\beta p + \beta' q) - k_0''\beta''^2 r\}. \end{aligned} \tag{7.6}$$

The dissipation coefficients k_0'' and k_1'' depend on the orientation of the satellite relative to **H**. An accurate determination of the coefficients k_0'', k_1'' is related to the actual specification of the

shape of the satellite. For example, in the case of a spherical shell $k_0 = k_1 = \text{const}$ and are given by a simple formula [6, 7]. The coefficients k_0'', k_1'' are essentially positive. We shall regard them as certain known constants, which are independent of the orientation and have the following structure:

$$k_s'' \approx \alpha_s I_s h \frac{1}{\mathcal{R}} \qquad (s = 0, 1),$$

where I_0, I_1 are the longitudinal and transverse moments of inertia of the surface of the satellite, h is the thickness of the satellite shell, $\mathcal{R}$ is the specific volume resistance of the shell material. If H and $\mathcal{R}$ are determined in electromagnetic units, α_0, α_1 are dimensionless coefficients. For example, for a spherical shell of radius a we have [6]

$$k_0'' = k_1'' = \frac{2\pi a^4 h}{3\mathcal{R}}.$$

In the assumption that $k_s'' = \text{const}$, let us consider the principal effects of the motion. For simplicity, we shall assume that the external field is plane-parallel and has a constant strength, i.e.,

$$\mathbf{H} = \text{const} \tag{7.7}$$

Condition (7.7) is approximately fulfilled in the case of equatorial earth satellites. Projecting (7.6) on the axes XYZ, we obtain the components of M along these axes:

$$\begin{aligned} M_x &= -H^2\left\{k_1''\frac{L_x}{A} + \left(k_0'' - k_1''\frac{C}{A}\right)r\alpha'\right\}, \\ M_y &= 0, \\ M_z &= -H^2\left\{k_1''\frac{L_z}{A} + \left(k_0'' - k_1''\frac{C}{A}\right)r\gamma'\right\}. \end{aligned} \tag{7.8}$$

Averaging with respect to the precession ψ and taking into account that $\cos \downarrow = Cr/L$, we obtain

$$\overline{M}_x = -H^2\left\{\frac{k_0''}{C}\cos^2\vartheta + \frac{k_1''}{A}\sin^2\vartheta\right\} L_x,$$
$$\overline{M}_y = 0, \qquad (7.9)$$
$$\overline{M}_z = -H^2\left\{\frac{k_0''}{C}\cos^2\vartheta + \frac{k_1''}{A}\sin^2\vartheta\right\} L_z.$$

We have the following equations of motion:

$$\dot{L}_x = \overline{M}_x, \quad \dot{L}_y = \overline{M}_y, \quad \dot{L}_z = \overline{M}_z, \qquad (7.10)$$

substituting (7.9) in which and assuming in the first approximation that $\vartheta = \vartheta_0$, after integration we obtain

$$L_y = L_y^0,$$
$$L_x = L_x^0 \exp\left\{-H^2\left(\frac{k_0''}{C}\cos^2\vartheta_0 + \frac{k_1''}{A}\sin^2\vartheta_0\right)\right\}(t - t_0), \qquad (7.11)$$
$$L_z = L_z^0 \exp\left\{-H^2\left(\frac{k_0''}{C}\cos^2\vartheta_0 + \frac{k_1''}{A}\sin^2\vartheta_0\right)\right\}(t - t_0).$$

Thus the plane passing through **L** (the axis Y) and **H** remains stationary:

$$\frac{L_X}{L_Z} = \text{const}. \qquad (7.12)$$

When $t \to \infty$, the magnitude of the vector

$$L = \sqrt{L_x^2 + L_y^2 + L_z^2} \to L_y^0, \qquad (7.13)$$

i.e., the vector **L** seeks to coincide in direction with **H**, while its magnitude tends to a constant value. At the same time the precession velocity

$$\dot{\psi} \approx \frac{L}{A} \to \frac{L_y^0}{A}. \qquad (7.14)$$

also tends to a constant value.

Now averaging M_z, from (7.6), we obtain:

$$\overline{M}_z = -H^2 r\left\{k_0''\left(1 - \frac{L_y^2}{L^2}\right) + \frac{1}{2}\sin^2\vartheta\left(3\frac{L_y^2}{L^2} - 1\right)\left[k_0'' - k_1''\frac{C}{A}\right]\right\}. \qquad (7.15)$$

But since

$$\cdot \quad \mathbf{M}_r = Cr, \frac{d}{dt}\cos\vartheta = \frac{\dot{Cr}}{L} - \frac{CrL}{L^2}, \tag{7.15a}$$

we obtain, now taking into account that r/L = cos φ/C:

$$\frac{d}{dt}\cos\vartheta = -H^2\cos\vartheta\sin^2\vartheta\left\{\frac{1}{2}\left(\frac{L_y^2}{L^2}+1\right)\left(\frac{k_0''}{C}-\frac{k_1''}{A}\right)\right\}, \tag{7.16}$$

i.e.,

$$\dot{\vartheta} = H^2\sin\vartheta\cos\vartheta\left\{\frac{1}{2}\left(\frac{L_y^2}{L^2}+1\right)\left(\frac{k_0''}{C}-\frac{k_1''}{A}\right)\right\}. \tag{7.17}$$

Integrating, we obtain

$$\tan\vartheta = \tan\vartheta_0 \exp H^2\int\left\{\frac{1}{2}\left(\frac{L_y^2}{L^2}+1\right)\left(\frac{k_0''}{C}-\frac{k_1''}{A}\right)\right\}dt. \tag{7.18}$$

Since, according to (7.13), $L \approx L_y$,

$$\tan\vartheta \approx \tan\vartheta_0 \exp\left[H^2\left(\frac{k_0''}{C}-\frac{k_1''}{A}\right)(t-t_0)\right], \tag{7.19}$$

i.e., $\varphi \to 0$, if

$$\frac{k_0''}{C}-\frac{k_1''}{A}<0 \qquad (A < C \text{ when } k_0'' \approx k_1''),$$

and $\varphi \to \pi/2$, if

$$\frac{k_0''}{C}-\frac{k_1''}{A}>0 \qquad (A > C \text{ when } k_0'' \approx k_1'').$$

Since $\cos\varphi = Cr/L$, we obtain $Cr \to L \to L_y^0 = \text{const}$ or $Cr \to 0$. In other words, a dynamically compressed satellite is stabilized in such a way that its rotation tends toward uniform rotation around the axis of symmetry, which seeks to coincide with **H**; a dynamically elongated satellite, on the other hand, tips over and seeks to put itself into uniform rotation (7.14) around the transverse axis, which seeks to coincide with **H**. However, an equatorial orbit (**H** = const) is an exceptional case. In the general case of an arbitrary orbit, owing to the rotation of the vector **H**, we must expect that all the components of the angular velocity will be

attenuated to zero, while the magnitude of the vector **L** will tend to zero (and not to a constant value, as in the case **H** = const). This follows from the fact that in such a case there will not be any fixed direction relative to which the force moment is equal to zero.

Let us consider, for example, the case of a polar orbit ($i = 90^\circ$), for the sake of simplicity taking $e = 0$ (a circular orbit). Then the axis $\bar{X}$ of the stationary system $\bar{X}\bar{Y}\bar{Z}$ (Fig. 11) is directed along the normal to the orbital plane:

$$H_{\bar{x}}=0,\ H_{\bar{z}}=\frac{3\mu_E}{R^3}\sin u\cos u,\quad H_{\bar{y}}=\frac{\mu_E}{R^3}[1-3\sin^2 u]. \tag{7.20}$$

Projecting the moment in (7.8) onto the axes XYZ and averaging with respect to ψ and ν, we obtain:

$$\begin{aligned}
\overline{M}_{\bar{x}} &= -\overline{H}^2\left\{\frac{k_0''}{C}\cos^2\vartheta+\frac{k_1''}{A}\sin^2\vartheta\right\}L_{\bar{x}},\\
\overline{M}_{\bar{y}} &= -\overline{H}_{\bar{z}}^2\left\{\frac{k_0''}{C}\cos^2\vartheta+\frac{k_1''}{A}\sin^2\vartheta\right\}L_{\bar{y}},\\
\overline{M}_{\bar{z}} &= -\overline{H}_{\bar{y}}^2\left\{\frac{k_0''}{C}\cos^2\vartheta+\frac{k_1''}{A}\sin^2\vartheta\right\}L_{\bar{z}},
\end{aligned} \tag{7.21}$$

where

$$\overline{H}_{\bar{y}}^2=\frac{11}{8}\frac{\mu_E^2}{R^6},\quad H_{\bar{z}}^2=\frac{9}{8}\frac{\mu_E^2}{R^6},\ \overline{H}^2=\frac{20}{8}\frac{\mu_E^2}{R^6}. \tag{7.22}$$

From

$$\dot{L}_{\bar{y}}=\overline{M}_{\bar{x}},\ \dot{L}_{\bar{y}}=\overline{M}_{\bar{y}},\ \dot{L}_{\bar{z}}=\overline{M}_{\bar{z}} \tag{7.23}$$

we have approximately (taking $\vartheta \approx \vartheta_0$):

$$\begin{aligned}
L_{\bar{x}} &= L_{\bar{x}}^0\exp\left\{-\overline{H}^2\left[\frac{k_0''}{C}\cos^2\vartheta_0+\frac{k_1''}{A}\sin^2\vartheta_0\right](t-t_0)\right\},\\
L_{\bar{y}} &= L_{\bar{y}}^0\exp\left\{-\overline{H}_{\bar{z}}^2\left[\frac{k_0''}{C}\cos^2\vartheta_0+\frac{k_1''}{A}\sin^2\vartheta_0\right](t-t_0)\right\},\\
L_{\bar{z}} &= L_{\bar{z}}^0\exp\left\{-\overline{H}_{\bar{y}}^2\left[\frac{k_0''}{C}\cos^2\vartheta_0+\frac{k_1''}{A}\sin^2\vartheta_0\right](t-t_0)\right\}.
\end{aligned} \tag{7.24}$$

That is, all the components of **L** tend to zero when $t \to \infty$. Hence we find that when $t \to +\infty$

$$L = \sqrt{L_x^2 + L_y^2 + L_z^2} \to 0 \qquad \dot{\psi} = \frac{L}{A} \to 0. \tag{7.25}$$

Let $\bar{\lambda}$ be the angle between the axis $\bar{Z}$ and the projection of the vector **L** on the orbital plane. Then from (7.24)

$$\tan \bar{\lambda} = \tan \bar{\lambda}_0 \exp \frac{1}{4} \frac{\mu_E}{r^3} \left[\frac{k_0''}{C} \cos^2 \vartheta_0 + \frac{k_1''}{A} \sin^2 \vartheta_0 \right] (t - t_0), \tag{7.26}$$

i.e.,

$$\lambda \to \frac{\pi}{2} \quad \text{when} \quad t \to \infty. \tag{7.27}$$

If θ is the angle between the vector **L** and the axis $\bar{X}$, then from (7.24) and (7.25) we have

$$\cos \theta = \frac{L_x^0 \exp \{-H^2 a (t - t_0)\}}{\sqrt{L_x^{02} \exp 2\{-\bar{H}^2 a (t-t_0)\} + L_y^{02} \exp 2\{-\bar{H}_z^2 a (t-t_0)\} + L_z^{02} \exp 2\{-H_y^2 a (t-t_0)\}}}, \tag{7.28}$$

$$a = \frac{k_0''}{C} \cos^2 \vartheta_0 + \frac{k_1''}{A} \sin^2 \vartheta_0.$$

Since $\bar{H}^2 > \bar{H}_{\bar{Z}}^2$ and $\bar{H}^2 > \bar{H}_{\bar{y}}^2$, from (7.28) it follows that when $t \to \infty$

$$\cos \theta \to 0. \tag{7.29}$$

Relationships (7.27) and (7.29) indicate that the kinetic-momentum vector seeks to make itself parallel to the axis of the magnetic dipole. Finally, writing out for the case under consideration the twice-averaged value of the projection of the moment on the axis of symmetry of the satellite, we obtain

$$\bar{M}_{z'} = -\bar{H}^2 r \left\{ k_0'' \left(1 - \frac{l^2}{L^2}\right) + \frac{1}{2} \sin^2 \vartheta \left(k_0'' - k_1'' \frac{C}{A} \right) \left(3 \frac{l^2}{L^2} - 1 \right) \right\}, \tag{7.30}$$

$$l^2 = L_y^2 \frac{\bar{H}_y^2}{\bar{H}^2} + L_z^2 \frac{\bar{H}_z^2}{\bar{H}^2}. \tag{7.31}$$

Using (7.15a), (7.30), and (7.21), we obtain an equation for the angle of nutation ϑ, analogous to (7.17), the integration of which gives

$$\tan\vartheta = \tan\vartheta_0 \exp\int_0^t \left\{\frac{1}{2}\left[\overline{H}_v^2\left(1+\frac{L_v^2}{D^2}\right) \mp \overline{H}_i^2\left(1+\frac{L_i^2}{D^2}\right)\right]\left(\frac{k_0^*}{C}-\frac{k_1^*}{A}\right)\right\}dt, \qquad (7.32)$$

in which case a formula analogous to (7.19) and the corollaries deriving from this formula will be asymptotically correct. Finally, since

$$Cr = L\cos\vartheta,$$

while $L \to 0$, according to (7.25), the axial component of the angular velocity $\mathbf{r}$ also tends to zero. In contrast to the case of an equatorial satellite, the rotation seeks to extinguish itself completely. A more detailed investigation of the effect of eddy currents on the rotation and orientation of a satellite is given by Yegorov [16].

8. The Effect of Moments of Light-Pressure Forces on a Solar Satellite

If a space vehicle is moving in an orbit around the sun, frequently, of the moments of external forces the moments of the forces of light pressure have the most significant effect on the rotational motion of the vehicle. An accurate calculation of the moments of light-pressure forces involves the same difficulties as the calculation of the moments of aerodynamic forces. In this case we cannot give preference to any one character of the reflection of light from the surface of a body, since it is determined by the properties of the surface of the body. The general integral formulas for the moments of light-pressure forces are given by A. A. Karymov

[12]. For studying the motion we can use the following approximate formula for the moment of light-pressure forces:

$$\mathbf{M} = \frac{a(\varepsilon) R_0^2}{R^2} \mathbf{e}_r \times \mathbf{k}'. \tag{8.1}$$

Here $\mathbf{e}_r$ is a unit vector of the radius vector of the satellite, $\mathbf{k}'$ is a unit vector of the axis of the satellite, ε is the angle between these vectors, so that $|\mathbf{e}_r \times \mathbf{k}'| = \sin \varepsilon$, R is the heliocentric radius vector of the center of mass of the satellite, R_0 is a fixed value of R (for example, at the initial moment), $a(\varepsilon)$ is a coefficient of the moment of light-pressure forces. The dimensionality of $\underline{a}$ coincides with the dimensionality of M. We shall assume that $\underline{a}$ is expressed explicitly in terms of cos ε:

$$a = a(\cos \varepsilon). \tag{8.2}$$

Then the following line of force corresponds to force moment (8.1)

$$U(\cos \varepsilon) = -\frac{R_0^2}{R^2} \int a(\cos \varepsilon)\, d(\cos \varepsilon), \tag{8.3}$$

i.e., according to (1.20), for an arbitrary elliptical orbit

$$U_\nu(\cos \varepsilon) = -\frac{R_0^2}{\sqrt{\mu P}} \int a(\cos \varepsilon)\, d(\cos \varepsilon). \tag{8.4}$$

Let us consider two cases: $a = a_0$ and $a = a_1 \cos \varepsilon$.

1. $a = a_0$. Then

$$U_\nu = -\frac{a_0 R_0^2}{\sqrt{\mu P}} \cos \varepsilon, \tag{8.5}$$

$$\cos \varepsilon = \gamma'' \cos \nu + \alpha'' \sin \nu, \tag{8.5a}$$

where γ'' and α'' are determined by Formulas (1.5). We find the average value with respect to Ψ of the function U_ν with the aid of (8.5):

$$\overline{U}_\nu = -\frac{a_0 R_0^2}{\sqrt{\mu P}} \cos \vartheta \sin \rho \cos(\sigma - \nu), \tag{8.6}$$

i.e., it has the form (1.25a); therefore, according to (1.28), the trajectory of the trace of the vector **L** is given by the formulas

$$\Phi = L_0 \cos\rho - \frac{a_0 R_0^2}{\sqrt{\mu P}} \cos\vartheta \cos\Psi = \text{const}, \tag{8.7}$$

$$\cos\Psi = \sin\rho \cos\bar{\varphi}, \quad \bar{\varphi} = \sigma - \nu. \tag{8.8}$$

Trajectory (8.7) is closed in a coordinate system rotating together with the radius vector R. Substituting (8.7)-(8.8) in (1.26), we can obtain the rates of change in the coordinates in the rotating system; however, the motion in Trajectory (8.7) allows a simpler interpretation. Let

$$n_0 = \frac{a_0 R_0^2}{L_0 \sqrt{\mu P}} \cos\vartheta, \tag{8.9}$$

$$\tan\rho^* = -n_0. \tag{8.10}$$

Then it turns out that Trajectory (8.7) on a unit sphere is a family of concentric circles

$$\cos\chi = \text{const} \tag{8.11}$$

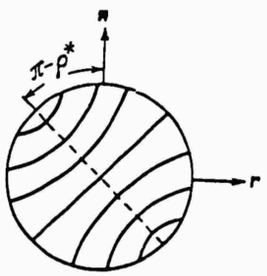

Fig. 14.

with the poles

$$\begin{aligned} &\text{a)}\ \varphi_1 = 0 \quad \rho_1 = \rho^*, \\ &\text{b)}\ \varphi_2 = \pi \quad \rho_2 = \pi - \rho^*, \end{aligned} \tag{8.12}$$

where ρ* is determined from (8.10). In Formula (8.11) χ denotes the angular distance from the first of the poles in (8.12) to the vector **L**. The trajectories for $n_0 > 0$ are shown in Fig. 14. Let λ_χ denote the angle of rotation of the vector **L** around the pole. Then the velocity of rotation of the vector **L** is given by the formula

$$\frac{d\lambda_\chi}{d\nu} = -\sqrt{1 + n_0^2}. \tag{8.13}$$

From (8.10) and (8.13) it can be seen that if the moments of light-pressure forces are small ($n_0 \approx 0$), the direction toward the pole is almost perpendicular to the orbital plane, and the velocity of motion $d\lambda_\chi/d\nu$ of the kinetic-momentum vector in the rotating coordinate system is close to -1, i.e., in a stationary coordinate system the vector **L** remains almost invariable. On the other hand, at high values of n_0 the stabilizing effect of light pressure is felt, and Poles (8.12) shift in the direction of the instantaneous radius vector ($\rho^* \to \pi/2$), while Velocity (8.13) increases. Similar results were reported to the author by D. Ye. Okhotsimskiy. Let us now consider Case 2.

2. $a = a_1 \cos \varepsilon$. Then

$$U_\nu = -\frac{a_1 R_0^2}{2\sqrt{\mu P}} \cos^2 \varepsilon, \tag{8.14}$$

$$\overline{U}_\nu = -\frac{a_1 R_0^2}{2\sqrt{\mu P}}\left(1 - \frac{3}{2}\sin^2 \vartheta\right) \sin^2 \rho \cos^2 (\delta - \nu). \tag{8.15}$$

The function $\overline{U}_\nu$ again has the form (1.25a); therefore, according to (1.27), the trajectory of the vector **L** in a rotating coordinate system will be

$$L_0 \cos \rho - \frac{a_1 R_0^2}{2\sqrt{\mu P}}\left(1 - \frac{3}{2}\sin^2 \vartheta\right) \cos^2 \Psi = \text{const}, \tag{8.16}$$

where Ψ is determined from (8.8).

The equations of motion in the coordinates ρ, σ, according to (8.15) and (1.22), have the form:

$$\frac{d\rho}{d\nu} = -\frac{a_1 R_0^2}{L_0 \sqrt{\mu P}}\left(1 - \frac{3}{2}\sin^2 \vartheta\right) \sin \rho \cos (\sigma - \nu) \sin (\sigma - \nu),$$

$$\frac{d\sigma}{d\nu} = -\frac{a_1 R_0^2}{L_0 \sqrt{\mu P}}\left(1 - \frac{3}{2}\sin^2 \vartheta\right) \cos \rho \cos^2 (\sigma - \nu). \tag{8.17}$$

Equations (8.17) completely coincide with the equations of motion (2.7) under the action of gravitational moments, if in (2.7)

we merely put e = 0 and choose N_0 appropriately. Therefore all the results of Section 2 for a circular orbit carry over to the given case of the effect of light pressure on the elliptical orbit of a solar satellite, if $N_0 = \varkappa$, where $\varkappa$ is determined by the formula:

$$\varkappa = -\frac{a_1 R_0^2}{L_0 \sqrt{\mu p}}\left(1 - \frac{3}{2}\sin^2\theta\right). \tag{8.18}$$

The main results of Section 2 refer to the case $|\varkappa| < 1$, for which the trajectories are shown in Fig. 4. In this case the stabilizing action of the light pressure is felt very slightly. For $|\varkappa| > 1$ the trajectories are shown in Fig. 5. Here the stabilizing action of the light pressure is already felt substantially, and there are regions in which the vector **L** "tracks" the radius vector of the orbit.

The poles of these regions are given by the formulas:

$$\varphi^* = 0, \pi, \quad \cos\rho^* = \frac{1}{\varkappa}. \tag{8.19}$$

Let us consider the case $\varkappa > 0$, to which the case $\varkappa < 0$ can be reduced without difficulty. The trajectories of the vector **L** are given in Fig. 5. The first of Eqs. (8.18) can be written in the form

$$\frac{d\rho}{d\nu} = \varkappa \sin\rho\cos\varphi\sin\varphi, \tag{8.20}$$

where, according to (8.16):

$$\cos^2\Psi + \frac{2}{\varkappa}\cos\rho = C_0. \tag{8.21}$$

Hence, taking (8.8) into account:

$$\cos\varphi = \frac{\sqrt{C_0 - \frac{2}{\varkappa}\cos\rho}}{\sin\rho}, \quad \sin\varphi = \frac{\sqrt{1 - \cos^2\rho - C_0 + \frac{2}{\varkappa}\cos\rho}}{\sin\rho}. \tag{8.22}$$

Substituting in (8.20), we obtain

$$\frac{dx}{dv} = -\sqrt{2\varkappa}\sqrt{\left(x-\frac{\varkappa}{2}C_0\right)\left[x^3-\frac{2}{\varkappa}x+C_0-1\right]} \quad (x=\cos\rho). \tag{8.23}$$

Taking into account that, according to (8.21) and (8.8):

$$C_0 = \cos^2\varphi_0 \sin^2\rho_0 + \frac{2}{\varkappa}\cos\rho_0 \tag{8.24}$$

and choosing the initial value of ν in such a way that when

$$\nu = \nu_0,\ \varphi_0 = 0, \tag{8.25}$$

we find that the polynomial under the radical sign in (8.23) has the roots

$$x_1 = \cos\rho_0 + \frac{\varkappa}{2}\sin^2\rho_0,\ x_2 = \frac{2}{\varkappa} - \cos\rho_0,\ x_3 = \cos\rho_0. \tag{8.26}$$

The following three cases are possible:

$$\begin{aligned} &\text{a)}\ x_2 > x_1 > x_3 \text{ when } -1 < \cos\rho_0 < \frac{2}{\varkappa} - 1, \\ &\text{b)}\ x_1 > x_2 > x_3 \text{ when } \frac{2}{\varkappa} - 1 < \cos\rho_0 < \frac{1}{\varkappa}, \\ &\text{c)}\ x_1 > x_3 > x_2 \text{ when } \frac{1}{\varkappa} < \cos\rho_0 < 1. \end{aligned} \tag{8.27}$$

In case "a" integration of Eq. (8.23) gives

$$\begin{aligned} &\cos\rho = \cos\rho_0 + \frac{\varkappa}{2}\sin^2\rho_0\,\mathrm{sn}^2(u, k), \\ &u = \sqrt{1-\varkappa\cos\rho_0}\,(\nu-\nu_0),\ k = \frac{\varkappa\sin\rho_0}{2\sqrt{1-\varkappa\cos\rho_0}}. \end{aligned} \tag{8.28}$$

This case corresponds to rotation around the normal to the orbital plane (Fig. 5). Instead of the second coordinate φ, it is more convenient to write out, according to (8.21), the angular distance Ψ from the radius vector of the orbit. We obtain

$$\cos\Psi = \cos\Psi_0\,\mathrm{cn}(u, k), \quad \cos\Psi_0 = \sin\rho_0. \tag{8.29}$$

The total period of rotation of the vector **L** will be

$$T = 4K(k^2)\sqrt{1-\varkappa\cos\rho_0}. \tag{8.30}$$

In case "b" the motion will occur in the neighborhood of the instantaneous radius vector of the orbit (Fig. 5), and integration of Eq. (8.23) gives

$$\cos\rho = \cos\rho_0 + 2\left(\frac{1}{\varkappa} - \cos\rho_0\right)\mathrm{sn}^2(u, k),$$
$$u = \frac{\varkappa}{2}\sin\rho_0\,(\nu - \nu_0),\quad k = \frac{2\sqrt{1-\varkappa\cos\rho_0}}{\varkappa\sin\rho_0}. \tag{8.31}$$

The total period of rotation of the vector **L**:

$$T = \frac{4K(k^2)}{\varkappa\sin\rho_0}, \tag{8.32}$$

while the angle Ψ is determined from the formula

$$\cos\Psi = \cos\Psi_0\,dn\,(u, k),\ \cos\Psi_0 = \pm\sin\rho_0. \tag{8.33}$$

Case "c" gives the same trajectories as case "b", but they are read off from the other extremum. However, for these trajectories it is convenient to write independent formulas:

$$\cos\rho = \cos\rho_0 - 2\left(\cos\rho_0 - \frac{1}{\varkappa}\right)\mathrm{sn}^2(u, k),$$
$$u = \sqrt{\frac{\varkappa^2}{4}\sin^2\rho_0 + \cos\rho_0(\varkappa - 1)}\,(\nu - \nu_0),$$
$$k = \frac{2\sqrt{\varkappa\cos\rho_0 - 1}}{\sqrt{\varkappa^2\sin^2\rho_0 + 4\cos\rho_0(\varkappa - 1)}}, \tag{8.34}$$
$$T = \frac{4K(k^2)}{\sqrt{\varkappa^2\sin^2\rho_0 + 4\cos\rho_0(\varkappa - 1)}},$$
$$\cos\Psi = \cos\Psi_0\,\mathrm{dn}\,(u, k),\ \cos\Psi_0 = \pm\sin\rho_0.$$

Narurally, when we substitute cos $\rho_0 \to 2/\varkappa$ - cos ρ_0 and vary the oscillation phase by T/2, Formulas (8.34) become Formulas (8.29)-(8.33).

Up to this time we have considered the case $\varkappa > 0$. If, on the other hand, $\varkappa < 0$, the substitution of $\bar{\rho} = \pi - \rho$ instead of ρ and $|\varkappa|$ instead of $\varkappa$ in the above formulas gives the solution for this case.

In conclusion, let us note that the above results are also applicable to a satellite with three unequal principal central moments of inertia, if the force moment has the form (8.1), where $\mathbf{k}''$ is a unit vector along one of the principal central axes of inertia (major or minor). The angle of nutation ϑ in this case should be averaged when introduced into the formulas. For the case of pure unperturbed rotation ($\vartheta = 0$) the results are completely applicable. A similar generalization is permissible with the above reservations for these same moments of other forces not depending on the moments of inertia of the body. The formulation of a theory of perturbed motion of a triaxial satellite under the action of gravitational moments, and also under the action of moments of forces of any nature requires a more rigorous analysis and formulation of the equations in osculating elements for the triaxial case, as was done, for example, in the article by F. L. Chernous'ko [17]. In this article the effect of gravitational moments on a triaxial satellite is considered, and the equations of motion for this case are reduced to the same form (2.7) as in the case of a biaxial satellite, except that the constant coefficient N_0 has a more complex structure and depends on the three moments of inertia A, B, C of the satellite.

Conclusion

The analysis carried out shows that the general equations in osculating elements (Section 1) are an effective apparatus for studying perturbed motion of a satellite. The main qualitative effects of motion studied in the present article are systematized in the table. The perturbing factors investigated are listed in

the first column; in the other columns the effects caused by these factors are described. The table is divided into two parts: effects of the 1st approximation are considered in the first part; additional effects revealed during an analysis of the 2nd approximation are indicated in the second part of the table; an analysis of the solution in the second approximation also enabled us to disclose certain "stabilizing" effects in an orbital (rotating) coordinate system; some of these effects are indicated in a special column in the second part of the table.

In the table the following notations are used:

$\mathbf{L}$, $|\mathbf{L}|$ = the kinetic-momentum vector and its absolute value,

$\mathbf{n}$ = the vector of the normal to the orbital plane,

$\boldsymbol{\tau}$ = the vector of the transversal of the orbit,

$\mathbf{r}$ = a vector along the direction of the instantaneous radius of the orbit,

$\mathbf{H}$, $\mathbf{H}_{av}$, $\mathbf{H}'_{av}$ = the vector of the earth's magnetic field strength and some of its "average" values,

$\boldsymbol{\tau}_{\pi}$ = a vector in the direction of the perigean tangent to the orbit,

i = the inclination of the orbit toward the equator,

$\bar{X}\bar{Y}\bar{Z}$ = a right-handed coordinate system connected to the earth and the orbit,

$\bar{Y}$ is parallel to the earth's axis,

$\bar{Z}$ is parallel to the nodal line of the orbit,

e = the eccentricity of the orbit,

W_0 = the angular velocity of rotation of the atmosphere (together with the earth),

A, C = the transverse and longitudinal moments of inertia of the satellite,

I_3, I_1 = the coefficients of aerodynamic dissipation along the transverse and longitudinal axes,

k_1'', k_0'' = the coefficients of electromagnetic dissipation (from eddy currents) along the transverse and longitudinal axes,

ϑ, $\dot{\psi}$, n = elements of the regular precession relative to the vector **L**: the angle of nutation, the angular velocity of precession, the axial component of the angular velocity (in Sections 2-8, instead of $\underline{n}$, we used the notation $\underline{r}$).

Within the framework of this table the most significant direction for further theoretical studies is a more accurate analysis of the role of dissipative effects. It seems probable that an analysis of the second approximation should reveal, for example, an asymptotic tending of the vector **L** toward certain moving directions (connected, for example, to the instantaneous vectors of velocity or magnetic strength).

More important, apparently, is an analysis of the combined effect of various factors and a comparison of the theoretical analysis and the observations of the actual motion of satellites relative to the center of mass. A number of studies have already been carried out in these directions. A theoretical analysis of the combined effect of aerodynamic and gravitational perturbations is given in an article by the author [9]. A number of effects in the rotation of the third Soviet artificial earth satellite [18] agreed with the theory. In the articles by Colombo and Naumann [1, 2, 19] the results of a numerical analysis of the combined effect of secular gravitational and magnetic perturbations are brought into good agreement with the results of observations of the rotation of certain American satellites. These studies will definitely be continued and developed.

TABLE

Main Effects of Perturbed Rotation of a Symmetrical Satellite

Perturbations		1st approximation (secular motion)			2nd approximation		
		Motion of the kinetic-momentum vector L		Motion relative to L	Motion of L		Motion relative to L
		Main effect	Other effects		Effects of supplementing the 1st approximation	Motion in the rotating system n, τ, r	
The presence of a force function	Gravitational	Precession relative to m	None	Regular precessions $\theta = \text{const}, n = \text{const}, \dot{\psi} = \text{const}$ (L = const)	Nutation relative to m	When e ≠ 0, a closed trajectory around m	Regular precessions $\theta = \text{const}, n = \text{const}, \dot{\psi} = \text{const}$ (L = const)
	Aerodynamic pressure	a) $e \neq 0$ precession around τ_π	1. Nutation relative to τ_π 2. A shifting of the precession pole due to W_0 3. Possible precession (and nutation) relative to m		Nutation relative to τ_π	When e ≠ 0, a closed trajectory with its pole on the meridian mv	
		b) $e = 0$ None	1. Possible precession relative to m				
	Constant symmetrical magnetic field of the satellite	Precession around H_{av} ($\theta \neq 90°$)	None		Precessional-nutational motion of the vector L completely described by Eqs. (1.22), (6.6), (6.10)-(6.11)	—	
	Magnetization of the satellite shell	Precessional-nutational motion a) around the pole on the meridian $\overline{YX}$ b) around the axis $\overline{Z}$				—	
	Light pressure	—	—		—	A closed trajectory with its pole on the meridian mr	
	Aerodynamic friction	1°. $e = 0 \mid L \mid \to 0$ 2°. $e \neq 0 \mid L \mid \to 0$: $\frac{L}{\mid L \mid} \to \frac{\tau_\pi}{\mid \tau_\pi \mid}$		$\dot{\psi} \to 0$; $n \to 0$ $\theta \to \begin{cases} 0, & \frac{I_1}{C} - \frac{I_2}{A} < 0 \\ \frac{\pi}{2}, & \frac{I_1}{C} - \frac{I_2}{A} > 0 \end{cases}$	—	—	
Dissipative effects	Eddy currents	1°. $i \neq 0 \mid L \mid \to 0$: $\frac{L}{\mid L \mid} \to \frac{H_{av}}{\mid H_{av} \mid}$		$\dot{\psi} \to 0$; $n \to 0$ $\theta \to \begin{cases} 0, & \frac{k'}{C} - \frac{k'}{A} < 0 \\ \frac{\pi}{2}, & \frac{k'}{C} - \frac{k'}{A} > 0 \end{cases}$			
		2°. $i = 0 \mid L \mid \to 0$: $\frac{L}{\mid L \mid} \to \frac{H}{\mid H \mid}$ (H = const)		a) $\frac{k'}{C} - \frac{k'}{A} < 0$ $\theta \to 0$; $\dot{\psi} \to 0$ $n \to n^\circ \neq 0$ b) $\frac{k'}{C} - \frac{k'}{A} > 0$ $\theta \to \frac{\pi}{2}$; $n \to 0$ $\dot{\psi} \to \dot{\psi}^\circ \neq 0$	—	—	

Finally, one more direction for further study should be noted: an analysis of the perturbing factors not considered (or considered very cursorily) until now, the ascertaining of new perturbing factors, and an analysis of their effect on the rotation of a satellite.

Received on
July 1, 1963

REFERENCES

1. R. I. Naumann. Preprint. Amer. Astron. Soc., No. 46, 30, 1962.

2. G. Colombo. Preprint. Amer. Astron. Soc., No. 45, 20, 1962.

3. Y. Hagihara. Smithsonian Contribs Astrophys. 5, No. 9, 113, 1961.

4. P. Notni, and H. Oleak. Veröff. Sternwarte Babelsberg, 13, No. 3, 1959; 13, No. 5, 45, 1960.

5. I. W. Warwick. Planetary and Space Sci., No. 1, 43-49, 1959.

6. Yu. V. Zonov. Sb. "Iskusstvennyye sputniki Zemli", No. 3, Izd-vo AN SSSR, 1959, pp. 118-124.

7. H. B. Rosenstock. Astronaut. Acta, 3, No. 3, 215, 1957.

8. V. V. Beletskiy. Sb. "Iskusstvennyye sputniki Zemli", No. 1, Izd-vo AN SSSR, 1958, pp. 26-43.

9. V. V. Beletskiy. Sb. "Iskusstvennyye sputniki Zemli", No. 6, Izd-vo AN SSSR, 1961, pp. 11-32.

10. N. N. Bogolyubov and Yu. A. Mitropol'skiy. Asimptoticheskiye metody v teorii nelineynykh kolebaniy. Gostekhizdat, 1955.

11. V. V. Beletskiy. Sb. "Iskusstvennyye sputniki Zemli", No. 3, Izd-vo AN SSSR, 1959, pp. 13-32.

12. A. A. Karymov. Prikl. matem. i mekhan., 26, No. 5, 867, 1962.

13. L. D. Landau and Ye. M. Lifshits. Elektrodinamika sploshnykh sred. Gostekhizdat, 1957.

14. L. D. Landau and Ye. M. Lifshits. Teoriya polya. Fizmatgiz, 1960.

15. V. A. Vdovin. Diplomnaya rabota. Moskovskiy fiziko-tekhnicheskiy in-t, 1963 (manuscript).

16. S. S. Yegorov. Diplomnaya rabota. Moskovskiy gosudarstvennyy universitet, 1963 (manuscript).

17. F. L. Chernous'ko. Prikl. matem. i mekhan., 27, No. 3, 474, 1963.

18. V. V. Beletskiy and Yu. V. Zonov. Sb. "Iskusstvennyye sputniki Zemli", No. 7, Izd-vo AN SSSR, 1961, p. 32.

19. R. I. Naumann. Dynamics of Satellites. Symposium, Paris May 28-30, 1962, Springer-Verlag, Berlin, 1963, p. 237.

ON THE ADIABATIC INVARIANTS OF MOTION OF A CHARGED PARTICLE IN A STATIONARY HETEROGENEOUS MAGNETIC FIELD

V. D. Plemnex and G. A. Skuridin

On the basis of the classical theory of adiabatic invariants, we examined the conditions of retaining conservation the first, second, and third invariants of the motion of a charged particle in a spatial magnetic system. Since such a motion of a particle in a magnetic field is not strictly conditionally periodic, theoretically there can be a divergence of the adiabatic approximation related to the inseparability of variables in the Hamilton-Jacobi equation.

The problem is raised concerning estimation of the accuracies of conserving the second and third invariants in a stationary magnetic field.

I. FORMULATION OF THE PROBLEM

1. Method of Averaging

As is known, motion of a charged particle in a stationary heterogeneous magnetic field is described by equations:

$$\frac{d\mathbf{v}}{dt} = \mathbf{F} + \frac{e}{mc}[\mathbf{v}\times\mathbf{H}], \quad \frac{d\mathbf{r}}{dt} = \mathbf{v}, \tag{I.1}$$

where $\mathbf{F} = e\mathbf{E}/m$ is the force acting on the particle in an electrical field, $\mathbf{v}$ is the velocity of the particle, and $\mathbf{H}$ is the magnetic

field. The rigorous solution of system (I.1) has considerable mathematic difficulties. Therefore, a number of methods for approximate solution of system (I.1) has been presently developed. One of the methods which is widely used is the so-called method of averaging, whose principles were previously established [1]. This method was subsequently developed [2, 3], while fundamental consideration was given to the theory of adiabatic invariants of the motion of a particle (or system of particles) [3].

Actually, the averaging method is one of the methods of the classical theory of perturbations. The theory of perturbations is in a less complete mathematical form, but was previously applied with greater clarity to the motion of a charged particle in stationary heterogeneous electrical and magnetic fields [4-6].

The physical sense of the method of averaging is as follows. In a zero approximation the true field is the actual heterogeneous magnetic field, averaged with respect to the volume of one Larmor rotation of a particle. Thus, the averaged heterogeneous magnetic field is replaced by the homogeneous field corresponding to it within one Larmor rotation of a particle.

Hence, the true motion of a particle in a zero approximation can be substituted by the motion of its center of rotation around magnetic lines of force or the so-called guiding center of the particle. Such averaging results in the regular heterogeneity associated with the constant gradient of a magnetic field perpendicular to the axis of the magnetic tube of force, which should be regarded in the first approximation. The effect of the remaining heterogeneities, causing deviations in the motion of a particle from the averaged motion, is mutually compensated owing to

symmetric rotation of the particle around a magnetic line of force. The presence of the constant gradient of the magnetic field perpendicular to this field causes the particle to drift perpendicular to the magnetic line of force. Drift of a particle due to distortion of the magnetic line of force is also added to this drift. Therefore, the equations of motion of a particle in a first approximation are called the drift approximation.

On the basis of these considerations, the solution of system of (I.1) is sought [1] as

$$x_k = \langle x_k \rangle - \sum_{n=1}^{\infty} \frac{1}{\omega_L^n} \xi_k^n (\langle \alpha \rangle, \langle x_1 \rangle, \ldots, \langle x_v \rangle), \qquad (I.2)$$

where x_k is the generalized coordinate of motion, α is the angle of rotation of a particle around a line of force in a plane perpendicular to this line, ω_L is the Larmor frequency. The mark $\langle \ldots \rangle$ denotes averaging over T_L, which is the period of Larmor rotation of a particle in a magnetic field. Here it is important to assume that $\omega_L \gg 1$*.

One of the results of using the method of averaging is the approximate conservation of the magnetic moment of a charged particle $\mu = mv_\perp^2/2H$, which in this case is an adiabatic invariant. The conditions of the conservation of μ as well as the degree of accuracy of this conservation follow directly from the classical mechanics of the motion of conditionally periodic systems and systems close to conditionally periodic.

Therefore, within the limits of the applicability of the method of averaging, it is expedient to study the character of the

---

*We can show that the method of averaging is essentially an asymptotic method which is at present widely used for solving many problems of mathematical physics.

motion of charged particles in a heterogeneous magnetic field based on the theory of adiabatic invariants which was developed in classical mechanics.

This examination as applied to the motion of a charged particle in an electromagnetic field has been carried out [7, 8].

This work examines the motion of a charged particle in a heterogeneous magnetic field based on a study of the conservation of all adiabatic invariants corresponding to the spatial symmetry of a magnetic system.

2. Elements of the Classical Theory of Adiabatic Invariants as Applied to the Motion of a Charged Particle in a Magnetic Field

The theory of adiabatic invariants in its most complete form was first developed by Yu. A. Krutkov, based on the methods of classical mechanics [9].

Yu. A. Krutkov examined the adiabatic invariants of conditionally periodic, cyclic, and erogodic systems, as well as the application of the theory of adiabatic invariants to quantum mechanics.

Previously, the value of the separability of variables in the Hamilton-Jacobi equation for adiabatic invariance was especially emphasized [9].

As is known [9, 10], if there is a system performing a homogeneous finite motion with period T in a field characterized by some parameter λ, and provided that

$$T\frac{d\lambda}{dt}\ll\lambda, \qquad (I.3)$$

then there is a combination of the energy of system $\mathcal{E}$ and parameter λ, which remains approximately constant. The degree of accuracy of

the approximation is limited by fulfillment of condition (I.3). This relationship between $\mathcal{E}$ and λ is an adiabatic invariant of a mechanical system. This adiabatic invariant for the system being examined in the most general case is a generalized impulse in the system of angle — action variables

$$I = \frac{1}{2\pi} \oint p dq, \qquad (I.4)$$

where integration is carried out along the closed trajectory on the phase plane of the generalized coordinates and of impulses $\underline{q}$ and $\underline{p}$. Condition (I.3) is actually a condition of linear change in time of energy ξ and parameter λ. Indeed, owing to (I.3) we can approximately assume that the complete energy of the system completing the motion changes with a velocity proportional to the velocity of change λ, i.e., $d\xi/dt \approx d\lambda/dt$ [10].

Thus, we disregrad the energy value for time T and approximately assume that the averaged values $\langle \mathcal{E} \rangle_T$ and $\langle \lambda \rangle_T$ are constant for time T and equal the effective values $\mathcal{E}$ and λ. When there is a system with many degrees of freedom which completes the periodic motion along each coordinate (so-called conditionally periodic system), expressions

$$I_k = \frac{1}{2\pi} \oint p_k dq_k \qquad (I.5)$$

can also be adiabatic invariants. However, in this case it is insufficient to only fulfill condition (I.3) for an approximate conservation of magnitudes I_k. For the adiabatic invariance of magnitudes I_k it is also necessary to fulfill the condition of complete separation of variables in the Hamilton-Jacobi motion equation [9, 11]. Mathematically, this condition is formulated as

the theorum of Stackler [9, 12], and physically it designates the complete independence of periodic motions on each other along each generalized coordinate.

Thus, under the condition of complete separation of variables and fulfillment of condition (I.3), I_k is an adiabatic invariant. An exception is the so-called case of degenerate systems where the frequencies of periodic motions along the generalized coordinates are commensurable i.e.,

$$\sum_{k=1}^{n} j_k \omega_k = 0, \tag{I.6}$$

where j_k are the integrals, and ω_k are the oscillation frequencies along each generalized coordinate q_k. A special case of disturbance of the invariance in a case of a two-dimensional oscillator during resonance of oscillations along each of the two coordinates was previously examined [8, 13].

As an illustration of an adiabatic homogeneous motion in mechanics we usually examine a one-dimensional oscillator whose Hamiltonian function is

$$G = \frac{p^2}{2m} + \frac{m\omega^2 q^2}{2}, \tag{I.7}$$

where ω is the normal mode of the oscillator. The equation of the phase trajectory here is found by the law of the conservation of energy

$$G(p; q) \quad \mathcal{E} = \text{const}. \tag{I.8}$$

Thus, the phase trajectory of a one-dimensional oscillator is an ellipse with semiaxes $\sqrt{2m\mathcal{E}}$ and $\sqrt{2\mathcal{E}/m\omega^2}$, and the area in this ellipse determine the magnitude of the adiabatic invariant

$$I = \frac{1}{2\pi}\int p\,dq = \frac{1}{2\pi}\iint dp\,dq = \frac{\mathcal{E}}{\omega}. \qquad \text{(I.9)}$$

Hence, with slow changes of the parameters of a one-dimensional oscillator (for instance, if ω changes adiabatically) the total energy of the system changes proportional to the frequency.

In the case of the motion of a charged particle in a slowly changing magnetic field (when parameter λ is the magnetic field strength H), a two-dimensional oscillator can be examined as the mechanical model. Motion along the azimuth here can be excluded, since it is not significant*. This examination was previously carried out [7, 8]. The corresponding mechanical system previously examined [7, 8] is a two-dimensional oscillator in which the material particle moves along a tube with plastic walls and reflects from these walls.

Let the coefficient of elasticity vary along the tube, increasing towards its ends. Then the kinetic energy of the longitudinal motion of the particle changes to energy of transverse motion, and the particle reflects from the ends of the tube, completing the periodic oscillations along the tube. The Hamiltonian of such a system is

$$G = \frac{x^2 + y^2 + \omega^2 y^2}{2}, \qquad \text{(I.10)}$$

where x is the coordinate along, and y is the coordinate across, the tube or magnetic field. Hence, the equations of motion of a particle in a tube are

---

*In zero approximation, as was pointed out above, the drift motion is generally disregarded.

$$\ddot{x} = -\frac{y^2}{2}\frac{d\omega^2}{dx}, \qquad \ddot{y} = -\omega^2 y. \tag{I.11}$$

Theoretically, we can substitute an examination of this two-dimensional oscillator by an examination of one-dimensional oscillations between the walls of a tube when the coefficient of elasticity varies as a function of time. The Hamiltonian of this new system will be

$$C = \frac{m\dot{y}^2 + m\omega^2(t)\,y^2}{2}. \tag{I.12}$$

In accordance with (I.9), during an adiabatic change of ω, and hence H, we arrive at the expression

$$I_1 = \frac{m\dot{y}^2 + m\omega^2 y}{2\omega}, \tag{I.13}$$

which is an adiabatic invariant. Changing from the motion of a mechanical system to the motion of a charged particle in magnetic field H, and accounting for the relationship

$$\dot{x}^2 = v_{\parallel}^2, \qquad \dot{y}^2 + \omega^2 y^2 = v_{\perp}^2, \tag{I.14}$$

we obtain [7]

$$I_1 = \frac{mv_{\perp}^2}{2\omega} = \frac{mc}{e}\mu, \tag{I.15}$$

where $\mu = mv^2 1/2H$.

An analogy of the coefficient of elasticity $m\omega^2$ for a magnetic field is the expression e^2H^2/mc^2.

Similarly, we can obtain two other adiabatic invariants of motion of charged particles in a magnetic field for a spatial case. Here, to obtain the second adiabatic invariant it is necessary to examine the motion of a charged particle averaged with respect to

T_e. If the conditions of this averaging are fulfilled, we can examine the oscillatory motion of a particle along a line of force and the drift motion as independent of the Larmor rotation of a particle (vibration). A one-dimensional oscillator can be examined as a mechanical analog of motion in an axiosymmetric magnetic field, since rotation about the axis of a magnetic system can be excluded owing to symmetry of the field. If the intensity of a magnetic field in the direction of drift changes sufficiently slowly, the motion has its own adiabatic invariant. The expression for this invariant is found especially simply if the problem is reduced to a one-dimensional oscillator with parameter H changing slowly in time. Then, according to (I.9), we obtain

$$I_2 = \frac{\langle \mathcal{E}_{\parallel} \rangle_{T_{osc}}}{\Omega}. \qquad (I.16)$$

Here the sign $< \ldots >_{T_{osc}}$ designates averaging with respect to the period of oscillations along a magnetic line of force. T_{osc} and Ω are the period and frequency of these oscillations, respectively. Thus

$$I_2 = \frac{\langle E_{\parallel} \rangle_{T_{osc}}}{\Omega} = \langle \mathcal{E}_{\parallel} \rangle_{T_{osc}} \cdot T_{osc} = \oint \frac{mv_{\parallel}^2}{2} \frac{ds}{v_{\parallel}}$$

or

$$I_2 = \frac{m}{2} \oint v_{\parallel} \, ds. \qquad (I.17)$$

Invariant I_2 is usually called the longitudinal adiabatic invariant or invariant of longitudinal action and is designated J.

To obtain the third adiabatic invariant let us examine the averaged motion of a particle with respect to the period of oscillations along the magnetic line of force. If the conditions of the

possibility of this averaging are fulfilled, then in this case the particle drifts in a stationary magnetic field over one and the same magnetic surface [14]. The magnetic surface over which the particle drifts (during absence of electric fields) is determined by $\mathcal{E}$, μ, and J. Since the magnetic flux across the transverse section of the drift surface does not change, conservation of J in the stationary field determines conservation of the so-called invariant of total flux

$$I_3 = \iint_S \mathbf{H} d\mathbf{S}. \qquad \text{(I.18)}$$

This invariant of the drift motion of charged particles in a magnetic field is usually designated by Φ. If there is a temporal change in the magnetic field, only a one-dimensional oscillator with a purely temporal change of parameters can be examined as the mechanical analog of drift motion. Based on (I.9), the adiabatic invariant here will be

$$I_3 \quad \oint \mathbf{u_d}\, d\mathbf{l} \quad \iint_S \mathbf{curl} \mathbf{u_d}\, d\mathbf{S}. \qquad \text{(I.19)}$$

Since the drift velocity of particles $\mathbf{u_d}$ with an accuracy up to a constant is determined by the vector potential of the magnetic field, we finally arrive at expression (I.18), i.e., the third adiabatic invariant. Approximation of the third adiabatic invariant in this case corresponds to averaging of the motion of a charged particle with respect to the period of its drift rotation (see Section II). Obtainment of these invariants is possible only on fulfillment of condition (I.3) and the approximated separations of motions as independent of each other with respect to each of the three coordinates. This separation of motions is accomplished in

systems close to the conditionally periodic. In particular, in a stationary heterogeneous magnetic field the possibility of this separation is related to the symmetry of the magnetic system.

II. CONDITIONS OF CONSERVATION OF ADIABATIC INVARIANTS IN A HETEROGENEOUS MAGNETIC FIELD

1. Conservation of the First Adiabatic Invariant

The condition of the approximated conservation of μ in a general case will be (I.3), where parameter λ is expressed by the magnetic field strength H, i.e.,

$$T_L \left| \frac{dH}{dt} \right| \ll H. \qquad \text{(II.1)}$$

For a stationary magnetic field condition, (II.1) assumes the form

$$T_L (v\nabla) H \ll H \qquad \text{(II.2)}$$

or

$$(\delta H)_L \ll H, \qquad \text{(II.3)}$$

where $(\delta H)_L$ is the change of field strength resulting from the motion of a charged particle over a trajectory along a magnetic line of force during time T_L. Condition (II.3) can be transformed to

$$(\delta H)_L = T_L \left(v_x \frac{\partial H}{\partial x} + v_y \frac{\partial H}{\partial y} \right) = T_L v_x \left(\frac{\partial H}{\partial x} + \frac{dy}{dx} \frac{\partial H}{\partial y} \right) = \qquad \text{(II.4)}$$
$$= v_y T_L \frac{v_x}{v_y} \frac{dH}{dx} = \rho_L \frac{v_\parallel}{v_\perp} \frac{dH}{dx} \ll H,$$

ρ_L is the Larmor radius.

Previously [2, 6], a special form of condition (II.4), corresponding to the case where $v_\perp \sim v_{||}$ was used. Then (II.4) can reduce to condition

$$\rho_L \frac{dH}{dx} \ll H \quad \text{or} \quad \rho_L \frac{\partial H}{\partial y} \ll H.$$

The causes, due to which an additional condition of applicability of an adiabatic approximation becomes necessary in the form

$$v_\perp \sim v_\parallel, \tag{II.5}$$

will be explained below.

On examination of the mechanical models of motion of a charged particle in a heterogeneous magnetic field, we assume that we are dealing with a conditionally periodic system. However, this is not entirely correct. The system of a charged particle in a strong magnetic field can be arbitrarily close to conditionally periodic, but nevertheless differs from the latter in that the total separation of variables in the Hamilton-Jacobi equation for such a system can be carried out only approximately. The fundamental purpose of the method of averaging, by which we obtain in an axiosymmetric magnetic field three periodic motions of a charged particle, is to separate the Larmor rotation (so-called "vibrations" of a charged particle) from drift about the axis of symmetry of the field and the oscillations of the particle along a magnetic line of force. The method of averaging allows us to carry out a corresponding separation of variables correct to any degree of expansion with respect to $1/\omega_L$. However, the character of expansion itself requires here some additional conditions of the applicability

of approximation.

Let us examine some examples. Let the velocity vector of a charged particle at the initial time of motion be directed tangentially to a magnetic line of force. Then $v_{\perp i} = 0$ and $\mu_i = 0$, (i = initial). Since a line of force of a heterogeneous magnetic field is distorted, during some subsequent instant, as is obvious from the simple mechanics of motion, $\mu \neq 0$, i.e., the magnetic moment of a charged particle changes, although its energy can be arbitrarily low, and the field arbitrarily strong. Condition (II.4) when $v_{\perp i} = 0$ leads to an indeterminate form, since $\rho_{\perp i} = 0$.

As another example, let us examine the case where $v_{\perp i} = 0$. Here the amplitude of oscillations of a particle along a magnetic line of force is of one order of magnitude with "vibrations" of the particle around a magnetic line of force. As was previously shown [2], as a result of "vibrations" within T_L the magnetic moment of a charged particle will not be a constant magnitude, but averaged over T_L it is constant. Hence, within T_L the amplitude of oscillations changes along a line of force. However, if the initial amplitude of oscillations is equal to zero, we cannot disregard the relation between oscillations along a line of force and "vibrations", since the contribution of "vibrations" to oscillations along a magnetic line of force will not be infinitesimal, in comparison with the amplitude of oscillations of the particle. Thus, when $v_{||i} = 0$, μ is not an adiabatic invariant, since the motion of a particle along a magnetic line of force and its "vibrations" around the line of force will not be independent. It is easy to verify the above through a mathematical examination of a first-order expansion with respect to $1/\omega_L$ [2]. This expansion has the

following form

$$r = \langle \bar{r} \rangle + \langle \rho_L \rangle (e_3 \cos \langle \alpha \rangle - e_2 \sin \langle \alpha \rangle),$$

$$v_\parallel = \langle v_\parallel \rangle - \frac{\langle v_\parallel \rangle \langle v_\perp \rangle}{\langle \omega_L \rangle} e_2 \frac{\partial e_1}{\partial x_1} \sin \langle \alpha \rangle + \frac{\langle v_\perp \rangle^2}{4 \langle \omega_L \rangle} \left(e_2 \frac{\partial e_1}{\partial x_3} + e_3 \frac{\partial e_1}{\partial x_2} \right) \cos 2 \langle \alpha \rangle - \quad \text{(II.6)}$$

$$- \frac{\langle v_\parallel \rangle^2}{4 \langle \omega_L \rangle} e_3 \frac{\partial e_1}{\partial x_2} \sin 2 \langle \alpha \rangle, \quad \text{(II.7)}$$

$$v_\perp = \langle v_\perp \rangle - \frac{\langle v_\parallel \rangle \langle v_\perp \rangle}{4 \langle \omega_L \rangle} \left(e_2 \frac{\partial e_1}{\partial x_3} + e_3 \frac{\partial e_1}{\partial x_2} \right) \cos 2 \langle \alpha \rangle +$$

$$+ \frac{\langle v_\parallel \rangle^2}{\langle \omega \rangle_L} e_2 \frac{\partial e_1}{\partial x_1} \sin \langle \alpha \rangle + \frac{\langle v_\parallel \rangle \langle v_\perp \rangle}{4 \langle \omega_L \rangle} \left(e_2 \frac{\partial e_1}{\partial x_2} - e_3 \frac{\partial e_1}{\partial x_3} \right) \sin 2 \langle \alpha \rangle. \quad \text{(II.8)}$$

Here $\underline{r}$ is the radius vector of the point where the charged particle is located, $v_\perp$ and $v_{||}$ are velocity components perpendicular and parallel respectively to the magnetic field strength vector, α is the angle of rotation of a particle in a plane which is perpendicular to **H**, and e_1, e_2, e_3 and x_1, x_2, x_3 are the unit vectors and coordinates, respectively, in a system of coordinates which is congruent with the magnetic line of force, i.e., e_1 coincides at each point with a direction tangential to the magnetic line of force, and e_2 and e_3 are determined by the relationships

$$e_2 = [e_3; e_1], \; e_3 = [e_1; e_2], \; e_1 = [e_2, e_3]. \quad \text{(II.9)}$$

In Eqs. (II.6)-(II.8) the systematic motion, defined by the terms $\langle \bar{r} \rangle$, $\langle v_\perp \rangle$, and $\langle v_{||} \rangle$, is separated from vibrations of a particle defined by the terms containing sin $\langle \alpha \rangle$ and cos $\langle \alpha \rangle$ correct to the terms of expansion of order of smallness $1/\omega_L^2$. In addition, from (II.6)-(II.8) it is apparent that the terms which correspond to "vibration" are terms of a higher order of

smallness than those of systematic motion. Thus, in Eq. (II.6) the term $\langle \mathbf{r} \rangle$, which describes the motion of the guiding center of a particle, is much larger than the term describing the Larmor rotation of a particle ("vibration") averaged over T_L. Actually, if $\omega_L \gg 1$, then $\langle \mathbf{r} \rangle \gg \rho_L$, since $\langle \rho_L \rangle = \langle v_\perp \rangle / \omega_L$. Therefore, the equations of motion of a particle obtained by the method of averaging, describe the motion of the guiding center of a particle, and in equalities (II.6) - (II.8) in a zero approximation we can obtain

$$v_\perp = \langle v_\perp \rangle, \; v_\parallel = \langle v_\parallel \rangle \text{ and } r = \langle r \rangle.$$

However, if $\langle v_{||} \rangle = 0$ at any instant of time, then it follows from (II.7) that

$$v_\parallel = \frac{\langle v_\perp \rangle^2}{4\langle \omega_L \rangle} \left(\mathbf{e}_2 \frac{\partial \mathbf{e}_1}{\partial x_3} + \mathbf{e}_3 \frac{\partial \mathbf{e}_1}{\partial x_2} \right) \cos 2\langle \alpha \rangle - \frac{\langle v_\perp \rangle^2}{4\langle \omega_L \rangle} \mathbf{e}_2 \frac{\partial \mathbf{e}_1}{\partial x_2} \sin 2\langle \alpha \rangle. \qquad \text{(II.10)}$$

Hence, $v_{||} \neq 0$, and as a result of "vibrations" related to a perpendicular motion of a particle $\langle v_{||} \rangle \neq 0$ can appear at some subsequent moment and lead to the nonconservation of the adiabatic invariant. Therefore, when $\langle v_{||} \rangle = 0$, the term of "vibrations" and the possible temporal divergence of the discarded terms of expansion, relating "vibrations" and systematic motion, are not negligible.

When $\langle v_\perp \rangle = 0$, from (II.8) we obtain

$$v_\perp = \frac{\langle v_\parallel \rangle^2}{\langle \omega_L \rangle} \mathbf{e}_2 \frac{\partial \mathbf{e}_1}{\partial x_1} \sin \langle \alpha \rangle. \qquad \text{(II.11)}$$

As is obvious from (II.11), the impossibility of an approximate separation of systematic motion and "vibrations" here is related to the parallel motion of the magnetic line of force of a charged

particle, which after a certain time leads to the appearance of $\langle v_\perp \rangle \neq 0$ and nonconservation of the adiabatic invariant. Our purpose is not an investigation of the nonconservation of μ when condition (II.5) is not fulfilled. However, as follows from above, this disturbance is theoretically possible and the results which were previously obtained [2, 4-6] are clearly valid for condition (II.5), although this condition is possibly too strong in special cases.

In addition, it is obvious that a more general condition relating $v_\perp$ and $v_{||}$ should exist which broaches all cases of conserving the first invariant.

2. Conservation of the Second and Third Adiabatic Invariants

The condition of the conservation of the second invariant for a magnetic field will be the condition

$$T_{\text{osc}} \left| \frac{dH}{dt} \right| \ll H. \qquad \text{(II.12)}$$

In the case of a stationary magnetic field, condition (II.12) has the form

$$\frac{v_d}{v_{||}} \frac{dH}{dl} v_\perp T_{\text{osc}} \ll H. \qquad \text{(II.13)}$$

Here dl is the element of arc of the drift motion of a particle. From (II.13) it is obvious that if $v_{||} = 0$, we obtain the same indeterminate form as in condition (II.14) when $v_\perp = 0$. This indeterminate form was characterized above. It should be remembered that conditions (II.4) and (II.13) are actually integral conditions. For instance, during oscillations of a particle between magnetic mirrors, the field can change by a considerable magnitude, but due

to the symmetry of motion relative to the equatorial plane, we have

$$\oint \frac{u_d}{v_\parallel} \frac{dH}{dl} ds \ll H, \qquad \text{(II.14)}$$

where $ds = v_{||}dt$. Condition (II.4) also has an integral character, since it implies that in a stationary magnetic field

$$\int_0^{\rho_L} \frac{v_\perp}{v_-} \frac{dH}{ds} dr \ll H. \qquad \text{(II.15)}$$

For ideal axial symmetry of a magnetic system

$$\frac{u_d}{v_\parallel} \frac{dH}{dl} v_\perp T_{osc} = 0$$

and J is conserved within the "vibrations" of a charged particle in a drift approximation.

Condition (II.13) means that in the approximation J = const the displacement of a particle form the magnetic line of force for time T_{osc} is negligible.

As was already indicated, in a stationary magnetic field the conditions of conserving J determine the conservation of invariant ϕ. For a field changing in time, the condition of conservation ϕ will be

$$T_d \left| \frac{\partial H}{\partial t} \right| \ll H, \qquad \text{(II.16)}$$

where T_d is period of rotation of a particle around the axis of a magnetic system. Condition (II.16) results from condition (I.3) when $\lambda = \lambda(t)$.

The canonical equations of motion of a particle in an approximation of the average for T_{osc} were previously obtained [15]. It was shown that on averaging equations of drift approximation in a stationary magnetic field for T_{osc}, J will be an adiabatic invariant.

A more general case of conserving J in a magnetic field which is temporally changing was previously examined [14]. The canonical equations of motion of a charged particle in an approximation of averaging for T_d were also obtained, and it was shown that here the adiabatic invariant will be Φ. In addition to the conditions of slowness in the change of the magnetic field within time interval T_{osc} or T_d, it was also assumed [14, 15] that approximations $J = \text{const}$ and $\Phi = \text{const}$ are possible only if $\omega_L \gg \Omega \gg \Sigma$, where Σ is the frequency of drift rotation of a charged particle. The equations of motion of a particle which were averaged for T_{osc} and T_d were previously obtained [14, 15] in a zero approximation.

However, the conditions of the conservation of the second and third adiabatic invariants in the form of (II.12), (II.13), and (II.16) in these works was not examined.

III. ACCURACY OF CONSERVING THE SECOND AND THIRD INVARIANTS IN A STATIONARY MAGNETIC FIELD

When examining the question about conserving adiabatic invariants in a stationary heterogeneous magnetic field, the problem arises concerning the degree of accuracy of their conservation. This problem has fundamental interest, not only theoretical, but practical. Therefore, we must state some preliminary considerations concerning this problem, disregarding, for the time being, its complete mathematical solution*.

---

*The complete solution of this problem will be published in the next issues of this journal.

Adiabatic approximations of the second and third invariants are possible only when oscillatory motion along a magnetic line of force and the drift motion of a particle are completely (accurately and approximately) independent of each other. However, it is not completely obvious that on averaging equations of motion of a particle in approximation μ = const for T_{osc}, we will obtain approximation J = const, in which the drift motion was separated from the oscillatory motion with the same degree of accuracy with which averaging equations of motion for T separates the Larmor "vibrations" of a particle from oscillations along a magnetic line of force and from drift.

Actually, the component of the field gradient $\nabla_{\perp} H$ perpendicular to the magnetic line of force and the component of field gradient $\nabla_{||} H$ parallel to the magnetic line of force are interrelated by equation div **H** = 0. This relation can be eliminated with some degree of accuracy within time interval T_L when conditions (II.4) and (II.5) are valid, while the difference between the actual values $\nabla_{\perp} H$ and $\nabla_{||} H$ and those averaged for T_L will be of the same order of smallness.

Therefore, the motion of a particle about a magnetic line of force during T_L can be considered almost a symmetric rotation. Symmetry of Larmor rotation, in turn, results in the corrections of the actual motion toward $\langle \nabla_{\perp} H \rangle$ and $\langle \nabla_{||} H \rangle$ being mutually compensated within T_L with a high degree of accuracy since they are of the same order of smallness . Thus, motions of a particle perpendicular to Larmor rotation and parallel to the magnetic field become independent during a time much greater than T_L.

The examined symmetry of motion, related to corrections of an

identical order of smallness toward $\nabla_{\perp} H$ and $\nabla_{||} H$ in expansion by $1/\omega_L$, is not inherent to oscillatory and drift motions of a particle in an approximation of averaging for T_{osc}. If (II.13) implies a slow change of the magnetic field in a direction perpendicular to the magnetic line of force, then, as was previously pointed out, motion along a line of force results in large changes of field strength within T_{osc}. Therefore, motion of a particle in an approximation of averaging for T_{osc} will not have complete symmetry and will be symmetric only relative to some plane (for instance, relative to the equatorial plane of an axiosymmetric magnetic field). Actually, in an axiosymmetric magnetic field the assignment of specific μ, J, and $\mathcal{E}$ uniquely determines the surface of the motion of a particle, while this surface is completely symmetric relative to the axis of the magnetic system. Thus, a shift of the particle from this surface with respect to height, changes its longitudinal invariant J.

With a completely axiosymmetric magnetic field the left side of inequality (II.13) becomes zero, since the particle is not shifted from the invariant surface and the intensity of the magnetic field does not vary from drift. Here the symmetry of the magnetic system compensates the asymmetry of approximation J = const. The oscillatory and drift motions here will be approximately independent, and the terms responsible for the relation of these motions will be small magnitudes nondivergent in time. Theoretically, J in an axiosymmetric magnetic system will be a constant of the motion with the same accuracy as when μ = const. However, even with a small asymmetry of a magnetic system, the asymmetry of approximation J = const relative to the radial shifts of the particle can result in

a temporal increase of the terms of expansion relating the motion of a particle along a magnetic line of force to the drift motion, even if these terms are small magnitudes of a high order at each moment of time.

Let us estimate the magnitude of disturbance J due to the drift motion of a particle in a field which is not ideally axiosymmetric. As will be shown, the cumulative effect of disturbances J is caused by the temporal divergence of the term which was related to distortion of the magnetic tube of force along which the charged particle moves. Due to distortion, a relation arises between the velocities of drift of a particle and oscillatory motion, i.e., a term appears connecting both motions. Although this term is of the first or even higher order of smallness, the presence of small deviations from an ideal symmetry nevertheless causes its temporal divergence and cumulative effect of disturbances J. For this purpose, let us examine a case where conditions (II.4), (II.5), and (II.13)* are fulfilled.

To estimate divergence J, let us introduce some auxiliary expressions for $\mathbf{u}_d$ and curl H in system of coordinates $\mathbf{e}_1$; $\mathbf{e}_2$; $\mathbf{e}_3$.

For $\mathbf{u}_d$ we have

$$\mathbf{u}_d = \frac{1}{\omega_L} \mathbf{e}_1 \times \left(v_\parallel^2 \frac{\partial \mathbf{e}_1}{\partial s_1} + \frac{v_\perp^2}{2H} \nabla H \right). \qquad \text{(III.1)}$$

Expression (III.1) was previously obtained in a general form [2]. By transforming (III.1) we obtain

---

*This work does not examine the case of large disturbances of axial symmetry, or, what is identical, the case where condition (II.13) is not fulfilled.

$$u_{\parallel} = -\frac{v_{\perp}^2}{2\omega_L}\frac{1}{H}\frac{\partial H}{\partial x_2}e_2 + \left(\frac{\rho_1 v_{\parallel}^2}{\omega_L} + \frac{v_{\perp}^2}{2\omega_L}\frac{1}{H}\frac{\partial H}{\partial x_3}\right)e_3, \qquad \text{(III.2)}$$

where ρ_1 is the curvature of a magnetic line of force.

For curl **H**, according to previous works [16], we will have:

$$\text{curl } \mathbf{H} = \left(H\rho_1 - \frac{\partial H}{\partial x_2}\right)e_3 + \frac{\partial H}{\partial x_3}e_2 - H(\tau_2 + \tau_3)e_1, \qquad \text{(III.3)}$$

where τ_2 and τ_3 are secondary torsion coefficients corresponding to partial derivatives $\partial e/\partial x_2$ and $\partial e/\partial x_3$ [16]. From (III.3) is follows that if curl **H** = 0,

$$\rho_1 = \frac{1}{H}\frac{\partial H}{\partial x_2}, \quad \frac{\partial H}{\partial x_3} = 0, \quad \tau_2 + \tau_3 = 0, \qquad \text{(III.4)}$$

and the magnetic system is axial symmetric. If curl **H** $\neq$ 0, from (III.2) and (III.3) we have

$$u_d = \frac{v_{\parallel}^2 + v_{\perp}^2}{2\omega_L H}[e_1 \times \nabla H] + \frac{v_{\parallel}^2}{\omega_L H}\{\text{curl } \mathbf{H} - e_1(e_1 \text{ curl } \mathbf{H})\}. \qquad \text{(III.5)}$$

Thus, term

$$\frac{v_{\parallel}^2}{\omega_L H}\{\text{curl } \mathbf{H} - e_1(e_1 \text{ curl } \mathbf{H})\}$$

corresponds to the correlation between the curvature of the magnetic line of force, along which the particle oscillates at velocity $v_{\parallel}$, and distortion of the magnetic surface of drift motion related to the deviation from axial symmetry.

We will average expression (III.5) for T_{osc} and will find how the magnetic field strength **H** changes due to the drift of a particle at velocity $\langle u_d \rangle T_{osc}$. Let us note that terms $\frac{v_{\parallel}^2 + v_{\perp}^2}{2\omega_L H} \cdot [e_1 \times \nabla H]$ in (III.5) and $\frac{v_{\perp}^2}{2H}[e_1 \times \nabla H]$ in (III.1) do not change H on the drift surface. Thus, the magnetic invariant surface J = const will be determined by conditions

$$\left\langle \frac{v_{\parallel}^2}{\omega_L H} \{ \mathrm{curl}\, \mathbf{H} - \mathbf{e}_1 (\mathbf{e}_1 \mathrm{curl}\, \mathbf{H}) \} \right\rangle_{T_{osc}} = 0 \qquad \text{(III.6)}$$

or

$$\left\langle \frac{v_{\parallel}^2 \rho_1}{\omega_L} \right\rangle_{T_{osc}} = 0. \qquad \text{(III.7)}$$

Really,

$$\left\langle \frac{v_{\parallel}^2 \rho_1}{\omega_L} \right\rangle_{T_{osc}} = \frac{1}{T_{osc}} \int_0^{T_{osc}} \frac{v_{\parallel}^2 \rho_1}{\omega_L} dt \neq 0,$$

since $v^2_{||}>0$, $\omega_L >0$, and ρ_1 does not change sign in time interval T_{osc} if $\delta H_\perp / H \ll 1$, which is analogous to fulfillment of condition (II.13). If condition (II.13) is valid, a change of the magnetic field along the drift trajectory is negligible for time T_{osc}. Actually from (II.13) and (III.2) we obtain

$$\begin{aligned} \oint \frac{u_d}{v_{\parallel}} \frac{dH}{dt} dx_1 &= \int_0^{T_{osc}} \left(\frac{\partial H}{\partial x_2} \frac{dx_2}{dt} + \frac{\partial H}{\partial x_3} \frac{dx_3}{dt} \right) dt = \\ &= -\int_0^{T_{osc}} \frac{\partial H}{\partial x_2} \frac{v_{\perp}^2}{2\omega_L} \frac{1}{H} \frac{\partial H}{\partial x_3} dt + \int_0^{T_{osc}} \frac{\partial H}{\partial x_3} \frac{v_{\perp}^2}{2\omega_L} \frac{1}{H} \frac{\partial H}{\partial x_2} dt + \\ &+ \int_0^{T_{osc}} \frac{v_{\parallel}^2 \rho_1}{\omega_L} \frac{\partial H}{\partial x_3} dt = \int_0^{T_{osc}} \frac{v_{\parallel}^2 \rho_1}{\omega_L} \frac{\partial H}{\partial x_2} dt \ll H. \end{aligned} \qquad \text{(III.8)}$$

However, it does not follow from (III.8) that

$$\int_0^{t_1} \frac{\partial H}{\partial x_3} \frac{v_{\parallel}^2 \rho_1}{\omega_L} dt \ll H, \quad \text{if} \quad t_1 \gg T_{osc}.$$

As was already pointed out, integral $\int_0^{t_1} v^2_{||} \rho_1/\omega_L dt$ directly increases with an increase of parameter t_L, while the sign of the component of gradient $\nabla_\perp H$ does not change. This can be similarly confirmed relative to integral

$$\int_0^{t_1} \frac{\partial H}{\partial x_3} \frac{v_\parallel^2 \rho_1}{\omega_L} dt.$$

Let us show that disturbance of invariance J is related to inequality

$$\frac{1}{T_{osc}} \int_0^{T_{osc}} \frac{v_\parallel^2 \rho_1}{\omega_L} \frac{\partial H}{\partial x_3} dt \neq 0. \qquad \text{(III.9)}$$

From (I.17) it follows that

$$J = mv^2 T_{osc} - 2\mu \int_0^{T_{osc}} H dt, \qquad \text{(III.10)}$$

since

$$v^2 = v_\parallel^2 + v_\perp^2 = \text{const and } \mu = \text{const.}$$

Hence

$$\frac{dJ}{dt} = mv^2 \frac{dT_{osc}}{dt} - 2\mu [H(t_1 + T_{osc}) - H(t_1)] \qquad \text{(III.11)}$$

and

$$\left\langle \frac{dJ}{dt} \right\rangle_{T_{osc}} = mv^2 \frac{\Delta T_{osc}}{T_{osc}} - \frac{2\mu}{T_{osc}} \left[\int_{t_1}^{t_1+T_{osc}} H(t + T_{osc})\, dt - \int_{t_1}^{t_1+T_{osc}} H(t)\, dt \right] =$$

$$= -2\mu (\langle H \rangle_{T_{osc}} - \langle H' \rangle_{T_{osc}})^1, \qquad \text{(III.12)}$$

---

* A change of T_{osc} for oscillation time, as well as a change in the length of an arc of a line of force can be negligible with respect to T_{osc} and the total length of arc. Thus, a change of $v_\parallel$ is most significant since it corresponds to a change of H during drift.

where T_{osc} is a change of T_{osc} for one oscillation along the magnetic line of force, $\langle H\rangle_{T_{osc}}$ is the average value of $H(t + T_{osc})$ for T_{osc}, and $\langle H'\rangle_{T_{osc}}$ is an analogous average value of $H(t)$. Let us recall that if the magnetic field strength changes along the drift trajectory,

$$H(t + T_{osc}) \neq H(t) \quad \text{and} \quad \langle H\rangle_{T_{osc}} \neq \langle H'\rangle_{T_{osc}}$$

If we take into account that $H \quad H' + T_{osc}\left\langle \frac{dH}{dt}\right\rangle_{T_{osc}}$ then from (III.12) we obtain*

$$\left\langle \frac{dJ}{dt}\right\rangle_{T_{osc}} = -\frac{2\mu}{T_{osc}} \int_0^{T_{osc}} \left(\int_0^{T_{osc}} \frac{dH}{dt}\, dt\right) dt =$$

$$= -\frac{2\mu}{T_{osc}} \int_0^{T_{osc}} \left[\int_0^{T_{osc}} \left(\frac{\partial H}{\partial x_1} v_{\parallel} + \frac{\partial H}{\partial x_2} v_{e_2} + \frac{\partial H}{\partial x_3} v_{e_3}\right) dt\right] dt =$$

$$= -\frac{2\mu}{T_{osc}} \int_0^{T_{osc}} \left[\oint \frac{\partial H}{\partial x_1} dx_1 + \int_0^{T_{osc}} \left(-\frac{\partial H}{\partial x_2}\frac{\partial H}{\partial x_3}\frac{v_{\perp}^2}{2\omega_L H} + \frac{\partial H}{\partial x_3}\frac{\partial H}{\partial x_2}\frac{v_{\perp}^2}{2\omega_L H}\right) dt + \right.$$

$$\left. + \int_0^{T_{osc}} \frac{\rho_1 r_{\parallel}^2}{\omega_L}\frac{\partial H}{\partial x_3}\, dt\right] dt = -\frac{2\mu}{T_{osc}} \int_0^{T_{osc}} \left(\int_0^{T_{osc}} \frac{\rho_1 v_{\parallel}^2}{\omega_L}\frac{\partial H}{\partial x_2}\, dt\right) dt. \qquad \text{(III.13)}$$

From (III.13) it follows that nonconservation of J is proportional to a change of H along the drift trajectory of the particle for time T_{osc}.

---

* Expression (III.13) can also be obtained directly from the general theory of adiabatic invariants if in the expression for the averaged derivative of an adiabatic invariant of one-dimensional motion $\left\langle \frac{dI}{dt}\right\rangle_T = \oint \left(\frac{\partial p}{\partial \mathcal{E}}\left\langle \frac{d\mathcal{E}}{dT}\right\rangle_T + \frac{\partial p}{\partial \lambda}\left\langle \frac{d\lambda}{dt}\right\rangle_T \right) dq$ (see [10]), we set I = J, $\mathcal{E} = \mathcal{E}_{||} = \frac{mv_{||}^2}{2}$, $p = p_{||} = mv_{||}$, $T = T_{osc}$ and $\lambda = H$.

Expression (III.13) can be transformed to

$$\left\langle \frac{dJ}{dt} \right\rangle_{T_{osc}} = \frac{2\mu}{T_{osc}} \int_0^{T_{osc}} \left(\int_0^{T_{osc}} \rho_1 v_\parallel^2 v_{e_1} dt \right) dt = \\ = \frac{2\mu}{T_{osc}} \int_0^{T_{osc}} \left(\int_0^{T_{osc}} \rho_1 v_\parallel^2 dx_2 \right) dt. \qquad \text{(III.14)}$$

From (III.14) it follows, particularly, that if $\rho_1 \approx 1/H \cdot dH/dx_2$,

$$\left\langle \frac{dJ}{dt} \right\rangle_{T_{osc}} = \frac{2\mu}{T_{osc}} \int_0^{T_{osc}} \left[\int_{x_2(0)}^{x_2(T_{osc})} \left(v^2 - \frac{2\mu H}{m} \right) \rho_1 dx_2 \right] dt = \\ = \frac{2\mu v^2}{T_{osc}} \int_0^{T_{osc}} \left(\int_{x_2(0)}^{x_2(T_{osc})} \frac{\partial \ln H}{\partial x_2} dx_2 \right) dt - \frac{4\mu}{T_{osc}} \int_0^{T_{osc}} \left(\int_{x_2(0)}^{x_2(T_{osc})} \frac{\partial H}{\partial x_2} dx_2 \right) dt = \qquad \text{(III.15)} \\ = \frac{2\mu}{T_{osc}} \int_0^{T_{osc}} \left[v^2 \ln \frac{H(T_{osc})}{H(0)} - v_\perp^2 \frac{H(T_{osc}) - H(0)}{H} \right] dt.$$

From (III.15) it is apparent that if the magnetic field strength along the drift trajectory increases for period T_{osc}, then $\langle dJ/dt \rangle_{T_{osc}}$ decreases and vice versa. This dependence has a simple physical sense. If H increases as a result of drift, μ does not change. Conservation of μ means that as a result of distorting the magnetic lines of force in the region of field anomalies, part of the kinetic energy of the particle parallel to the field changes into perpendicular energy so that $v_\perp^2/H$ does not change, and $\langle v_\parallel^2 \rangle_{T_{osc}}$ decreases.

From (III.13) it is apparent that the rate of a systematic (unaverageable) nonconservation of the second invariant through a term temporally diverging will be determined by expression

$$\frac{dJ}{dt} = -\frac{2\mu}{T_{osc}} \int_0^{T_{osc}} \frac{\rho_1 v_\parallel^2}{\omega_L} \frac{\partial H}{\partial x_3} dt. \qquad \text{(III.16)}$$

We will find the velocity of a T_{osc}-unaverageable displacement of a particle from an invariant surface when this displacement increases directly in time. It is clear from above that this velocity will be that part of the drift velocity which leads to a T_{osc}-unaverageable change of the field strength H along the trajectory of the particle. Let us show more rigorously that $\delta H_{\perp}$, which corresponds to the drift of a particle with velocity $v_{||}^2 \rho_1/\omega_L$ does not change in T_{osc}. Actually

$$\delta H_{\perp} = \int_0^{T_{osc}} \frac{\partial H}{\partial x_3} \frac{v_{||}^2 \rho_1}{\omega_L} dt = \int_0^{T_{osc}} \frac{1}{\omega_L} \left(v^2 - \frac{2\mu}{m} \right) \rho_1 \frac{\partial H}{\partial x_3} dt =$$

$$= \frac{mcv^2}{e} \int_0^{T_{osc}} \rho_1 \frac{\partial H}{\partial x_3} dt - \frac{2\mu c}{e} \int_0^{T_{osc}} \rho_1 \frac{\partial H}{\partial x_3} dt.$$

When condition (II.13) is valid, curvature $\rho_1 = 1/R$ does not change sign within T_{osc}, since distortions of the field through anomalies are small as compared to the magnitudes of the field. Under this same condition, $\partial H/\partial x_3$ also does not change sign within T_{osc}. Actually, a change of the sign of the anomaly gradient when the particle shifts perpendicular to the magnetic line of force and along the line is at variance with condition (II.13). With such a change of sign, the problem becomes nonlinear and disturbance of the second invariant, obviously, will have not a cumulative, but a resonant character.

Let us examine the effect of anomalies with gradients of different sign on the drift surface for particles postively and negatively charged. For this we use expression (III.2). Let $\partial H/\partial x_2 < 0$ and $\partial H/\partial x_3 > 0$. This means that during motion from the center of the magnetic system the field decreases, and during motion in direction e_3 the field increases. Let us note that in the

earth's magnetic field, which corresponds to a dipole with small deviations from axial symmetry (anomalies), e_2 is directed from earth and e_3 is directed eastward. Hence, $\partial H/\partial x_3 < 0$ corresponds to an increase of strength H in the anomaly region in an easterly direction. Protons moving in a field with gradient $\partial H/\partial x_2 < 0$ will drift westward and the field strength due to this drift will decrease. The drift due to $\partial H/\partial x_3$ here will be earthward and will basically compensate the decrease of H and increase of J. However, a partial change of H which corresponds to drift in direction $-e_3$ with velocity $v_{||}^2 \rho 1/\omega_L$ remains uncompensated. Thus, when $\partial H/\partial x_3 > 0$ and $\partial H/\partial x_2 < 0$, protons shift from the invariant surface away from earth. Due to the dependence of u_d on the sign of the particle charge, electrons will shift from surface J = const to the opposite side, i.e., earthward.

When $v_{||}^2 = 0$, expression (III.2) yields the total mutual compensation of changes of field strength during drift shift along e_2 and e_3. However, here, as was pointed out above, condition (II.5) is disturbed and the approximation becomes inapplicable.

Presently, the so-called McIlwain system of coordinates is widely used to estimate the density distribution and intensity of particles in an actual geomagnetic field [17]. This system of coordinates is based on the conservation of the second invariant, through which it is assumed that a particle moves continuously along the same magnetic surface. As was already pointed out, the invariant surface of motion of a charged particle is uniquely determined by specific values μ, J and ξ. The significance of introducing McIlwain coordinates is that the invariant surface of

the motion of a particle in an actual geomagnetic field is replaced by the corresponding dipole invariant surface which has the same μ and J as the actual. This substitution does not complicate the equation of motion of a particle by taking into account the deviations of the geomagnetic field from the dipole, and also makes it possible to estimate the effect of these deviations on the distribution of particles in the field.

From what was pointed out above concerning the accuracy of the conservation of the second invariant, it seems to us that this system of coordinates has limited applicability. Its applicability is determined by the time intervals during which particles do not shift significant distances from the invariant surfaces.

In conclusion, let us point out that the drift displacement of charged particles examined above from invariant surfaces can lead to radial "shifting" of particles in the earth's radiation belts. Here, the densities and intensities of the flows of charged particles at each point of space will change as a function of time even in a stationary magnetic field. The cause of the change of densities, as was already pointed out, is the transfer of the energy component of the particle which is parallel to the field to perpendicular or vice versa. Here, the second invariant J is not conserved, and the first invariant μ remains constant.

REFERENCES

1. N. M. Krylov and N. N. Bogolyubov. Vvedeniye v nelineynuyu mekhaniku. Kiyev, 1937.

2. N. N. Bogolyubov and Yu. A. Mitropol'skiy. Asimptoticheskiye

metody v teorii neleneykh kolebaniy. Fizmatgiz, Moscow, 1955.

3. M. Kruskal. Adiadaticheskiye invarianty. IL, Moscow, 1962.

4. Ya. P. Terletskiy. Vestn. Mosk. Gos. un-ta, No. 1, 75, 1948.

5. Ya. P. Terletskiy. Vestn. Mosk. Gos. un-ta, No. 11, 53, 1949.

6. Kh. Al'fven. Kosmicheskaya elektrodinamika, IL., Moscow, 1952.

7. O. B. Firsov. Fizika plazmy i problema unprablyayemykh permoyadernykh reaktsiy, Vol. 3, Izd-vo AN SSSR, pg. 259, 1958.

8. B. V. Chirikov. Atomnaya energiya, 6, Vol. 6, 1959.

9. Yu. A. Krutkov. Adiabaticheskiye invarianty i ikh promeneniye v teroeticheskoy fizike, Tr. Gos. optichesk. in-ta, 2, No. 12, 1922.

10. L. D. Landau and Ye. M. Lifshits. Mekhanika. Fizmatgiz, 1958.

11. G. Goldsteyn. Klassicheskaya Mekhanika. Fizmatgiz, 1957.

12. L. I. Lur'ye. Analiticheskaya mekhanika. Fizmatgiz, 1952.

13. V. D. Fedorchenko, B. N. Rutkevich, and B. M. Chernyy. Zh. tekhn. fiziki, 29, Vol. 10, 1212, 1959.

14. T. Nortrop and others. Sb. "Solnechnyye korpuskulyarnyye potoki i ikh fzamioveystviye s. magnitnym polmen Zemli." IL, Moscow, page 99, 1962.

15. B. B. Kadomtsyev. Fizika plazmy i problema upravlyayemykh termoyadermykh rektsiy, Vol. 3, Izd-vo AN SSSR pg. 285.

16. S. Chandrasekar, A. Kaufman, and K. Vatson. Problemy sovremennoy fiziki, No. 2, 111, 1959.

17. C. E. McIlwain. J. Geophys. Res., 66, No. 11, 3681, 1961.

ON THE DENSITY DISTRIBUTION AND INTENSITY OF CHARGED PARTICLES WITHOUT TAKING INTO ACCOUNT INTERACTION IN A STATIONARY GEOMAGNETIC FIELD

V. D. Pletnev

An asymptotic method of solving the Boltzmann equation for a low-density ionized gas in a strong stationary magnetic field is used to estimate the density distribution and intensity of charged particles in the Van Allen radiation belts. This method, which was previously developed [1] and which is based on expansion of the distribution function of charged particles with respect to the inverse powers of the Larmor frequency, is applicable when conserving the invariant of the longitudinal effect of a particle in a magnetic field. For this, additional averaging of the distribution function is carried out for the period of vibrations of a particle between magnetic mirrors. This work examines the different possible forms of the distribution function in these approximations and their corresponding density distributions and intensity of charged particles in the field.

1. METHOD OF SOLVING THE BOLTZMANN EQUATION

The method of solving a Boltzmann equation for stationary conditions of a low-density ionized gas in a strong magnetic field was examined previously [1]. The Boltzmann equation for this gas is

$$v_j \frac{\partial f}{\partial x_j} + A_j \frac{\partial f}{\partial v_j} + \frac{e}{mc} \varepsilon_{ijk} \frac{\partial f}{\partial v_i} v_j H_k = 0, \tag{1.1}$$

where $\underline{f}$ is the distribution function, v_j is velocity component of a charged particle, H_k is the intensity component of a magnetic field, mA_j is the component of the external force acting on a charged particle. The action of a constant electric field can be examined as this force.

The essence of the method of solving Eq. (1.1) in an approximation of the first adiabatic invariant of the motion of a particle $\mu = mv_\perp^2/2H = \text{const}$ lies in the asymptotic expansion of distribution function $\underline{f}$ with respect to the inverse powers of the frequency of Larmor rotation ω_L, so that $f = \sum_{n=0}^{\infty} \omega_L^{-n} f_n$ providing $\omega_L \gg 1$, and in the successive determination of solutions for f_0, f_1, etc. The possibility of finding a series of such solutions is related to operator $L = \varepsilon_{ijk} v_j \frac{\partial}{\partial v_i} = \text{const}\, \partial f/\partial\varphi$, where φ is the azimuth angle in the velocity space in a plane perpendicular to the magnetic field, i.e., in the plane of symmetric rotation of a particle. Therefore, with conditions

$$T_L \left|\frac{dH}{dt}\right| \ll H \tag{1.2}$$

and

$$v_\perp \sim v_\parallel, \tag{1.3}$$

where $v_\perp$ and $v_{||}$ are the particle velocity components perpendicular and parallel to the magnetic field (see [2]), we can average operator L for period T_L and assume that the effect of this averaging of the operator on $\underline{f}$ is approximately equal to zero. This results in a system of successive equations for determining f_0, f_1, f_2, ..., f_n, viz.,

$$\begin{aligned} &Lf_0 = 0, \ \langle Df_0\rangle_{T_L} = 0, \\ &Df_0 + \lambda Lf_1 = 0, \ \langle Df_1\rangle_{T_L} = 0, \\ &\cdots\cdots\cdots\cdots\cdots\cdots \\ &Df_{n-1} + \lambda Lf_n = 0, \ \langle Df_n\rangle_{T_L} = 0, \end{aligned} \tag{1.4}$$

where operator

$$D = v\frac{\partial}{\partial x_j} + A_j\frac{\partial}{\partial v_j}, \tag{1.5}$$

and the magnetic field is

$$\mathbf{H} = \langle H\rangle_{T_L}\lambda(x_i)\,\mathbf{n}. \tag{1.6}$$

Index $\langle\ldots\rangle T_L$ designates averaging of the period of Larmor rotation of a charged particle T_L. Vector $\mathbf{n}$ is a unit vector directed along the magnetic field and $\langle H \rangle T_L\ \lambda\ (x_i) = H$.

The purpose of this work is to obtain a series of solutions for the distribution function in approximation J = const, where $J = \oint v_{||}\,ds$ is the second adiabatic invariant of the motion of a charged particle in a magnetic field. These solutions will be compared with solutions in approximation μ = const. Therefore, subsequent results corresponding to approximation J = const will be examined along with the previously obtained [1] results of approximation μ = const. These results will be simultaneously applied to a geomagnetic field. The case examined in this work lacks electric fields and other external forces. The interaction of charged particles is negligible.

2. DISTRIBUTION FUNCTION OF CHARGED PARTICLES IN ZERO APPROXIMATION OF EXPANSION IN $1/\omega_L$

In a zero approximation, drift of a particle can be negligible, since ω_L is a very large magnitude. Therefore, we can assume that the particle moves along the same magnetic line of force. Mathematically, disregard of drift due to magnetic heterogeneity in zero approximation follows from condition

$$Lf_0 = 0. \tag{2.1}$$

Condition

$$\langle Df_0\rangle_{T_L} = 0 \tag{2.2}$$

yields here an equation for determining f_0, viz.,

$$n_j \frac{\partial f_0}{\partial x_j} - v_\perp^2 \frac{n_j}{H} \frac{\partial H}{\partial x_j}\left(\frac{\partial f_0}{\partial v_\parallel^2} - \frac{\partial f_0}{\partial v_\perp^2}\right) = 0, \tag{2.3}$$

where n_j is the unit vector component of magnetic field $\underline{n}$ for x_j. The solution of this homogeneous equation of the first order in partial derivatives will be an arbitrary function of the integrals of a system of characteristic equations, to wit, equations [1]:

$$\begin{aligned} \frac{dx_j}{dt} &= n_j, \\ \frac{dv_\perp^2}{dt} &= -\frac{v_\perp^2}{H} n_j \frac{\partial H}{\partial x_j}, \\ \frac{dv_\parallel^2}{dt} &= \frac{v_\perp^2}{H} n_j \frac{\partial H}{\partial x_j}. \end{aligned} \tag{2.4}$$

Hence, in zero approximation of expansion in $1/\omega_L$, the solution will be

$$f_0 \equiv f_0\left(G, \mu, \int_{r_1}^{r_2} [dr \times n]\right), \tag{2.5}$$

where $G = m(v_\perp^2 + v_\parallel^2)/2$ is the kinetic energy of a particle, $\mathbf{r}$ is the vector radius of the point in which the moving charged particle is found. Since G = const in a stationary magnetic field, μ = const in this approximation (see [3]) and $\int_{r_1}^{r_2} [dr \times n]$ = const provided the particle moves only along the magnetic line of force, then

$$\frac{df_0}{ds} = 0, \tag{2.6}$$

where ds is the element of arc of a magnetic line of force. This result corresponds to the Louisville theorem.

If we assume that

$$n_j \frac{\partial}{\partial x_j} = \frac{\partial}{\partial s},$$

and select as the parameter of the characteristic system the independent variable s or (what is more suitable for subsequent calculations) the intensity of magnetic field H, which is a function determined only from s, we obtain

$$f_0 \equiv f_0(G, \mu). \tag{2.7}$$

Let us define the form of function f_0 as a function of independent variables $x_1 = v$, $x_2 = \alpha$, $x_3 = H$, where v is the velocity modulus of a particle, α is the angle between vectors **v** and **H**. The variables x_1, x_2, and x_3 are related through integrals of motion

$$x_1 = \sqrt{G},\ x_2 = \arcsin \frac{\sqrt{2\mu x_3}}{x_1}. \tag{2.8}$$

After assigning a specific form of distribution function at a point of the magnetic field of force where the field intensity is minimal,*

$$f_0|_{H_0 = H_{\min}} = \varphi(x_1, x_2, x_2^0),$$

we obtain by (2.7) and (2.8)

$$f_0(x_1, x_2, x_3) = \varphi\left[v, \arcsin\left(\sqrt{\frac{H_0}{H}} \sin\alpha\right)\right]. \tag{2.9}$$

Any values of variables v and α at point $H_0 = H_{\min}$ will be designated as v_0 and α_0. For a monoenergetic flow of particles we obtain

$$f_0|_{H_0} = C\delta(v_0 - v_0) f_0(\alpha_0). \tag{2.10}$$

---

* We can show that the value of the starting form of a distribution function at any other point of the magnetic line of force does not completely determine the form of this function at other points of the line of force, since the trajectories of all particles moving along this line of force pass only through the point in which $H_0 = H_{\min}$.

Then due to (2.9), at any other point of this line of force

$$f_0 = C\delta(v' - v) f_0\left[\arcsin\left(\sqrt{\frac{H_0}{H}}\sin\alpha\right)\right]. \qquad (2.11)$$

From f_0 in a stationary magnetic field it is easy to change to the density distribution of particles along the magnetic line of force, as well as to the distribution of intensity of the Van Allen radiation belt. Actually, the density of charged particles is defined by the distribution function as

$$N = \int f_0\, dU, \qquad (2.12)$$

where dU is the element of volume in velocity space.

In this space let us introduce the spherical system of coordinates in which $\mathbf{v}$ is the vector radius, longitude is some angle Φ, and α corresponds to latitude, i.e., we assume that axis OZ of the corresponding Cartesian system of coordinates directionally coincides with vector **H**. Then

$$dU = v^2\, dv\, d\Omega, \qquad (2.13)$$

where the solid angle element in velocity space

$$d\Omega = \sin\alpha\, d\alpha\, d\Phi.$$

Hence, the density distribution of particles of a monoenergetic flow along a magnetic line of force is

$$N = C\int_0^{2\pi}\int_0^{\infty}\delta(v'-v) f_0'\left[\arcsin\left(\sqrt{\frac{H_0}{H}}\sin\alpha\right)\right] v^2\sin\alpha\, dv\, d\alpha\, d\Phi =$$

$$= 8\pi C v'^2\int_0^{\frac{\pi}{2}} f_0\left[\arcsin\left(\sqrt{\frac{H_0}{H}}\sin\alpha\right)\right]\sin\alpha\, d\alpha^1. \qquad (2.14)$$

---

* From the theory of δ-functions it is known that

$$\int\delta(x' - x)\, f(x)\, dx = f(x').$$

The intensity of a directed flow of radiation of some energy is defined as

$$j = N(\tilde{\alpha})\, v, \tag{2.15}$$

where α is the fixed value of α, which corresponds to the specific direction of flow relative to the magnetic line of force. For total (integral) intensity of a particle flux of some energy moving at different angles to the magnetic line of force, we have

$$I = N_0 v', \tag{2.16}$$

where I has dimensionality [cm^{-2} sec^{-1}]. Hence, analogous to (2.14) we obtain

$$I = 8\pi c v'^3 \int_0^{\frac{\pi}{2}} f_0' \left[\arcsin\left(\sqrt{\frac{H_0}{H}}\sin\alpha\right)\right] \sin\alpha\, d\alpha. \tag{2.17}$$

Let us determine the density of ray j from equality

$$I = \int_0^{\pi/2} j(\tilde{\alpha}) \sin\tilde{\alpha}\, d\tilde{\alpha}. \tag{2.18}$$

Then from (2.9) and (1.17)

$$j(\tilde{\alpha}) = 8\pi c v'^3 f_0' \left[\arcsin\left(\sqrt{\frac{H_0}{H}}\sin\tilde{\alpha}\right)\right] = \text{const}. \tag{2.19}$$

along a magnetic line of force. Although $j(\tilde{\alpha}_0) = j(\tilde{\alpha})$ along a line of force (where j_0 is the intensity of a ray at point $H_0 = H_{min}$), nevertheless, the form of function $j_0(\tilde{\alpha}_0)$ does not correspond to the form of function $j(\tilde{\alpha})$ at any other point. Hence, the anisotropic character of radiation with respect to angles with a line of force in the general case changes along the trajectory of particle motion with this

$\tilde{\alpha}_0$ (i.e., along the magnetic line of force from some reflection point to another). An exception is when $dj_0/d\alpha_0 = 0$, i.e., the distribution function at point $H_0 = H_{min}$ is isotropic relative to α_0. From (2.17) it follows that for an isotropic distribution with respect to angles α_0, $I = I_0$ along the entire line of force, since $j_0 = \text{const}$ and

$$I_0 = \int_0^{\pi/2} j_0 \sin \tilde{\alpha}_0 \, d\tilde{\alpha}_0. \tag{2.20}$$

From above it is clear that in a general case (for an anisotropic distribution function) $I \neq I_0$.

Different cases of angular anisoptropic Van Allen belt radiation in a stationary geomagnetic field in a dipole approximation (when $H_0 = H_{min}$ corresponds to the geomagnetic equator) and their corresponding intensity distributions along a magnetic line of force were previously examined [4]. This study will additionally examine the angular anisotropy of radiation of particles of different energies in a zero approximation.

If $f_0|H_{min} = C_1$, i.e., the distribution function is isotropic on the equator relative to particle energies and angles α, then from (2.7) and (2.9) we obtain

$$N = 8\pi C_1 \int_{v_{min}}^{v_{max}} \int_0^{\frac{\pi}{2}} v^2 \sin \alpha \, dv \, d\alpha = \frac{8\pi}{3} C_1 (v_{max}^3 - v_{min}^3) \tag{2.21}$$

and from (2.17)

$$I_1 = \int_{v_{min}}^{v_{max}} vN dv = C_2 (v_{max}^2 - v_{min}^2)(v_{max}^2 - v_{min}^2), \tag{2.22}$$

where I_1 is the total intensity of particles of all energies and directions and has dimensionality [erg/cm^2 sec] and $C_2 = 4/3\pi C_1$. From

(2.21) and (2.22) it follows that I_1 and N are constant along a magnetic line of force. Here it is assumed that v_{max} and v_{min} are also constant along a line of force, i.e., the distribution is examined in the same energy range. When $df_0/dv \neq 0$, but the spectral distribution of charged particles is not a function of angle α_0 or α, N and I_1 will also be constant along a magnetic line of force. The only change will be the character of functional dependence of I_1 on v_{max} and v_{min} as compared with (2.21) and (2.22).

Fundamentally new will be the case where the character of the energy spectrum changes along a magnetic line of force or, what is the same thing, when the spectral distribution changes its character at any point of the magnetic line of force (for instance, on the equator) as a function of angle α. Here, the distribution function cannot be the product of two functions, one of which is a function only of v, and the other a function only of α. Therefore, the expression for I_1 must be sought in a most general form:

$$I_1 = \int_{v_{min}}^{v_{max}} vN dv = 8\pi \int_{v_{min}}^{v_{max}} v \left\{ \int_{r_{min}}^{r_{max}} \int_0^{\frac{\pi}{2}} \varphi\left[v;\ \arcsin\left(\sqrt{\frac{H_0}{H}}\sin\alpha\right)\right] \cdot \right. \tag{2.23}$$
$$\left. \cdot \sin\alpha\, v^2\, dv\, d\alpha \right\} dv.$$

These examples apply to zero approximation of expansion in $1/\omega_L$. However, as we shall see later, the results do not fundamentally change if we transfer to a drift approximation in a magnetic system having axial symmetry. As follows from the equations of motion of a separate particle in the drift approximation, the particle in this approximation without an electric field and with axial symmetry of a magnetic system will strictly move along the same surface which is being formed by identical magnetic lines of force. Therefore, instead

of drift motion, we can examine here only vibrations of a charged particle along the same magnetic line of force and apply these results to a case of, for instance, a magnetic field, such as an ideal dipole field.

The equation for the distribution function in approximation J = = const is obtained by further averaging of Eq. (2.2). Here

$$\langle Df_0 \rangle_{T_L T_{osc}} = 0, \tag{2.24}$$

where $< \ldots > T_{osc}$ designates averaging for T_{osc} for the vibration period of a charged particle between magnetic mirrors. Let us designate the distribution function in this approximation as f_{oo}. Then

$$\left\langle n_j \frac{\partial f_0}{\partial x_j} - v_\perp^2 \frac{n_j}{H} \frac{\partial H}{\partial x_j} \left(\frac{\partial f_0}{\partial v_\parallel^2} - \frac{\partial f_0}{\partial v_\perp^2} \right) \right\rangle_{T_{osc}} = 0 \tag{2.25}$$

or, since

$$- v_\perp^2 \frac{n_j}{H} \frac{\partial H}{\partial x_j} \left(\frac{\partial f_0}{\partial v_\parallel^2} - \frac{\partial f_0}{\partial v_\perp^2} \right) = \frac{v_\perp^2}{H} \left(\mathfrak{n} \frac{\partial H}{\partial \tau} \right) \frac{1}{v_\perp v_\parallel} \frac{\partial f_0}{\partial \alpha} =$$

$$= \frac{v_\perp^2}{H} \left(\mathfrak{n} \frac{\partial H}{\partial \tau} \right) \frac{2H_k}{v^2} \frac{\partial f_0}{\partial H} = 2 \frac{\partial H}{\partial s} \frac{\partial f_0}{\partial H} = 2n_j \frac{\partial f_0}{\partial x_j},$$

then from (2.25) we obtain

$$\left\langle 3n_j \frac{\partial f_0}{\partial x_j} \right\rangle_{T_{osc}} = 0. \tag{2.26}$$

Hence it follows that

$$n_j \frac{\partial f_{oo}}{\partial x_j} \equiv 0. \tag{2.27}$$

and f_{oo} does not change during motion along a magnetic line of force. The result obtained is trivial. Its physical significance is that f_{oo} is f_0 averaged for the period or for the amplitude of vibrations of a particle along a magnetic line of force.

However, from this result we can make some conclusions which are important for subsequent investigation. First, from (2.26) it follows that the equation for f_{oo} does not have an L-type correction operator in approximation μ = const. Therefore, all subsequent approximations of averaging for T_{osc} will equal f_{oo}:

$$f_{00} = f_{01} = f_{02} = \ldots \tag{2.28}$$

Equality (2.28) results from the conservation of J in a stationary magnetic field with that degree of accuracy with which a change of the field intensity due to shifting of a charged particle from a given line of force for period T_{osc} is negligible (see [2]). In zero approximation of expansion in $1/\omega_L$, this condition is fulfilled with absolute accuracy, since it is assumed that $\omega_L \to \infty$. Second, in a first approximation of expansion in $1/\omega_L$ when changing to approximation J = const in a field where there is no axial symmetry, the drift shift of a charged particle for time T_{osc} must be disregarded, since this shift changes the intensity of the magnetic field in which the particle moves. Therefore, function f_{1o} provided conservation of J will be a superposition of the distribution functions f_{oo} which are constant along each magnetic line of force. Thus, in approximation J = const the character of the distribution function along the magnetic line of force does not change when passing from zero approximation of expansion in $1/\omega_L$ to first approximation. Mathematically, this fact is expressed as follows. Let the general solution of Eq. (1.1) in a first approximation of expansion in $1/\omega_L$ be

$$f_1 = \frac{1}{\lambda}\varphi_1 + \psi_1, \tag{2.29}$$

where $L_{\psi_1} = 0$. Then, according to (1.4), we obtain

$$L\varphi_1 = \langle Df_0 \rangle_{\tau_L} - Df_0. \tag{2.30}$$

φ_1 is the partial solution of Eq. (2.30) for a distribution function in a first (drift) approximation taking into account (in the first order of smallness of expansion in $1/\omega_L$) the effect of the heterogeneity of the magnetic field averaged over T_L.

The effect of heterogeneity is calculated by correction operator L. However, it is obvious that there is no type L correction operator in the drift approximation for f_{1o}. Actually, in approximation j = const we have

$$\langle L\varphi_1 \rangle_{\tau_L} = \langle Df_0 \rangle_{\tau_L} - \langle Df_0 \rangle_{\tau_L} = 0. \tag{2.31}$$

Thus, the unique equation which determines f_{1o} will be

$$\langle Df_1 \rangle_{\tau_L \tau_{osc}} = 0. \tag{2.32}$$

3. DRIFT APPROXIMATION

According to (1.4), the equations for distribution function f_1 in a drift approximation will be

$$\lambda L f_1 = \langle Df_0 \rangle_{\tau_L} - Df_0 \tag{3.1}$$

and

$$\langle Df_1 \rangle_{\tau_L} = 0. \tag{3.2}$$

After presenting the general solution as (2.29), we find the following equations for determining φ_1 and ψ_1:

$$L\varphi_1 = \langle Df_0 \rangle_{\tau_L} - Df_0 \tag{3.3}$$

and

$$\langle D\psi_1\rangle_{\tau_L} + \frac{1}{\lambda}\langle D\varphi_1\rangle_{\tau_L} + \left\langle \varphi_1 D\left(\frac{1}{\lambda}\right)\right\rangle_{\tau_L} = 0. \tag{3.4}$$

As was previously point out, the partial solution of Eq. (2.30) in a drift approximation allows us to take into account the effect of the heterogeneity of a magnetic field in a Larmor circle. Substitution of the solution for φ_1 into (3.4) leads to a solution for the distribution function taking into account the drift in a heterogeneous magnetic field caused by the gradient component of the field perpendicular to the magnetic line of force [3].

The partial solution of Eq. (2.34) is (see [1])

$$\varphi_1 = \varepsilon_{ijk}\left(\Phi_i + \frac{1}{2}\Phi_{il}\, v_{\perp l}\right) v_j n_k, \tag{3.5}$$

where

$$\Phi_j = \frac{\partial f_0}{\partial x_j} + 2v_{\parallel}^2 n_i \frac{\partial n_j}{\partial x_i}\left(\frac{\partial f_0}{\partial v_{\parallel}^2} - \frac{\partial f_0}{\partial v_{\perp}^2}\right), \tag{3.6}$$

$$\Phi_{ij} = v_{\parallel}\left(\frac{\partial f_0}{\partial v_{\parallel}^2} - \frac{\partial f_0}{\partial v_{\perp}^2}\right)\left(\frac{\partial n_i}{\partial x_j} + \frac{\partial n_j}{\partial x_i}\right). \tag{3.7}$$

Calculation of term $1/\lambda \cdot \varphi_1$ in a general solution leads to a calculation of the "vibrations" of a particle and, therefore, does not introduce significant changes in the distribution of charged particles in a magnetic field. When averaging equations of motion of a charged particle over T_{osc}, the "vibrations" are generally negligible. Therefore, when interpreting the solution of system of Eqs. (2.30) and (3.4) we will be basically interested in the solution for function ψ_1. Equation (3.4) in vector form is

$$\frac{\lambda v_{\parallel}}{\omega_L}\frac{\partial \psi_1}{\partial x_i} + \mathbf{v}_d \nabla f_0 - \frac{1}{H}\nabla_{\perp}(H\mathbf{v}_d)\mu\frac{\partial f_0}{\partial \mu} = 0, \tag{3.8}$$

where

$$\mathbf{v}_d = \frac{1}{\omega_L} \mathbf{n} \times \left(v_\parallel^2 \frac{\partial \mathbf{n}}{\partial x_1} + \frac{v_\perp^2}{2} \nabla \ln \lambda \right). \tag{3.9}$$

and coordinate x_1 corresponds to the direction along the magnetic line of force.

We will examine an axiosymmetric magnetic field. Here, as previously pointed out [1], Eq. (3.8) takes the form

$$\frac{\lambda v_\parallel}{\omega_L} \frac{\partial \psi_1}{\partial x_1} + \frac{v_d}{r} \frac{\partial f_0}{\partial \theta} = 0, \tag{3.10}$$

where $\underline{r}$ is the distance from the axis of the system to the point at which the particle is found, θ is the azimuth angle, $v_d = \frac{1}{\lambda \omega_L} \left(v_\parallel^2 + \frac{v_\perp^2}{2} \right)$.

Averaging (3.10) over T_{osc}, we obtain

$$\frac{1}{T_{osc}} \frac{\partial f_0}{\partial \theta} \int \frac{v_d}{r} \frac{dx_1}{v_\parallel} = 0, \tag{3.11}$$

since

$$\frac{\text{const}}{T_{osc}} \oint \frac{\partial \psi_1}{\partial x_1} dx_1 = 0.$$

Since $v_{dr}/r = d\theta/dt$, then from (3.11) it follows that

$$\frac{\partial f_0}{\partial \theta} \left\langle \frac{d\theta}{dt} \right\rangle_{T_{osc}} = 0. \tag{3.12}$$

If $\langle d\theta/dt \rangle_{T_{osc}} \neq 0$, then $\partial f_L / \partial \theta = 0$, i.e., the distribution function does not depend on θ and does not change along the surface of magnetic lines of force on which the particle drifts. Since v_d also does not change here, the distribution of particles with respect to density and intensity along each magnetic surface remains the same. Thus, for an axiosymmetric magnetic pole, $f_{oo} = f_{1o}$. We can arrive at this result directly without averaging over T_{osc} if we take into account the remark made in the preceding section concerning the

identity of distribution functions of the zeroth and first approximations of expansion in $1/\omega_L$ for an axiosymmetric magnetic field. Assuming $\psi_1 = f_0$, we obtain

$$\frac{\partial f_0}{\partial \theta}\frac{d\theta}{dt} = 0. \tag{3.13}$$

From (3.13) it follows that in this case $f_1 = f_0$.

Let us now examine a case where axial symmetry is absent. Here, Eq. (3.8) is converted by introducing some parameter determining the magnetic surface along which the charged particle moves. In a stationary magnetic field such a parameter can be second invariant J (see [5]).

Actually,

$$\begin{aligned} v_d \nabla f_0 = \frac{dx_3}{dt}\frac{\partial f_0}{\partial x_3} + \frac{dx_3}{dt}\frac{\partial f_0}{\partial x_3} - \frac{\partial f_0}{\partial J}\frac{\partial J}{\partial x_3}\frac{dx_3}{dt} + \frac{\partial f_0}{\partial J}\frac{\partial J}{\partial x_3}\frac{dx_3}{dt} = \\ = \frac{\partial f_0}{\partial J}\left(\frac{\partial J}{\partial x_3}\frac{dx_3}{dt} + \frac{\partial J}{\partial x_3}\frac{\partial x_3}{dt}\right) = \frac{\partial f_0}{\partial J}\frac{dJ}{dt}. \end{aligned} \tag{3.14}$$

Substituting (3.14) into (3.8) and averaging the obtained equation over T_{osc}, we obtain the following equation for f_{10}:

$$\left\langle \frac{dJ}{dt} \right\rangle_{T_{osc}} \frac{\partial f_{10}}{\partial J} - \left\langle \frac{1}{H}\nabla_\perp (H v_d) \right\rangle_{T_{osc}} \mu \frac{\partial f_{10}}{\partial \mu} = 0. \tag{3.15}$$

Since in the approximation of averaging over T_{osc} we have (see [2])

$$\left\langle \frac{dJ}{dt} \right\rangle_{T_{osc}} \approx 0. \tag{3.16}$$

and

$$\left\langle \frac{1}{H}\nabla_\perp (H v_d) \right\rangle_{T_{osc}} \approx 0, \tag{3.17}$$

then in this approximation the distribution function is an arbitrary function of G, μ, and J, i.e.,

$$f_{10} \equiv f_{10}(G, \mu; J). \tag{3.18}$$

We will show that (3.17) is fulfilled with the same degree of accuracy as J = const. For an axiosymmetric magnetic field, the velocity drift is determined as

$$v_d = \frac{mc(v^2 + v_\parallel^2)}{2eH^3}[H; \nabla H]. \tag{3.19}$$

Hence

$$\frac{1}{H}\nabla_\perp(Hv_d) = \frac{v_d}{H}\nabla H + \nabla_\perp v_d = 0, \tag{3.20}$$

since

$$\frac{v_d}{H}\nabla_\perp H = \text{const}\cdot[H; \nabla_\perp H]\nabla_\perp H = 0,$$

$$\nabla_\perp \text{const}\cdot[H; \nabla_\perp H] = 0,$$

if curl H = 0, i.e., if the field is axiosymmetric. If the magnetic system is not completely axiosymmetric, curl $\mathbf{H} \neq 0$. Nevertheless, when fulfilling the condition of conserving the second invariant (see [2]) we obtain

$$\left\langle \frac{1}{H}\nabla_\perp(H v_d)\right\rangle_{T_{osc}} \approx 0.$$

Actually, if we assume $|v_d| = dl/dt$, then

$$\frac{v_d}{H}\nabla_\perp H = \frac{1}{H}\frac{dl}{dt}\frac{dH}{dl} = \frac{1}{H}\frac{dH}{dt}$$

and

$$\left\langle \frac{v_d}{H}\nabla_\perp H\right\rangle_{T_{osc}} = \frac{1}{T_{osc}}\int_0^{T_{osc}} \frac{1}{H}\frac{dH}{dt}dt \approx 0. \tag{3.21}$$

A change in v_d in the direction of drift also is negligible within a time interval equal to T_{osc}. This is obvious since a calculation of the change of v_d for T_{osc} is equivalent to calculating the change of H in the direction of drift over T_{osc} which contradicts the condition of conserving J. Hence,

$$\langle \nabla_\perp v_d\rangle_{T_{osc}} \approx 0. \tag{3.22}$$

Thus, condition (3.17) is fulfilled with the same accuracy with which J is conserved in our approximation.

Strictly speaking, in an approximation of averaging over T_{osc} we should have excluded the dependence of density distribution of particles and total intensity on x_1, the coordinates along the line of force of a magnetic field, and should have examined the motion with values $v_{||}$ and v_v averaged over T_{osc}. However, we cannot make such an exception of the dependence of the distribution of particles on x_1 without basic errors. At the same time, the distribution of particles with respect to density and intensity remains constant on this drift magnetic surface of an asymmetric magnetic field. The last conclusion is not trivial. Actually, condition (3.22) does not mean that in approximation J = const the change of v_d for any period of time is negligible. Conditions (3.21) and (3.22) actually reduce all changes of H in a direction perpendicular to H for T_{osc} to changes of H in the plane of the same magnetic line of force. Here, changes $\nabla_{\perp} H$ in the direction of drift can be approximately examined as changes $|\nabla_{e_2} H|$ where the unit vector e_2 is perpendicular to the drift surface. For instance, let the particle enter the area of positive heterogeneity of the field during drift motion along the surface of magnetic lines of force.* Then $|\nabla_{e_2} H|$ increases and hence, v_d increases (see (3.19)). In the region of negative heterogeneity $|\nabla_{e_2} H|$ and v_d decrease. Nevertheless, in the regions of positive and negative heterogeneity the total particle flux, and hence, the

* By the positive heterogeneity of a magnetic field we mean the region on the drift surface in which the intensity of the magnetic field is greater than the mean intensity on the magnetic surface. By a negative heterogeneity we mean the region where the intensity is less than mean.

total intensity of radiation, does not change. The appearance of positive heterogeneity is related to contraction of the magnetic lines of force, and the appearance of negative heterogeneity is related to expansion of the lines of force. Thus, as previously pointed out [5], the total particle flux moving in this magnetic tube of force does not change during drift motion along the same magnetic surface, J = const. This means, particularly, that if the "distorted" lines of force in the region of the magnetic anomaly are replaced by their corresponding lines of force of an axiosymmetric field with the same J, then the intensity of Van Allen belt radiation will be constant on the drift surface along a line equal to the intensity of the magnetic field. This examination of the distribution of charged particles in a real geomagnetic field was previously carried out [6]. Here, naturally, it was assumed that J is conserved with absolute accuracy.

The author expresses his gratitude to G. A. Skuridin and B. A. Tverskiy for their valuable instructions and observations during this work.

REFERENCES

1. S. Chandrasekar, A. Kaufman and K. Vatson. Probvlemy Sovremennoy fiziki, No. 2, 11, 1959.

2. V. D. Pletnev and G. A. Skuridin. Kosm. issled, nast, vyp., pp. 387.

3. N. N. Bogolyubov and Yu. A. Mitropol'skiy. Asimptoticheskiye metody v teorii nelineynikh kolebaniy Fizmatgiz, 1959.

4. V. D. Pletnev. Izv. AN SSSR, ser, geofiz., No. 1, 150, 1961.

5. T. Nortrop and E. Teller. Sb. "Solnechnyye korpuskulyarnyye potoki i ikh vzaimodeystviye s nagnitnym polem Zemli," IL, Moscow, pp. 99, 1962.

6. C. E. McIlwain. J. Geophys. Res., 66, No. 11, 3681, 1961.

MOTION OF CHARGED PARTICLES IN A MAGNETIC DIPOLE FIELD WITH ALLOWANCE FOR DISSIPATION OF ENERGY*

V. M. Vakhnin, G. A. Skuridin,
and I. N. Shvachunov

In this article we consider the problem of the motion of charged particles in a magnetic field in a conservative approximation while also making an allowance for dissipative perturbation for the following three idealized systems: a) a magnetic dipole field in the absence of an outer magnetic field, b) a magnetic dipole in a space having a homogeneous magnetic field parallel to the magnetic dipole field strength vector in its equatorial plane, and c) a magnetic dipole in a space with a homogenous magnetic field antiparallel to the magnetic dipole field strength vector in its equatorial plane.

We examined the problem at the equatorial dipole plane. The motion of charged particles in a magnetic field was analyzed by using the phase plane method in a conservative approximation, which made it possible to detect a number of critical trajectories and to obtain a qualitative picture of the effect of kinetic energy loss on the shape of the trajectory. These losses were taken into account as small dissipative perturbations of the conservative approximation.

---

* These results were reported at the XIII International Astronautic Congress (Varna, 1962) and at the annual gathering of the COSPAR (Warsaw, 1963).

At present the problem of the motion of charged particles in a magnetic field has taken on great importance in conjunction with the theory of the origin of the earth's radiation belts. We know that a calculation of the motion of charged particles, in a conservative approximation, i.e., without allowance for the energy loss by particles, for example, in Störmer's [1] and Boguslavskiy's [2] theories, leads us to infer the impossibility of particle capture by the magnetic field, since any "conservative" solution should be reversible with respect to time.

A conservative solution, however, is not completely rigorous since, according to the classical radiation theory, any curvature in the trajectory of a charged particle entails a certain radiation energy loss [3]. Other possible causes for energy losses exist, e.g., magnetic scattering, losses due to collisions, ionization losses, etc.

Previous works on investigations into particle trajectories in a magnetic dipole field generally disregard these causes of energy losses [4].

In this article we analyze the motion of charged particles in a magnetic dipole field by using the phase plane method both in a conservative approximation [5] and by taking into account their kinetic energy loss to radiation, thus making it possible to obtain a qualitative picture of the effect of kinetic energy loss on the trajectory shape. These losses were taken into account as small dissipative perturbations of the conservative approximation. We also showed the existence of critical trajectories for which particle capture by the magnetic field are effected with the smallest energy losses desired [6]. Particle capture can apparently take place in the presence of

small, though finite losses, even for other trajectories close to critical.

The phase plane method proved to be especially convenient in considering the particle motion in a composite field having both dipole and homogeneous constituents.

In this work conservative approximations and their dissipative perturbation are considered for three idealized systems: a) a magnetic dipole in the absence of an outer magnetic field, b) a magnetic dipole in a space with a homogeneous field parallel to the magnetic dipole field strength vector in its equatorial plane, and c) a magnetic dipole in a space with homogeneous field antiparallel to the magnetic dipole field strength vector on its equatorial plane. These systems were analyzed at the equatorial plane of the dipole.

I. Motion of a Charged Particle in a Magnetic Dipole Field in the Absence an Outer Magnetic Field

1. Differential Equation of the "Phase Trajectory" of Charged Particle Motion

The differential equation for the motion of a charged particle in equatorial plane of a magnetic dipole can be conveniently represented in polar coordinates ρ, φ. The magnetic vector H_d is perpendicular to this plane and equal in value to

$$H_d = \frac{M}{\rho^3}, \tag{1.1}$$

where M is the magnetic dipole moment.

The trajectory curvature of a freely moving charged particle in a magnetic field equals

$$K = \frac{eH_\varphi}{mvc}, \tag{1.2}$$

where m is the particle mass, e is the charge, v is the velocity, and c is the electrodynamic constant.

On the other hand, curvature in polar coordinates is expressed as

$$K = \frac{\rho^2 + 2\rho'^2 - \rho\rho''}{(\rho^2 + \rho'^2)^{3/2}}. \tag{1.3}$$

Using (1.1) and (1.3), the differential equation for the motion of the charged particle at the equatorial plane in a magnetic dipole field has the form

$$\frac{\rho^2 + 2\rho'^2 - \rho\rho''}{(\rho^2 + \rho'^2)^{3/2}} = \frac{a^2}{\rho^3}, \tag{1.4}$$

where $a = \sqrt{eM/mvc}$ is Störmer's characteristic coefficient.

In a conservative approximation, as stated above, the kinetic energy and velocity of the particle are regarded as fixed, i.e., they do not change even with respect to the value of the characteristic coefficient a. For an electron, in absolute gaussian units, we have

$$a^2 = 1{,}75 \cdot 10^7 \frac{M}{v},$$

and for the proton

$$a^2 = 0{,}95 \cdot 10^4 \frac{M}{v}.$$

By changing in (1.4) to phase coordinates

$$w = \frac{\rho}{a}, \qquad u = \frac{d\rho}{d\varphi}\frac{1}{a}, \tag{1.5}$$

we obtain the equation for the "phase trajectory" of the electron particle

$$\frac{du}{dw} = \frac{w}{u} + 2\frac{u}{w} \mp \frac{[1 + (u/w)^2]^{3/2}}{uw}, \tag{1.6}$$

where the minus sign in the right-hand side corresponds to trajectory segments of positive curvature, i.e., convex from the origin. The plus sign corresponds to the trajectory segments of negative curvature.

We can analyze Eq. (1.6) by the isocline method and by constructing the graph of the direction field, and by inspection of the asymplotic formulas for the vicinity of singular points and at infinitely large and infinitely small values of the phase coordinates u, w. This enables us to determine the characteristic features of all possible phase trajectories, and consequently (by changing from the variables w, u, to ρ, and φ) to determine the motion of charged particles in the magnetic dipole field.

2. Plotting the "Isoclines" and the "Direction Fields" on the Phase Plane in the Conservative Approximation

To construct the isoclines of Eq. (1.6), we set du/dw = ϰ = = const. The equation of the isoclines which directly relates u and w, is an equation of the sixth order and has the form

$$\frac{w}{u}+2\frac{u}{w}\mp\frac{[1+(u/w)^2]^{3/2}}{uw}=\varkappa=\text{const}. \tag{1.7}$$

When we set u/w = ξ, (1.7) becomes

$$w^3=\pm\frac{(1+\xi^2)^{3/2}}{1+2\xi^2-\xi\varkappa}. \tag{1.8}$$

Figure 1 shows the family of curves $w^2 = f(\xi,\varkappa)$ in the plane (w^2,ξ) for different values of ϰ.

From Eq. (1.8) for any ϰ when $\xi \to \infty$, we obtain the asymptotic value $w^2 \approx \xi/2$ shown in Fig. 1 as the sloping dashed line, and when $\xi \to 0$, $w^2 \to 1$.

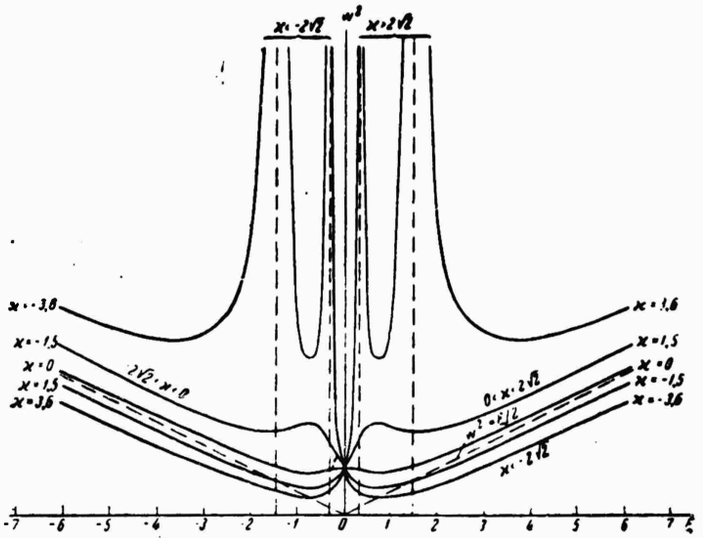

Fig. 1.

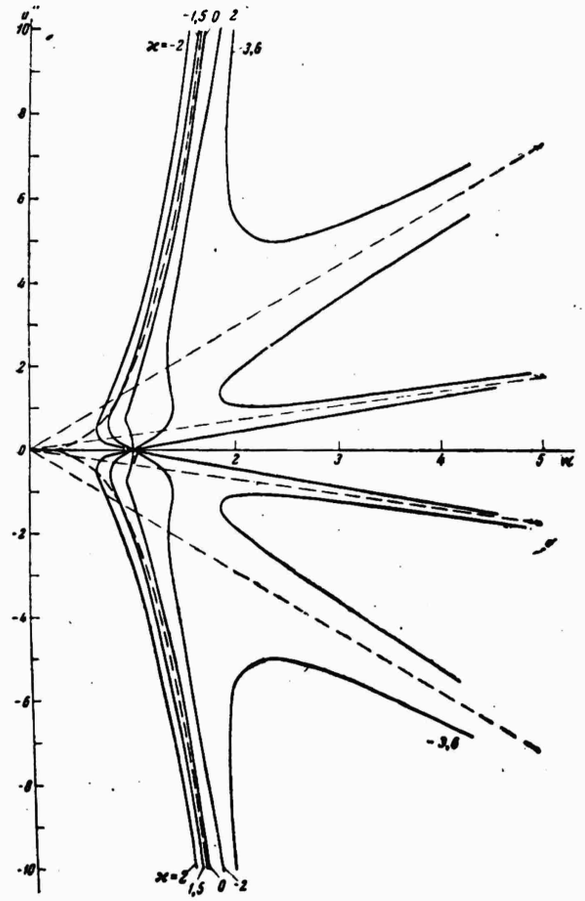

Fig. 2.

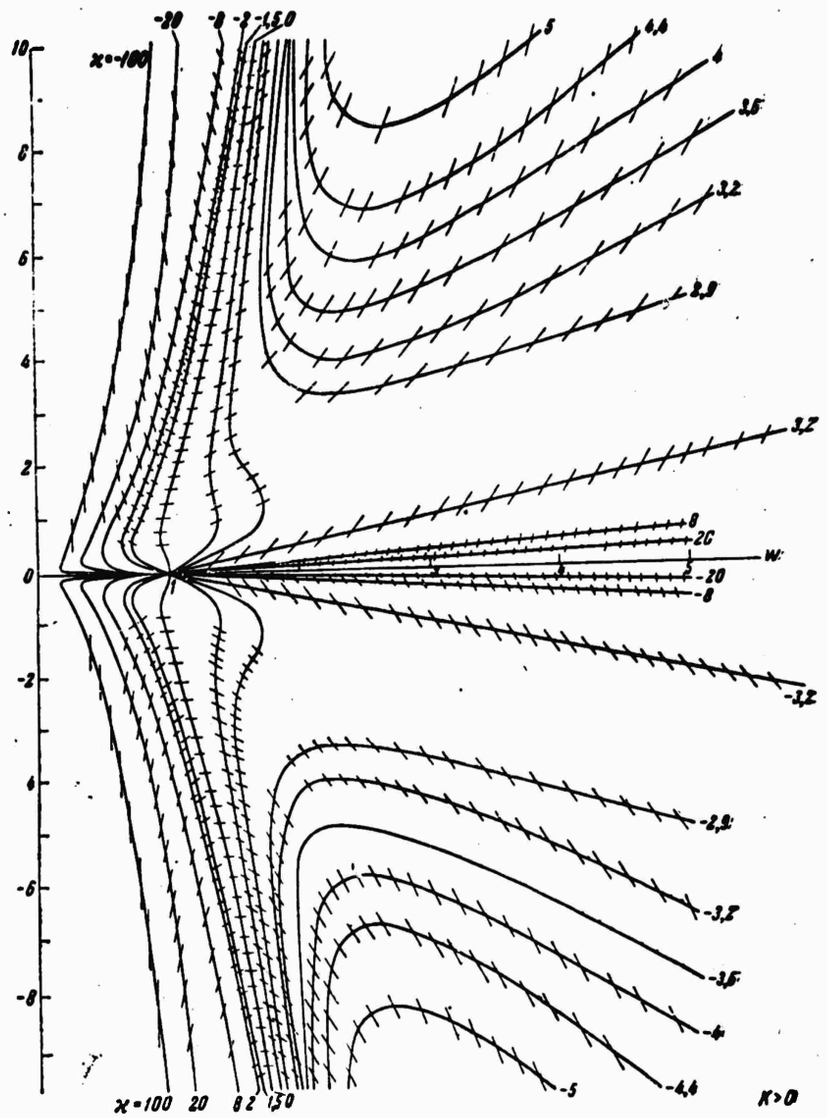
x=100
-20
-8
-2
-1,5
0
5
4,4
4
3,5
3,2
2,9
3,2
8
20
W
-20
-8
-3,2
-2,9
-3,2
-3,5
-4
-4,4
-5
x=100
20
8
2
1,5
0
K>0

Fig. 3.

For $\varkappa > 2\sqrt{2}$ there are also two vertical asymptotes (shown by the dashed line) which correspond to finite values of ξ which at $\varkappa = 2\sqrt{2}$ merge into the one limiting asymptote.

We thus see that the function $w^2 = f(\xi,\varkappa)$ is continuous.

The obtained family of curves with different values of $\varkappa$ on the plane (w^2,ξ) should be converted to coordinates (w,u) by a nonlinear change in the scale along the w^2-axis and then by transformation $u/w = \xi$, at which the lines parallel to the y-axis become inclined lines passing through the origin. As a result of this transformation of scales, we obtain the isocline field shown in Fig. 2. When we map its corresponding "direction element" on each isocline, we obtain the direction field for both positive ($K > 0$) (see Fig. 3) and negative ($K < 0$) curvature, along which, as is known, the phase trajectories respectively, for $K > 0$ and $K < 0$ are readily obtained.

Behavior of Phase Trajectories at Large and Small Values of u and w

At large and small values of u and w, the behavior of the phase trajectories can be studied by inspection of Eq. (1.6).

Let $u \to 0$ and $w \neq 0$, when $u/w \to 0$, then from (1.6) we get

$$\frac{du}{dw} = \frac{1}{u}\left[w \mp \frac{1}{w}\right]. \tag{1.9}$$

Let us consider (1.9) with the plus sign ($K < 0$) for any values of $w \neq 0$. In this case when $u \to 0$, $du/dw \to \infty$, i.e., all phase trajectories at the points of intersection of the w-axis have vertical tangents. Thus when $K < 0$ Eq. (1.6) has no singular points [5].

If in (1.9) we set $w = 1$ and take the minus sign ($K > 0$), then when $u \to 0$, we get the indeterminate form 0/0.

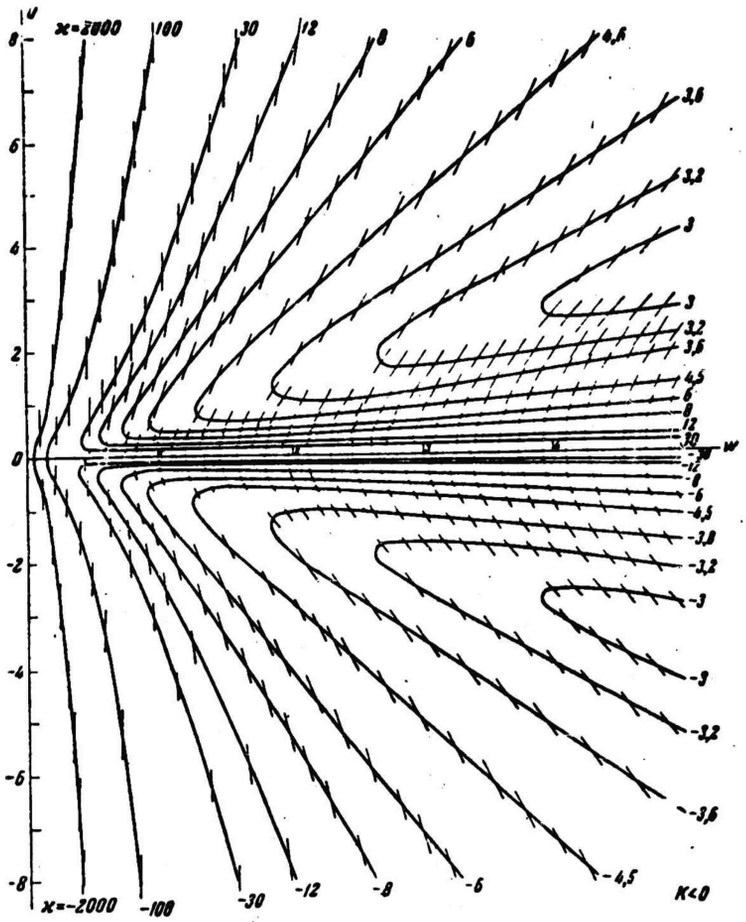
u
x=2000
100
30
12
8
6
4,5
3,6
3,2
3
3
3,2
3,6
4,5
6
8
12
30
w
-30
-12
-8
-6
-4,5
-3,6
-3,2
-3
-3
-3,2
-3,6
-4,5
K<0
x=-2000
-100
-30
-12
-8
-6
8
6
4
2
0
-2
-4
-6
-8

Fig. 4.

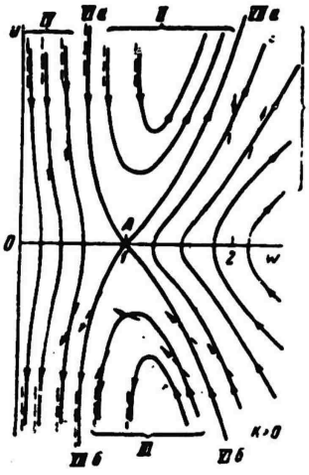

Fig. 5.

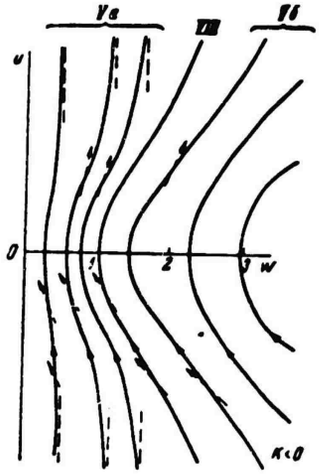

Fig. 6.

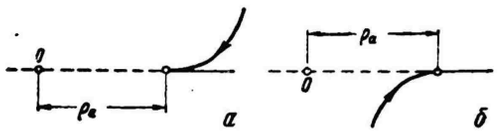

Fig. 7.

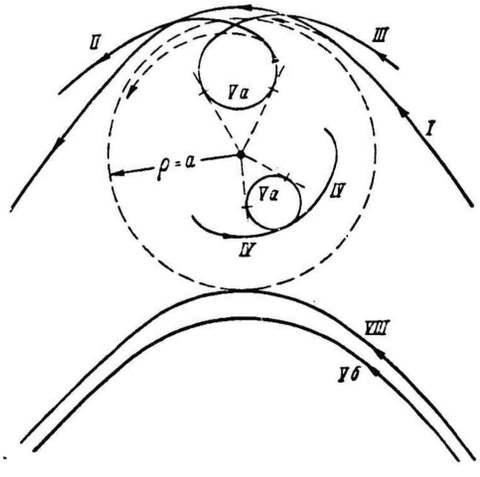

Fig. 8.

Let us develop this indeterminacy:

$$\frac{du}{dw} = \frac{2w\frac{dw}{du}}{\frac{dw}{du}u + w}$$

or

$$\left(\frac{du}{dw}\right)^2 = \frac{2w}{w + u\frac{dw}{du}}.$$

When $w \neq 1$, and $u \to 0$, we get

$$\frac{du}{dw} = \pm\sqrt{2}. \tag{1.10}$$

Thus, the point ($u = 0$, $w = 1$) is singular for (.16). It is readily seen that this singular point is unique and acts somewhat as a saddle point.

Suppose now that $w \to 0$, $u \neq 0$, then $w/u \to 0$ and Eq. (1.6) takes the form of Bernoulli's equation

$$\frac{du}{dw} = \frac{1}{w}\left[2u \mp \frac{u^2}{w^2}\right], \tag{1.11}$$

the solution of which has the form

$$u = \frac{w^3}{Cw \pm 1}. \tag{1.12}$$

Here the phase trajectories will have, when $C \neq 0$, vertical asymptotes at the points $w = 1/C$. With an increase in C, the phase trajectories are rectified, which when $C \to \infty$ degenerate into the asymptote $w = 0$.

Let us consider the behavior of phase trajectories at large values of u and w.

Suppose $w \to \infty$ and $u/w \to 0$, then (1.6) gives

$$\frac{du}{dw} = \frac{w}{u}, \tag{1.13}$$

i.e., $du/dw \to \infty$ from which it follows that there are no asymptotes parallel to the axis of the abscissa.

On the other hand, by integrating (1.13) we obtain $u^2 - w^2 = C^2$, i.e., the phase curves at large values of w are in the form of an equilateral hyperbola.

We will now consider the case where $u \to \infty$ and $w/u \to 0$. As a result, Eq. (1.6) is again transformed into the Bernoulli equation whose solution has form (1.12). The phase curves here will have vertical asymptotes for $w = \pm 1/C$ and $C \neq 0$.

Unlike the aforementioned case for $w \to 0$ and $C = 0$, we obtain $u = \pm w^3$. The phase trajectories take the form of a cubic parabola lacking a vertical asymptote.

It follows from the above cases of $w \to \infty$ or $u \to \infty$, that the phase trajectories separate on the plane (w,u) into equilateral hyperbolas ($w \to \infty$) or cubic parabolas ($u \to \infty$), respectively.

This is easily detected if we consider the nature of the phase curves at $w \to \infty$ and $u \to \infty$. In this case, Eq. (1.6) transforms into the two equations

$$\frac{du}{dw} = \frac{w}{u} \quad (w \to \infty), \tag{1.14}$$

$$\frac{du}{dw} = 3\frac{u}{w} \quad (u \to \infty). \tag{1.15}$$

From (1.14) we derive $u^2 - w^2 = C^2$, and from (1.15), $u = \pm Cw^3$.

The curves separating the corresponding branches of the hyperbolas and parabolas on the (w,u) plane are the separatrixes which pass through the singular point ($u = 0$, $w = 1$).

4. Phase Trajectories and the Trajectories of Charged Particles in a Magnetic Field

Figures 5 and 6 show the phase trajectories plotted according to the previously cited "direction fields" and also from an analysis of Eq. (1.6). The instantaneous state of the charged particle is

characterized by the coordinates w_0, u_0 of the representative point. The motion of the particle along the trajectory corresponds to the motion of the representative point along the phase trajectory. The direction of the representative point is easily determined, if we take into account the fact that positive values of u correspond to an increase in w with an increase in the polar angle φ, since $u = dw/d\varphi$.

It is apparent from Figs. 5 and 6 that the set of phase trajectories can be grouped into several types designated by Roman numerals I-VIII.

To elicit what segments of the particle trajectories correspond to the indicated kinds of phase trajectories, we will examine the relation between the simplest lines and points of the phase plane and the trajectories defined by them in the equatorial plane of the dipole.

1. The points distributed along the w-axis correspond to circular trajectories about the dipole with radius $\rho = aw = \text{const}$.

2. The lines $u = \text{const} \neq 0$ correspond to the spiral of Archimedes, $\rho = a\varphi$.

3. The branch tending asymptotically to the vertical line corresponds to a trajectory tangent to a radius coming from the origin, since in this case $du/dw = \rho'/\rho'' \to \infty$ or $\rho = 0$. The point of tangency is at $\rho_a = aw_a$, where w_a is the asymptotic value of w.

Figure 7a shows a trajectory corresponding to the phase trajectory approaching w from the direction of large values of w, and Fig. 7b shows the same trajectory approaching w from small values of w.

4. The branch approaching infinite values of w corresponds to

the particle trajectory going off to infinity (or the trajectory coming from infinity).

With the above we have sufficient information to determine the nature of the trajectories depicted in the phase curves shown in Figs. 5 and 6. Type I phase curves which have two branches going off to infinity (to infinite $\underline{w}$ values) and which correspond to positive curvature determined the enveloping trajectory (Fig. 8).

Types II and III phase trajectories correspond to the separate trajectory segments which with the Va type phase trajectory determine the "nonenvoloping loop" type of trajectory having branches going off to infinity.

Type IV phase trajectories combined with Va type trajectories to form a "captured" trajectory.

Type Vb phase trajectories and the type VII boundary trajectory determine the hyperbolic enveloping trajectories.

Lastly, VIa,b, VIIa,b, and VIII phase trajectories are the boundary trajectories (separatrixes) dividing the trajectory as of the enveloping, loop, and captured types, whereas the singular point A defines the unstable circular trajectory of radius $\rho = a = \text{const}$ enveloping the dipole.

5. Phase Trajectories and Corresponding Trajectories of a Charged Particle With Allowance for Energy Dissipation

In accordance with classical radiation theory, any curvature in the trajectory of a charged particle is assoicated with a certain radiation energy loss. We know [3] that a particle with charge $\underline{e}$ and which is accelerating radiates in unit time an energy of

$$S = \frac{2}{3}\frac{e^2\dot{v}^2}{c^3}.$$

The relative losses to radiation on a small arc dφ of the trajectory of the moving particle will be

$$\frac{dS_0}{S_0} = \frac{4}{3}\frac{e^2H_0^2}{c^2m}d\varphi.$$

These relative energy losses involve a change in the velocity of the particle, and consequently a change in the characteristic coefficient a. For small energy losses a valid approximation is

$$\frac{\Delta r}{r} \approx \frac{1}{2}\frac{\Delta S_0}{S_0} \approx -2\frac{\Delta a}{a}. \tag{1.16}$$

Let us consider the image of a change in the kinetic energy on the phase plane. An instantaneous change by a value ΔS_0 without a discontinuity and break in the trajectory particle results in a change of the coefficient a while keeping the previous values for ρ and dρ/dφ.

We shall find Δu and Δw of the representative point characterizing the instantaneous state of the particle on the phase plane

$$\Delta u = \frac{\partial u}{\partial a}\Delta a = -\frac{1}{a^2}\frac{\partial \rho}{\partial \varphi}\Delta a$$

or

$$\Delta u = -u\frac{\Delta a}{a}.$$

In accordance with (1.16) we obtain

$$\Delta u \approx \frac{1}{4}u\frac{\Delta S_0}{S_0} = \frac{1}{2}u\frac{\Delta v}{v}. \tag{1.17}$$

Similarly for Δw

$$\Delta w \approx \frac{1}{4}w\frac{\Delta S_0}{S_0} = \frac{1}{2}w\frac{\Delta v}{v}. \tag{1.18}$$

Thus, with energy losses $\Delta S_0 < 0$ and, consequently, the representative point shift toward the origin. For uninterrupted energy losses, the movement of the representative point on the phase curve will proceed in such a manner that it will always be displaced

toward the origin, with respect to the conservative phase curves which is readily confirmed if we represent the continuous energy loss in terms of the sum of infinitely small discrete loss and use expressions (1.17) and (1.18).

Figures 5, 6 and 8 (dashed arrors) give a systematic representation of the direction of movement of the representative point during a loss in kinetic energy. If the phase curve for a particle moving over the envoloping trajectory, is, in a conservative approximation, close enough to the separatrix, the energy losses will cause the phase curve to intersect the separatrix VIb,a and, consequently, the particle will change from an enveloping trajector to a "loop" trajectory. Furthermore, when the representative point moves along the left branch of the type III phase curve (Fig. 5), the extended energy losses can effect an intersection of the representative point and the second separatrix VIIb, resulting in the particle changing to a capture trajectory defined by the phase curves IV and Va. Figure 3 gives a systematic representation of this process in a phase trajectory, and Fig. 8 (the dashed line) shows this process on the equatorial plane of the dipole.

Motion of a Charged Particle in a Magnetic Dipole Field In an Outer Homogeneous Magnetic Field Parallel to the Magnetic Dipole Vector at its Equatorial Plane

1. Differential Equation for the Phase Trajectory of a Charged Particle

In the case under consideration the value of the resulting magnetic field will be

$$H = \frac{M}{\rho^3} + H_0, \tag{2.1}$$

where H_0 is the outer magnetic field strength.

The trajectory curvature of a freely moving charged particle in this case will be

$$K = \frac{eH}{mvc} = \frac{eM}{mvc}\frac{1}{\rho^3} + \frac{eH_0}{mvc}. \qquad (2.2)$$

Using (2.1) and (2.2) we obtain the differential equation for the motion of a charged particle in polar coordinates in a magnetic field

$$\frac{\rho^3 + 2\rho'^2 - \rho\rho''}{(\rho^2 + \rho'^2)^{3/2}} = \frac{a^3}{\rho^3} + k, \qquad (2.3)$$

where $k = eH_0/mvc$ is a supplementary term taking into account the effect of the homogeneous magnetic field H_0.

When we transfer to phase coordinates w,u, we obtain the differential equation for the phase trajectories of the charged particle

$$\frac{du}{dw} = \frac{w}{v} + 2\frac{u}{w} \mp \frac{[1 + (u/w)^2]^{3/2}}{uw}(1 + hw^3), \qquad (2.4)$$

where $h = ak = \frac{H_0}{H_d(a)}\left(H_d(a) = \frac{M}{a^3}\right)$.

The minus sign in front of the third term in the right-hand side, as before, represents a trajectory with positive curvature, whereas the plus sign corresponds to a negative curvature.

2. Behavior of Phase Trajectories for Small and Large Values of u and w

At small and large values of u and w the behavior of phase trajectories can be studies by an inspection of Eq. (1.14). Let $u \to 0$ and $w \neq 0$. By letting $u/w \to 0$, from (2.4) we get

$$\frac{du}{dw} = \frac{1}{u}\left[w \mp \frac{1 + hw^3}{w}\right]. \qquad (2.5)$$

In this case the derivative du/dw will be either finite or infinite depending on whether the expression in brackets in (2.5) has positive real roots for w at different values of the parameter h. With this in mind, we first consider the equation

$$hw^3 - w^3 + 1 = 0 \tag{2.6}$$

for K > 0:

a) at $0 < h < 2/3\sqrt{3}$ this equation has two positive real roots

$$w_1 = \frac{1}{3h}\left\{1 + 2\cos\left[\frac{\pi}{3} + \frac{\arccos(13.5h^2 - 1)}{3}\right]\right\}, \tag{2.7}$$

$$w_2 = \frac{1}{3h}\left\{1 + 2\cos\left[\frac{\pi}{3} - \frac{\arccos(13.5h^2 - 1)}{3}\right]\right\}; \tag{2.8}$$

b) at $h = 2/3\sqrt{3}$ the equation has one positive real root

$$w_0 = \frac{1}{3h}\left(1 + 2\cos\frac{\pi}{3}\right) = \sqrt{3}; \tag{2.9}$$

c) at $h > 2/3\sqrt{3}$ there are no positive real roots.

At the points w_γ ($\gamma = 0, 1, 2$) as $u \to 0$, (2.5) becomes the indeterminate form 0/0. When we evaluate this indeterminate form, we obtain

$$\frac{du}{dw} = \pm\sqrt{2 - 3hw_\gamma}. \tag{2.10}$$

It follows from (2.7) that $3hw_1 < 2$, and hence Eq. (2.10) has a real value, and w_1 is the singular type of saddle. Analogously, from (2.8) it follows that $3hw_2 > 2$, thus Eq. (2.10) is imaginary and the point w_2 is a singular type of saddle.

At point $w_0 = \sqrt{3}$, we have

$$\frac{du}{dw} = 0. \tag{2.11}$$

In this case the singular points w_1 and w_2 merge into one: $w_0 = \sqrt{3}$. It is easily shown that these singular points are the only ones for $K > 0$.

We consider Eq. (2.5) for $K < 0$ and for any other values of $w \neq 0$, as $u \to 0$.

$$hw^3 + w^3 + 1 = 0. \tag{2.12}$$

For all values of the parameter $h(0 < h < \infty)$, Eq. (2.12) does not have even one positive real root, and consequently the quantity in brackets in (2.5) for $K < 0$ for any values of h and w do not vanish.

Consequently as $u \to 0$, $du/dw \to 0$, i.e., all phase trajectories at the points of intersection of the w-axis have vertical tangents. Thus when $K < 0$, and as $u \to 0$, Eq. (2.4) has no singular points.

When $w \to 0$, and $u \neq 0$, $w/u \to 0$ and (2.4) takes the form of the Bernoulli equation

$$\frac{du}{dw} = \frac{1}{w}\left[2u \mp \frac{u^2}{w^3}\right]. \tag{2.13}$$

Equation (2.13) does not depend on the parameter h and coincides with (1.11). As indicated in paragraph 3, Section 1, the phase curves will have vertical asymptotes at the points $w = 1/C$ when $c \neq 0$. With an increase in C, there is a rectification in the phase curves which as $C \to \infty$ degenerate into the asymptote $w = 0$.

We will now consider the behavior of phase trajectories at large values of u and w.

If $w \to \infty$ and $u/w \to 0$, then

$$\frac{du}{dw} = \frac{w}{u}\left[1 \mp hw\right] \to \infty. \tag{2.14}$$

It follows that at all values of the parameter $h(0 < h < \infty)$ the phase trajectories have no asymptotes parallel to the w-axis.

To determine whether the phase curves have vertical asymptotes parallel to the u-axis, we consider the case where $u \to \infty$ and $w/u \to 0$

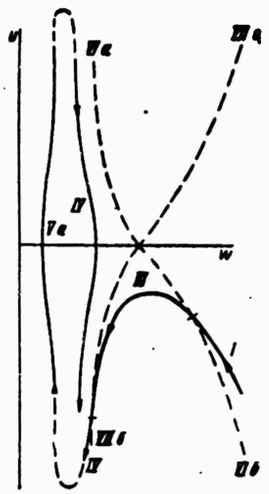

Fig. 9.

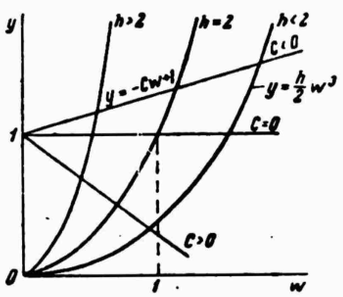

Fig. 10.

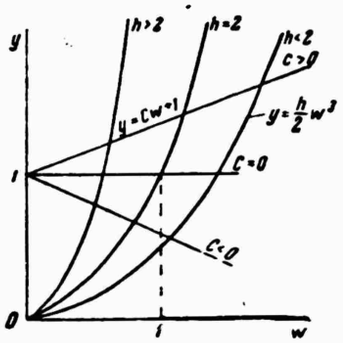

Fig. 11.

In this case (2.14) becomes the Bernoulli equation

$$\frac{du}{dw} \approx 2\frac{u}{w} \mp \frac{u^2(1+hw^3)}{w^4}, \tag{2.15}$$

the solution of which has the form

$$u = \frac{1}{\pm\left(-\frac{1}{w^3}+\frac{h}{2}\right)\frac{C}{w^3}}. \tag{2.16}$$

The phase curves will have vertical asymptotes at those values of w where the denominator in (2.16) becomes zero.

We investigate this equation first for K > 0

$$hw^3 + 2Cw - 2 = 0. \tag{2.17}$$

The graphs of the equation $hw^3/2 = -Cw^3 + 1$ at $w > 0$ are shown in Fig. 10. We see that for all h and for all $C \gtrless 0$ there will always be one real positive root w_1 of Eq. (2.17), i.e., when $w = w_1$ in Eq. (2.16), $u \to \infty$. This indicates that for all h all the phase trajectories for $K > 0$ have vertical asymptotes parallel to the u-axis.

We now inspect Eq. (2.16) for negative curvature ($K < 0$)

$$hw^3 - 2Cw - 2 = 0. \tag{2.18}$$

The graph of $(h/2)w = Cw + 1$ for $w > 0$ is shown in Fig. 11. This figure shows that at all values of the parameter h and for all $C \gtrless 0$ there will always be one positive root w_1 satisfying Eq. (2.18) at which $u \to \infty$ in Eq. (2.16). Hence all the phase trajectories have vertical asymptotes parallel to the u-axis.

3. Phase Trajectories and the Associated Trajectories of Charged Particles in a Magnetic Field

We shall consider the phase trajectories and the corresponding trajectories of charged particles in the magnetic field $H = H_d + H_o$ for various values of the parameter h in a conservative approximation based on our analysis of Eq. (2.4).

a) For $0 < h < 2/3\sqrt{3}$ the phase trajectories have the shape shown in Figs. 12 and 13.

The trajectories of charged particles in an equatorial plane corresponding to the different values of the phase trajectories are

shown in Fig. 14. The closed phase trajectory I (Fig. 12) corresponds to the "loopless" type trajectory enveloping the dipole which at sufficient distances $\rho \gg \sqrt[3]{M/N_0}$ from the dipole can be as close as possible to a simple circular trajectory of radius $r = mvc/eH_0$, whereas, at even closer distances from the dipole the trajectory noticeably diverges from a circular trajectory owing to a linear change in the magnetic dipole vector with increasing distance from the dipole.

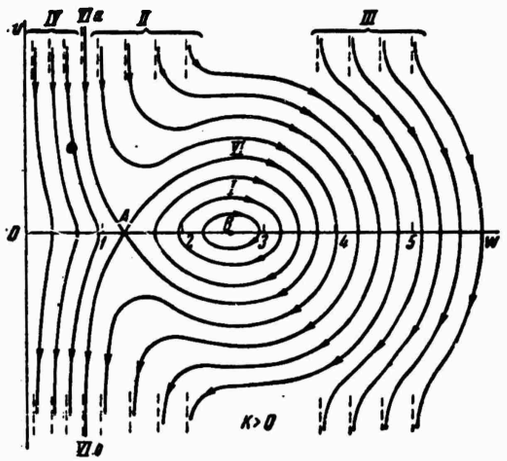

Fig. 12.

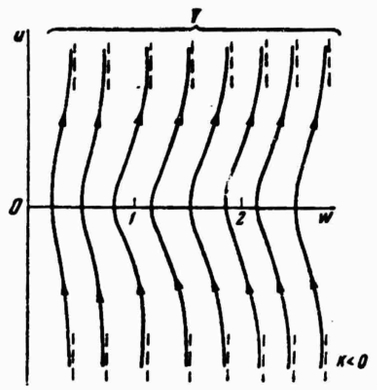

Fig. 13.

Phase trajectories II and V simultaneously define the loop trajectory enveloping the dipole. This trajectory is similar to trajectory I with the only difference being that it forms loop V when near the dipole.

It is essential to point out that as a result of the nonlinear change in H, the entire motion cycle of the representative point along the phase trajectories I and II-V corresponds to rotation of particles about the dipole at an angle exceeding 360°, since the trajectories of the charged particles are open during one revolution. Therefore, they will rotate relative to the dipole center and in infinite time

they will fill the entire ring between the two boundaries of the circles whose radii are at maximum and minimum distances from the center of the dipole [7].

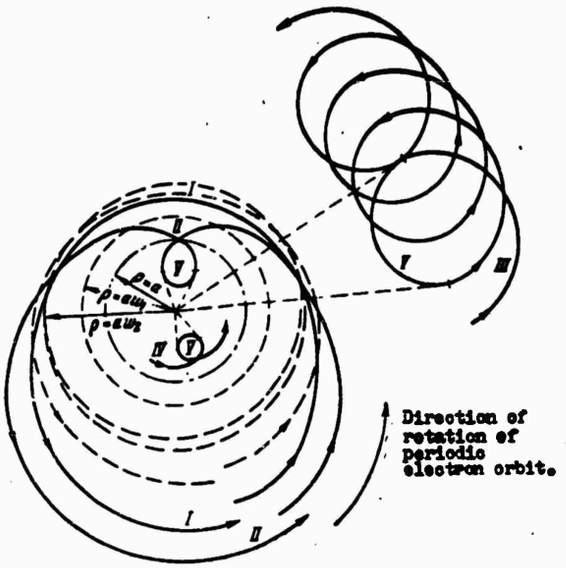

Fig. 14.

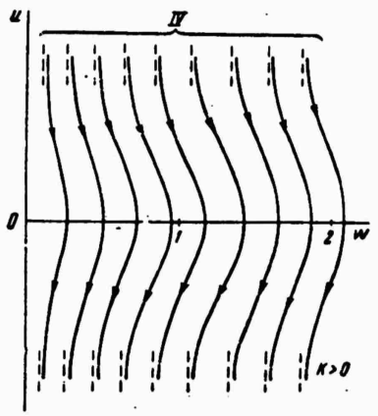

Fig. 15.

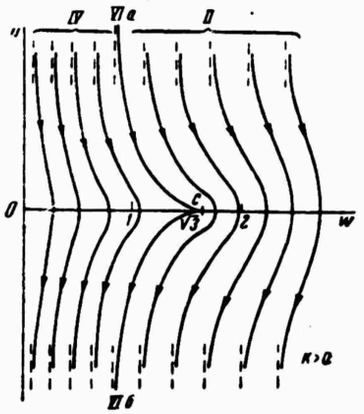

Fig. 16.

Phase trajectories III and V simultaneously define the loop trajectory at $\rho \gg \sqrt[3]{M/H_0}$ from the dipole center, while phase trajectories IV and V also correspond to the loop trajectory but are $\rho \ll \sqrt[3]{M/H_0}$

from the center of the dipole. These loop trajectories are open for the same reason as trajectories I and II-v, and in a "drift" approximation they can be represented [8] as the movement of a charged particle about circles of radii $r = mvc/eH_0$ (trajectories III-V) and $r = mvc/eH_d$ (trajectories IV-V) with a homogeneous drift of their leading centers about the dipole center owing to the presence of ∇H_d.

The singular point A corresponds to the unstable circular trajectory of radius $\rho = aw_1(h) = const$, while the singular point B corresponds to the stable periodic trajectory of radius $\rho = aw_2(h) = = const$. Phase trajectories VI, VIa, and VIb which pass through A are the separatrixes dividing the phase trajectories into their respective types.

b) $h > 2/3\sqrt{3}$. The phase trajectories for his case are shown in Figs. 13 and 15. Figure 15 shows that the region of type I phase trajectories and the separatrixes bounding it vanish, so that loopless enveloping trajectories are not present. The remaining picture of motion is the same as that for case a).

c) $h = 2/3\sqrt{3}$. This is the transitional case between a) and b). In the first case when $h(k > 0)$ increased, both singular points A and B draw nearer and for $h = 2/3\sqrt{3}$, merged forming the one singular point C at $w = \sqrt{3}$ (Fig. 16).

4. Phase Trajectories and Their Associated Trajectories of a Charged Particle with an Allowance for Energy Dissipation

In this case the motion of charged particles in qualitatively differs in many ways from the case of a magnetic dipole lacking an outer field. When we have an outer magnetic field, H_0, and lines of

force of the resultant magnetic field, $H = H_d + H_o$, normal to the equatorial dipole plane, all charged particles whose trajectories lie in this plane are already captured by the outer magnetic field H_o. The magnetic dipole will exite the homogeneous field by the magnitude of H_d, as a result of which, as stated above, the leading centers of all trajectories drift relative to the center of the dipole. If in this case the dipole lacks an outer field we can speak of the capture (IV-V) and noncapture (I, II-V) of particles by the magnetic dipole field, where as in the presence of an outer magnetic field H_o there is no principal difference between the trajectories of particles proceeding at extremely large (II-V, III-V) and relatively small (IV-V) distances from the center of the dipole.

For a dipole lacking an outer magnetic field the transition of a charged particle trajectory from a remote to a near-lying trajectory (with respect to the center of the dipole) in the presence of dissipative perturbations occurs at a well-defined distance ρ_{cr} where the nature of its movement qualtitatively changes: this particle is captured by the magnetic dipole field, i.e., a transition from a "noncaptured" to a "captured" trajectory. In the phase plane the capture process corresponds to the intersection between the representative point and the separatrix VIIb (Fig. 9). In the presence, however, of an outer magnetic field H_o, the transistion from a sufficiently remote to closer trajectories in the presence dissipative perturbations, according to Formulas (1.17) and (1.18) occurs continuously without qualtitative changes in the motion of this particle. The intersection of the representative point and the separatrix VIa or VIb in the phase plane (Fig. 12) does not change the nature of the movement, since, as indicated above, there is fundamental difference

between trajectories II-V, III-V, and IV-V.

The charged particle moving over the loopless trajectory and losing kinetic energy to radiation finally changes from the loopless enveloping trajectory I to the loop trajectory IV-V.

Actually, the representative point, corresponding to a charged particle moving over the loopless enveloping trajectory I and losing kinetic energy to radiation will in the phase plane proceed along a twisting spiral in accordance with Formulas (1.17) and (1.18), while approaching singular point B. With an energy loss ΔS_0 (velocity Δv) the characteristic coefficient a, and consequently the parameter h, will increase.

$$\frac{\Delta h}{h} = 3\frac{\Delta a}{a}. \tag{2.19}$$

We see from (2.7) and (2.8) that with an increase in h, the singular points $A(w_1)$ and $B(w_2)$ (Fig. 12) approach along the w-axis and at $h = 2/3\sqrt{3}$ will merge into point $w_0 = \sqrt{3}$ (Fig. 16); the closed region of the phase trajectories I (Fig. 12) bounded by the separatrix VI draw together to this point (Fig. 16).

Furthermore, in the presence of the smallest possible loss in kinetic energy of the particle, i.e., the smallest possible increase in h, this particle hits the loop trajectory IV-V, since $h > 2/3 > \sqrt{3}$ and the separatrixes VIa and VIb vanish (Fig. 15).

III. Motion of a Charged Particle in a Magnetic Dipole Field in an Outer Homogeneous Magnetic Field Antiparallel to the Magnetic Field Strength of a Dipole in its Equatorial Plane

1. Differential Equation for the Phase Trajectory of a Charged Particle

In the case under consideration the resultant magnetic field

equals

$$H = \frac{M}{\rho^3} - H_0. \tag{3.1}$$

The trajectory curvature of a freely moving charged particle is

$$K = \frac{eH}{mvc}\frac{1}{\rho^3} - \frac{eH_0}{mvc}. \tag{3.2}$$

As before, on the basis of Eqs. (3.1) and (3.2)

$$\frac{\rho^2 + 2\rho'^2 - \rho\rho''}{(\rho^2 + \rho'^2)^{3/2}} = \frac{a^2}{\rho^3} - k. \tag{3.3}$$

By converting to the phase coordinates w, u, we obtain the differential equation for the phase trajectories conforming to Eq. (2.3) in the form

$$\frac{du}{dw} = \frac{w}{u} + 2\frac{u}{w} \mp \frac{[1 + (u/w)^2]^{3/2}}{uw}(1 - hw^3). \tag{3.4}$$

The minus sign in front of the fraction corresponds to the previous positive curvature ($K > 0$) and the plus sign corresponds to the negative curvature ($K < 0$) on all regions where the magnetic dipole field vector of the resulting magnetic field coincides with the magnetic dipole field vector, i.e., at $w < \sqrt[3]{1/h}$. In those regions where the field vector reverses the direction ($w > \sqrt[3]{1/h}$), the relationship between the sign in front of the fraction and the trajectory curvature changes.

2. Behavior of Phase Trajectories at Large and Small Values of u and w

As before, we can study the behavior of phase trajectories by an inspection of Eq. (3.4).

When $w \to 0$ and $u \neq 0$, $w/u \to 0$, and the equation takes the form of the Bernoulli equation

$$\frac{du}{dw} = \frac{1}{w}\left[2u \mp \frac{w^2}{w^3}\right]. \tag{3.5}$$

This equation does not depend on the parameter h and is identical to Eqs. (1.11) and (2.13). Consequently, here also the phase curves will have vertical asymptotes at w = 1/C when C ≠ 0. When C increases, there is a rectification in the phase curves which, as C → ∞, degenerates into the asymptote w = 0.

If u → 0, and w ≠ 0, u/w → 0, and Eq. (3.4) has the reduced form

$$\frac{du}{dw} = \frac{1}{u}\left[w \mp \frac{1 - hw^3}{w}\right]. \tag{3.6}$$

In this case the derivative du/dw will be finite or infinite depending on whether the expression in brackets has positive real roots of w at different values of h.

We will analyze this expression first for K > 0 when $hw^3 < 1$, and for K < 0 when $hw^3 > 1$.

We get

$$hw^3 + w^2 - 1 = 0. \tag{3.7}$$

For any h, Eq. (3.7) will always have one positive real root. For different values of h, this root can be represented as

$$w_1 = \begin{cases} \frac{1}{3h}\left\{2\cos\left[\frac{\arccos(1-13{,}5h^2)}{3}\right] - 1\right\}, & 0 < h \leqslant \frac{\sqrt{2}}{3\sqrt{3}}, \\ \frac{1}{3h}\left\{2\cos\left[\frac{\arccos(13{,}5h^2-1)}{3}\right] - 1\right\}, & \frac{\sqrt{2}}{3\sqrt{3}} \leqslant h \leqslant \frac{2}{3\sqrt{3}}, \\ \frac{1}{3h}\left\{2\operatorname{ch}\left[\frac{\operatorname{Ar\,ch}(13{,}5h^2-1)}{3}\right] - 1\right\}, & h > \frac{2}{3\sqrt{3}}. \end{cases} \tag{3.8}$$

It is easily seen that this root varies in the interval $0 < w_1 \leq 1$. At point w_1 as u → 0, Eq. (3.6) becomes the indeterminate form

0/0. Evaluating this, we obtain

$$\frac{du}{dw} = \mp \sqrt{2 + 3hw_1}. \tag{3.9}$$

Equation (3.9) always has one real value, i.e., the point w_1 is the only singular "saddle" point of Eq. (3.4).

We now inspect the quantity in brackets in (3.6) when there is a plus sign in front of the fraction. This corresponds to $K < 0$ when $hw^3 < 1$, and to $K > 0$ when $hw^3 > 1$.

$$hw^3 - w^2 - 1 = 0. \tag{3.10}$$

For all h, Eq. (3.10) has one positive real root

$$w_2 = \frac{1}{3h}\left\{1 + 2\operatorname{ch}\left[\frac{\operatorname{Arch}(13{,}5h^2 + 1)}{3}\right]\right\}. \tag{3.11}$$

The analysis of Eq. (3.10) shows that the value of w_2 as a function of the parameter h takes values from $0 < w_2 < \infty$.

At point w_2, when $u \to 0$, Eq. (3.6) becomes the indeterminate form 0/0. Evaluating it, we obtain

$$\frac{du}{dw} = \pm \sqrt{2 - 3hw_2}. \tag{3.12}$$

Let us now examine the behavior of phase trajectories at large values of w and u.

If $w \to \infty$ and $u/w \to 0$, then

$$\frac{du}{dw} = \frac{w}{u}[1 \pm hw] \to \infty \tag{3.13}$$

Hence, it all values of the parameter h for phase trajectories there are no assymptotes parallel to the w-axis.

To determine whether the phase trajectories have vertical asymptotes parallel to the u-axis, we consider the case where $u \to \infty$ and $w/u \to 0$. Equation (3.4) then becomes the Bernoulli type differential

equation

$$\frac{du}{dw} = 2\frac{u}{w} \mp \frac{u^3(1-hw^3)}{w^4}, \tag{3.14}$$

the solution of which has the form

$$u = \frac{1}{\mp\left(\frac{1}{w^2}+\frac{h}{2}\right)+\frac{C}{w^2}}. \tag{3.15}$$

The phase curves will have vertical asymptotes for those w at which the denominator in (3.5) becomes zero.

We will investigate this equation first for $K > 0$ when $hw^3 < 1$, and then for $K < 0$ when $hw^3 > 1$.

We get

$$hw^3 - 2Cw + 2 = 0. \tag{3.16}$$

Equation (3.16) has positive real roots only for $C \geq 3/2 \sqrt[3]{h}$. Thus only in this case do the corresponding phase trajectories have branches going off to infinity with vertical asymptotes parallel to the u-axis.

We will now consider Eq. (3.15) for $K < 0$ when $hw^3 < 1$, and for $K > 0$ when $hw^3 > 1$

$$hw^3 + 2Cw + 2 = 0. \tag{3.17}$$

Equation (3.17) has positive real roots only for $C \leq 3/2 \sqrt[3]{h}$, and the corresponding trajectories have branches with vertical asymptotes parallel to the u-axis going off to infinity.

3. Phase Trajectories and the Corresponding Trajectories Of Charged Particles in a Magnetic Field

We shall consider the phase trajectories and their corresponding trajectories of charge particles in the magnetic field $H = H_d - H_o$ in a conservative approximation based on an analysis of Eq. (3.4).

In this case the shape of the phase plane does not vary qualitatively for any value of the parameter h, and the phase trajectories

have the shape shown in Figs. 17 and 18.

Figure 19 shows the trajectory of charged particles in the equatorial plane corresponding to the various phase trajectories.

The point $w_o = \sqrt[3]{1/h}$ on the phase plane (Figs. 17 and 18) represents a circle of radius $\rho_o = aw_o = \sqrt[3]{|M/H_o|}$ (Fig. 19) on which numerically $H_d = M/\rho^3 = H_o$, i.e., the resulting magnetic field $H = 0$. Apparently, in the region interior to the exterior to the neutral circle, the resulting field H has opposite signs and consequently, when it is intersected by the charged particle the curvature of the trajectory of the latter changes its sign.

Phase trajectory I (Fig. 17) corresponds to the loopless type trajectory enveloping the dipole (Fig. 19). Phase trajectories II, III, and V simultaneously define the loopless trajectory enveloping the dipole.

Trajectories I, II, and III, intersecting the neutral circle of radius $\rho_o = aw_o = \text{const}$, change the sign of their curvature ($K > 0 \rightleftarrows K < 0$) and change to curvilinear trajectory VI, which at sufficiently large distances $\rho \gg \sqrt[3]{M/H_o}$ from the center of the dipole can be as close as possible to the circular trajectory of radius $r = mvc/eH_o$.

Phase trajectories IV and V simultaneously defind the loop trajectory at $\rho \ll \sqrt[3]{M/H_o}$ from the center of the dipole, while the phase trajectories V-Vl also correspond to the loop trajectory though at $\rho \gg \sqrt[3]{M/H_o}$ from the dipole center. These loop trajectories, just as loop trajectories IV-V and III-V in paragraph 3 Section 2, in a drift approximation can be regarded as the movement of a charged particle along a circle of radius $r_1 = mvc/eH_d$ (trajectories IV-V) and $r_2 = mvc/eH_o$ (trajectories V-VI) with homogeneous drift of their

leading centers around the center of the dipole resulting from H_d. Obviously, the motion of the charged particles (having similar charge signs) along the circles r_1 and r_2 and also the drift of the leading centers of these circles will proceed in the opposite direction.

The closed phase trajectory VII (Fig. 18) corresponds to an undulating trajectory of the charged particle about a stable circular trajectory of radius $\rho = aw_2 = \text{const}$ (Fig. 19). This circle in the plane is determined by the singular point B. The singular saddle type point A corresponds to an unstable circular trajectory of radius $\rho = aw_1 = \text{const}$, and the phase trajectories VIa, b, and VIIa, b which pass through a are the separatrixes dividing the phase trajectories into their different types.

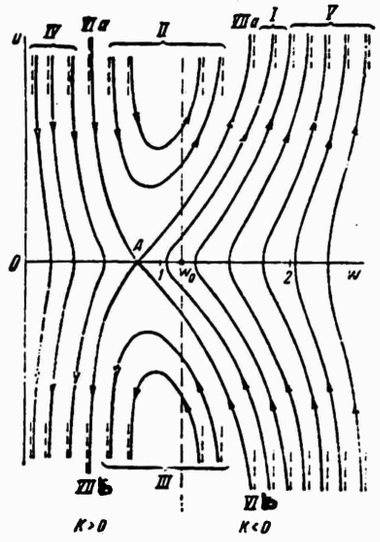

Fig. 17.

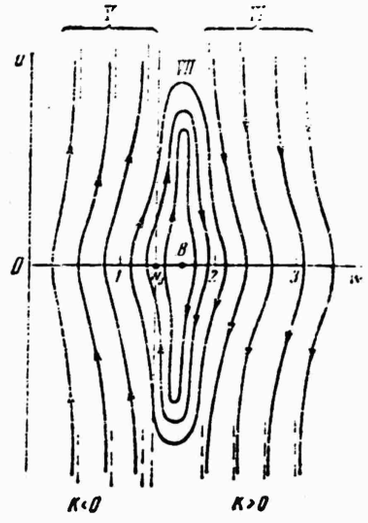

Fig. 18.

4. Phase Trajectories and Corresponding Trajectories of a Charged Particle with an Allowance for Dissipation of Energy

In this case, as in that of the dipole in an outer homogeneous field parallel to the magnetic dipole field vector at its equatorial plane (par. 2), due to the presence of the outer magnetic field all the charged particles whose trajectories lie in the equatorial plane have already been captured by this outer field. All that was said

above in par. 4, Section 2 with respect to the nature of the motion of charged particles along the loop trajectories IV-V and III-V also hold in this case (trajectories III-V in par. 4, Section 2 here correspond to the trajectory VI-V, and trajectories IV-V are completely analogous) with the only difference being that (as stated in par. 3, Section 3) the charged particles with identical charges will move along trajectories IV-V and VI-V in the opposite direction.

Just as in the case of a dipole with a parallel outer magnetic field, the change of the charged particle from a remote to a nearby trajectory in the presence of dissipative perturbations, in agreement with (1.17) and (1.18), occurs continuously without any qualitative changes in the nature of motion of this particle. The intersection between the representative point and separatrix VIb and VIIa, and also VIa and VIIb in the phase plane (Fig. 17) does not qualitatively change the character of the movement.

Unlike the dipole with a parallel outer magnetic field, in this case the particle capture by the magnetic dipole field can be effected in a stable circular trajectory. We shall consider this capture in greater detail. The representative point corresponding to the charged particle moving along trajectory VII enveloping the dipole (Figs. 18 and 19) and osing kinetic energy to radiation, will proceed along the twisting spiral of Formulas (1.17) and (1.18), while approaching the singular point B. And as shown in par. 4, Section 2, the parameter $\underline{h}$ increases according to (2.19), which results in the midpoint $B(w_2)$ being displaced along the w-axis. For sufficiently large $\underline{h}$ (or sufficient small $\underline{v}$), from (3.11) we get

$$w_2 = \frac{1}{3h}\left\{1 + 2\operatorname{ch}\left[\frac{\operatorname{Arch}(13{,}5h^2+1)}{3}\right]\right\} \approx \sqrt[3]{\frac{1}{h}} = w_0. \qquad (3.18)$$

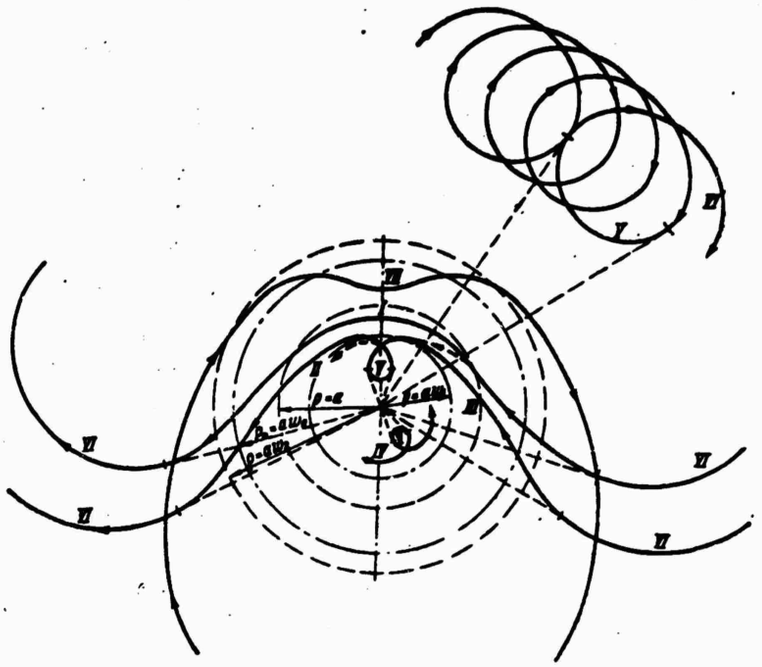

Fig. 19.

Hence as h increases, the singular point $B(w_2)$ approaches the neutral point w_0, and at sufficiently large h they merge.

In the equatorial dipole plane the movement of the charged particle corresponding to the previously described motion of the representative point in a phase plane will proceed over an undulating trajectory with constantly decreasing amplitude of oscillations about a circle of radius $\rho_0 = aw_0 = \text{const}$. At sufficiently large h, the particle is practically in a neutral circle when the kinetic energy approaches zero.

REFERENCES

1. S. K. Mitra. Verkhnyaya atmosfera. IL, M., 1955.

2. S. A. Boguslavskiy. Izbrannyye trudy po fizike. Fizmatgiz, 1961.

3. L. D. Iandau, and Ye. M. Lifshits. Teoriya polya. Fizmatgiz, 1961.

4. S. N. Vernov, and A. Ye. Chudakov. Usp. fiz., n., 70, No. 4, 585, 1960.

5. A. A. Andronov, A. A. Vitt, and S. E. Khaykin. Teoriya kolebaniy. Fizmatgiz, 1959.

6. V. M. Vakhnin, and G. A. Skuridin. Dokl. AN SSSR, 135, 1354, 1960.

7. L. D. Landau, and Ye. M. Lifshits. Mekhanika. Fizmatgiz, 1958.

8. Kh. Al'fven. Kosmicheskaya elektrodinamika, IL, M., 1952.

INVESTIGATIONS OF COSMIC RADIATION BEYOND THE ATMOSPHERE

N. L. Grigorov, D. A. Zhuravlev, M. A. Kondrat'eva,
I. D. Rapoport, and I. A. Savenko

Measurements of the tracks of charged particles in an emulsion irradiated at a height of 306-339 km showed that the intensity of the recorded radiation is three times greater than the intensity of primary cosmic radiation. Nearly 50% of the excess particles were nonnuclear active particles with minimum ionization (electrons are the fastest). The remaining 50% are strongly ionized particles which are nuclear fission products.

Measurements made on rockets and earth satelites have shown that at heights of 200-300 km the radiation flux is several times greater than that of primary cosmic rays, even though the radiation belts are well-defined at high altitudes.

This excess of radiation over primary cosmic radiation was recorded by instruments mounted on the second spaceship (Aug. 19, 1960) whose orbit was 306-309 km above the earth's surface within the latitudes $\pm$ 65°.

Figure 1 shows the results of measurements made with counters on the second spaceship, and also the intensity of primary cosmic

radiation measured by A. N. Charakhch'yan and T. N. Charakhch'yan [3].

Curve 1 shows the results of the measurements made by means of a single gas-discharge counter mounted inside the spaceship [1]. The higher count in the gas-discharge counter over that expected from primary cosmic radiation in Savenko's et al. work [1] is explained by secondary charged particles (with near minimum ionization) generated by primary cosmic radiation. Curve 2 shows the results of measurements obtained by a telescope consisting of two gas-discharge counters [2]. These same authors also obtained a similar value of charged particle intensity during the third cosmic space flight. The authors consider that the increase in the number of telescope readings as compared to those expected from primary cosmic radiation most probably results from protons of energies $E > 60$ Mev, which as a result of diffusion drop-out from the inner belt to heights of 200-300 km.

The existence of excess radiation as charged particles has been noted in a number of works devoted to the investigation of radiation at heights of 200-300 km, although the nature of this radiation at the present time is vague.

An explanation of this radiation and its mechanism of formation is of definite interest. If the "excess" particles are protons of the inner radiation belt, a study of their distribution in space at low heights of 200-300 km can yield valuable information on the mechanism causing particle drop-out from the belt. In this case the varying radiation effects primarily involve the dynamics of the inner radiation belt and not variations in primary cosmic radiation. If, however, the "excess" particles are genetically

associated with primary cosmic radiations, as some authors hold [1], then despite their great intensity, they will not hamper a study of variations in cosmic rays at these low heights.

The second cosmic spaceship contained a photoemulsion section of 489 NIKFI"R" photoemulsion layers, 10 x 10 cm square and 400 μ thick (the shielding of the outer emulsion edge was 6-8 g/cm^2). Since the emulsion registers all particles integrally without distinguishing them with respect to time, then to compare the emulsion data with the data registered by the counters, the latter must be averaged for the entire flight time by taking into account the different times the devices were at different latitudes and the dependence of the radiation intensity on the latitude at which the recordings were observed.

This averaging for the flight time of the second cosmic spaceship, according to Savenko's data [1], gives an average radiation intensity (2.19 ± 0.06) particles/cm^2 sec; according to Ginzburg's data [2], an average intensity of 2.52 ± 0.11 particles/cm^2 sec; and for primary cosmic radiation according to Charakhch'yan's data [3], an average intensity of 0.65 particles/cm^2 sec. Thus according to the data recorded by the counters, the intensity of the recorded radiation is approximately three times greater than that of primary cosmic radiation.

At the time of the development of the film pile, the sensitivity of emulsion was high enough to ensure reliable recording of minimum-ionized particles (the sensitivity was determined with respect to electrons resulting from π-, μ-, and e- disintegrations). In 37 of 38 cases the electrons had an average track density of $g_{min} = (27 \pm 0.5)$ grains/100 μ.

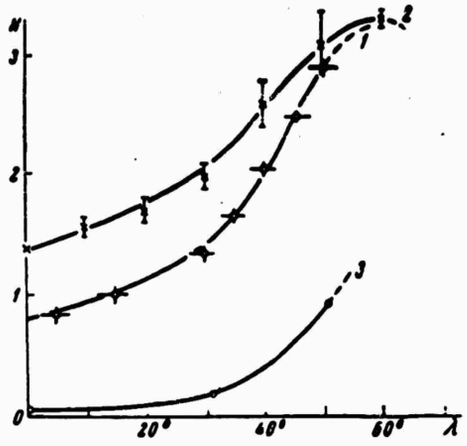

Fig. 1. Radiation intensity recorded during flight of the second cosmic spaceship

The x-axis represents the geomagnetic latitude; the y-axis represents the number of particles per cm^2 per sec. Curve 1 is the radiation intensity recorded by a single-stage gas-discharge counter; curve 2 is the radiation intensity recorded by the telescope of the two-series counters; curve 3 is the intensity of the primary cosmic radiation

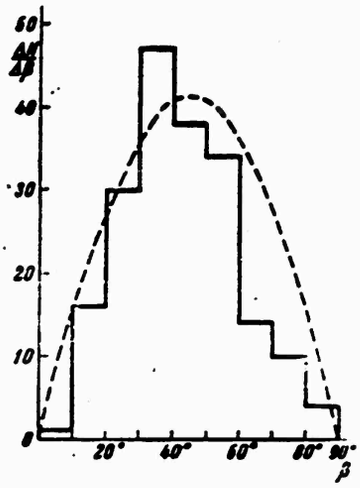

Fig. 2. Angular distribution of the recorded particles

The x-axis represents the angle which the particle makes with the emulsion plane; the y-axis shows the number of particles in angle intervals of 10^o

If all the particles recordable by counters are recorded in the photoemulsion, we can analyze the nature of "excess" particles by means of photoemulsion data. To ascertain whether all the particles are recorded in the photoemulsion, we determined the absolute intensity of the particles.

To accomplish this, in all layers of emulsion Nos. 51 and 347, on areas 1 mm from the outer edge of the emulsion, at a magnification of 1350, we made sketches of all recorded particles intersecting the surface of the emulsion layer. Two observers examined every field of view. On an area of 0.18 mm^2, 196 tracks were sketched. For all tracks we measured the angle ψ (the angle at the emulsion plane), and β, the angle formed by a perpendicular to the emulsion plane. The distribution with respect to ψ is isotropic and therefore we shall consider the distribution of particles with respect to the angles β as also isotropic. Figure 2 also shows the particle distributions with respect to β. The curve is drawn on the assumption of an isotropic distribution. The curve was normalized with respect to the number of particles in the interval of β from 30 to 60°, since for small and especially large angles of β there is a chance of miscalculation. Half of the particles should occur in the interval from 30 to 60°. In our calculations, as a result of a miscalculation, there are more than half (119 out of 196) and we consider the total number recorded in this area from the time of preparing the emulsion to be $119 \times 2 = (238 \pm 22.0)$ particles.

To obtain the number of particles recorded in the emulsion during the flight time, on the control layers which were kept on earth and which were developed together with the film plates, we

measured the background, which over an area 0.18 mm^2 consisted of (40 ± 4.6) particles. Thus, during a 27-hour flight we recorded (110.0 ± 12.0) $\times 10^3$ particles/cm^2.

From the average global intensity of particles measured by counters, (2.19 ± 0.06) particles/cm^2 sec, we should expect a particle flux through the emulsion surface of (106 ± 3) $\times 10^3$ particles/cm^2, which agrees nicely with the flux observed in the emulsion. Therefore, we can assert that all those "excess" particles present in the cabin of the second spaceship which we recorded by a single counter [1], were also recorded by the emulsion.

We measured the density of the grains g and calculated their ratio g/g_{min} on 175 of the 196 tracks. Twenty one tracks had a small angle β and it was difficult to make measurements.

The same measurements were made on the background tracks. Figure shows the particle distribution by ionization. Figure 4 gives the same distributions after allowances for the background.

We see that over 60% of the particles in the emulsion recordings had minimum ionization; 40% had an ionization of $g/g_{min} > 1.4$. Among these particles with heightened ionization capacity there can be particles, the nuclear disintegration products, occurring in the material surrounding the emulsion or in the emulsion itself. To reveal what fraction of the recorded heavily ionizing particles resulted from nuclear fission, we proceed in the following manner.

Grigorv's work [4] showed that at different atmospheric heights (9 and 20 km) the heavily ionizing particle fluxes were the same under different filters (graphite, parafin, and lead) and in air, and were proportional to the star-producing component at this height,

i.e., proportional to the number of "stars" formed per cm^3 per unit time.

Therefore, the heavily ionizing particle flux resulting from nuclear disintegration during the flight of the second spaceship should be proportional to the number of "stars" per cm^3 of the emulsion.

For determining the number of stars we examined a volume, 0.072 cm^3, of the emulsion at a magnification of 450x. Stars with a number of gray and black tracks $N_h \geq 3$ were recorded. To diminish star omission, the same area was examined by three observers. The contribution of the second observer was 10-15% of the total number of stars found by the first observer, the contribution of the third observer was no more than 5%.

We found (183 ± 13.5) stars of $N_h \geq 3$, which is (2260 ± 170) stars/cm^3 per day.

N. L. Grigorov [4] recorded (2350 ± 120) stars/cm^3 a day with $N_h \geq 3$ and (2.5 ± 0.1) particles/cm^2/min/sterad with 20 Mev < E < 180 Mev, which is (0.26 ± 0.01) particles/cm^2/sec of the global flux. According to the literature [5], particles (protons) with this energy have $7.8 > g/g_{min} > 2.4$. We recorded (2260 ± 170) stars/cm^3/day with $N_h \geq 3$, i.e., the fraction of nuclear disintegrations that can be anticipated (0.25 ± 0.04) particles/cm^2/sec.

Figure 4 shows that in the ionization range $2.4 < g/g_{min} < 7.8$, (15.0 ± 3.2)% of all the particles were recorded. Hence, the global flux of heavily ionizing particles recorded by emulsion in this ionization range was (0.31 ± 0.06) particles/cm^2/sec.

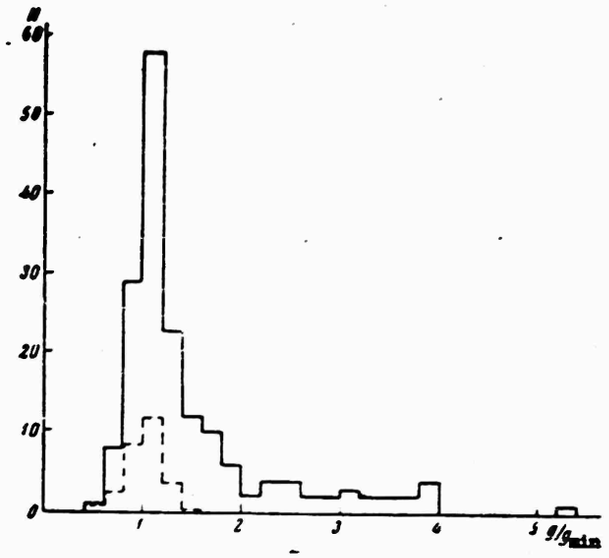

Fig. 3. Emulsion recording of particle distribution by ionization

The x-axis represents the density ratio of the grains seen in the tracks, g/g_{min}; the y-axis represents the number of particles in the given ionization interval; the solid line shows the particles recorded (inclusive of the background) during the flight; the dotted line represents the control layer background on the same area.

Since these figures are within our accuracy limits, we can regard all particles with $g/g_{min} > 2.4$ observed in the emulsion to be due to nuclear disintegration. If, however, we base our calculations on absolute values, we must note a certain excess in the

heavily ionizing particles (0.06 ± 0.08) particles/cm^2/sec which can be attributed to the protons in the inner belt, as the "belt" protons mainly fall within this range (if we assume that their energy spectrum at the height of 200-300 km is the same as in the center of the belt [6]). Thus, the inner radiation belt protons with $2.4 < g/g_{min} < 7.8$ after passing through the spaceship wall can comprise (3 ± 4)% of all particles recordable by counters.

It is theoretically possible that high-energy protons falling within the range $g/g_{min} < 2.4$ are diffused most intensely out of the inner belt. Figure 4 shows that particles with $g/g_{min} < 2.4$ amount to (85 ± 3.2)% of all particles, i.e., their global flux equals (1.74 ± 0.16) particles/cm^2/sec. The particle fluxes with $1.4 < g/g_{min} < 2.4$ equal (0.46 ± 0.08) particles/cm^2/sec, and those with $g/g_{min} \leq 1.4$ equal (1.28 ± 0.13) particles/cm^2/sec; the last value includes the primary cosmic particles with a global flux of 0.65 particles/cm^2/sec. If all the particles were protons, there should have been a large number of stars in the emulsion.

Having compared the observed number of stars with those that should be expected, assuming that the excess particles are protons or other nuclear-active particles generated by the primary cosmic radiation in the substance surrounding the emulsion, we can obtain definite knowledge concerning the excess particles.

We shall consider the part played by particles with $g/g_{min} \leq 1.4$ in the formation of the stars. They comprise 45% of the excess particles. The stars generated by these particles should contain at least one relativistic particle, i.e., with $n_s \geq 1$.

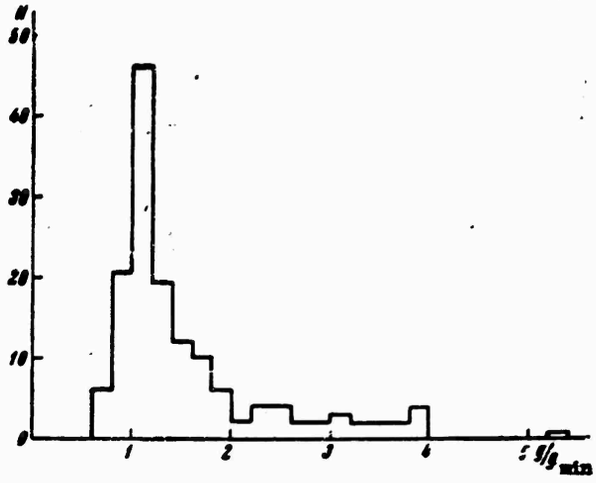

Fig. 4. Emulsion recordings of particle distribution by ionization (exclusive of background)

All stars found with $N_h \leq 3$ were examined with magnification of a 630 × or 900 × and the number of tracks with $g/g_{min} \leq 1.4$ in each star was determined. There were (74 ± 8.6) stars with $N_h \geq 3$ and $n_s \geq 1$, which comprise (915 ± 110) stars/cm³/day. To introduce a correction for stars with $N_h < 3$, we used the distributions with respect to N_h of the stars which were produced by protons with an energy of 6.2 Bev [7] and found by following the proton tracks in the emulsion. The correction coefficient was $N_h \geq 0/N_h \geq 3 = 1.36 \pm 0.13$. Applying this value to stars with $n_s \geq 1$, we obtained the number of stars with $N_h \geq 0$ (1250 ± 150) stars/cm³/day.

The primary protons having an emulsion interaction path of 37 cm yields 1500 stars/cm³/day, thus the excess particle flux with $g/g_{min} \leq 1.4$ was (0.63 ± 0.13) particles/cm²/sec; no stars were

formed within the error limits of our measurements.

Consequently these particles are neither relativistic protons nor $\pi^{\pm}$ mesons generated by the primary cosmic particles.

Based on this analysis we consider the relativistic excess particles as sufficiently energetic electrons.

Protons with $1.4 \leq g/g_{min} < 1.8$ have an interaction path λ in the emulsion of about 50 cm [8], and for protons with $1.8 < g/g_{min} < 2.4$, an interaction path λ of approximately 80 cm [9]. Hence, protons with $1.4 < g/g_{min} < 2.4$ would yield (700 ± 120) stars/cm^3/day. The stars resulting from these protons will not have a relativistic track. We have almost twice as many stars with a number of rays $N_h \geq 3$ (1340 ± 130) stars/cm^3/day than could be expected from protons with ionization of $1.4 < g/g_{min} < 2.4$. It is possible that these stars were produced by secondary neutrons. For estimates we use previous data [10] on the distribution of stars by the number of rays and by the nature of the particles producing stars at 54° N and 29 km. The distribution of these stars by number of rays coincides nicely with the distributions shown by J. J. Lord [10] (Fig. 5.). The ratio of the number of stars produced by neutrons to the number of stars produced by protons (in agreement with Lord's data [10]) is 1.6. Our ratio was 1.3. Since the shielding thickness behind which the emulsions were kept is less than that of the atmosphere at 29 km, and as this ratio diminishes with height, we can consider that our data does not contradict the fact that the excess of stars with $n_s = 0$ over that which should be expected from protons with $1.4 < g/g_{min} < 2.4$ is explained by the interaction between the neutrons resulting from nuclear disintegration produced by primary cosmic particles in the

substance surrounding the emulsion.

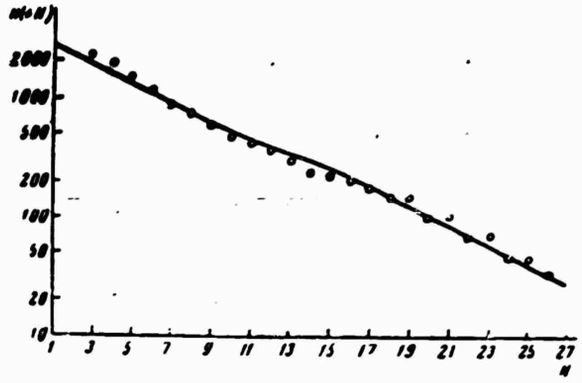

Fig. 5. Distribution of stars by number of rays

The x-axis shows the number of rays N, the y-axis shows the number of stars with the number of rays greater than that given in 1 cm^3 per day, $n(\geq N)$; the solid line gives the data cited by J. J. Lord [10] for latitude 54° N and height of 29 km; the points show our obtained distribution

Conclusions

1. Excess particles at heights of 200-300 km can be divided by specific ionization into two groups: relativistic particles ($g/g_{min} \leq 1.4$) and "gray" particles ($g/g_{min} > 1.4$). The relativistic particles make up 45% of all particles, and the "gray", 55%.

2. The relativistic excess particles are not nuclear active. They are most probably electrons. The "gray" tracks are nuclear

fission products (mostly proton products) and not protons of the inner radiation belt.

3. The inner radiation belt protons, if they are present among the excess particles within the spaceship, do not comprise more than 4 ± 6% of all excess particles.

4. The bulk, and possibly all excess particles are genetically associated with primary cosmic radiation at the point of observation.

5. In conclusion the authors thank V. V. Bobrovskaya and E. A. Orlova for carrying out the measurements.

REFERENCES

1. I. A. Savenko; N. F. Pisarenko; P. I. Shavrin. Sb. "Iskusstvennyye sputniki Zemli," No. 9, Izd-vo AN SSSR, 1961, p. 71.

2. V. L. Ginzburg; L. V. Kurnosova; V. I. Logachev; L. A. Razorenov; I. A. Sirotkin, M. I. Fradkin. Sb. "Iskusstvenyye sputniki Zemli," No. 10, Izd-vo AN SSSR, 1961, p. 22.

3. A. N. Charakhch'yan; T. N. Charkhch'yan. Zh. eksperim. i teoret. fiz., 35, 1088, 1958.

4. N. L. Grigorov; A. V. Podgurskaya; A. I. Savel'yeva; L. M. Poperevkeya. Aj. eksperim. i teret. fiz., 35, 3, 1958.

5. K. F. Pauell, U. Kamerini; P. Fauler i dr. Uspekhi fiz. n., 43, 54, 1951.

6. E. C. Freden, R. S. White. Phys. Rev. Letters., 3, 9, 1959.

7. H. Winzeler, B. Klaiber, W. Koch, M. Nikolic, M. S. Schnecberger. 17, 8, 1960.

8. G. Bernardini, E. T. Booth, S. J. Lindenbaum. Phys. Rev., 85, 826, 1952.

9. L. S. Germain. Phys. Rev., 82, 596, 1951.

10. J. J. Lord. Phys. Rev., 81, 901, 1951.

OUTGOING RADIANT FLUXES ONTO VARIOUSLY ORIENTED SURFACES AT A HEIGHT OF 300 km

K. Ya. Kondrat'yev and M. N. Fedorova

This article gives the results of calculating outgoing long-wave and short-wave radiant fluxes onto variously oriented plane surfaces at a height of 300 km. The calculations were made from the angular distribution of the intensity of the outgoing radiation. Conclusions were reached on the feasibility of using an isotropic approximation for calculating the outgoing long-wave radiation.

The problem of the arrival of terrestrial radiation onto variously oriented surfaces at a given height is extremely important for resolving problems of the thermal balance of artificial earth satellites, for interpreting data on the measurements of outgoing radiation by means of weather satellites, and for considering other problems. Authors in earlier works [1] found that outgoing long-wave radiant fluxes diminish rather smoothly with an increase in the angle of inclination of a surface. In this article we will mainly use relative values of the radiant fluxes (the values were determined by the flux on a horizontal surface).

The relative values of the outgoing long-wave radiant fluxes F/F_h, calculated from the angular distribution of the intensity of outgoing radiation at the equator and 65° latitude in a cloudless sky and in the presence of a total sky cover with an upper boundary of the layers and 9 km, are represented by circles in Fig. 1. An examination of this figure shows that the dependence of the relative radiation fluxes on the inclination angle is practically universal. The relative magnitudes calculated from this outgoing radiation intensity distribution [1] is very close to the relative values calculated by an "isotropic" approximation. Hence, isotropic approximation can be used for approximate calculations of the relative outgoing long-wave radiation fluxes onto variously oriented surfaces in the atmosphere. We must stipulate, however, that the case of a partial, horizontally inhomogeneously distributed cloud cover must be investigated further.

On the basis of calculations of outgoing long-wave radiation fluxes we can estimate the magnitude of the angle at the apex of a cone on which 90% of the flux striking the given surface falls. Calculations show that for all the differently selected surface orientations, the magnitude of this angle (or the so-called "effective zone") is approximately 60°. Only for surfaces with inclination angle $\alpha > 70^\circ$ does the effective zone reach 70°.

The magnitude of the effective zone within which 50% of the outgoing long-wave radiation falls is approximately 30° for surfaces with an inclination angle $\alpha < 70^\circ$ and 45-50° for surfaces with $\alpha > > 70^\circ$.

We will now consider the results of the calculations of outgoing short-wave radiation onto variously oriented surfaces.

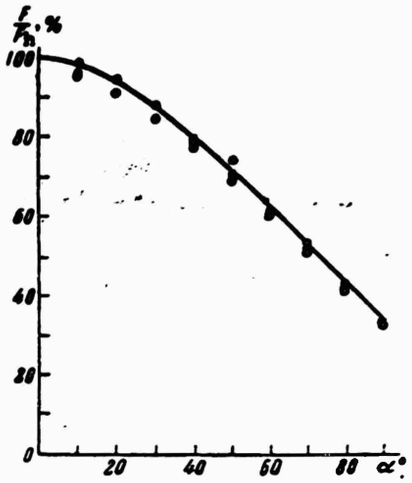

Fig. 1. The dependence of the relative values of the outgoing long-wave radiant fluxes on the inclination angle of the surface circles F/F_h for the equator and 65% Ne for cloudless sky and total sky cover. The solid curve is the dependence of relative fluxes on the inclination angle for outgoing radiation.

The outgoing short-wave radiant fluxes were calculated from the angular distribution of the intensity of the outgoing radiation obtained by theoretical calculations in Ye. M. Feygel'son's work [2].

We must bear in mind that the calculations of the angular distribution of the intensity of outgoing short-wave radiation were carried out in this earlier work [2] for the case of a plane-parallel, horizontally stratified atmosphere onto whose outer boundary a parallel beam of solar rays impinged. We assume that the earth's surface reflects the impinging radiation according to Lambert's law. The scattering coefficient and the scattering indicatrix are considered assigned. The polarization of light is not taken into account. We measure the change in scattering coefficient with height by using an extremely simple method: the atmosphere was divided into two layers with respect to height, and in each the indicatrix was assumed constant.

The angular distribution of the intensity of the outgoing short-wave radiation can be rather involved depending on the distribution of cloudiness over the area of the earth's surface under consideration, on the albedo of the underlying surface, and on the illumination conditions of the area by direct solar radiation. Calculations of

the intensity of the outgoing short-wave radiation made earlier [2] for a fully lighted illuminated area of the earth with a homogeneous albedo showed that at small zenith angles of a visible point (up to 45°), the intensity of the outgoing radiation for real and isotropic scattering is close in order of magnitude at all azimuths. At large zenith angles the radiant intensities differ markedly, the differences increasing with decrease of azimuth of the point in question (the azimuth is reckoned from the direction to the sun). We must emphasize that these results were obtained for a plane-parallel atmosphere under the simplest optical conditions. Hence, in reality, we may consider the field of outgoing short-wave radiations to be essentially anisotropic.

Consequently, accurate values of the outgoing short-wave radiant fluxes onto variously oriented surfaces can only be calculated by numerical integration from the given angular distribution of the intensity of the outgoing radiation.

In this work we calculate the outgoing short-wave radiation fluxes onto variously oriented surfaces at a height of 300 km. All the calculations in Feygel'son's work [2] were made in relative units. Since in this article we are studying the variability of outgoing radiation scattering on inclined surfaces as functions of their orientations and fluxes on inclined surfaces, we can compare them with fluxes on a horizontal surface and can also determine the fluxes in relative units.

We calculate the short-wave outgoing radiant fluxes for surfaces with inclination angles relative to the horizontal plane, α = 0, 10, 30, 50, 70, and 90°, oriented along the azimuth angle ψ = 90° and 180° relative to the sun's direction; we also calculated these fluxes

TABLE 1

Outgoing Short-Wave Radiation Fluxes (In Relative Units) Onto Variously Oriented Plane Surfaces; $\tau^* = 0.8$, $q = 0.1$

$z_\odot$, °	30				75				F/F_h for isotropic radiation, %
	ψ, °								
z, °	0		180		0		180		
	F	F/F_h, %	F	F/F_h %	F	F/F_h, %	F	F/F_h, %	
0	1,117	100	1,117	100	0,570	100	0,570	100	100
10	1,077	96,4	1,083	97	0,546	95,8	0,547	96,1	98,5
30	0,963	86,2	0,952	85,3	0,544	95,6	0,484	85	87,8
50	0,816	73	0,901	80,6	0,494	86,8	0,418	73,4	72
70	0,625	56	0,698	62,5	0,416	73,1	0,361	63,4	53,8
90	0,413	37	0,437	39,1	0,307	54	0,239	41,9	35,2

TABLE 2

Outgoing Short-Wave Radiation Fluxes (In Relative Units) Onto Variously Oriented Plane Surfaces; $\tau^* = 0.2$, $q = 0.8$

$z_\odot$, °	30				75				F/F_h for isotropic radiation, %
	ψ, °								
z, °	0		180		0		180		
	F	F/F_h, %	F	F/F_h, %	F	F/F_h, %	F	F/F_h, %	
0	3,733	100	3,733	100	1,127	100	1,127	100	100
10	3,874	103,8	3,880	103,9	1,118	99,2	1,102	97,8	98,5
30	3,461	92,7	3,480	93,2	1,019	90,4	0,984	87,4	87,8
50	2,847	76,3	2,768	74,2	0,864	76,7	0,823	73	72
70	2,130	57	2,156	57,8	0,675	59,9	0,631	56	53,8
90	1,339	35,9	1,358	36,4	0,453	40,2	0,411	36,4	35,2

TABLE 3

Outgoing Short-Wave Radiation Fluxes (In Relative Units) Onto Variously Oriented Plane Surfaces; $\tau^* = 0.2$, $q = 0.8$

$z_\odot$, °	30						60						F/F_h for isotropic radiation, %
	ψ, °												
z, °	0		90		180		0		90		180		
	F	F/F_h, %	F	F/F_h, %	F	F/F_h, %	F	F/F_h, %	F	F/F_h, %	F	F/F_h, %	
0	1,656	100	1,656	100	1,656	100	1,055	100	1,055	100	1,055	100	100
10	1,626	98,2	1,631	98,5	1,636	98,8	1,042	98,7	1,039	98,5	1,037	98,2	98,5
30	1,448	87,4	1,646	88,4	1,482	89,4	0,945	89,5	0,936	88,6	0,936	88,6	87,8
50	1,308	78,9	1,214	73,3	1,240	74,9	0,805	76,3	0,785	74,4	0,795	75,3	72
70	1,109	67	0,917	55,3	1,051	63,4	0,633	60	0,601	57	0,621	58,8	53,8
90	0,577	34,8	0,582	35,2	0,610	36,8	0,429	40,7	0,388	36,7	0,414	39,3	35,2

for the following optical parameters: optical thickness of the entire atmosphere $\tau^* = 0.2$, 0.4, and 0.8; zenith distances from the sun $z_\odot$ 30, 60, and 75°; and the values of the albedo of the subjacent layer $q = 0.1$, 0.3, and 0.8. The results are given in Tables 1-3.

An analysis of the obtained results shows that the variability in the outgoing short-wave radiant fluxes as a function of the inclination angle of the surface is approximately the same as in the case of long-wave radiation (see [1]). The magnitudes of the outgoing radiant fluxes, calculated in relative units, vary markedly depending on the sun's zenith distance, the optical atmospheric thickness, and the albedo of the subjacent surface. A comparison of the different values of the outgoing radiant fluxes showed that at large albedos ($q = 0.1$) for a given zenith distance of the sun, the outgoing radiant fluxes on variously oriented plane surfaces increased as the optical thickness of the atmosphere increased. At large values of albedo ($q = 0.8$) the magnitudes of outgoing short-wave radiation decrease with increase of atmospheric thickness at a constant zenith distance. These results are apparently explained by atmospheric haze, which increases the albedo of the earth's surface-atmosphere system for a small albedo of the subjacent surface and decreases it at a large albedo. For constant values of τ^* and $z_\odot$, the outgoing short-wave radiant fluxes increase with increase in the albedo of the surface from 0.1 to 0.8 by 3 to 5-fold.

The dependence of the relative values of the short-wave radiant fluxes (with respect to the flux on a horizontal surface F/F_h) on the steepness and azimuth of the surface is shown graphically in Figs. 2-4.

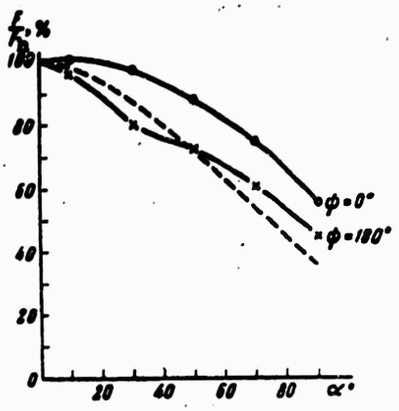

Fig. 2. The dependence of the relative outgoing short-wave radiant fluxes on the inclination angle to the surface for $z_{\odot} = 75^{\circ}$, $\tau^* = 0.2$, and $q = 0.1$.

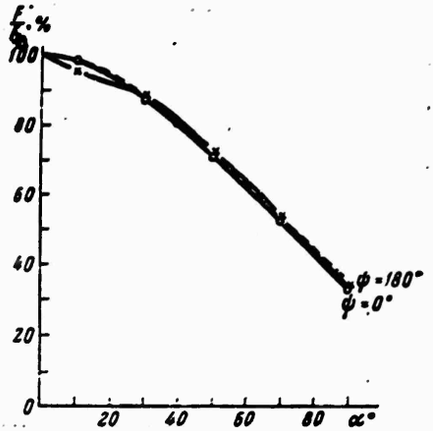

Fig. 3. The dependence of the relative outgoing short-wave radiant fluxes on the inclination angle to the surface for $z_{\odot} = 30^{\circ}$, $\tau^* = 0.8$, and $q = 0.8$.

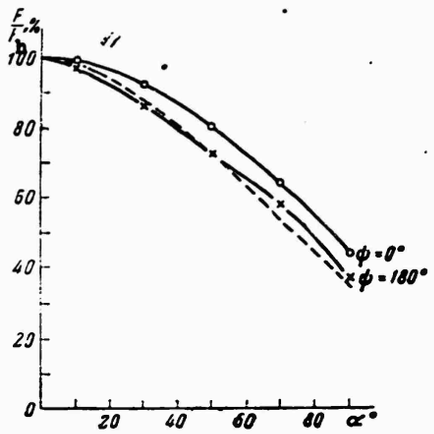

Fig. 4. The dependence of the relative outgoing short-wave radiant fluxes on the surface inclination angle for $z_{\odot} = 75^{\circ}$, $\tau^* = 0.8$ and $q = 0.8$.

The broken curve was calculated for the relative values of isotropic short-wave radiant fluxes. The graphs show that for large albedo, the relative radiant fluxes calculated from an angular distribution of the intensity of the outgoing short-wave radiation differed little

from the corresponding values calculated for an isotropic radiation field. Marked differences were observed for small albedo values (Fig. 2; q = 0.1) and large zenith distances. As already noted [2], this is caused by the fact that with decrease in the albedo of the underlying surface, there is an increase in the effect of anisotropic scattering.

The relative values of the outgoing short-wave radiant fluxes for small zenith distances ($z_\odot = 30^\circ$) proved to be fairly close to the various combinations of the optical characteristics τ^* and q.

The dependence of the relative flux magnitudes on the azimuth are insignificant for small zenith distances and more substantial for larger zenith distances.

Hence, we consider that under the simple atmospheric conditions which we chose, the angular dependence of the relative values of the outgoing short-wave radiant fluxes in general are practically identical and closely correspond to the dependence for an isotropic radiation field.

For more involved cases, where an area of the earth's atmosphere in the instrument's field of vision is partially illuminated by the sun and where partial cloudiness is present, it becomes necessary to determine the values of the outgoing radiant fluxes for each specific case. Therefore, in the future, it will be necessary to calculate the outgoing radiant fluxes for more complicated cases and for conditions of partial cloudiness in order to obtain sufficient data for statistical generalizations.

REFERENCES

1. K. Ya. Kondrat'yev and M. P. Fedotova. Sb. "Iskusstvennyye sputniki Zemli," No. 14, Izd-vo AN SSSR, p. 133.

2. Ye. M. Feygel'son, M. S. Malkevich, S. Ya. Kogan, T. D. Koronatova, K. S. Glazova, and M. A. Kuzntsova. Tr. In-ta fiziki atmosfery. No. 1, 1958.

BALLOON INVESTIGATIONS OF THE RADIATION BALANCE OF THE EARTH'S SURFACE-ATMOSPHERE SYSTEM

K. Ya. Kondrat'yev, G. N. Gavvskaya, and
G. A. Nikol'skiy

This article considers the vertical profiles of the radiation balance and its components during the summer and fall measured by standard actinometric devices mounted on free balloons.

The launching of several American weather satellites (the Tiros series) has resulted in securing abundant experimental data on the earth's radiation balance (in an earth's surface-atmosphere system). Although there is great promise in using satellites for this type of investigation (primarily from the standpoint of the "global" nature of information), the inadequate reliability of existing data (see, for example, [1]) point up the need for developing and using additional methods of investigation.

In this connection the ascent of actinometric devices on automatic balloons to heights of 25-30 km has the following virtues: 1) the possibility of obtaining highly accurate measurements; 2) the possibility of obtaining comprehensive information on the radiant

fluxes and the major factors governing them; 3) the possibility of obtaining information not only on the outgoing radiation and radiation balance, but also on the vertical profiles on the radiant fluxes in a free atmosphere (the latter is extremely essential for resolving problems of interpretation of the results gathered by antinometric measurements on satellites).

Therefore, several years ago the authors to begin to fabricate and test a series of balloon instruments designed to measure the radiation balance, its components, and the major meteorological characteristics determining the radiation field. An earlier work [2] gave a description of the equipment and also presented the first results obtained in this direction from the data of two ascents. The table below gives the results of an analysis of nine ascents made in 1962 under differing weather conditions. The flight dates are given below.

Flight number	Date	Flight number	Date
1	7.VI 1961	7	22.VI 1962
2	14.XI	8	4.VII
3	25.V 1962	9	7.VII
4	30.V	10	12.VII
5	5.VI	11	22.XI
6	12.VI		

These data include information on the vertical profiles of direct solar, global, and reflected short-wave radiant fluxes, and also information on the vertical profiles of short-wave and total radiation balances. We calculate the values of the albedo from the measured values of the global and reflected short-wave radiation.

In addition to the radiant fluxes we also measured: 1) the air temperature (by a platinum resistance thermometer), 2) the temperature of all the radiation sensors (using thermistors), 3) the air pressure (by a radiosonde atmospheric pressure sensor).

All the instruments were calibrated before the flight under laboratory and natural conditions.

Since the actinometric instruments on the supporting frame were relative instruments, we determined the conversion factors under both laboratory (on a photometric bench) and field conditions.

Since the radiant fluxes were continuously recorded on a N-70 loop oscillograph, it was possible to construct the vertical profiles of the measured values. To do this, a time signal was recorded on the oscillograph tape during the flight. Every other minute the recording line broke off. Then, since we knew the starting time, we were able to figure out the total flight time and thus find the height of ascent.

Since each element to be measured will have a zero recording every 36 seconds (by opening the sensor circuit), if we measure the distance from the zero recording on the line to the corresponding measured value, and if we know the conversion factor of the two loop-instruments, we can obtain absolute values of the radiant fluxes per cal/cm^2 min.

The declination of the supporting stage from the horizontal resulted in a wave-like curve recording. To obtain reliable data, while processing the measured values for 1961, we averaged 10-12 points for every minute. By using the recording curve, we plotted all the experimental points observed per minute. In processing the measurement data of the 1962 radiant fluxes, the averaging was done directly on the tape, for which purpose we drew an average curve which smoothed out the fluctuations of the flux to be recorded.

In processing the measurement values of the radiation balance and its components, we introduced a correction factor for the height

of the sun and for the instrument temperature and pressure.

We will now discuss the results of the different conditions observed, bearing in mind that we are primarily concerned with standard conditions.

1. One instrument set was launched on a clear day, May 25, 1962, at 1013 hr local time (mean solar time) with approximately a 10 km visibility at the time of launch. The height of the sun varied between $55^{\circ}6'$ and $58^{\circ}45'$.

As a result of the flight we obtained vertical distribution of direct solar, global, and reflected short-wave radiant fluxes, short-wave and total radiation balances, and also the albedo. .

The direct solar radiation S (Fig. 1) increased with distance from the earth's surface, where it was 1.2 cal/cm^2 min, and where at 16 km it reached 1.83 cal/cm^2 min. From 16 km to the sounding ceiling, the direct solar radiation flux remained practically constant (within the limits of accuracy of the measurements). The appreciable increase in direct solar radiation at 16 km was determined by severe turbidity of the lower atmospheric layers and by attenuation of solar radiation by haze.

The global radiation increases in the lower 2-km layer from 1.29 cal/cm^2 min at the earth's surface to 1.42 cal/cm^2 min. From 8 to 16 km, the global radiation was constant, and then increased practically linearly to 1.63 cal/cm^2 min at the outer sounding point. The rather large increase in the lower 2-km layer and insignificant variation in the 2 to 4-km layer was determined by attenuation of the radiant fluxes owing to severe turbidity in the lower atmosphere by aerosols.

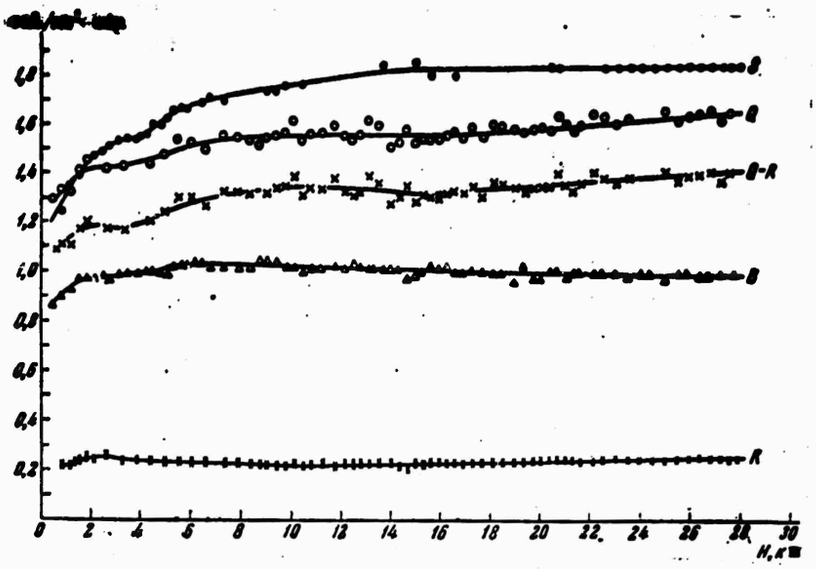

Fig. 1. Vertical profiles of the radiation balance and its components (flight 3, May 25, 1962) S) direct solar radiation; R) reflected short-wave radiation; Q-R) short-wave balance; B) radiation balance.

The reflected radiation had a weakly defined maximum of 0.25 cal/cm^2 min at 2.5 km produced by increased reflection from the formation of dense light-gray haze. At about 9.5 km, the reflected radiation was 0.22 cal/cm^2 min, and at greater heights, up to 28 km, a linear increase to 0.25 cal/cm^2 min was observed. The change in the reflected radiation from 9.5 to 28 km was only 0.03 cal/cm^2 min. As a result of the increase in the reflected radiation at 3.5 km, a weak minimum at 1.18 cal/cm^2 min is observed in the radiation of the short-wave balance. At about 10.5 km, due to the decrease in the reflected radiation at this height, a small maximum appears (1.35 cal/cm^2 min). At the outer sounding point, the short-wave balance reaches 1.4 cal/cm^2 min.

The total radiation balance increases up to 6 km where it is 1.03 cal/cm^2 min; from 6 km to the sounding ceiling, it decreases linearly, finally becoming 0.98 cal/cm^2 min owing to the increase in

reflected radiation in the upper sounding layers.

Figure 2 shows the change in the albedo of the subjacent surface and the underlying air layer with height. We see that the maximum albedo at approximately 3 km is 18%. Above 7 km, the albedo is practically constant, being about 15%.

2. The sixth flight obtained vertical profiles of the radiation balance and its components up to 27 km. The measurements were made June 12, 1962 at 1057 hr local time. The horizontal visibility at flight time was 10 km. Individual cumuliform clouds, which developed into a heavy cumuliform cloud cover, were noted at the flight start. There was an over-all cloudiness of 8 scale units in the middle of the flight. The instrument package could be clearly seen through the cloud gaps. A heavy haze was observed near the ground.

The presence of a severely turbid layer near the earth's surface and cloudiness were reflected in the abnormal course of the reflected short-wave radiation and the short-wave and total radiation balances. (Fig. 3).

As a result of attenuation by the thick aerosol layer, the direct solar radiation varied in the lower 10-km layer from 1.18 to 1.80 cal/cm^2 min, whereas from 11-27 km it was practically constant.

The global radiation at the 4-km layer increased from 1.2 to 1.5 cal/cm^2 min. At greater heights the increase in global radiant flux became considerably slower. At 27 km, the global radiant flux reached its maximum, 1.58 cal/cm^2 min.

The maximum values of the reflected short-wave radiation was 0.61 cal/cm^2 min at 11 km, and then fell to 0.54 cal/cm^2 min at the maximum sounding point. The pronounced increase in reflected radiation beginning from 4 km upwards is caused by the rapidly developing

cloudiness.

The part played by reflected radiations in changing the vertical profiles of the short-wave balance shows up graphically in a vertical distribution of the short-wave balance.

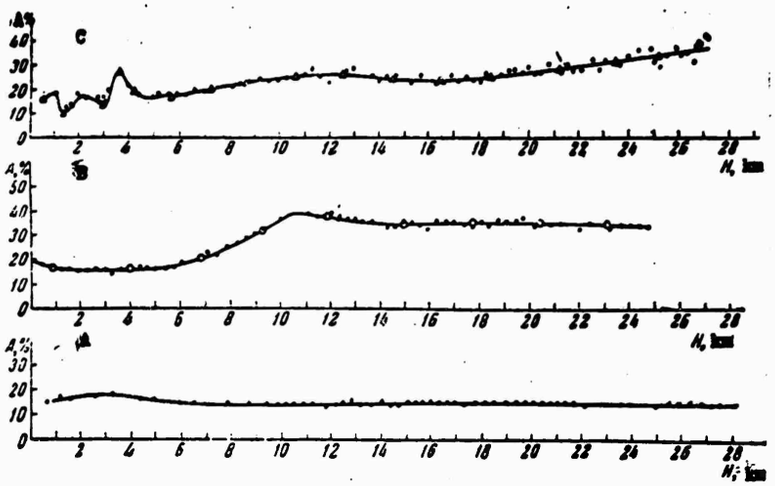

Fig. 2. Albedo distribution by height. a) flight No. 3, May 25, 1962; b) flight No. 6, June 12, 1962; c) flight No. 7, June 22, 1962.

The short-wave balance of 0.96 cal/cm^2 min near the earth reaches a maximum of 1.26 cal/cm^2 min at 4.5 km. At 11 km, a second maximum is observed. Above 11 km, the short-wave balance increases linearly as result of a drop in reflected radiation and increase in the global radiant flux.

Just as in the short-wave balance, the total radiation balance varies substantially owing to reflected radiation in the entire sounding layer.

As in the short-wave balance, a maximum of 0.95 cal/cm^2 min was first observed at 4 km which then fell to 0.62 cal/cm^2 min near 11 km. Above 11 km, the vertical profile of the radiation balance was distinguished by an increase in the balance resulting from a decrease of

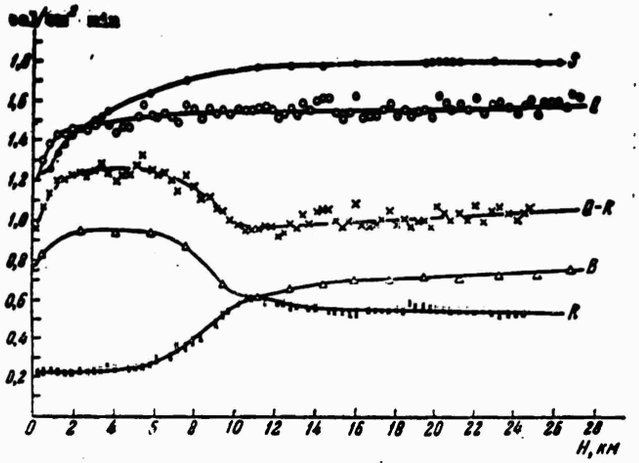

Fig. 3. Vertical profiles on the radiation balance and its components (Flight No. 6, June 12, 1962).

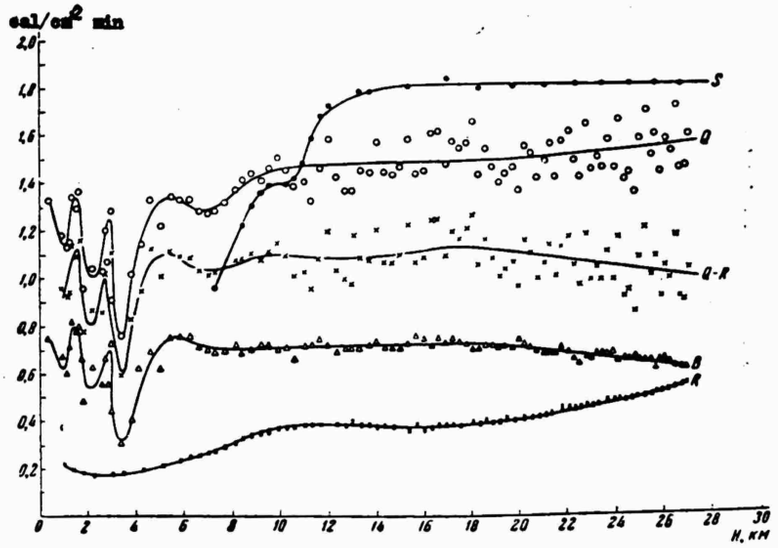

Fig. 4. Vertical profiles of the radiation balance and its components (Flight No. 7, June 22, 1962).

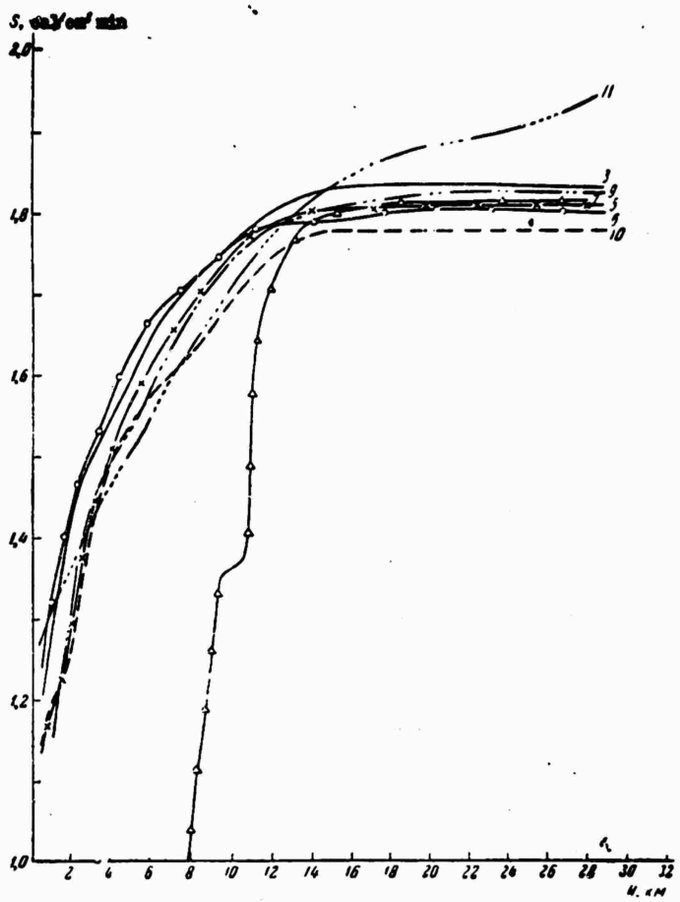

Fig. 5. Vertical profiles of direct solar radiation. The numbers on the curves correspond to the flights.

the reflected radiant flux in the 11 to 27-km layer. The sharp decrease in the vertical profile of the albedo (Fig. 2) in the lower 12-km layer is caused by a considerable horizontal nonhomogeneous atmosphere. We see that there is a minimum near the earth's surface (16-18%) and a maximum (41%) near 11 km, which falls to 34% in the vicinity of the sounding ceiling.

3. The seventh instrument set was sent aloft on June 22, 1962 at 1033 hr local time. Unlike the earlier flight, we observed a cirrus and stratocumulous cloudiness of 8/7 scale units at the start of flight, which by the end of the flight rose to 9/8. Owing to the presence of dense cloudiness with some gaps, the radiation-balance components varied sharply in the lower 6-km layer, and there was no continuous recording of solar radiation (Fig. 4). The cloudiness strongly attenuated the direct solar radiation up to 13 km. The constancy of the direct solar radiation in the layer 9.5 to 10.5 km revealed the presence of a cloudless interlayer here. The rapid rise in direct solar radiation above 10 km is due to the passage of the balloon through semitransparent clouds. From 7.5 to 17 km, direct solar radiation varies from 0.96 to 1.76 cal/cm^2 min, and above this the radiation rises slowly to 1.81 cal/cm^2 min at the outermost sounding point. At 7 km, the minimum global radiation (1.28 cal/cm^2 min) was replaced first by a rather rapid and then a gradual increase in the global radiant flux. At the outermost sounding, the global radiation nearly reached 1.57 cal/cm^2 min.

The reflected radiation was minimum (0.17 cal/cm^2 min) at 2.5 km. The second weakly defined minimum was observed at 16 km, after which the reflected radiant flux rose rapidly to 0.56 cal/cm^2 min at 27 km. This rapid rise in reflected radiation was produced by increasing

cloudiness under the balloon.

The maximum values of the short-wave balance (1.1 and 1.3 cal/cm^2 min) were at 10 and 17 km respectively. The minima in the short-wave balance were produced either by an increase in the reflected radiant flux, for example at heights of 13 and 27 km, or by a decrease in the downcoming flux in the lower 8-km layer.

The total radiation flux in the 10 to 19-km layer was almost constant (0.70 cal/cm^2 min). Above this, it decreases owing to a marked increase of the reflected radiation in the 18 to 27-km layer.

It is apparent that despite the substantial variability with height of the direct solar global radiation, the outer troposphere and stratosphere are close to radiant equilibrium. A comparison of curves S, Q, and B illustrate how erroneous can be the calculations of the radiant thermal influx based on a calculation of only the absorbed direct radiation and radiant heat exchange resulting from long-wave radiation. Figure 4 clearly indicates the major role played by the absorption of scattered and reflected radiation. The vertical profile of the albedo (Fig. 2) shows the horizontal nonhomogeneity of the subjacent surface and mainly of the atmosphere. The albedo varies from 18% at the earth's surface up to 35% at 27 km. The rather wide scatterings of points in these graphs (Figs. 1-4) was caused by the rotation and oscillations of the supporting stage, which resulted in a declination of the instrument surfaces from the horizontal.

4. Figure 5 shows the vertical distributions of the direct solar radiant fluxes during the entire probe.

As expected the most marked variations in the direct solar radiation occurred in the lower atmosphere. The radiant flux impinging here was substantially attenuated owing to the high concentration of

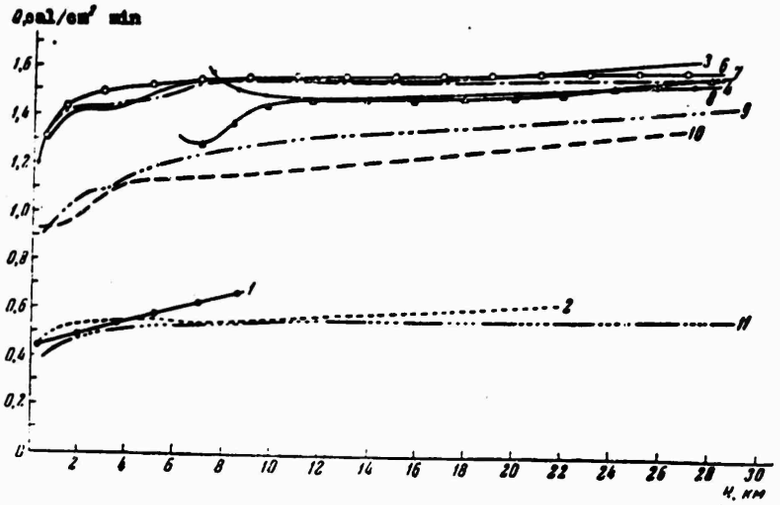

Fig. 6. Vertical profiles of global radiation numbers on the curves correspond to the flight number.

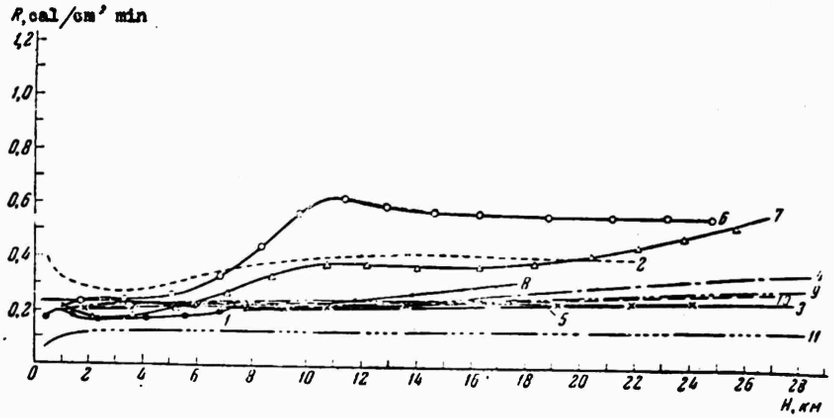

Fig. 7. Vertical profiles of reflected short-wave radiation.

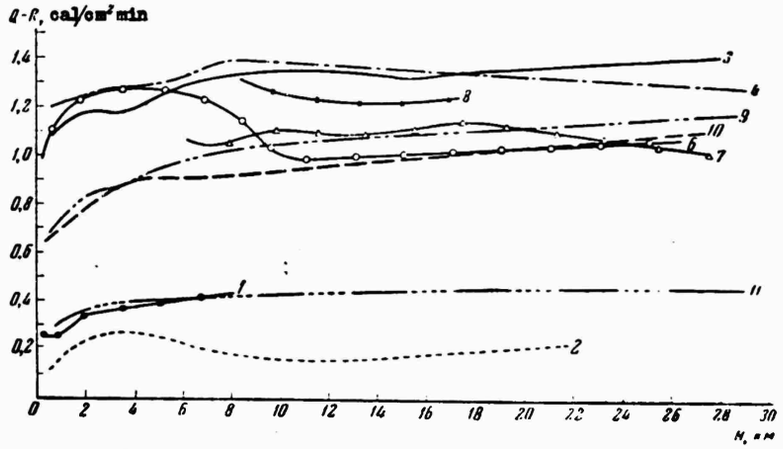

Fig. 8. Vertical profiles of the short-wave balance.

aerosols and the presence of cloudiness. Above 12 km, variations in the direct solar radiant flux were insignificant. In the summer (curves 1, 3, 5-10 in Fig. 5) in the 12 to 29-km layer, the measurements of the direct solar radiant flux varied from flight to flight (from 1.79 to 1.83 cal/cm^2 min). Discrepancies in the values of the direct solar radiant flux in different flights are explained by the change in the solar constant represented as a function of the distance between the earth and the sun, by the stratification characteristics of the troposphere, and by random measurement errors.

In the autumn months (November, curve 11) the variation of direct solar radiation with height was more uniform than in the summer. At 29 km, it reached 1.94 cal/cm^2 min. This increase over that measured in the summer results from the decreasing distance between the earth and the sun.

The global radiation, just as the direct solar radiation, undergoes the greatest changes in the lower atmosphere (Fig. 6). Above, 12 km, the global radiant flux continues to increase up to the sounding ceiling. This is partly due to the change in height of the sun during flight. A considerably important part is also played here by the "illumination" resulting from the radiation scattering off the balloon. Figure 6 shows clearly two series of curves, one of which (curves 3-10) denotes the summer measurements and the second (curves 2, 11) the fall measurements. In the fall, the global radiant flux is almost one-third that of summer. Both autumn flights were made in November 1961 and 1962. The autumn soundings yielded similar values for the global radiant fluxes.

The vertical profiles of reflected radiation for all 11 flights highlight either the horizontal homogeneity or nonhomogeneity of the

underlying surface and of the atmosphere (Fig. 7).

The reflected radiant flux rose sharply when the instrument set passed above dense cloud strata (Fig. 7, curves 6 and 7).

The maximum reflected radiation was 0.61 cal/cm^2 min. The presence of a snow cover during the November 11, 1961 launch resulted in a threefold increase in the short-wave radiant flux over that measured in the November 2, 1962 flight (no snow cover) in the 10 to 22-km layer (curves 2,11). Near 3 km, the differences in the reflected radiant fluxes in these two cases diminished; the difference was only 0.16 cal/cm^2 min. This decrease was the result of a decreasing albedo when the balloon passed over an unfrozen river (curve 2, Fig. 7).

The diminished reflected radiant flux observed on the 11-th flight compared to the flux in the other flights was produced by a decrease in the albedo of the moist underlying surface.

Figure 8 shows the variations of the short-wave balance with height. The values of the short-wave balance differ considerably from flight to flight owing either to a rather substantial variation of the short-wave radiant flux or the effect of the aerosol layer in attenuating the downcoming radiant flux.

The decrease in the short-wave balance in the autumn below that in the summer is explained by the slower arrival of global radiation and an increase in the reflected radiant flux.

The differences in the values of the short-wave balance in the fall (Fig. 8) are also associated with differing values of albedo. The presence of the snow cover on Nov. 14, 1961 strongly decreased the short-wave balance.

The horizontal nonhomogeneity of the underlying surface also affects the distributions of the total radiation balance with respect

to height (Fig. 9).

In the summer the radiation balance differs from day to day by 0.60 cal/cm^2 min. In the fall, this difference diminishes, becoming approximately 0.05 cal/cm^2 min. We see from Fig. 9 that the radiation balance markedly changes in the 0 to 12-km layer, whereas above this it is either practically constant which characterizes atmospheric conditions near to radiation equilibrium, or diminishes slightly owing to the increase in the reflected radiant flux from the dense cloud cover.

On cloudy days the values of the total radiation balance in the 12 to 29-km layer were similar (curves 7, 8, Fig. 9).

Figure 10 represents the variations of the albedo with height as a function of the season. A horizontal nonhomogeneity of the underlying surface or of the atmosphere appears in the path of the albedo. In clear weather the albedo either varies negligibly with height or remains constant. In clear summer weather, the albedo varies from flight to flight from 18 to 21%. On cloudy days, the albedo varies markedly throughout the entire sounding layer. If there are cumulus clouds (curves 6, 7) the albedo may increase to 35-40%.

The albedo increases sharply when a snow cover is present. For example, the flight of Nov. 14, 1961 passed over the surface of a level snow cover, while the flight of Nov. 22, 1962 was over the dark moist earth surface. This difference strongly affected the albedo values In the first flight, the albedo reached 65-70% and in the second, 20-22%.

The following table summarizes the measured values of the radiation balance and its components in the upper sounding layers. The blank spaces in the table refer to cases where no recordings were

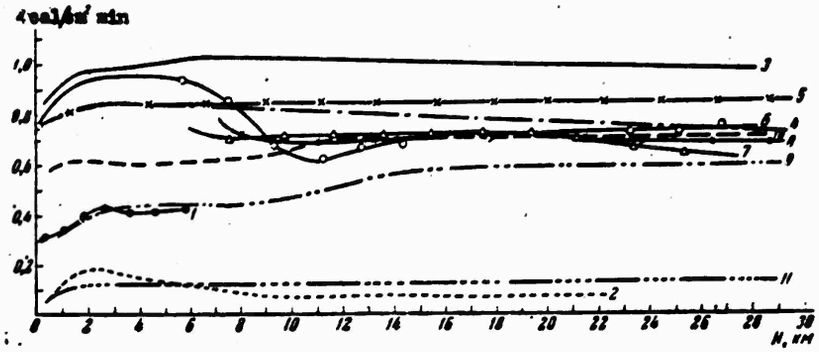

Fig. 9. Vertical profiles of total radiation balance.

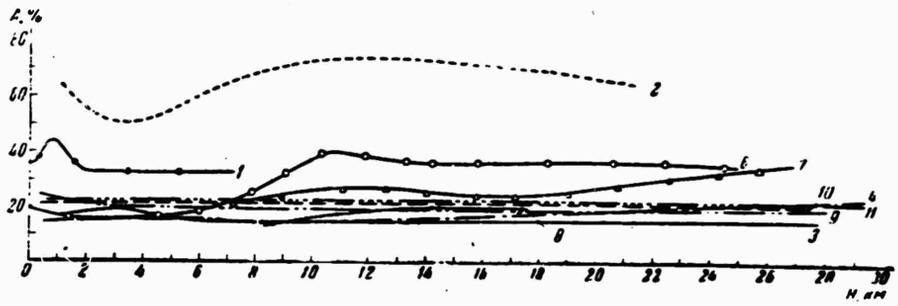

Fig. 10. Albedo distribution with respect to height.

made due to technical difficulties. An examination of the table shows that the direct solar radiant flux at the outermost sounding point varies from 1.79 to 1.94 cal/cm² min. The value of the direct solar radiant flux reduced to the mean distance between the earth and the sun varies for the sounding ceiling from flight to flight between 1.85 and 1.89 cal/cm² min.

Radiation Balance and its Components at the Outermost Sounding Points

Date	Time in hr and min.	H, km	S	Q	$Q_\perp$	R	Q − R	R	A, %
14.XI 1961	11 48	22		0,64	1,91	0,40	0,24	0,145	62
25.V 1962	11 47	26	1,83	1,64	1,92	0,25	1,39	0,99	15,3
	11 50	27	1,83	1,64	1,92	0,25	1,39	0,98	15,5
30.V	11 44	26		1,57	1,84	0,34	1,23	0,74	21
	11 47	27		1,57	1,84	0,34	1,23	0,74	21,3
	11 50	28		1,57	1,85	0,35	1,22	0,73	22
5.VI	11 15	26	1,81			0,24		0,85	
	11 18	27	1,81			0,24		0,85	
	11 22	28	1,81			0,24		0,85	
12.VI	12 00	25	1,80	1,58	1,81	0,54	1,04	0,74	34
	12 03	26	1,80	1,58	1,81	0,54	1,04	0,74	34
	12 06	27	1,80	1,58	1,81	0,53	1,05	0,75	34
22.VI	11 42	25	1,81	1,55	1,77	0,51	1,04	0,66	33
	11 46	26	1,81	1,56	1,78	0,54	1,02	0,65	34
	11 53	27	1,81	1,57	1,80	0,56	1,01	0,64	35
4.VII	11 46	26	1,81	1,54	1,77			0,68	
	11 50	27	1,81	1,54	1,77			0,68	
	11 54	28	1,81	1,55	1,78			0,68	
	12 00	29	1,81	1,55	1,78			0,68	
7.VII	10 00	26	1,82	1,43	1,79	0,29	1,14	0,60	19
	10 03	27	1,82	1,44	1,80	0,30	1,14	0,60	19
	10 06	28	1,82	1,44	1,80	0,30	1,14	0,60	19
12.VII	9 40	25	1,79	1,34	1,74	0,28	1,06	0,71	20,5
	9 42	26	1,79	1,35	1,74	0,28	1,07	0,71	20,3
	9 45	27	1,79	1,36	1,75	0,29	1,07	0,71	20,2
22.XI	11 39	26	1,92	0,56	1,87	0,13	0,43		21
	11 41	27	1,92	0,56	1,88	0,13	0,43		21
	11 43	28	1,925	0,57	1,89	0,13	0,44		21
	11 45	29	1,94	0,57	1,89	0,13	0,44		21

The sixth column of the table shows the values of the global radiant flux calculated from the formula $Q_\perp = Q/\sin h_\odot$, where $h_\odot$ is the height of the sun. With the exception of two flights, this value is somewhat less than that of the direct solar radiant flux, varying from 1.74 to 1.92 cal/cm² min. The inequality $Q_\perp < S$ can only be explained by systematic errors in the global radiation measurements.

The reflected radiant flux R in the summer months varies from 0.24 to 0.56 cal/cm^2 min at the outermost sounding point.

The sharp increase in the reflected radiation on the June 12 and 22, 1962 flights is due to the presence of cloudiness under the balloon.

The value of the short-wave balance (column 8) varies from flight to flight from 0.24 - 1.39 cal/cm^2 min; the total radiation balance (column 9) varies from 0.145 to 0.99 cal/cm^2 min. In the summer the albedo at the outermost sounding point varies between 15 and 35%.

An analysis of the measurement results shows that the most pronounced variations in the radiation balance and its components occur in the lower atmosphere where there is a more marked effect of the aerosol haze, nonhomogenity of the underlying surface, and cloudiness. In the summer this layer extends to a height of 11-12 km and in the fall, to 8-9 km. Above these levels, the changes of the radiation balance and its components generally remain within the accuracy limits of our measurements.

The authors express their thanks to I. V. Andreev, N. M. Yevdokimova and S. V. Maryuskin for their help in launching the instruments and in processing the obtained data.

REFERENCES

1. N. Ya. Kondrat'yev. Meteorologicheskiye sputniki. Gidrometeoizdat, 1963.

2. K. Ya. Kondrat'yev, G N. Gayevakaya, and G. A. Nikol'skiy. Sb. "Iskusstvennyye sputniki Zemli," No. 14, Izd-vo AN SSSR, p. 86, 1962.

THE VALUE OF GEOGRAPHIC-GEOLOGICAL METHODS OF STUDYING THE MOON

Yu. A. Khodak, V. V. Kozlov, I. N. Tomson, L. V. Khoroshilov

The value of geographic-geophysical methods of studying the moon, especially structural-geomorphological and structural and historical-geological methods is substantiated. It is proposed that there is a close connection between geographic-geological (with regard to material comparable to the earth) and astronomical methods in the study of the moon. An evaluation is made of the geographic-geological studies already completed in the USSR (by A. V. Khabakov and Yu. A. Khodak) and in other countries and also of the meteroritic approach to explaining the development of the relief and structure of the moon.

The origin and history of development of the relief and structure of the moon is attracting ever more attention from geologists, astronomers and geographers. An attempt to clarify the structure of the visible side of the moon from the geological aspect was first undertaken by the Soviet scientist A. V. Khabakov [1-3], who explained the basic formations of the relief of the moon in an age sequence of their formation. A detailed "geomorphological" study of the form of the relief of the visible side of the moon was made by the American geologist Spurr [4].

Geological and tectonic schemes for a number of regions on the visible side of the moon have been presented in numerous works by Bülov [5-8], Benes [9-13], Hedevari [14, 15], Mason, Hackman and Shoemaker [16-19], Miyamoto [20, 21], Fielder [22-31], Warner [32-35], McDonald [36], Cameron and O'Keefe [37], Compte [38], Mohacsi [39], Schlichta [40], and other investigators.

From the photos made in October 1959 from aboard the Soviet space rocket, mankind received its first information about the far side of the moon [41, 42].

The tectonic scheme of the moon as a whole (near and far sides) is based on analysis of the character and arrangement of mountainous formations (walled plains, craters, walled-plain and crater chains and ridges), lunar seas, valleys, and clefts by Yu. A. Khodak [43], who singled out the most important structural elements, dividing them into blocks of a deep rill zone (cf. article in this issue).

It is very clear that at this stage of investigation when man has yet to set foot on the surface of the moon, it is impossible to understand the nature and history of the development of the interior, crust, and surface of the moon and the processes of its formation and development as a planetary body without a "geographic-geological" approach. Astronomers alone, without the participation of geologists, are in no position to formulate, not to mention solve, the problem of studying the structural elements of the moon. Close cooperation in a joint effort using geographic-geological (taking into account material comparable to the earth) and astronomical methods must be the start of a qualitatively new stage in the study of the moon.

At present the use of the results from astronomical observations alone is characteristic in the geographic-geological study of the moon by geographers and geologists. First the geologist must use the most accurate photographs, such as those in the atlas edited by Kuiper [44] and the photos and drawings from Wilkin's atlas [45], of the lunar surface to study separate areas and regions of the moon and to obtain a complete picture of both the near and far sides of the moon. Of absolute necessity is direct visual observation by geologists of the surface of the moon through a telescope, with correction of available photos (including those taken in the invisible portions of the spectrum) by sketching from them the ("most minute" within the limits of telescope resolution) details of the form of lunar relief and of the correlations between them.

To make a structural-geographical and a structural-geological study it is extremely important to obtain the most accurate topographic schematic map possible (schematic maps of the differences of elevation between the forms of lunar relief) of the individual areas, seas, and regions of the entire visible side of the moon. Structural-geomorphological and structural-geological deciphering and correction must be carried out jointly by geologists and astronomers during visual observation and when compiling topographic schematic maps.

Of great importance are geomorphological studies, using photographic methods (including the invisible regions of the spectrum), of the character of individual walled plains, large and small craters, the nature of clefts, the superposition of walled plains and craters of different size, of the form and structure of the

steepness, freshness, the interrelationship of clefts with certain types of walled plains and craters, the interrelationship of various types and systems of clefts and with series of chains, with chains, and with types of plains craters, etc. (even within seas). The assembly and classification of these details must be made with concomitant topographical corrections.

Of great importance is an understanding of the structure of the moon is the structural-geomorphological, structural-geological deciphering and correcting of data on the physical characteristics of the surface and interior of the moon (albedo, color, temperature, polarization properties, magnetic, spectroscopic, radioastronomical and other kinds of data), on individual characteristics, and on complexes of characteristics by revealing the changes in their relations in individual sections and regions, seas, and over the entire visible surface of the moon as a whole and changes in these relations relative to the character of the topography, geomorphology, and structure, cleft networks, individual walled plains and craters and their series, etc. Of great interest is the comparison of schematic maps of these constants with topographical and structural-geologioal schematics such as the radar topographical map of the moon by Pettengill [46].

Since geologists cannot presently conduct a direct study of the composition of lunar rock (primarily a mineral-petrographic study), it is necessary to use data on the physical characteristics of the moon for preliminary interpretation of the character and properties of the rock making up the surface (and, perhaps, the interior also) and for revealing the possible areas of their distribution. It is desirable to correlate these "petrographic" [1, 47, 48],

topographical, geomorphological, and structural-geological data for the various areas and regions, seas, and for the entire visible side, as well as for individual walled-plain and crater chains, for cleft networks, centers of walled plains, craters, fracture zones, etc., (as well as inside of individual seas).

To reveal the genesis of the polygonal-ring structures (walled plains and craters), it is necessary to make a detailed structural-geological study of individual plains and craters of the moon by means of visual and other kinds of observations and by comparing them with analogous polygonal-ring structures of ancient strata of the earth. The basic problems concerned with the moon are as follows: study of the character, form, and relation with clefts or cleft networks of separate walled plains and craters, the character of the shape of chains of walled plains and craters, of the direction of their long axes* along the chains, clefts or network of clefts, valleys, mountain ridges, etc., (inside of seas as well); the development of the polygonal-ring character of the structure of the walled plains and craters, of the structural and other relationships of individual plains and craters, of individual parallel or intersecting networks of walled plains and craters, different degrees and stages of superposition, of the proximity of individual plains and craters inside and outside of the chains; the development of a connection between polygonal-ring structures of walled plains and craters, which apparently appear as unique grabenlike forms

---

* In this connection we note the works of M. M. Shemyakin [49], Fielder and Jordan [30].

(with polygonal-ring blocks, downthrown along faults) with topographical and other data ("petrographic," physical, etc.). Data and conclusions on the formation of polygonal-ring structures of the moon would be of great value for revealing the concealed geological history of analogous structures of the ancient strata of the earth.

On the basis of the studies listed above, structural-geological and historical-geological analysis is carried out with separation of the main structural elements of "continental" masses, belts of belts of sea depressions, individual large blocks of these masses and depressions and deep fault zones separating them, with an elucidation of the differentiation of the inheritance and superposition of their development from ancient times to the present, with a revelation of the pattern of development of various regions and of general patterns in the development of the lunar crust and of the moon as a planetary body.

In Soviet literature may be found two attempts at a structural-geological and historical-geological analysis of the moon: A. V. Khabakov [1-3] for the near side of the moon and Yu. A. Khodak [43] for the near and far sides of the moon. Both studies tend toward a general conclusion concerning the block structure of the moon and the polygonality of its massive structural elements of "continents" and "seas." The polygonal outlines of lunar seas was noted by V. G. Fesenkov [50] and a number of other astronomers. Yu. A. Khodak [43] emphasized the important role in the geological development of the moon and the formation of its crust of the system of deep fault zones which appear to be the most tectonically active portions along which occurred the most intense formation of

polygonal-ring structures, differentiated uplifting and subsiding of blocks of various character and dimension, the formation of grabens and horsts, rills, valleys, etc.

The block structure of the lunar crust, which if found on Mars [52] as well as on the earth [51], evidences a general regularity in the development of the solid crust of planets belonging to the earth group. Study of the block structure of the lunar crust with the abundance of polygonal-ring structures would be of importance for an interpretation of a number of regularities of the earth's crust, especially its lower (older) portions and in the water-filled oceanic and marine basins, which to a considerable degree are concealed from our observations.

The above-described approach to the study of the moon, i.e., an explanation of the causes for the formation of its relief and the geomorphological and structural forms of its crust and interior, appears to be diametrically opposed to the so-called meteoritic approach which explains the formation of all forms of the lunar relief by meteoritic bombardment [53, 54]. For the present, before a preliminary structural geographic-geological study of the moon, we will not enter into a fruitless discussion, and will use everything valuable and useful contained in the remarks of B. Yu. Levin [53, 54] and other supporters of the meteoritic hypothysis concerning the role of intensive cosmic bombardments of the already formed (as a planetary body) moon. We will note only briefly our main comments concerning the "meteoritic hypothysis."

From the principles of B. Yu. Levin [53, 54] it follows that after the formation of the moon as a planetary body, when the moon,

as all planets of the earth group, absorbed practically all of the solid objects present in the region of its orbit, that "meteoritic" relief of the moon began to form, which, we now see in form which took hundreds of millions, if not billions of (up to 4 billions) of years to solidify. According to Levin, the intensive meteoritic bombardment of the moon which formed the relief now visible to us, continued even after the disappearance of that cluster of particles from which the moon must have been formed.

The supporters of the "meteoritic" hypothesis, without analyzing the accumulated material concerning the regular and inherited distribution of the main forms of the relief and structural elements of the moon, deny all that is now being done by many specialist (geologists, astronomers, geographers, geophysicists) of the most diverse opinions in the USSR, Czechoslovakia, Hungary, USA, England, Japan, and other countries on the study of the problem of the formation of the lunar relief.

Such a one-sided approach to an explanation of the development of the relief and structure of the moon might lead this problem to an impasse and cannot methodically further its solution. Only constructing the various schematic maps proposed above on the same data and by analyzing and examining them, is it possible to approach a solution of the questions posed.

One of the important and interesting aspects of the proposed problems is the explanation of the effect of the rotational and orbital motion of the moon on the formation of its structures. (of course, the relief is their reflection in a surface section) and systems of deep fault zones during its development. Similar unsystematic studies concerning the earth have already been

described [55-58].

In conclusion it must be emphasized that without enlisting geologists it would be impossible to solve the problem of the origin of the relief and structure of the moon, their regular distribution, or to draw up topographical, geographical, geological (selenological) schematics and maps corresponding to the present level of science.

The authors express gratitude to Doctor of Physical-Mathematical Sciences A. G. Masevich for his assistance in the study.

Received 9 May 1963

REFERENCES

1. A. V. Khabakov. Sb. "Luna." Fizmatgiz, 1960, str. 241.

2. A. V. Khabakov. Ob osnovnykh voprosakh istoriy razvitiya poverkhnosty Luny. Geografgiz, 1949.

3. A. V. Khabakov. Sb. "Iskusstvennyye sputniki Zemli," vyp. 9. Izk-vo AN SSSR, 1961, str. 52.

4. J. Spurr. Geology Applied to Selenology. Pennsylvania, 1945.

5. K. Bülov. Geologie, H. 6/7, 1957, S. 565-609.

6. K. Bülov. Wiss. Z. Univ. R., H. 1, 1959.

7. K. Bülov. Raketentechn. u. Raumfahrtforsch., 4, No. 3, 1960, p. 93-97.

8. K. Bülov. Forsch. u. Fortschr., 35, No. 8, 225, 1961.

9. K. Benes. Risé hvezd, 40, No. 11, 1959.

10. K. Benes. Tr. Gorn. in-ta, Ostrava, No. 5/6, 1960.

11. K. Benes. Izv. AN SSSR, ser. geol. No. 11, 50, 1962.

12. K. Benes. Risé hvezd, 41, No. 8, 153, 1960.

13. K. Benes. Risé hvezd, 41, No. 11, 213, 1960.

14. P. Hedervari. Magyar fiz. folyóirat, 8, No. 4, 261, 1960.

15. P. Hedervari. Magyar fiz. folyóirat, 9, No. 4, 251, 1960.

16. A. Mason, R. Hackman. Bull. Geol. Soc. America, 71, No. 12, pt. 2, 2103, 1960.

17. Yu. M. Shoemaker, R. D. Hackman. Sb. "Novoye o Lune." Izd-vo AN SSSR, 1963, str. 220.

18. A. Mason, R. Hackman. Symp. No. 14 Intern. Astron. Union, the Moon, 1962, p. 301.

19. A. Shoemaker, R. Hackman. Bull. Geol. Soc. America, 71, No. 2, pt. 2, 2112, 1960.

20. S. Miyamoto. Planet. a. Space Sci., 2. No. 4, 256, 1960.

21. S. Miyamoto. Contribs. Inst. Astrophys. A. Kwasan Observ. Univ. Kyoto, No. 96, 6, 1960.

22. G. Fielder. Sky a. Telescope, No. 19, 334, 1960.

23. G. Fielder. Monthly Notices Roy Astron. Soc., 123, No. 1, 15, 1961.

24. G. Fielder. Planet. a. Space Sci., 5, No. 4, 286, 1961.

25. G. Fielder. Planet. a. Space Sci., 8, No. 1, 1961.

26. G. Fielder. Observatory, 81, No. 923, 140, 1961.

27. G. Fielder. J. Brit. Astron. Assoc., 66, No. 341, 1957.

28. G. Fielder. Nature, 193, No. 4812, 258, 1962.

29. G. Fielder, T. Kiang. Observatory, 82, No. 926, 8, 1962.

30. G. Fielder, C. Jordan. Planet. a. Space. Sci., No. 9, 1962.

31. G. Fielder, B. Warner. Planet. a. Space. Sci., No. 9, 1962.

32. B. Warner. Publs. Astron. Soc., Pacif., 73, No. 434, 349, 1961.

33. B. Warner. J. Brit. Astron. Assoc., 71, No. 8, 388, 1961.

34. B. Warner. J. Brit. Astron. Assoc., 71, No. 3, 104, 1961.

35. B. Warner. Planet. a. Space Sci., 5, No. 4, 283, 1961.

36. G. McDonald. Planet. a. Space Sci., 2, No. 4, 249, 1960.

37. W. Cameron, J. O'Keefe. Astron. J., 66, No. 7, 280, 1961.

38. P. Compte. Urania, 43, No. 248, 199, 1958.

39. B. Mohacsi. Magyar tud. akad. Mat. és. fiz. tud. oszt. kölz., 10, No. 4, 421, 1960.

40. O. Schlichta. Bull. Geol. Soc. America, 71, No. 12, pt. 2, 2111, 1960.

41. Atlas Obratnoy Storony Luvy, Izd., AN SSSR, 1960.

42. Yu. N. Lipskiy. Sb. "Iskusstvennyye sputniki Zemli," vyp. 9, Izd-vo AN SSSR, 1961, str. 3.

43. Yu. A. Khodak. Tez. dokl. IV soveshch. po probl. astrogeol., L., 1962, str. 40.

44. Photographic Lunar Atlas. Edited by G. Kuiper. The University of Chicago, 1960.

45. H. Wilkins. Moon Maps. The Macmillan Company, 1969.

46. G. Pettengill. Proc. I. R. E., 48(5), 933, 1960.

47. V. Sharonov. Astron. zh., 31, No. 5, 442, 1954.

48. C. Haynes. Mines Mag., 52, No. 1, 26, 1962.

49. M. M. Shemyakin. Byull. VAGO, No. 30 (37), 33, 1962.

50. V. G. Fesenkov. Sb. "Problemy evolyutsiy Zemli i planet," vyp. 5, Izd-vo AN KazSSR, 1951, str. 19.

51. A. V. Peyve. Sb. "Structura zemnoy kory i deformatsiy gornykh porod." Izd-vo AN SSSR, 1960, str. 67.

52. G. N. Katterfel'd. Izv. Vses. geogr. o-va, 91, No. 272, 1959.

53. B. Yu. Levin. Byull. VAGO, No. 30 (37), 6, 1962.

54. B. Yu. Levin, Ye. L. Ruskol. Sb. "Voprosy kosmogoniy," t. 8, Izd-vo AN SSSR, 1962, str. 109.

55. G. N. Katterfel'd. Lik Zemli i ego proiskhozhdeniye. Geografizdat, 1962.

56. M. V. Stovas, D. N. Usenko. Izv. AN SSSR, ser. geol., No. 11, 101, 1962.

57. M. V. Stovas. Geogr. sb. No. 15, Izd-vo AN SSSR, 1962, str. 29.

58. Chang Wen-yu. Scientia Sinica. 10, No. 3, 361, 1961.

MAIN STRUCTURAL ELEMENTS OF THE MOON

Yu. A. Khodak

A description is given of the main structural elements of the near and far sides of the moon and a series of deep-fracture zones in four directions which segment the lunar crust into huge blocks is noted.

In connection with the growing study of outer space, including the region of the moon, it has become necessary to elicit the structural elements of the moon.

In 1960 the compilation of geological moon maps began simultaniously both in the USSR and USA [1]. The U.S. Geological Survey, under the direction of R. J. Hackman, compiled a generalized photogeological map of the visible side of the moon (1:3, 800, 000), on which are distinguished three differently developed complexes of lunar rock, and a preliminary photogeological map of the region of the crater Copernicus (1:1, 000, 000), on which are distinguished five differently developed complexes of lunar rock. This map also shows anticlines, synclines and monoclines, and areas of eruption of various rocks [2-5].

On the basis of an analysis of the nature and distribution of mountain formations (cirques, craters, cirque and crater chains and ridges), maria, clefts and rills, the author has attempted in this

paper to note the most important structural elements of the moon as a whole, both visible and far sides. For this purpose the following information concerning the relief of the moon was used: A. V. Khabakov's map of the relief formations of the visible portion of the moon [6], the latest atlases of photos and drawings of the visible side of the moon (the atlas of photographs edited by Kuiper [7] and Wilkin's atlas of photos and drawings [8]), a map of the reverse side of the moon compiled from photos obtained from the Soviet automatic interplanetary station in 1959 [9-11], as well as other material.

From what we can see of the moon, there are three major structural elements (Fig. 1): 1) a meridionally elongated ancient massif embracing the southern portion of the reverse side (more than half) and the southern part of the visible side; 2) the Great Belt of deep depressions (seas) within the massif and extending as a semi-ring convex northward from Mare Australe to Mare Humorum; 3) a meridional belt of deep depressions on the reverse side of the moon at the edge of the yet-unphotographed region of the moon. The junctions of these elements are linear, angular, and similar to the deep fractures of the earth as represented by A. V. Peyve [12, 13], V. M. Sinitsyn [14], and other geologists [15, 16]. For example, the junction zone of the ancient massif with the Great Belt of large lunar depressions (seas) extends westward along a submeridional angular fracture from Mare Humboldtianum to the Joliot-Curie Montes, the western edge of Mare Marginis and Mare Smythii, the Skodowska-Curie Montes, the western edge of Mare Australe. Another somewhat more easterly zone of the meridional jointing of the western segment of the Great Belt of depressions extends along an angular fracture over the eastern edge of Mare Nectaris and Mare Tranquillitatus and northward to Mare Frigoris.

In the eastern segments of the Great Belt of lunar depressions, the junction zone with the ancient massif extends along a sharply defined meridional cirque chain Licetus-Walter-Ptolemeaus. This fracture zone is traced farther north along the Caucusus Mts., delimiting Mare Serenitatis and Mare Imbrium.

Within the limits of the chief structural elements noted, which were, in our opinion, formed in the ancient period of development (ca. 300 million years ago), it is possible to note structural elements of subsequent periods which appear as blocks delimited by a system of global, deep fractures of four directions, viz., meridional, submeridional, latitudinal, and sublatitudinal, traced for thousands of kilometers. The fracture zones bound lunar seas whose polygonal outlines were noted by B. G. Fesenkov [17].

The meridional and submeridional fractures separate the massifs from the belts of large depressions and extend coincident with the main directions of mountainous structures and internal uplifts within the depressions. Latitudinal and sublatitudinal fractures separate the chief blocks of the massif and zones of large depressions at the intersection of the course of mountainous structures and uplifts. The oldest systems of fractures are comprised of the following zones (Fig. 2a): a) meridional and submeridional fracture zones: 1) central zone, from the region of the southern zone approximately from the Zach cirque through the cirque chain of Licetus-Walter-Ptolemeaus, the region of the Fresnel prominance and farther to the north pole; 2) western zone along the estern boundary of Mare Nectaris and Mare Tranquillitatus, the western boundary of Mare Serenitatis, and northward to Mare Frigoris; 3) eastern zone along the eastern margin of Oceanus Procellarum and Mare Imbrium; 4) on the reverse side of the

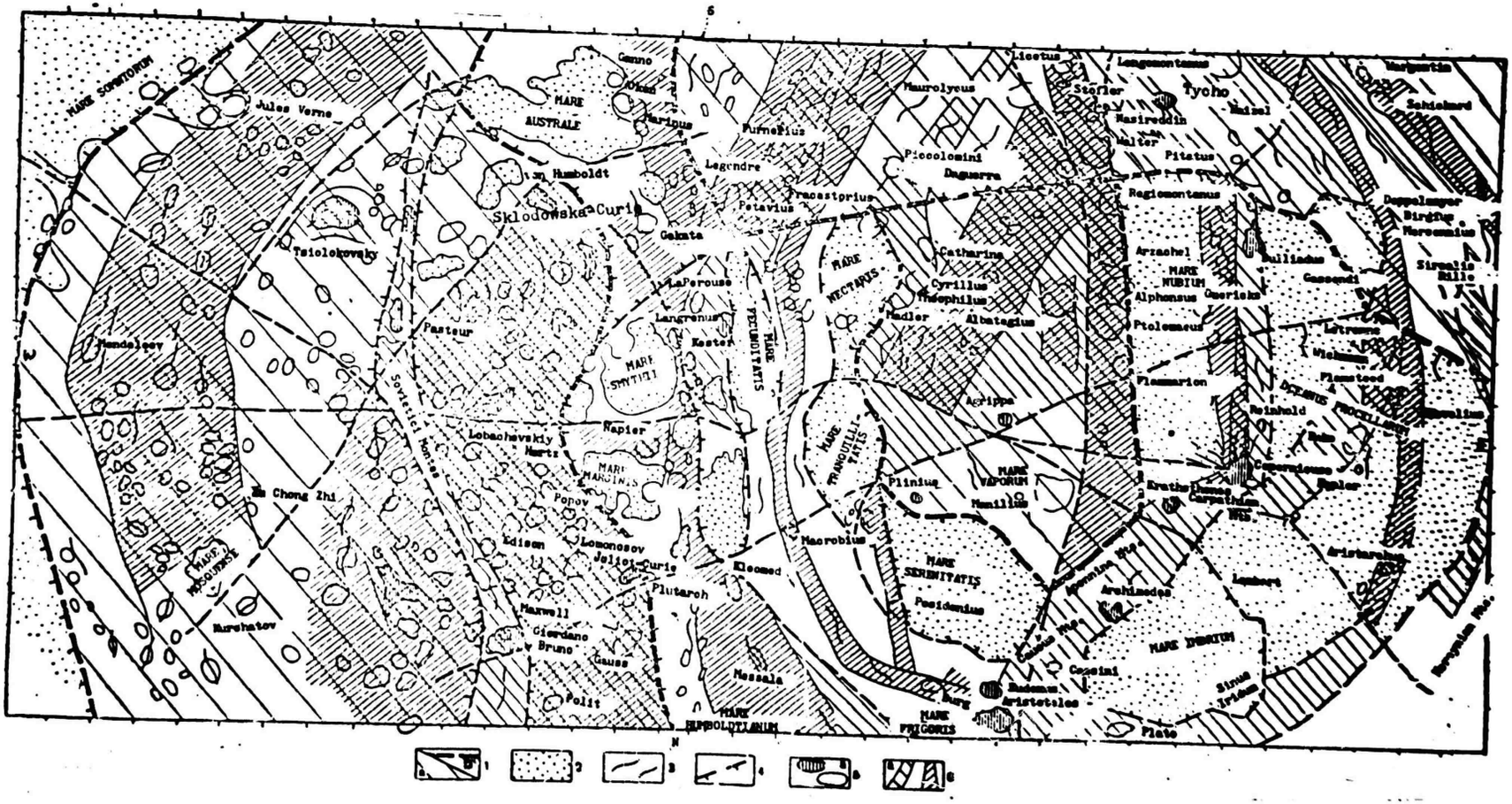

Fig. 1. Diagram of the main structural elements of the moon.
1a) ancient massif; b) boundary massif; 2) depressions (maria); 3) course of mountainous structures and upheavals; 4) deep fractures (direction of subsidence of blocks given); 5) chief cirques and craters, a) young; 6) mountainous structures and upheavals, a) young.

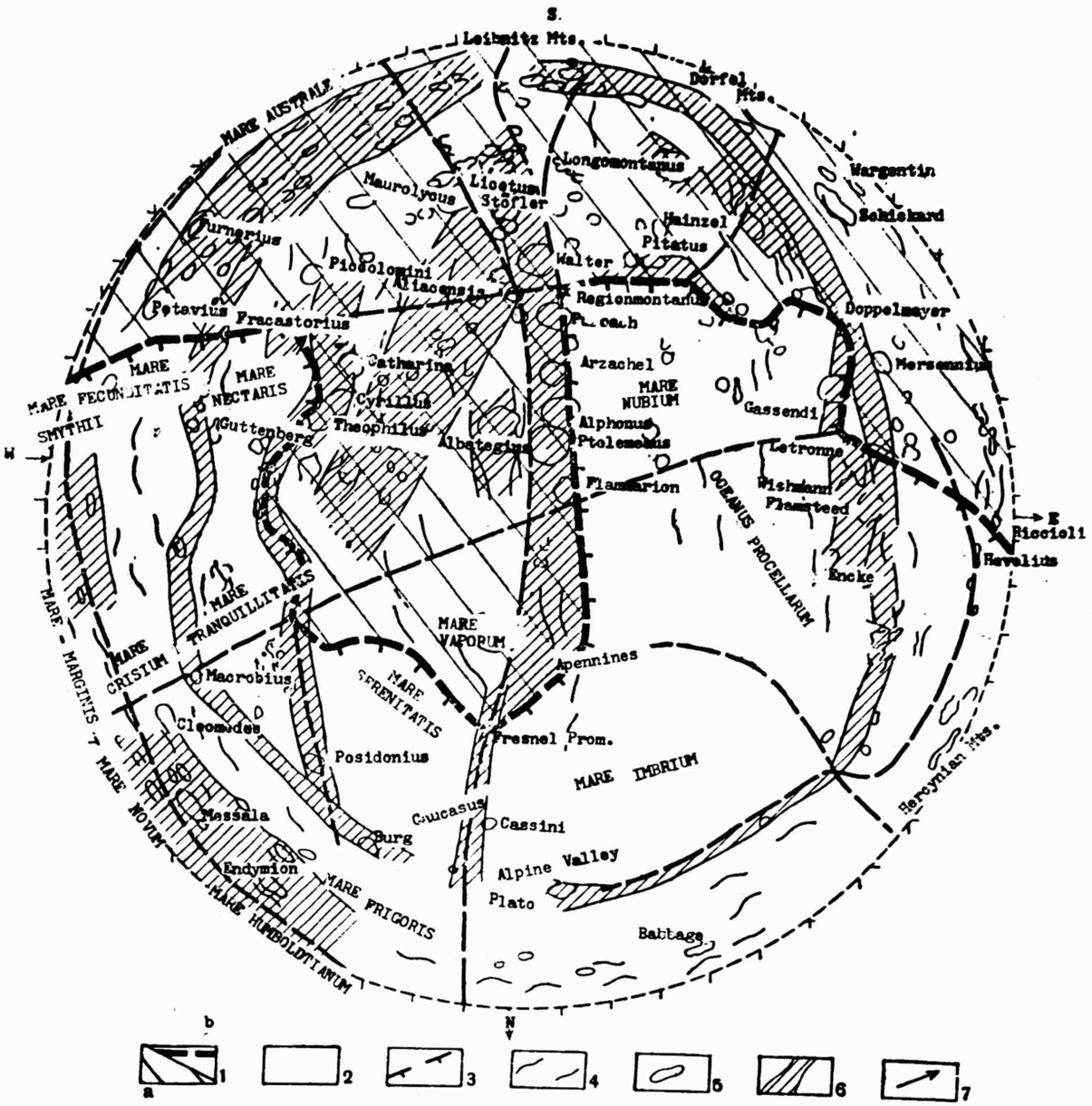

Fig. 2. Diagrams of main structural elements:

a) ancient and Ptolemaic periods of the visible side of the moon: 1a) ancient massif, b) boundary of massif; 2) depressions; 3) deep fractures (direction of subsidence of blocks given); 4) course of ancient mountainous structures and upheavals; 5) chief cirques and craters of the Ptolemaic period; 6) mountainous structures and zones of major upheavals of the Ptolemaic period; 7) direction of stress.

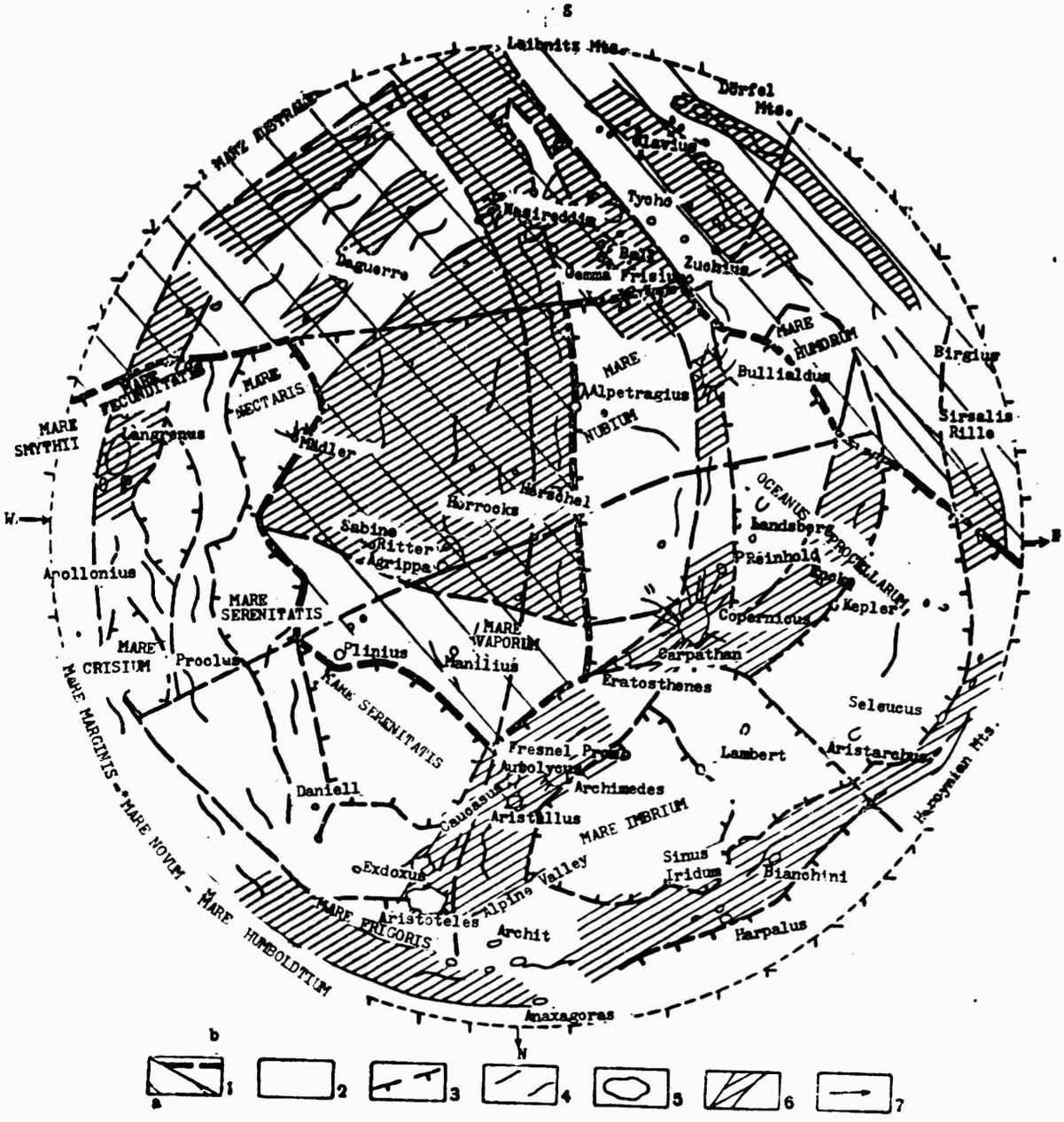

Fig. 2 (continued)

b) Copernican and Recent periods of the visible side of the moon: 1a) ancient massif; b) boundary of massif; 2) depressions; 3) deep fractures (direction of subsidence of blocks given); 4) course of ancient mountainous structures and upheavals; 5) major cirques and craters of the Copernican and Recent periods; 6) mountainous structures and zones of major upheavals in the Copernican and Recent periods; 7) direction of stress.

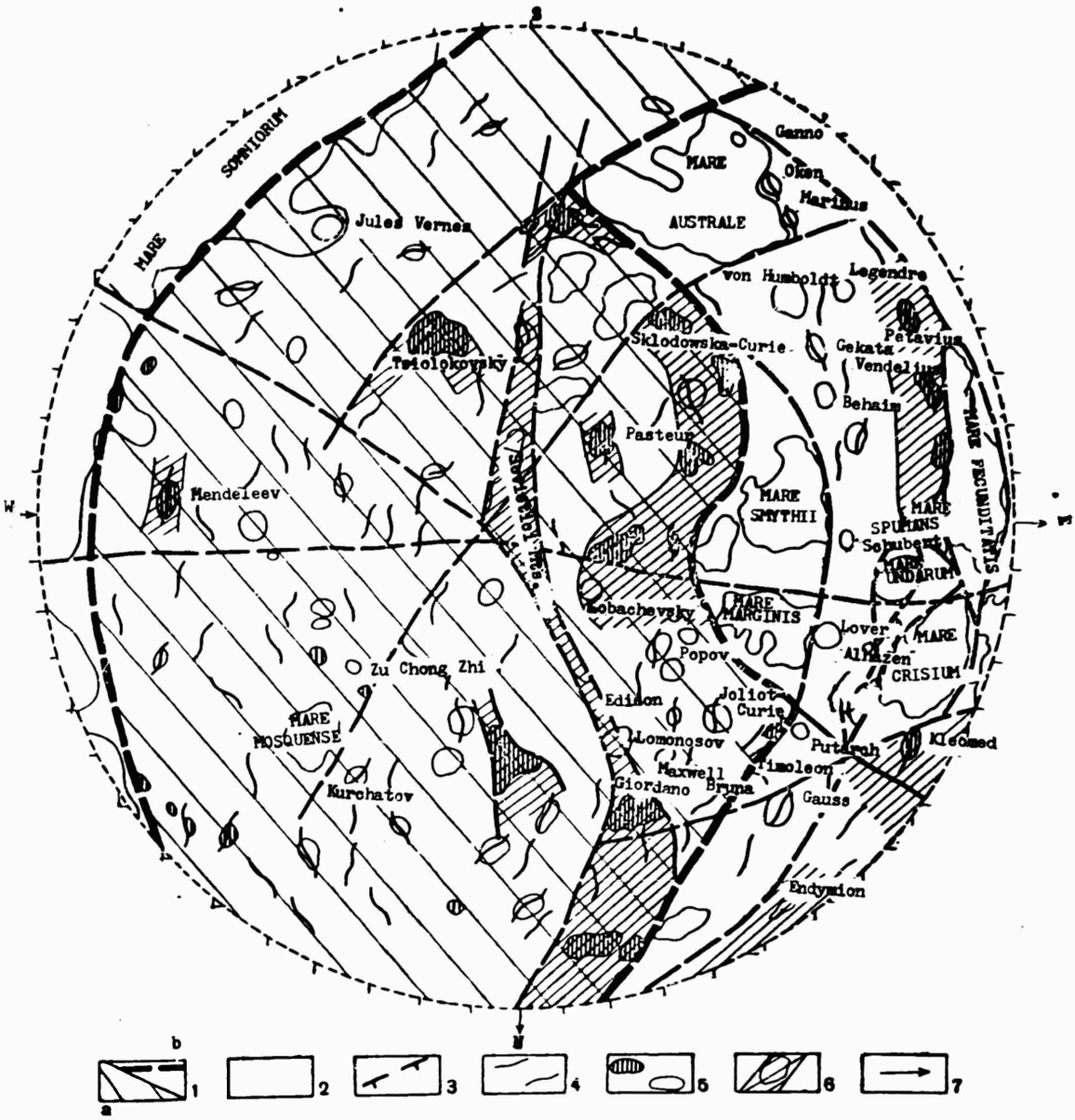

Fig. 2 (concluded)

c) reverse side of the moon: 1a) ancient massif, b) boundary of massif; 2) depressions; 3) deep fractures (direction of subsidence of blocks given); 4) course of mountainous structures and upheavals; 5) major cirques and craters, a) young; 6) major mountainous structures and zones of upheaval; 7) direction of stress.

moon are traced two zones of meridional and submeridional fractures: a) eastern boundary of Mare Somniorum and the seas located north of it, and b) in the middle part of the massif, from the mountainous structures located near Giordano Bruno along the edge of the Sovietici Montes and farther to the western edge of Mare Australe.

b) Latitudinal and sublatitudinal fracture zones: 1) southern zone along the sourthern limit of Mare Smythii, Mare Fecunditatus, and Mare Nectaris to the sourthern edge of Mare Nubium and Mare Humorum, delimiting a large block of massif jutting out northward as a wedge; 2) northern zone, along the northern edge of Mare Crisium and Mare Serenitatis, one branch of this fracture zone is traced eastward as far as the region of Flammarion, another branch of this deviates northward and extends along the southern limit of Mare Serenitatis and Mare Imbrium, separating them from the northern, less mountainous part of the massif. On the reverse side of the moon the northern sublatitudinal fracture zone terminates along the northern border of Mare Smythii and Mare Fecunditatis, intersects the Sovietici Mts. [11] at their angular bend, and is traced to the region of Mendeleev (Fig. 2c).

The most elevated portion of the massifs in the ancient period, it seemed to us, is its northern projection on the visible side of the moon: the region around Mare Vaporum, separated from the core of the massif by a northern sublatitudinal fracture. The portion of the massif on the reverse side of the moon was stable, especially its central areas which abut the Sovietici Mts.

During the Ptolemaic period (about 100-150 million years ago as defined by Khabakov [6, 18]) the moon in many respects inherited its early structural plan. The most active zone in this development

period was the central meridional fracture zone of the southern hemisphere, in which emerged the vast meridional mountain chain consisting of the Licetus-Ptolemaeus chain. The mobility of the zone diminishes north of Ptolemaeus where it may be traced along gradual, fault-block fractures between Mare Serenitatis and Mare Imbrium. Less mobile meridional and submeridional zones are distinguished along the border of Mare Nectaris and Mare Tranquillitatis, onward to the region of the western limit of Mare Frigoris and also within the Great Belt of depressions: 1) along the western border of Mare Nectaris and Mare Tranquillitatis and north to Mare Frigoris; 2) in the eastern portion of Oceanus Procellarum and Mare Imbrium, from the region of the Dörfel Mts. in the south to the region of Plato in the north.

The reverse side of the moon during the Ptolemaic period was relatively stable. In all probability the most mobile zones were the meridional and submeridional junction zones of the massif with the zones of large depressions situated further west and east, as well as the middle portion of the massif separated from the north pole by the Giodano Bruno Mts., and Sovietici Mts. into two large-scale block segments, western and eastern.

The activities of the zones of latitudinal and sublatitudinal directions of the Ptolemaic period are rather weakly detected.

During the Copernican and Recent periods (according to Khabakov [6, 18]) further differentiation of the structural elements took place along the zones of deep fractures which occurred in preceding periods, breaking them up into huge blocks (Fig. 2b). The linked system of zones of meridional and sublatitudinal (NW) directions, which may be traced from the Leibnitz Mts. in the south to the large

craters of Tycho, Bullialdus, and Copernicus and northwestward to the crater Aristoteles, which separates the most subsided northern portion of Oceanus Procellarum and Mare Imbrium from the uplifted massif of the southern hemisphere and near-equatorial region, appears to be the most mobile [19-25]. Less uplifted meridional zones are noted: 1) along the ancient central meridional zone, 2) along the border of Mare Australe, Mare Fecunditatis and Mare Crisium and northward to Mare Frigoris, where the zone joins with the most mobile belt of the Leibnitz Mts. and the creaters Copernicus and Aristoteles; both of these zones girdle the most uplifted section of the moon, 3) along the northeast border of Mare Imbrium, the east border of Oceanus Procellarum, and southward along the Sirsalis Rille in the region of the crater Birgius.

On the reverse side of the moon the most mobile zone is the meridional fracture zone which is traced in the northern portion of the massif along the Giordano Bruno Mts., the Sovietici Mts. and farther to the mountains close to the edge of Mare Australe. It is possible to divide the sublatitudinal zone of fractures: 1) from the northern edge of Mare Serenitatis to the Apennines and northward to the mountains of Aristarchus: 2) from the mountains of Giordano Bruno and Joliot-Curie to the reverse side of the moon along the north border of Mare Crisius, Mare Tranquillitatis, Mare Nubium (bisecting the massif) to the junction of Mare Humorum, Oceanus Procellarum, and the southwestern portion of the massif in the region of Letronne, 3) in addition, two extensive fracture zones overlapping at the point of the angular bend in the Sovietici Montes are noted on the reverse side of the moon. The southwestern fracture extends from the angular bend in the Sovietici Montes (more northeasterly it proceeds along

this ridge) to the northern border of Mare Somniorum; the northwestern fracture extends from the northern border of Mare Australe and Sklodowska-Curie to the northeastern border of Mare Mosquense.

From what has been stated, one may conclude a block structure of the moon, and an inheritance of development from the chief structural elements and from their differential movements along the zones of deep fractures from the ancient period to the Recent. The block structure of the lunar crust, which exists also on the earth [13] and on Mars [26], evidences the general pattern of development of the solid crust of these planets, which make it possible to continue a planetological investigation in a comparative historical aspect.

The author expresses his thanks to Doctor of Physical-Mathematical Sciences, A. G. Masevich for assistance in organizing the study.

REFERENCES

1. A. V. Khabakov. Gaz. "Izvestiya", 3 April, 1963.

2. Generalized Photogeologic Map of the Moon. U.S. Geol. Serv., 1960.

3. A. Mason and R. Hackman. Bull. Geol. Soc. America, 71, No. 2, pt. 2, 2103, 1960.

4. A. Mason and R. Hackman. Symp. No. 14. Intern. Astron. Union, the Moon, p. 301, 1962.

5. E. Shoemaker and R. Hackman. Symp. No. 14, Intern. Astron. Union, the Moon, p. 289, 1962

6. A. V. Khabakov. Sb. "Luna". Fizmatgiz, str. 241, 1960.

7. Photographic Lunar Atlas. Edited by G. Kuiper. Chicago, 1960.

8. H. Wilkins. Moon Maps. The Macmillan Company, 1960.

9. Atlas obratnoy storony Luny. Izd-vo AN SSSR, 1960.

10. I. I. Breydo, A. A. Mardelova, and L. Sh. Shchegoleva. Sb. "Iskusstvennyye sputniki Zemli", vyp. 9, Izd-vo AN SSSR, str. 30-40 1961.

11. Yu. N. Kipskiy. Sb. "Iskusstvennyye sputniki Zemli", vyp. 9. Izd-vo AN SSSR, str. 3-19, 1961.

12. A. V. Peyve. Izv. AN SSSR, ser. geol., No. 5, 23, 1945.

13. A. V. Peyve. Sb. "Struktura zemnoy kory i deformatsiya gornykh porod". Izd-vl AN SSSR, str. 67, 1960.

14. V. M. Sinitsyn. Sb. "Voprosy geologiy Aziy", t.2. Izd-vo AN SSSR, str. 81, 1955.

15. G. D. Azhgiriy. Sb. Muzeya semlevedeniya MGU "Zhizn' Semli", No. 1, str. 53-64, 1961.

16. Yu. A. Khodak and Sun-Shu, Izv. AN SSSR, ser. geol,, No. 10, str. 97, 1960.

17. V. G. Fesenkov. Sb. "Problemy evolyutsii Zemli i planet", vyp. 5. Izd-vo AN KazSSR, 1951.

18. A. V. Khabakov. Ob osnovnykh voprosakh istoriy razvitiya poverkhnosti Luny. Geografizdat, 1949.

19. V. B. Neyman. Byull. VAGO, No. 30 (37), a8, 1962.

20. R. B. Boldwin. Sky a. Telescope, 21, No. 2, 84, 1961.

21. R. W. Carder. Symp. No. 14, Intern. Astron. Union, the Moon, p. 117, 1962.

22. E. Du-Frensne. Astrophys. J., 124, No. 3, 638, 1950.

23. Ch. U. S. LaFond. Missiles a. Rockets, 8, No. 14, 34, 1961.

24. G. Schrutka-Rechtenstamm. Mitt. Univ. Sternwarte Wien., 7, 1955.

25. G. Schrutka-Rechtenstamm and I. Hopmann. Abteilung II, Sitzungsberichte, 167, No. 8-10, Wien, p. 283, 1958.

26. G. N. Katterfel'd. Izv. Vses. geogr. o-va, 91, No. 272, 1959.

CHRONICLE

DISCUSSION OF SPACE RESEARCH PROBLEMS AT THE XIV GENERAL ASSEMBLY OF THE URSI

The XIV General Assembly of the International Scientific Radio Union (URSI) was held in Tokyo from Sept. 9 through Sept. 20, 1963. Participating in the conferences were delegates from 26 countries who are carrying on investigations in various fields of radio engineering and radiophysics. On the whole, over 1000 scientists (approximately 600 Japanese delegates) participated in the proceedings. V. I. Siforov headed a 21 man delegation from the Soviet Academy of Sciences.

URSI is made up of seven commissions whose work encompasses all scientific investigations in the field of radio. Three commissions are directly associated with space research (Commission III deals with the ionosphere, IV with the magnetosphere, and V with radio-astronomy); a Committee of Space Research coordinates the activity pertaining to space investigation performed by URSI with the works in this field carried out by other scientific unions and organizations, particularly by COSPAR.

An appreciable place in the work of the XIV General Assembly of the URSI was devoted to problems involving space research:

ionospheric investigation by satellites and rockets, radiation investigations of planets and planetary atmospheres by their millimetric and infracted radiations, and the use of radio-communication satellite systems, etc.

This article aims only at a preliminary and partial presentation of the proceedings of the assembly which dealt with space research. The most comprehensive information is given for Commission III (ionospheric investigation) since this author participated mainly in the work of this commission.

The day following the opening of the General Assembly there was a joint gathering of commissions, i.e., in essence a plenary gathering.

The first paper read was, "Ionospheric Investigation By Means Of Rockets And Satellites." This paper, the work of the American delegate Bourdeau, the Canadian, Chapman, and the Japanese, K. Mayeda, was divided into the three following categories:

1) results of scientific investigations using rocket probes;

2) results of ionospheric investigations based on satellite-gathered data;

3) investigation procedures and rocket and satellite to be used.

This report is the most comprehensive in its field to date.

In brief, it considers the following wide range of problems: satellites and rocket investigations of ionospheric structure including the D and E regions both in the presence and absence of disturbances; solar radiation intensity in the lower ionosphere; electron and ion concentration measurements above the main ionization maximum; measurements of the electron temperature; determination of

ion composition, and upper ionospheric radiosoundings (above the ionization maximum).

Under the first category dealing with rocket and satellite ionospheric measurements, data was presented on instruments to be used for satellite ionospheric radiosoundings, data on Langmuir probes, reasonance probes, and impedance probes. Data were also presented on the Doppler shift, the Farraday effect, and rocket and satellite findings. The article's conclusion summarizes the work and investigations to be carried out by research rockets and satellites in the International Year of the Quiet Sun (1964-1965).

A shortcoming of the report is that the authors limit their considerations only to 1000-1500 km and, so to speak, disregard the higher ionized regions of the ionosphere, the groundlessness of which was shown by the Soviet investigations with Lunar rockets and "Mars-I."

The next paper read, dealing with the means of investigating millimeter and infrared radiation waves, was the work of two Americans, Weaver, director of the Radioastronomy Laboratory at Berkeley, and Silver, director of the Space Research Laboratory also at Berkeley. The paper dealt with solving the problems of the structure of the atmosphere and surfaces of planets by studying their radiation spectra in specific frequency ranges. The authors showed that polarized radiation could be used for determining the dielectric constant of both the surface layer and certain other details of surface structure.

In this article, the authors considered the problems of radiation sources in millimeter and infrared frequency ranges of waves observed in space (solar radiation, planet radiation, nonthermal

radiation, and atmospheric radiation), of receiving the radiation of planets in these frequency ranges (planet temperature, problems of antennas and receivers), and of observation methods to be used in studying the planets. This article also summarized the work dealing with the moon, Venus, Jupiter, and also considers briefly the problems involved in the experiemtnal instruments mounted on balloons and space rockets, and those associated with radiometers and receivers.

The report of O'Neil, the Bell Laboratory (USA) representative, was titled "Space Communication Systems — Results and Problems." After briefly outlining the history of American communication satellites ("Score" –1958, "Courier" – 1960, "Echo" I – 1960, "Telstar" – 1962, "Relay" – 1962), the author went into greater detail on the Telstar satellite on which he had worked. He presented data on satellite temperature, its rotational velocity change, its rotational axis, and the effect of the radiation belts on its solar-operated battery output. O'Neil pointed out that the causes of the satellite's operation failure were apparently the ionization effects falling onto the transistor surfaces of the instrument decoding the incoming signal. To avoid them in the future, these effects were simulated in the laboratory. (A more detailed account of this is given in "Bell System Technology Journal," Vol. 42, January, 1963.) The author also gave a brief summary of the ground stations operating in conjunction with the American communication satellites, and pointed out that large antenna stations are currently being constructed in West Germany and Japan (a number of the Soviet delegates had visited the Japanese station near Takahasi on Sept. 15, 1963). The author also presented

information on the communication satellite ground station at Andover (Maine, USA). This station has a 175-foot horn antenna; the mobile horn mounting stand weighed 370 tons; the antenna gain at 6390 Mc was 61 db, at 4179, 58 db. A 210-ft diameter and 165-ft high shell protected the antenna, thus making it possible to orient the antenna under all weather conditions. The over-all temperature of the receiver system was 50° K at a 5° angle of elevation, and 32°K at the zenith (in dry weather). When it rains, a temperature of 80 to 100° K is observed, and under unusual conditions temperatures from 130 to 150° K have been recorded (this temperature increase is mostly due to the wet shell). The report stressed the prime importance of accuracy in satellite ground tracking stations. The author pointed out that even an error in antenna orientation of several hundredths of a degree could pronouncedly decrease the attainable signal-to-noise ratio.

The article then considers the problems associated with the powers emitted from the satellites and the use of frequency modulations. For the further development of efficiently operating satellite communication systems, the authors contended that there must be progress in the following areas:

1) satellites should be designed which can operate continuously for longer periods and which can generate greater power than the previous satellites;

2) the average satellite service life should be increased by several years while the cost of setting it in, or if need be, removing it from orbit should be minimized;

3) problems involving the delay of signals and the suppression of reflected signals should play a much greater role than they do

in ground systems. Much greater attention should be given to the major role (especially in low orbiting satellites) played by doppler shifts;

4) the problems of simultaneous signal transmission between several different pairs of ground stations by means of a signal satellite should be the object of greater study. The methods for both achieving and determining the feasibility of creating such systems should be thoroughly analyzed.

In conclusion the authors cite the importance of increasing the power generated by the satellite, and in this connection, increasing the volume of information relayed by the satellite. Therefore, the use of directional antennas on the satellite and the appropriate orientation areof major importance. The authors discussed these problems briefly. On the question of the reliable operation of the instruments, the authors pointed out that the causes of the malfunctioning in the "Relay I", the "Syncom I", and "Telstar II" which was (launched May 7, 1963, and stopped operating June 16, 1963) had not yet been determined. He noted however that the experimental satellites were much more intricate than those which will be used for operation and accordingly the latter will be much more reliable.

In the last article read at the plenary session by Golomb (of the California Jet Propulsion Laboratory (USA)), the author presented different approaches to the problem of coding the information transmitted from outer space (for example from Mars). One such approach is to use a code where each information unit is protected in the best possible manner from distortions coming from the noise of the transmission canal; another possible approach is to evaluate the

information from the standpoint of its importance, and then to furnish the best possible conditions for transmission of the most pertinent information. In pointing out the fact that in experiments conducted in space rockets it was more advantageous to process complicated information on earth rather than process the experimental data on board the spaceship, the author indicated possibilites where the reverse was true (for example, if the distribution of the magnitudes to be measured are known as priori).

The work of the Ionospheric Commission was under the directorship of its recently elected representative Ratcliffe (England), one of the foremost specialists in the field of the physics of the ionosphere and the ionospheric distribution of radio waves. Participating in this conference were the leading experts in this area from many different countries: from the USA, Bourdeau, Bowhill, Boyles, Bauer, Dessler, F. Johnson, Garriott, Carpenter, Pfister, Friedman, Hinteregger, Evans, Nisbet, Farley, Schmerling; from England, Baynon; from Canada, Chapman; from France, Vassy; from East Germany, Lauter; from West Germany, Dimminger; from Italy, Pancci; and also the president of the International Association of Geomagnetism and Aeronomy, Nicolet, and the former president of URSI, Berkner.

An extremely large group of Japanese research scientists worked on Commission III (K. Mayeda, Aono, Obayashi, Takayama). This group made the work of Commission III one of the most representative and serious discussions on the structure of the ionosphere and the ionospheric distribution of radio waves held in recent years.

The characteristic feature of the work of Commission III was the major importance granted to the discussion on the methods of rocket and artificial satellite study of the ionosphere. Two meetings

of the Commission were devoted to the themes, "The Ionososphere and Space Research" and "The Electron Profile of the Ionosphere." In addition to these, Commission III sessions discussed the following problems: ionizing radiation and atmospheric compositions, waveguide propagation of radio waves in the ionosphere and troposphere (jointly with Commisssions II and IV), questions associated with the International Year of the Quiet Sun, and problems of the nonhomogeneous structure of the ionosphere.

The work of Commission III began with a summary of the most important results obtained in ionospheric research since the preceding meeting of URSI (1960-1963). This summary was given by the commission representative Ratcliffe.

Ratcliffe noted the majcr successes achieved in the study of the D layer, the electron distribution from 50 to 90 km, and the behavior of the D layer in the polar regions and of the ionizing agents creating the D layer.

According to the author, no significant results were obtained in studying the normal E layer, whereas certain valuable data were obtained on the sporadic E layer; in particular, a number of independent rocket measurements showed the reality of the existence of layers with greater than 1 to 2-km thick electron concentrations.

The upper ionosphere above the maximum layer was studied by the following methods:

1) by ionospheric radio soundings "from above" by means of various ionospheric sounding stations mounted on satellites;

b) by incoherent scattering. In this method the energy of a powerful, upward incoherently scattered radiation is used for determining the electron concentrations at different heights;

c) by direct study of the electron concentration and the ion masses by using probes installed in artificial earth satellites.

Naturally, a certain fraction of the large volume of the latest information gathered in these probes requires additional corrections.

The author cited as two of the most important results gathered in ionospheric research, the detection of layers where helium and hydrogen were the predominant elements and the establishment that these boundaries change with time. The effective temperature of the ionosopheric electrons T_e can apparently be higher than the temperature of the ions T_i (especially during the day); this relationship can reach two. The factors causing this are yet to be explained.

The data for determining the total electron concentration by means of observing radio signal "beacons" mounted on the satellites, and for determining the Faraday effect in the radiolocation of the moon indicate that during ionospheric storms, there is a decrease not only in the electron content in the "lower" ionosphere (a fact long known), but also a decrease in the electron content above the F layer. The observation of whistlers shows that a similar decrease in electrons occurs at heights of the order of one to two earth radii.

The causes of ionospheric heating continue to remain unknown. Ultraviolet radiation, corpuscular solar fluxes, Joule heating, and (during storms) hydromagnetic waves are being considered as possible causes.

Attempts to formulate a theory which would describe the behavior of antennas in the ionosphere operating on a frequency close to the plasma frequency near the antenna have had only partial successes. Experiments with probes supplied by a voltage with an alternating

frequency, carried out in laboratory plasma and in the ionosphere, showed that a rectified current across the probe attains a maximum at a voltage frequency close to the plasma frequency. Attempts to explain this phenomenon have not been entirely successful.

The recently developed theory of incoherent scattering of radio waves in the ionosphere indicates that the study of the spectrum shape of the echo-signal broadened as a result of the Doppler effect enables us to determine the ratio of the electron to ion temperature. The author also showed that in any case a detailed study of the spectrum should result in determining the ion masses.

In Ratcliffe's summary, as well as in Bourdeau's, Chapman's, and Mayeda's reports, insufficient attention was given to the upper ionosphere (heights greater than approximately 1500 km) and to the question of its upper boundary.

Friedman's report was concerned with the role played by the different region of the solar radiation spectrum in the formation of the ionosphere at different heights. His report used measurement data of solar radiation obtained by American satellites and rockets. Friedman's major conclusions may be summarized as follows.

Ionospheric behavior depends on the solar radiation flux in the X-ray and ultraviolet frequency ranges. In each ionospheric region the specific length of wavelengths play the major role. Under quiet solar conditions Lyman-α (1216 A) is the chief ionization source of the D layer. When the sun is active its increase in ionic activity is proportional to the X-radiation from 1 to 10 A. At heights greater than the E layer (100-150 km), ionization is created by X-radiation in the wide range from 10 to 100 A; the Lyman-β (1025.7 A) radiation can define the shape of the base of

the E region, whereas C III (977 A) and the Lyman continuum (910-800 A) are the most important ionization sources in the higher areas of the E region. The major contribution in the ionization of the F layer is made by the ultraviolet radiation in the range from 175 to 400 A, which includes the resonance line of He II (304 A).

The report of the Belgian, Nicolet, was devoted to a theoretical substantiation of the chemical composition of the ionosphere, by considering the different variants of elementary processes which yield results close to those observed in rockets and satellites by ion mass-spectroscopes.

Chapman's (Canada) report dealt with a summary of the results gathered by the "Alouette" satellite developed and manufactured in Canada and launched Sept. 29, 1962 in the USA. The satellite is an ionospheric station completing a near circular orbit at approximately 1000 km inclined to the equator at 80.5°. The orbital plane rotated relative to the earth at a rate of approximately 2° per day. The measurement results were transmitted by a telemetric system.

The basic characteristics of the station are as follows: the frequency varies from 0.5 to 11.5 Mc; the rate of frequency change is 1 Mc/sec; there are three frequency swings per minute; the duration of the pulse lasts 100 μsec; the recurrent frequency is 67 cps, and the pulse power is 10 w. The antenna is made up of two adjacent dipoles, one 150 ft long (the total sweep) and other, 75 ft long.

The satellites are guided by transmitting stations in North and South America, Europe and Australia.

The results of the measurements made by the satellite are of major value. Large volumes of data were obtained on the global

nature of the upper atmosphere; included in these data were facts on the anomalous concentration of high electron concentrations within the magnetic equator and facts on diurnal variations. Chapman indicated that ionospheric stations installed on satellites are especially valuable for representing ground and space data measurements as functions of latitude and height. To explain certain results obtained by the "Alouette" satellite, it is necessary to assume that the energy imparted to the ionosphere by the charged particle fluxes is greater than we had considered earlier, especially in high latitudes.

In the future, ionospheric satellite radiosoundings should be combined with measurements of the ion and electron temperatures and energy particle fluxes. The satellite-gathered ionograms will be transmitted to World Data Collection Center A (in the USA), from where all stations desiring either to process the ionograms independently or to clarify some detail will be able to obtain them.

Gringauz's report (USSR) summarized the results of certain 1961-62 experiments which were part of the Soviet research program of satellite and rocket investigations of the upper atmosphere and outer space.

The report primarily presented ionospheric data gathered by Soviet geophysical rockets. These experiments were used, first, for determining the electron concentration from measurements of the radio wave scattering from rockets and, second, for determining the electron concentration from the Faraday effect. A comparison of these measurements (1962-63) with analogous measurements made in 1958-59 indicated that the height distribution of the electrons above the major ionization maximum varies with a decrease in solar

activity (the electron concentration drop-off with height is accelerated). A comparison between the on-board measured data and simultaneous ground measurements made by the ionospheric station at launch time showed that, by using the ground ionospheric station measured data it is possible to determine with sufficient accuracy the true distribution of electron concentration below the major ionization maxium (using the method of solving the integral equation with the Shinn-Kelso coefficients).

The second group of ionosphere experiments elucidated in the works of Gdalevich, Imyanitov, and Schwarts dealt with measuring the electrical fields by using electrostatic fluxmeters adapted to operate in plasma. These experiments demcstrated the existence of outer electrical fields in the ionosphere during the measurements. These fields at 300-500 km were estimated to be of the order of 10^{-3} w/cm.

The report then gave certain results of the ion trap experiments conducted April, 1962 with the "Kosmos-2" satellite. A comparison of these results with experimental data gathered by the ion traps on the third Soviet artificial earth satellite (May, 1962) showed that with a decrease in solar activity not only does the height distribution of the charged particles vary substantially, but even the chemical composition of the ions varies markedly. The region where atomic oxygen predominates, which in 1958 extended above 1000 km, in 1962 terminated at heights of 600-700 km, and above this a region began where helium ions predominate. These results are in good agreement with Soviet geophysical rocket experiemtnal data, and apprently are the result of the over-all cooling of the upper atmosphere as minimum solar activity is approached.

The article concludes with the results of the measurements pertaining to that part of the atmosphere investigated with the "Mars-1" ion traps in 1962. These results confirm that the earth's ionized gaseous envelop extends to heights of the order of 20,000 km. The "Mars-1" experiments were the first to successfully observe at these high geomagnetic latitudes the intersection of the earth's gaseous envelop with the outermost charged particle belt composed of comparatively low-energy electrons.

Ratcliffe, chairman of Commission III, noted that certain important and interesting results were presented in the Soviet report. He especially emphasized the experiments on the direct detection of the ionospheric electrical fields, having stressed the fundamental importance of the problems of ionospheric electrical fields for a thorough comprehension of a number of processes, particularly the motion of ionospheric inhomogeneities.

The American scientists, Carpenter, reported at the joint session of Commissions III and IV devoted to the height distribution of ionospheric electron concentrations. He outlined a method for determining the electron concentration distribution in the equatorial regions by observing whistlers. Comparison of several different investigations indicated good agreement with respect to the shape of the distributions. The distribution obtained coincides with the experimental data on the incoherent radio wave scattering research made up to heights of 500 km in the neighborhood of the geomagnetic equator. In the electron concentration distribution curve for the equatorial region, Carpenter noted a region where the curve bent, which he termed a "knee." This "knee" is distinguished by a rapid electron concentration drop-off n_e (sixfold and more). Carpenter

considers that this "knee" is a constant phenomenon and its height does not vary with magnetic activity. Carpenter noted that his results pertaining to the "knee" in the curve agree with the results made with the charged particle traps on the Soviet "Lunar-2" station.

In considering this report we must note that the agreement between Carpenter's results pertaining to the region of rapid drop-off n_e at heights of 3-4 Earth radii and the Soviet (1959) results had heretofore not been confirmed by any other independent method or by any other scientists.

In his notes on Carpenter's report, Gringauz indicated that actually the effect of a relatively rapid drop-off of the charged particle concentration above 15,000 km was first observed not on the second Soviet rocket, as stated in the report, but on the first lunar rocket. To confirm this, Gringauz exhibited a graph published in 1960.

The reports of the two American, Bauer and Jackson, were of great interest. Their reports cited results of near simultaneous measurements of the high-altitutde distribution of electrons and ions in the outer ionosphere made directly over Wallops Island in the USA July 2, 1963. The electron concentration distribution was measured by an ionospheric radiosounding from an "Alouette" satellite and by measuring incoherent radio wave scattering, using a device developed by the Lincoln Laboratories (designed by Evans) and by scattering measurements of coherent signals emitted by a two-frequency transmitter installed on the vertically launched "NASA" rocket. This rocket contained an ion trap for measuring the ion concentration.

All four measurements gave practically similar results (less

than 10% divergence).

Boyle in his report devoted to the problems of ionospheric investigation by the incoherent scattering method pointed out that the rapid development in the use of incoherent scattering methods for measuring the ionospheric electron concentration and temperature profiles entails a number of difficulties. Perhaps the only possible way to obtain the electron profile of the ionosphere will be to measure the Faraday effect of the polarization plane of radio waves scattered at different heights.

A number of reports were devoted to questions of the inhomogeneous structure of the ionosphere.

Farley's (USA) theoretical reports, and Teuda's (Japan) dealt with the mechanism causing the formation of inhomegeneities.

Getmantsev and Densisov (USSR) presented the following results of the investigation of small-scale and large-scale ionospheric inhomogeneities by radioastronomy, vertical sounding, and artificial earth satellite methods:

1. Data on small-scale inhomogeneities were gathered by observing the radiation fluctuations of discrete sources.

2. Data on the size and movement of ionospheric inhomogeneities were obtained by spatially diverse reception of reflected ionospheric signals.

3. Data on the height and scope of the inhomogeneities were obtained by using space diverse reception of artificial earth satellite (AES) signals.

4. Investigation results of the large-scale inhomogeneities in the F layer were obtained by measuring the phase difference of signal, of the coherent frequencies of the AES.

5. Results of the theoretical calculation of the statistical parameters of the field occurring at the earth's surface owing to diffraction of waves on an inhomogenous screen (on the ionospheric layer).

Pfister (USA) reported on the results of the direct measurements of electron concentration by artificial earth satellites. Observations demonstrated the existence of ionospheric inhomogeneities with only a 10% deviation for the charged particle concentration, having dimensions of the order of 700 km.

Certain reports concerning space research were also given in the sessions of Commission VII.

P. Lust (West Germany) read a paper on plasma on geophysical and astrophysical scales. He noted the the prime impetus to the development of plasma physics was furnished by geophysical and astrophysical problems, and that this field is still of major interest since the greater part of the universe exists in the form of plasma (the only exceptions are celestial bodies similar to the earth and planets* which comprise only a minor fraction of the entire mass of the universe). The author goes on to note that one of the most interesting aspects of plasma physics is the interaction between interstellar, interplanetary, stellar, and planetary matter and the cosmic magnetic fields. The author briefly reviews certain properties of plasma in different regions of the universe. The report concludes by giving a useful resume of the different parameters of plasma (plasma frequencies, Debye radii, proton and electron

*Also cosmic dust and neutral hydrogen.

hydrostatics, the collision frequencies required for charged and neutral particles, the free path, the velocity of sound, etc.) present in the ionosphere, in the interplanetary medium, the corona, the sun's photosphere, and in the interstellar medium.

Sonnet (USA) reported on the structure of the interplanetary magnetic field both during quiescent periods and during disturbances, using measurement data gathered by the "Mariner-2."

Even this rather incomplete treatment of the scientific research discussions at the XIV General Assembly of URSI indicates that it was one of the major scientific gatherings in the field of space research (especially ionospheric research) and that its findings merit serious attention.

K. I. Gringauz

DISTRIBUTION LIST

DEPARTMENT OF DEFENSE	Nr. Copies
HEADQUARTERS USAF	
AFCIN-3D2	1
ARL (ARB)	1
AFCIN-M	1
OTHER AGENCIES	
CIA	1
NSA	6
DIA	4
AID	2
OTS	2
AEC	2
PWS	1
NASA (ATSS-T)	1
ARMY (FSTC)	3
NAVY	3
NAFEC	1
RAND	1
AFCRL (CRXLR)	1

MAJOR AIR COMMANDS	Nr. Copies
AFSC	
SCFDD	1
DDC	25
TDBTL	5
TDBDP	82
TDGS	1
TDC	1
TDF	3
TDES	1
TDEWT	1
TDFS	1
TDSPAO	4
AEDC (AEY)	1
AFFTC (FTY)	1
AFMDC (MDF)	1
AFMTC (MTW)	1
AFWL (WLF)	1
AMD (AMRF)	1
APGC (PGF)	1
ASD (ASFA)	32
BSD (BSF)	1
ESD (ESY)	1
RADC (RAY)	1
SSD (SSF)	2